PACIFIC EARTHQUAKE ENGINEERING
RESEARCH CENTER

Spectral Damping Scaling Factors for Shallow Crustal Earthquakes in Active Tectonic Regions

Sanaz Rezaeian
U.S. Geological Survey, Golden, CO

Yousef Bozorgnia
Pacific Earthquake Engineering Research Center
University of California, Berkeley

I. M. Idriss
University of California, Davis

Kenneth Campbell
EQECAT, Inc., Beaverton, OR

Norman Abrahamson
Pacific Gas & Electric Company, San Francisco, CA

Walter Silva
Pacific Engineering & Analysis, El Cerrito, CA

PEER 2012/01
JULY 2012

Spectral Damping Scaling Factors for Shallow Crustal Earthquakes in Active Tectonic Regions

Sanaz Rezaeian
U.S. Geological Survey, Golden, CO

Yousef Bozorgnia
Pacific Earthquake Engineering Research Center
University of California, Berkeley

I. M. Idriss
University of California, Davis

Kenneth Campbell
EQECAT, Inc., Beaverton, OR

Norman Abrahamson
Pacific Gas & Electric Company, San Francisco, CA

Walter Silva
Pacific Engineering & Analysis, El Cerrito, CA

PEER Report 2012/01
Pacific Earthquake Engineering Research Center
Headquarters at the University of California, Berkeley
July 2012

ABSTRACT

Ground motion prediction equations (GMPEs) for elastic response spectra, including the Next Generation Attenuation (NGA) models, are typically developed at a 5% viscous damping ratio. In reality, however, structural and non-structural systems can have damping ratios other than 5%, depending on various factors such as structural types, construction materials, level of ground motion excitations, among others. This report provides the findings of a comprehensive study to develop a new model for a Damping Scaling Factor (*DSF*) that can be used to adjust the 5% damped spectral ordinates predicted by a GMPE to spectral ordinates with damping ratios between 0.5 to 30%. Using the updated, 2011 version of the NGA database of ground motions recorded in worldwide shallow crustal earthquakes in active tectonic regions (i.e., the NGA-West2 database), dependencies of the *DSF* on variables including damping ratio, spectral period, moment magnitude, source-to-site distance, duration, and local site conditions are examined. The strong influence of duration is captured by inclusion of both magnitude and distance in the *DSF* model. Site conditions are found to have less significant influence on *DSF* and are not included in the model. The proposed model for *DSF* provides functional forms for the median value and the logarithmic standard deviation of *DSF*. This model is heteroscedastic, where the variance is a function of the damping ratio. Damping Scaling Factor models are developed for the "average" horizontal ground motion components, i.e., RotD50 and GMRotI50, as well as the vertical component of ground motion.

ACKNOWLEDGMENTS

This study is part of the Second Phase of the Next Generation Attenuation relations for shallow crustal earthquakes in active tectonic regions (NGA-West2). The NGA-West2 research program is coordinated by the Pacific Earthquake Engineering Research Center (PEER) and supported by the California Earthquake Authority (CEA), California Department of Transportation (Caltrans), and the Pacific Gas & Electric Company. Any opinions, findings, and conclusions or recommendations expressed in this material are those of the authors and do not necessarily reflect those of the sponsoring organizations.

We would like to thank all of the NGA model developers and supporting researchers for their assistance and lively discussions throughout the project. Such technical interactions resulted in more robust models. Numerous individuals and organizations contributed to the development of the NGA-West2 ground motion database; foremost, we thank Dr. Tim Ancheta for his time, efforts and cooperation. Dr. Bob Darragh and Dr. Walt Silva were key in the development of the database.

We would also like to thank Dr. Badie Rowshandel and Tom Shantz for their continued encouragement.

CONTENTS

LIST OF FIGURES

LIST OF TABLES

1 Introduction

1.1 BACKGROUND AND SCOPE OF THE PROJECT

Ground motion prediction equations (GMPEs) are models that predict intensity measures (IMs) of ground shaking in an earthquake event. They are of great importance in seismic hazard calculations and the design and analysis of engineered facilities. Traditionally, these models are developed for elastic response spectra at a 5% viscous damping ratio. The next generation attenuation (NGA) GMPEs for shallow crustal earthquakes in active tectonic regions (NGA-West1 models [Power et al. 2008] and their upcoming updated versions, NGA-West2 models [Bozorgnia el al. 2012]) are no exception.

However, in reality, structural and non-structural systems can have damping ratios other than 5%. The damping ratio represents the level of energy dissipation in structural, non-structural, and geotechnical systems. Within the structural dynamics framework, two types of damping are usually considered: viscous and hysteretic. Our focus in this study is on the former. In an actual structure, many damping mechanisms are present. Largely for mathematical convenience, an idealized concept called equivalent viscous damping [Chopra 2012] is used to approximate the overall viscous damping of the structure. Equivalent viscous damping is sometimes used to account for systems with hysteretic damping as well (see, e.g., Iwan and Gates [1979]). Its value depends on the structure type, construction material, and level of ground shaking, among other characteristics. For example, base-isolated structures and structures with added energy dissipation devices can have damping ratios higher than 5%, while some non-structural components can have damping ratios lower than 5%. As another example, the recent guidelines for performance-based seismic design of tall buildings [PEER 2010] specify a damping ratio of 2.5% for tall buildings at the serviceability hazard level. Generally, a lower damping ratio is expected if the structure remains elastic; on the other hand, if the ground shaking is severe enough to cause yielding or damage to the structural and non-structural components, the effective (equivalent) damping ratio could increase significantly. The damping ratios for different types of structures and ground motion levels are a subject of debate, but recommended values are available in the literature and building codes (e.g., Newmark and Hall [1982]; ATC [2010]). ATC [2010] provides a good review of available studies in estimating equivalent damping ratios for various structural systems and ground motion levels. As another example, Regulatory Guide 1.61 [2007] provides guidance on damping values to be used in the elastic design of nuclear power plant structures, systems, and components.

In any engineering application where the system has an equivalent viscous damping ratio other than 5%, it can be beneficial to adjust the predicted 5% damped ground motion intensity to reflect the difference. For example, the classic work of Newmark and Hall [1982], or variations

of it, has been extensively used worldwide to scale design spectra for different damping ratios. It is noted that the pioneering work of Newmark and Hall was based on only 28 records from 9 earthquakes prior to 1973. A review of damping scaling rules is provided by Bozorgnia and Campbell [2004] and Naeim and Kircher [2001].

Following the publication of the NGA-West1 GMPEs in 2008 [Power et al. 2008], the Pacific Earthquake Engineering Research Center (PEER) initiated a follow-up research program, NGA-West2, to expand the original NGA-West1 database and update the ground motion relations. One of the tasks in NGA-West2 is to develop a model to adjust the GMPEs to predict response spectra for damping ratios other than 5%. This report addresses the damping scaling task. In the new NGA-West2 database, ground motions recorded in several events since 2003 have been added; thus, the new database is larger than that in NGA-West1 by a factor of 2.2. This extensive NGA-West2 database is used to develop the damping scaling model in the present study.

The new damping model is developed by examining the NGA-West2 database, and building the model step-by-step by testing the key explanatory variables influencing the damping scaling. It should be noted that the new damping scaling model is not dependent on the NGA GMPEs, or any other specific GMPE, as the damping model is developed directly from the spectral ordinates of the recorded data. Therefore, the damping scaling model is general enough to be applicable to a wide range of GMPEs for elastic response spectra. Our damping scaling model is applicable to a range of damping ratios from 0.5 to 30%. Also, two damping models are developed for: (1) the "average" of the horizontal components, and (2) the vertical ground motion.

1.2 DIFFERENT APPROACHES TO MODELING OF DAMPING SCALING

In the past two decades, a rather large number of studies have been conducted on this topic (see Appendix A). Although the new damping scaling model is developed starting with few assumptions, we begin our modeling process by examining the overall behavior and the general trends of spectral ordinates with various factors (i.e., damping ratio, spectral period, ground motion duration, earthquake magnitude, source-to-site distance, and site characteristics) that were explored by previous researchers.

As also pointed out by Stafford et al. [2008], there are two possible approaches to obtain response spectral models for damping ratios other than 5%:

1. Develop prediction equations that directly estimate the spectral ordinate at various levels of damping. Thus, different GMPE coefficients need to be provided for each damping ratio. This is the approach taken by Akkar and Bommer [2007] and Faccioli et al. [2004]. A review of similar methods (e.g., Berge-Thierry et al. [2003], Bommer et al. [1998], Boore et al. [1993], and Trifunac and Lee [1989]) is provided in Bommer and Mendis [2005].
2. Develop models of multiplicative factors to scale existing GMPEs for 5% damped spectral ordinates into ordinates for other damping ratios. The majority of the existing literature and building codes follow this approach.

In the literature, various terminologies and symbols are used for the scaling factor, for example:

- DCF, "Damping Correction Factor," is used by Cameron and Green [2007] as well as in the Eurocode 8 [2004];
- $DR_{x\%}$ stands for "Damping Ratio" with x denoting a ratio other than 5% and is used by Atkinson and Pierre [2004];
- B is used by Stafford et al. [2008], Lin et al. [2005], Lin and Chang [2003; 2004], NEHRP [2003], and several other researchers;
- Other terminologies seen in the literature include: "damping reduction factor," "damping adjustment factor," and "response spectrum amplification factor."

In this study, we adopt the second approach as it allows the use of existing GMPEs and allows more efficient modeling, and use the term *Damping Scaling Factor*, or DSF. The approach is to predict:

$$DSF = \frac{Spectral\ ordinate\ for\ a\ \beta\%\ damping\ ratio}{Spectral\ ordinate\ for\ a\ 5\%\ damping\ ratio} \tag{1.1}$$

where β represents the damping ratio of interest.

We divide different approaches to modeling DSF into three categories:

1. Random vibration theory is the most theoretically consistent method of modeling the DSF [McGuire et al. 2001]. The procedure recommended by McGuire et al. [2001] uses different formulas for different ranges of spectral period. For periods between 0.2 to 1 sec, the DSF ratio is based on the procedure developed by Rosenblueth [1980], which is dependent on the damping ratio, spectral period, and duration of motion. For periods less than 0.2 sec, the DSF ratio is based on the procedure developed by Vanmarcke [1976], which depends additionally on peak ground acceleration (PGA). A shortcoming of this method is that it is only applicable to periods less than 1 sec. By simply assuming a white-noise process as the earthquake ground motion and using random vibration theory, one can approximate the DSF as $\sqrt{5/\beta}$ (where β is given in percentage, e.g., $\beta = 5$ for 5% damping). But due to the wide-band assumption of white-noise, this approximation is not applicable to large β values. Even at low β, this is a very rough approximation since, unlike the white-noise process, real earthquake ground motions have non-stationary characteristics.
2. Other analytical studies can be used to examine the dependence of the *DSF* on various parameters. For example, Cameron and Green [2007] examined the analytical response of a single-degree-of-freedom elastic oscillator to finite-duration, sinusoidal excitations in order to show the dependence of the *DSF* on the frequency content and the duration of

motion. They used point-source simulation models to show that frequency and duration depend on earthquake magnitude, source-to-site distance, and tectonic setting. These analytical trends identified the most influential factors, then they used recorded and simulated ground motions to calculate the DSF empirically.

3. The majority of existing models, starting with the pioneering work of Newmark and Hall [1982], are based on empirical methods. Reviews of existing models and building code guidelines are presented in Stafford et al. [2008], Cameron and Green [2007], Bommer and Mendis [2005], Lin et al. [2005], and Bozorgnia and Campbell [2004]. Naeim and Kircher [2001] provide a history of the guidelines for DSFs in U.S.-based codes.

In this study, we use the newly developed NGA-West2 database of recorded ground motions and empirically develop a predictive equation for the *DSF*. The goal is to arrive at a model of the form:

$$\ln(DSF) = \mu(\beta, T, earthquake, site; \mathbf{b}) + \epsilon \tag{1.2}$$

where μ represents the mean of $\ln(DSF)$ and is a function of the damping ratio β, the spectral period T, and the earthquake and site characteristics such as magnitude, distance, and soil conditions; $\mathbf{b}$ is the vector of regression coefficients; and ϵ represents the error that has zero mean and is assumed to be normally distributed.

To identify possible predictor variables, patterns are extracted and trends are examined between DSF and various variables in the database. We begin with the variables already identified in the literature to have influence on the DSF. β is a common predictor variable in all existing empirical models, and in fact, it is the only predictor variable in Priestley [2003], Tolis and Faccioli [1999], and Ashour [1987]. Another important predictor variable considered in the majority of existing models is vibration period T (Lin and Chang [2003]; Idriss [1993]; Wu and Hanson [1989]; and Newmark and Hall [1982]). Abrahamson and Silva [1996] additionally included earthquake magnitude as one of the predictor variables. Lin and Chang [2004] considered the influence of site effects on the *DSF*. More recent studies have considered the effects of duration, magnitude, and distance on the *DSF*. The majority of these studies (Cameron and Green [2007]; Bommer and Mendis [2005]; Atkinson and Pierre [2004]; Naeim and Kircher [2001]), however, limited their results to tabulating or plotting the *DSF* for various magnitude-distance bins, different soil conditions, or different tectonic settings, and they did not provide a single unified predictive equation for the *DSF*. Stafford et al. [2008] directly included a measure of duration in their predictive equation, but T was not a predictor variable in their model. (Spectral ordinates were averaged over periods of 1.5 to 3 sec to form the database.) According to literature reviews, there are significant disagreements among existing proposed models (see, e.g., Bommer and Mendis [2005], Lin et al. [2005], and Naeim and Kircher [2001]). But one should have in mind that different models have used different databases and considered different ranges of β and T. Despite the discrepancies, the majority of the models qualitatively agree on the overall behavior and the general trends of the *DSF* with the potential predictor variables.

1.3 ORGANIZATION OF THE REPORT

Chapter 2 describes the database of strong ground motion records that is used in this study for empirical modeling. This is followed by a summary of the observed general trends between the *DSF* and the potential predictor variables in Chapter 3. The procedure to develop a model of the form in Equation (1.2) is described next in Chapter 4. Predictive models for the median *DSF* and its logarithmic standard deviation for the horizontal component of ground motion are proposed. The proposed model for median *DSF* is then validated by studying the residual diagnostic plots at the end of Chapter 4, and it is compared to data and several existing models in Chapter 5. Finally, in Chapter 6, the model is extended to the vertical component of ground motion, and the differences between the horizontal and vertical components are highlighted. Appendices A-E provide additional information on literature review, details of the regression process, regression coefficients for alternative models, and residual diagnostic plots.

2 Ground Motion Database

A new database of over 8,000 three-component recordings has been developed for the NGA-West2 project [Ancheta et al. 2012]. The magnitude-distance distribution of the NGA-West2 database is shown in Figure 2.1. In this database, the elastic response spectra for the horizontal components (i.e., RotD50 and GMRotI50) and the vertical component were calculated for eleven different damping ratios: 0.5, 1, 2, 3, 5, 7, 10, 15, 20, 25, and 30%. RotD50 [Boore 2010] and GMRotI50 [Boore et al. 2006] are measures of horizontal ground motion that are independent from the *in-situ* orientations of the sensors. These measures are calculated from response spectra of two horizontal components of ground motion rotated in small increments over $180°$ and $90°$ range (respectively, corresponding to RotD50 and GMRotI50). GMRotI50 is based on the geometric mean of the two components, and a single rotation angle is used for all oscillator periods (period-independent). RotD50 is obtained without computing geometric means and uses a period-dependent rotation angle. The term "50" in both expressions stands for the 50^{th}-percentile and indicates a median measure of the horizontal ground motion.

A subset of the above mentioned database with the closest distance to rupture $R_{rup} < 50$ km is selected in this study for empirical modeling. Focusing on this subset ensures a proper damping scaling for near-source data. This subset contains 2250 records for the horizontal components and 2229 records for the vertical component. The moment magnitude **M** ranges from 4.2 to 7.9. The magnitude-distance distribution of the selected records is shown in Figure 2.2. The validity of the developed empirical damping model is later verified for distances beyond 50 km by examining the residuals of the remaining records in the NGA-West2 database.

The NGA-West2 database also contains various measures of duration to examine the expected dependence of the DSF on the duration of the motion. In this study, the duration for RotD50 and GMRotI50 components is calculated as the arithmetic average of D_{5-75} for the two horizontal components. D_{5-75} represents the significant duration from 5-75% of Arias intensity. This measure of duration for the selected records in the database ranges from between 0.25 to 59.32 sec for the horizontal components with a mean of about 7.5 sec and 0.48 to 89.29 sec with a mean of about 9.1 sec for the vertical component. The distributions of **M**, R_{rup}, and D_{5-75}, along with the distribution of the time-averaged shear wave velocity of the top 30 m of the soil, V_{S30}, (ranging between 116 to 2016 m/sec) for the records in the selected database are shown as normalized frequency diagrams in Figures 2.3 and 2.4.

This study uses the pseudo-spectral acceleration (*PSA*) to calculate the *DSF*,

$$DSF = \frac{PSA_{\beta\%}}{PSA_{5\%}} \tag{2.1}$$

Some previous studies (e.g., Lin and Chang [2003]) argue that the absolute spectral acceleration (SA) should be used instead of PSA to calculate the DSF. They reason that the DSF calculated for the pseudo-spectral acceleration is in fact derived for the spectral displacement (SD), $DSF = (SD_{\beta\%})/(SD_{5\%}) = (PSA_{\beta\%})/(PSA_{5\%})$, and therefore the use of it to reduce design forces is inappropriate. These studies show significant differences between $(PSA_{\beta\%})/(PSA_{5\%})$ and $(SA_{\beta\%})/(SA_{5\%})$ especially for $\beta > 10\%$ and $T > 0.15$ sec. Bearing in mind that (a) a purpose of this study is to develop a damping scaling model to be applied to PSA-based GMPEs, (b) the use of $(PSA_{\beta\%})/(PSA_{5\%})$ versus $(SA_{\beta\%})/(SA_{5\%})$ depends on the structural analysis method, and (c) the relatively recent engineering practice is being driven towards displacement-based design, we follow Equation (2.1). Therefore, PSA has been calculated for each record in the database for all 11 damping ratios and for the 21 periods considered in the NGA-West1 project : T = 0.01, 0.02, 0.03, 0.05, 0.075, 0.1, 0.15, 0.2, 0.25, 0.3, 0.4, 0.5, 0.75, 1, 1.5, 2, 3, 4, 5, 7.5, and 10 sec). Validity of the calculated PSA at long periods is record dependent and based on the filtering process for each record. If the filter corner period is not adequate for the period of interest, the record is eliminated for the long-period calculations.

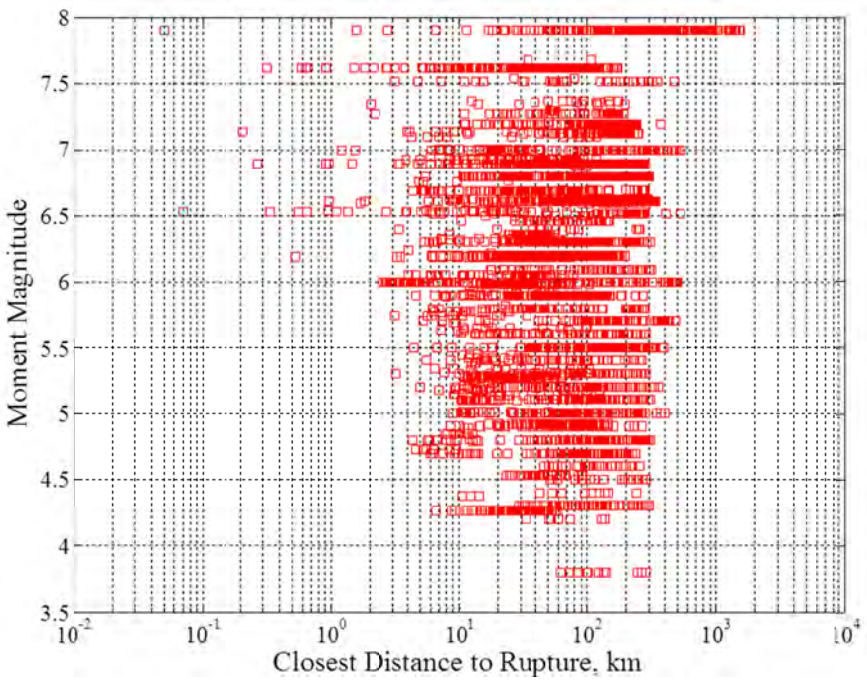

Figure 2.1 Magnitude-distance distribution of the NGA-West2 database (horizontal component).

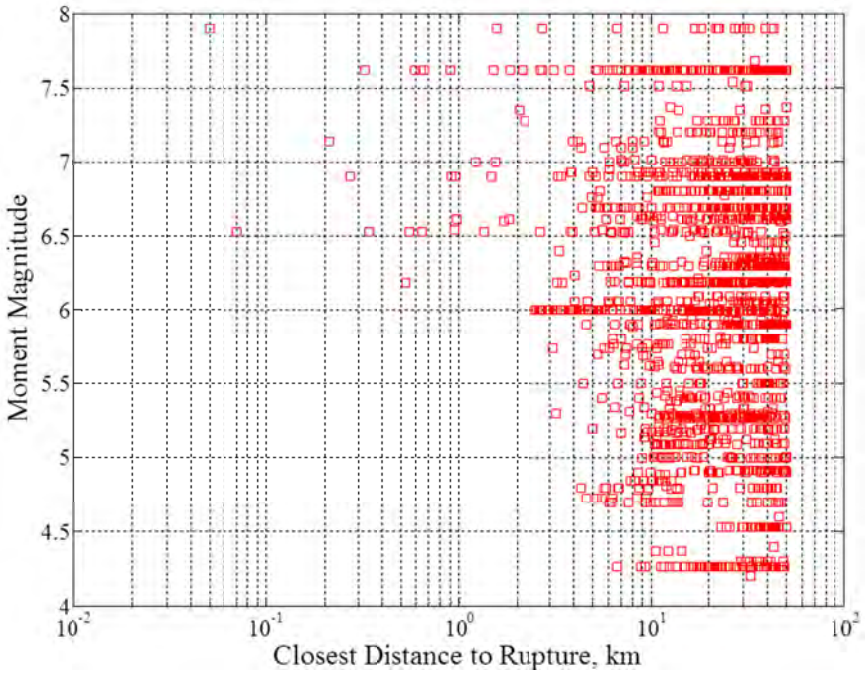

Figure 2.2 **Magnitude-distance distribution of the selected database (horizontal component).**

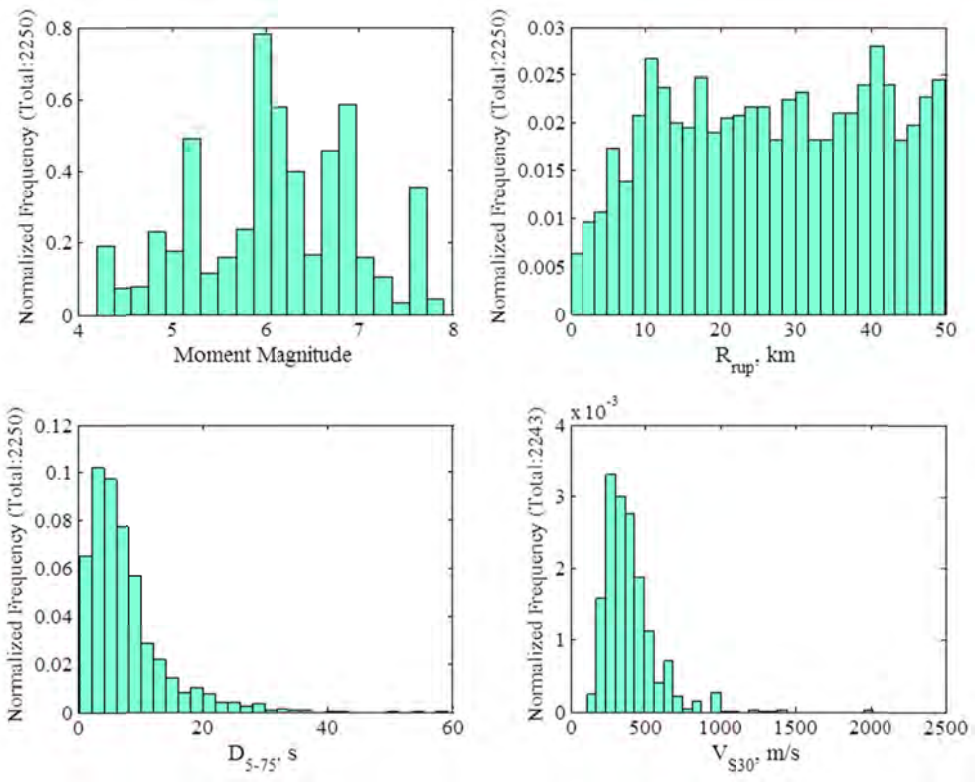

Figure 2.3 **Distributions of parameters in the selected database (horizontal component).**

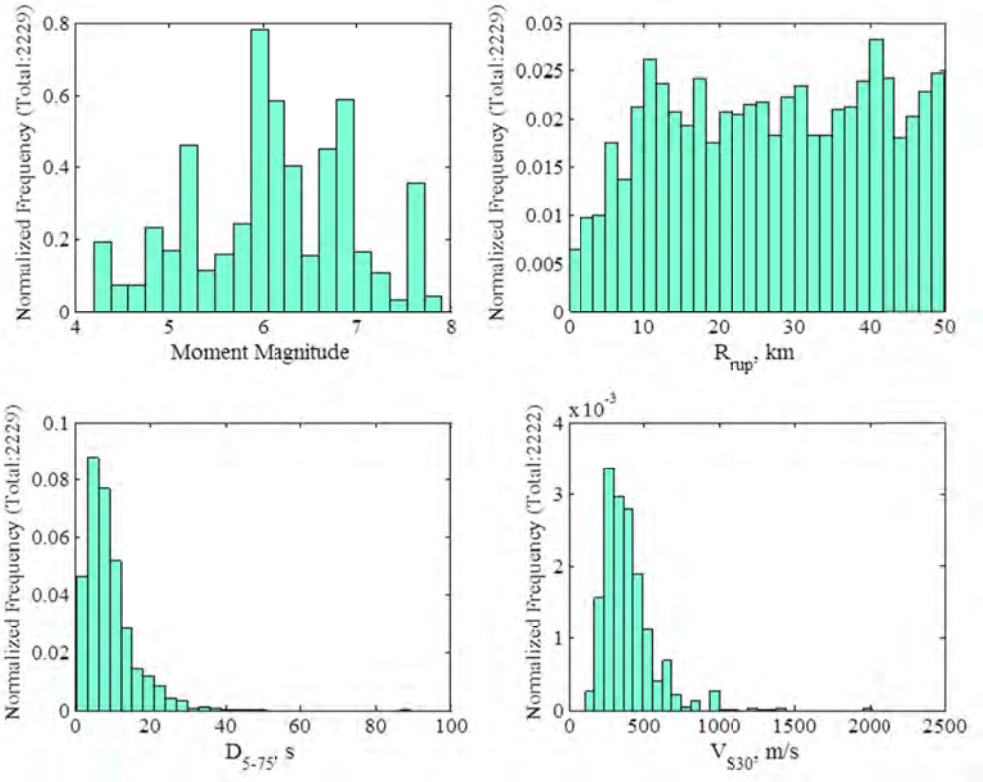

Figure 2.4 Distributions of parameters in the selected database (vertical component).

3 General Observed Trends

This chapter discusses the variables that might influence the *DSF*, as well as the general trends observed in our database and reported in the literature. The focus in this chapter is on the horizontal component. All figures in this chapter correspond to the RotD50 component (similar patterns are observed for the GMRotI50 component); the vertical component will be discussed in Chapter 6. Variables that have been seen to influence the *DSF* in previous studies are as follows: damping ratio, spectral period, duration, magnitude, distance, soil conditions, and tectonic setting. Our statistical data analysis revealed useful information about the dependence of the *DSF* on the above-mentioned variables. The findings are summarized in this chapter and are used to identify the potential predictor variables for the regression analysis in Chapter 4.

3.1 INFLUENCE OF DAMPING AND PERIOD ON *DSF*

The most fundamental predictor variables for the *DSF* are the damping ratio β, and the vibration period T. While there is no question that the *DSF* depends on these two variables (based on the definition of the *DSF* and the dependence of *PSA* on *T*), different degrees of dependence have been reported in different studies. For example, mild, weak and very weak dependence on T has been reported by Stafford et al. [2008], Bommer and Mendis [2005], and Naeim and Kircher [2001], respectively. Lin and Chang [2003] stated that the *DSF* for *PSA* varies little with T, but the *DSF* for *SA* shows much more variation with T. Note that each study considered a different range of periods and damping ratios, and a different selection of recorded ground motions. It is expected that the *DSF* to be unity at PGA (and very short spectral periods) and also at very long T because the forces in a very stiff or a very flexible structure are relatively independent of the damping ratio. This phenomenon was also noted in Stafford et al. [2008] and is taken into consideration in the model of Eurocode 8 [2004].

The new NGA-West2 ground motion database was analyzed to explore the effects of β and T on the DSF, revealing systematic patterns as shown in Figures 3.1 and 3.2. Almost no dependence on T is seen between 0.2–2 sec for $\beta \geq 2\%$, but there is a strong dependence as we move away from this period range when the *DSF* approaches unity for very low and very high T. The dependence on T is much higher for $\beta \leq 1\%$. Finally, not only does the *DSF* decrease as damping increases, but the decrements (i.e., rate of reduction in the DSF as β increases) reduce as well (see Figure 3.1).

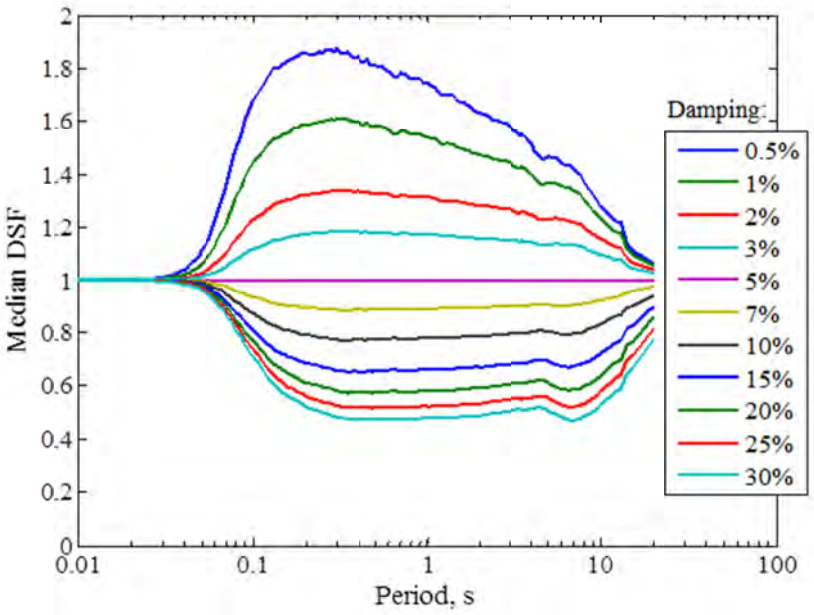

(a)

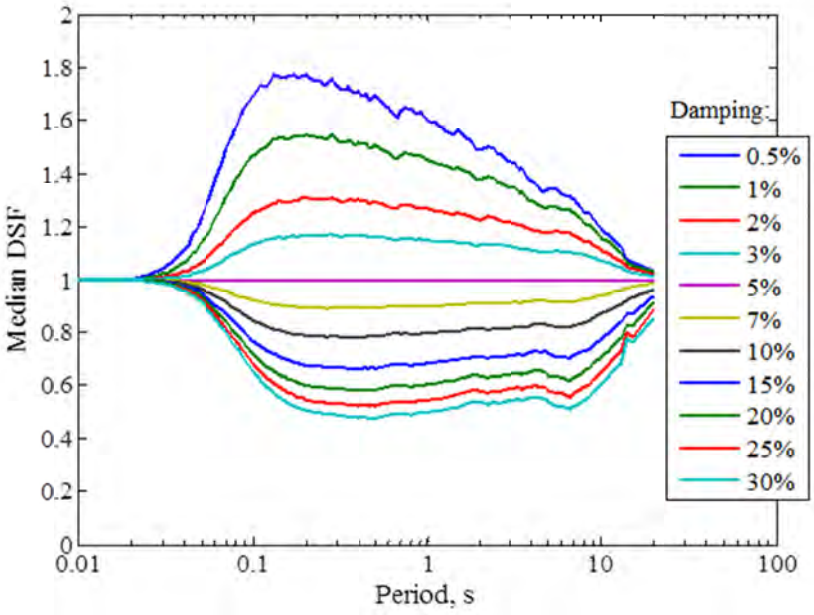

(b)

Figure 3.1 Influence of spectral period and damping ratio on *DSF*: (a) all data used; and (b) only records with R_{rup} < 50 km are used.

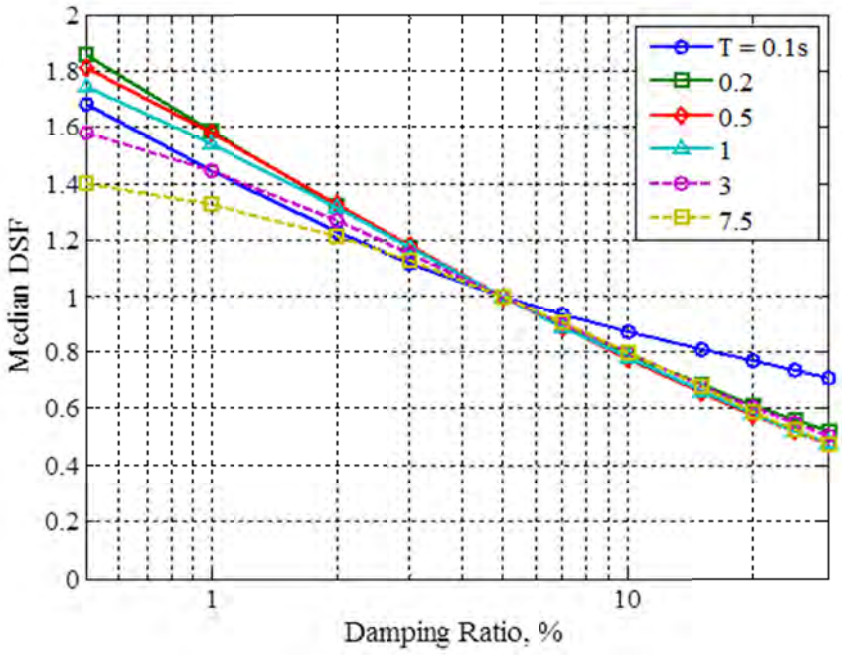

(a)

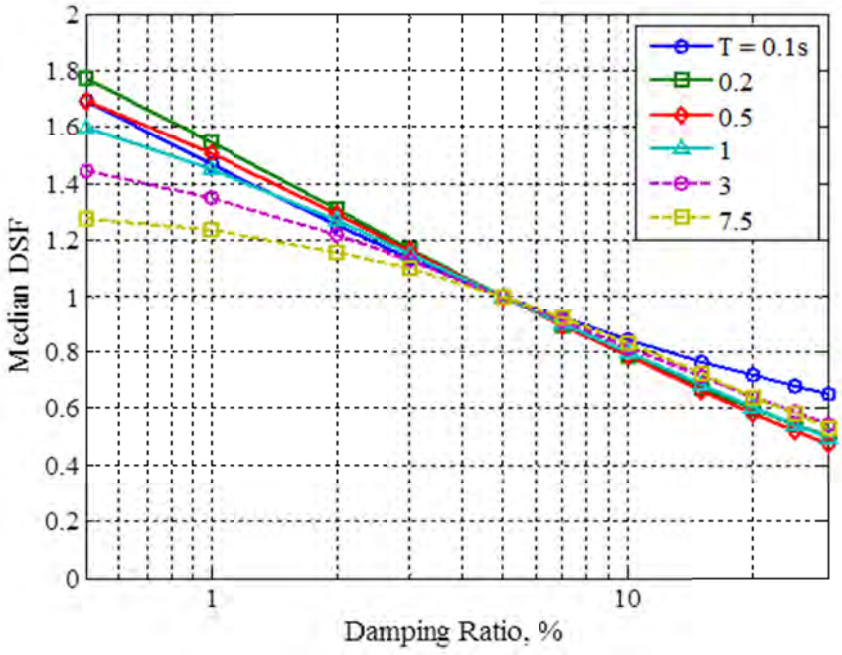

(b)

Figure 3.2 **Influence of spectral period and damping ratio on *DSF*: (a) all data used; and (b) only records with R_{rup} < 50 km are used.**

3.2 INFLUENCE OF DURATION, MAGNITUDE, AND DISTANCE ON *DSF*

Duration of the motion can be an important factor controlling the *DSF*, as the number of energy dissipating cycles can be influential. Stafford et al. [2008]—one of the few models that explicitly included duration as a predictor variable—considered three measures of duration: significant duration from 5–75% of Arias intensity D_{5-75}; significant duration from 5–95% of Arias intensity D_{5-95}; and the number of equivalent load cycles $N_{rr}(2.0)$ (using the rainflow range counting method with relative thresholds and a damage exponent of 2.0). The only other predictor variable in their model was β. Because the data for spectral ordinates were averaged over a period range of 1.5 to 3.0 sec, their model was period independent.

Cameron and Green [2007] also considered the influence of duration. According to their study, the *DSF* depends on the frequency content and duration of the motion. For $\beta \geq 2\%$, they tabulated the *DSF* for specified values of β and T, and for: different magnitude bins (5–6, 6–7, and 7+); tectonic settings; and site classifications (rock or soil). These parameters (i.e., earthquake magnitude, tectonic setting, and site classification) have significant influence on the frequency content of the motion. For $\beta = 1\%$, Cameron and Green considered distance as an additional parameter because it significantly influences the duration of the motion. They tabulated the *DSF* for distance bins of 0–50 km and 50–100 km (or 50–200 km, depending on the magnitude).

Bommer and Mendis [2005] also acknowledged the influence of duration on the *DSF*. Since their study was limited to damping ratios higher than 5%, they observed that the *DSF* decreased as magnitude and distance increased. Since an increase in magnitude and distance is associated with an increase in duration (see, for example, Kempton and Stewart [2006]), they implied that the *DSF* decreases as duration increases. Furthermore, they reported an increase in the dependence of the DSF on duration with the damping ratio.

Analysis of the NGA-West2 database of recorded ground motions reveals trends in the data that are opposite in the direction for $\beta < 5\%$ versus $\beta > 5\%$ (see Figure 3.3). The DSF increases with duration if $\beta < 5\%$, but it decreases with duration if $\beta > 5\%$. Figure 3.3 shows the data at $T = 1$ sec along with a fitted line to simply capture the linear pattern between DSF and $\log(D_{5-75})$ for visual purposes. The pattern with duration is much more significant at longer periods. For example, almost no pattern is seen at $T = 0.2$ sec, but a very strong dependence is observed at $T = 7.5$ sec. Figure 3.3 also shows evidence of heteroscedasticity in the data with respect to β and D_{5-75}. Note that the scatter in the data increases as β deviates from 5%; this dependence will later be incorporated into the variance model. A change in the data scatter as a function of D_{5-75} can be seen, but is not as pronounced. This change could be due to the relatively low number of data points at short durations. (Under consideration are moderate to large magnitude events that, in general, are expected to result in longer durations.) In modeling, the dependence of variance on D_{5-75} will be ignored.

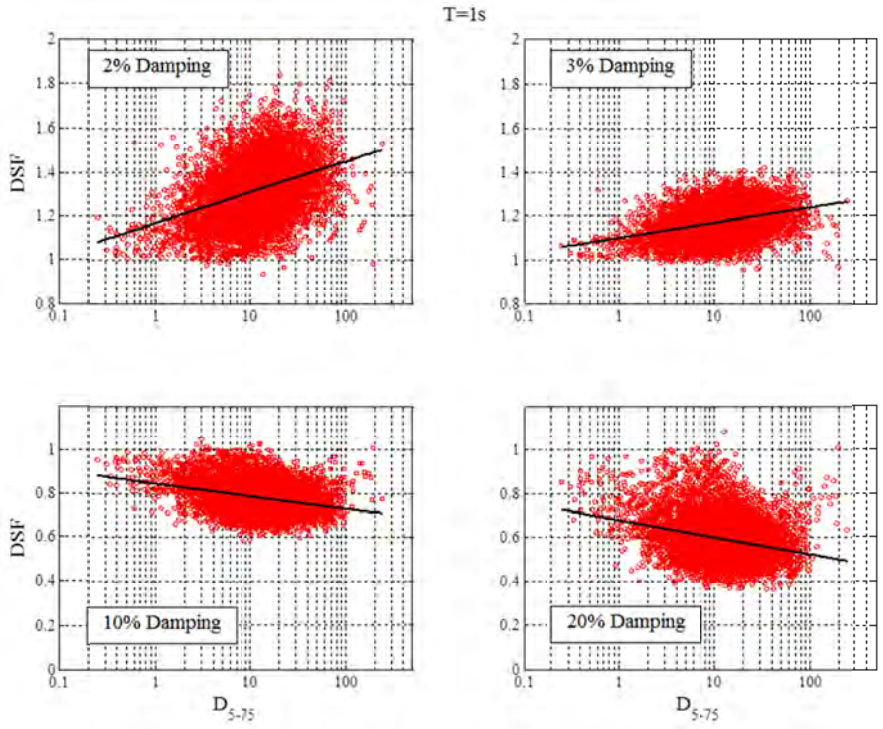

(a)

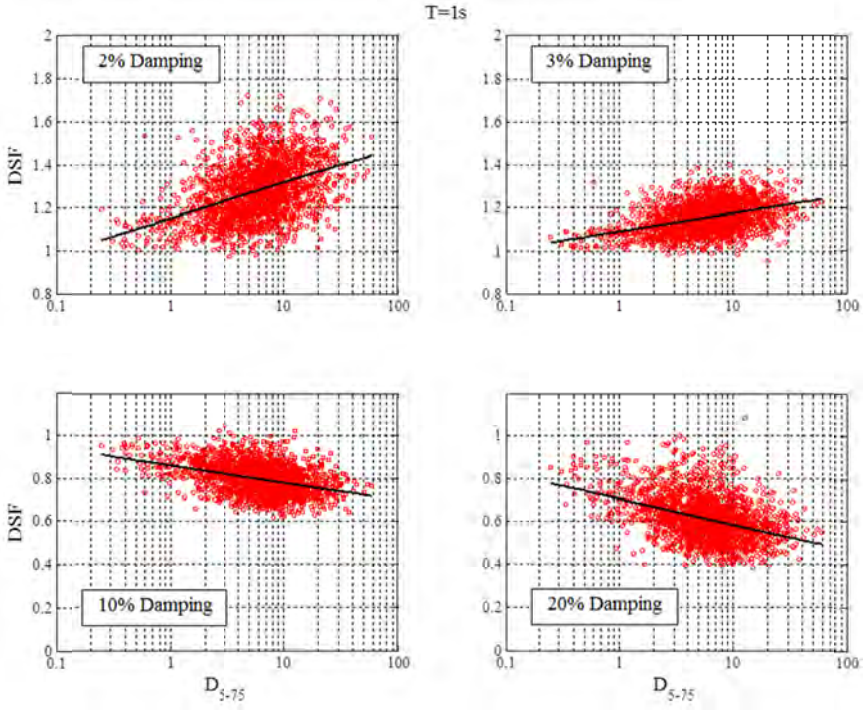

(b)

Figure 3.3 **Influence of duration on *DSF* at T = 1 sec and β = 2, 3, 10, 20%: (a) all data used; and (b) only records with R_{rup} < 50 km are used.**

Explicit inclusion of duration in the model is not ideal in practice because duration is generally not specified as part of a seismic design scenario. Therefore, the possibility of capturing the influence of duration on the DSF by including both magnitude and distance in the model is considered. In general, a strong positive correlation between duration and earthquake magnitude and a moderate positive correlation between duration and distance is expected (see, for example, Kempton and Stewart [2006]). In this study, we find that most of the influence of duration on the DSF can be captured through inclusion of magnitude and distance in the model (more details are provided in Chapter 4). A similar approach was taken by Cameron and Green [2007], where they tabulated the DSF for various magnitude-distance bins.

As shown in Figure 3.4, there is a significant dependence between DSF and the moment magnitude **M**. Figure 3.4 is for $T = 1$ sec along with a fitted line to capture the trend in the data. Bommer and Mendis [2005] is one of the few studies that investigated the effect of magnitude on the DSF. Their study was limited to $\beta > 5\%$, suggesting a decrease in the DSF as **M** increases. This is consistent with the pattern shown in Figure 3.4. Patterns similar to Figure 3.4 are more pronounced at longer T, but at shorter periods (around 0.2 sec) they are not as significant and are opposite in the direction. These observations suggest a linear relation between DSF and **M**.

Figure 3.5 shows similar but far less significant patterns between DSF and R_{rup}. This weak relation is consistent with what has been reported in the literature. For example, Cameron and Green [2007] only distinguished between distances of less than or greater than 50 km (a higher *DSF* for distances greater than 50 km was reported at $\beta = 1\%$). Atkinson and Pierre [2004] also saw a weak dependence between *DSF* and distance and reported an increase in the dependence at lower damping levels. As shown in Figure 3.5, the dependence of DSF on R_{rup} is more pronounced when only looking at data with $R_{rup} < 50$ km. We see an increase in DSF with distance if $\beta < 5\%$ and a decrease if $\beta > 5\%$. Despite the weak influence of R_{rup} on *DSF*, some of the effects of duration on *DSF* can be captured by including R_{rup} as one of the predictor variables in the model in addition to **M**.

The influence of magnitude and distance on the *DSF* is also shown in Figure 3.6, where the median *DSF* is plotted versus T for selected magnitude-distance bins. Here, as **M** increases, *DSF* decreases for $\beta > 5\%$ and $T > 1$ sec, but a general increase in *DSF* is observed for $\beta < 5\%$. Also, a deviation from unity at long periods is observed as distance increases. Furthermore, the DSF increases with distance if $\beta < 5\%$, and decreases if $\beta > 5\%$; this effect is more pronounced in the low magnitude range.

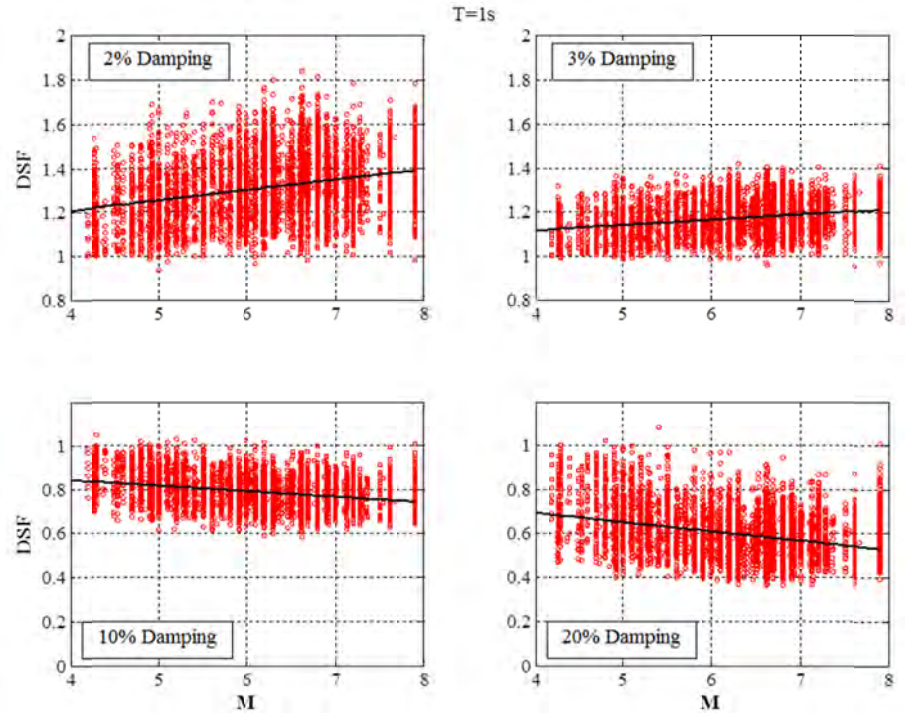

(a)

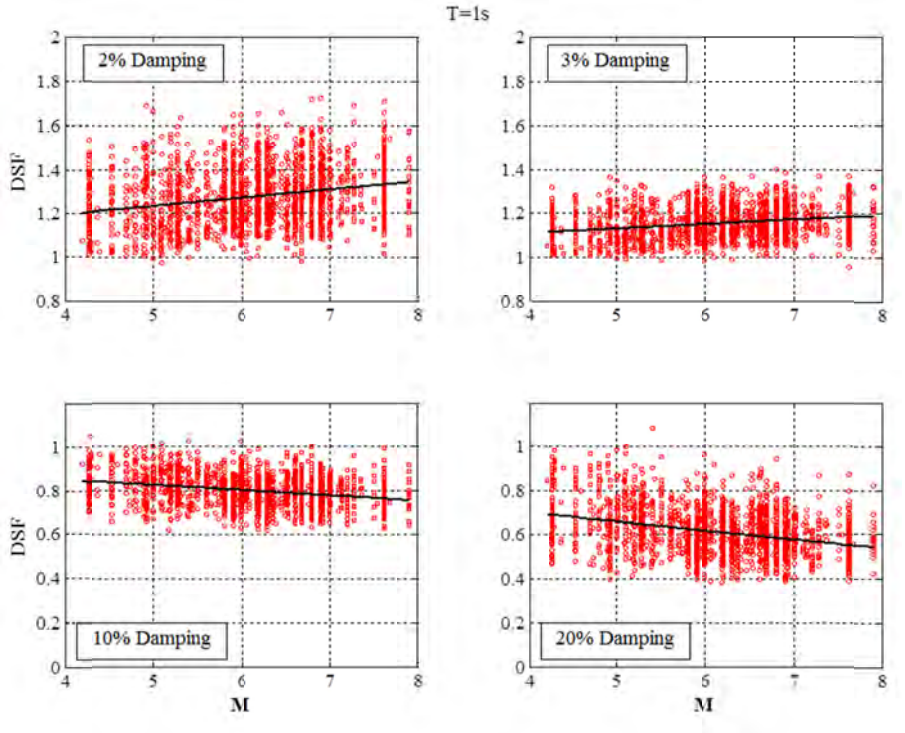

(b)

Figure 3.4 **Influence of magnitude on *DSF* at T = 1 sec and β = 2, 3, 10, 20%: (a) all data used; and (b) only records with R_{rup} < 50 km are used.**

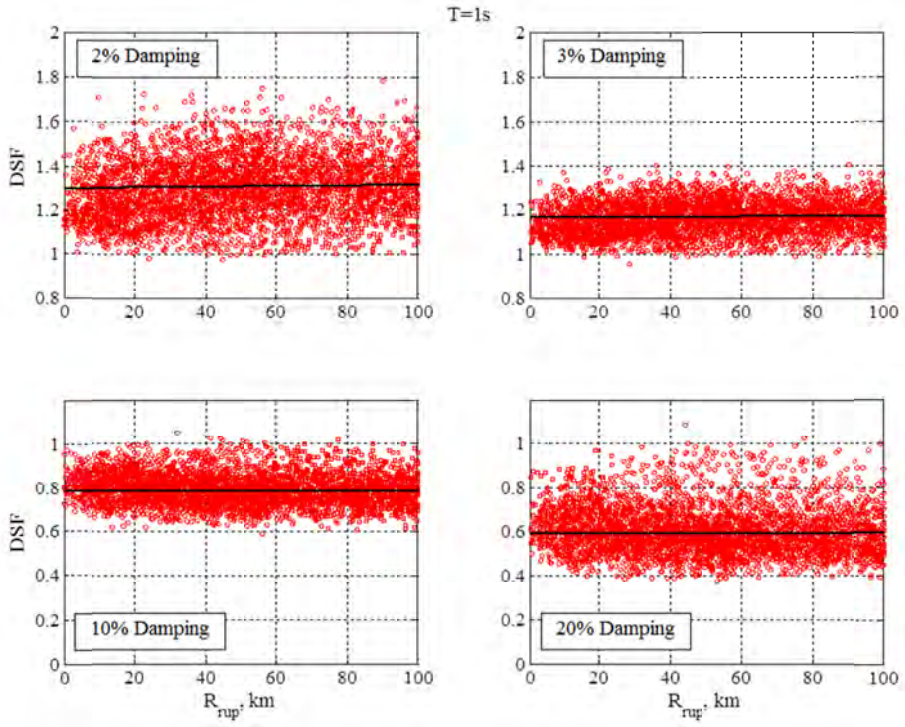

(a)

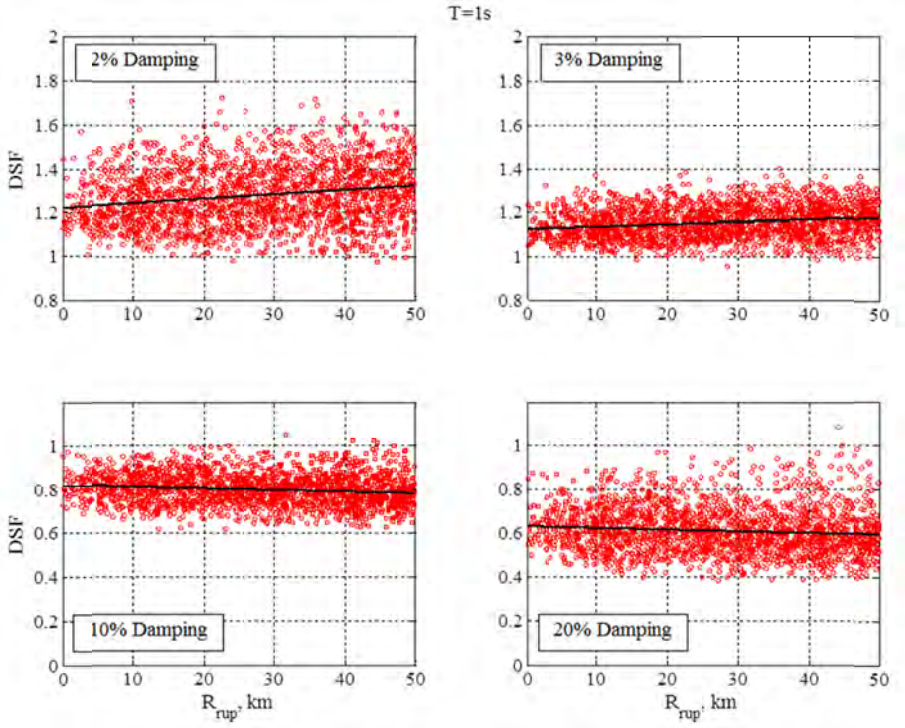

(b)

Figure 3.5 **Influence of distance *DSF* at T = 1 sec and β = 2, 3, 10, 20%: (a) all data used; and (b) only records with R_{rup} < 50 km are used..**

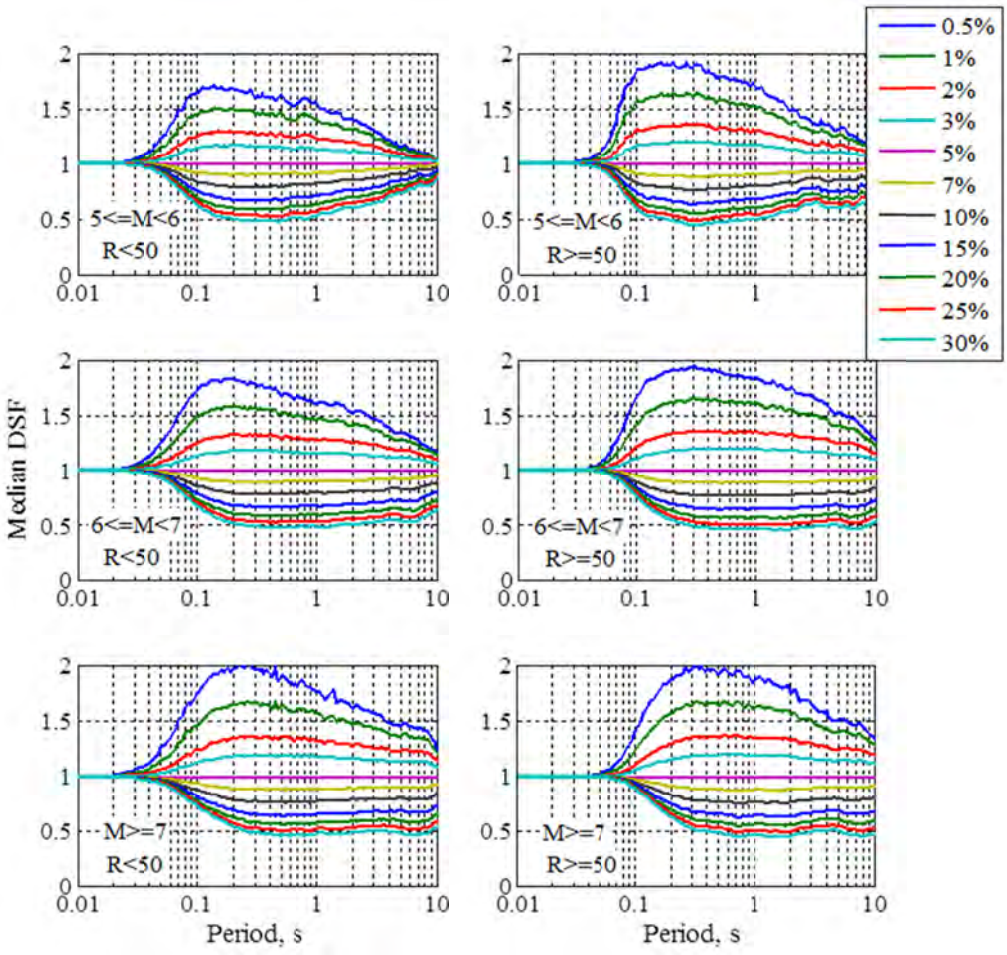

Figure 3.6 **Median *DSF* versus period plotted for different magnitude-distance bins.**

3.3 INFLUENCE OF SITE CONDITIONS AND TECTONIC SETTINGS ON *DSF*

Site conditions and tectonic settings have been considered in some existing literature. Cameron and Green [2007] distinguished between Western United States (WUS) and Central and Eastern United States (CEUS). Atkinson and Pierre [2004] was one of the few studies that focused on the CEUS. Given that the focus here is on shallow crustal events in active tectonic regions (e.g., WUS); the stable continental regions (e.g., CEUS) are outside the scope.

To consider the effect of site conditions, the influence of V_{S30} on DSF was examined, and insignificant dependence was observed (see Figure 3.7 as an example for $T = 1$ sec). The slight pattern seen in this figure is not consistent for all periods. This observation is consistent with the literature. Bommer and Mendis [2005] reported that soft soil influences the *DSF* but to a much lesser degree than magnitude and distance. Lin and Chang [2004] was the only study that directly included the site class in their model. They found that this factor can be neglected when the *DSF* is calculated for PSA. The *DSF* for SA is more sensitive to the site class. Since we are interested in the *DSF* for PSA, we do not consider V_{S30} as a predictor variable.

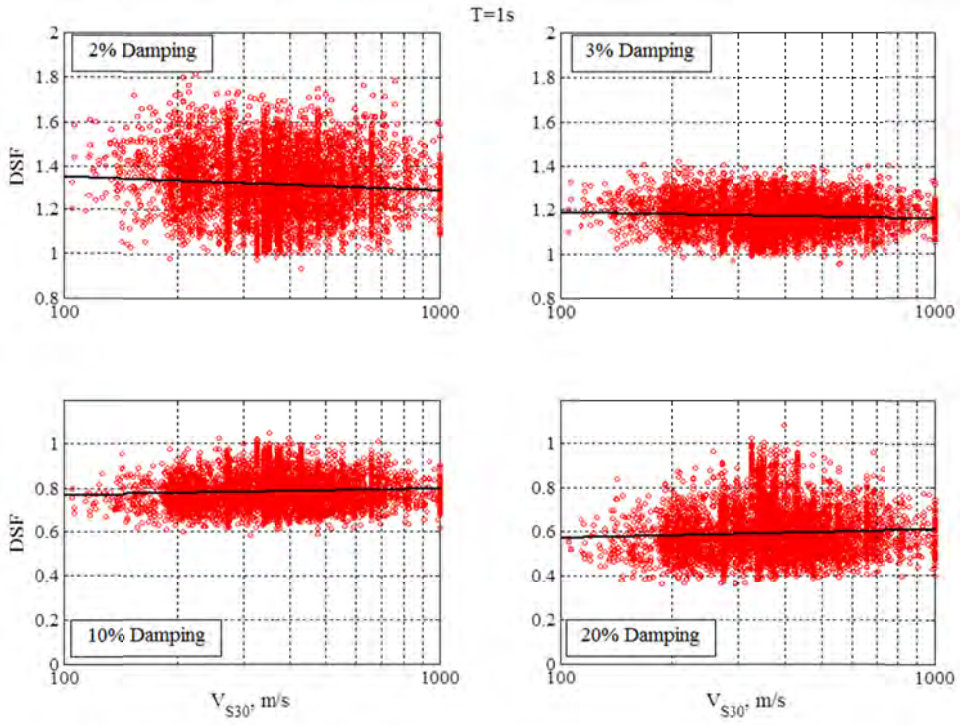

(a)

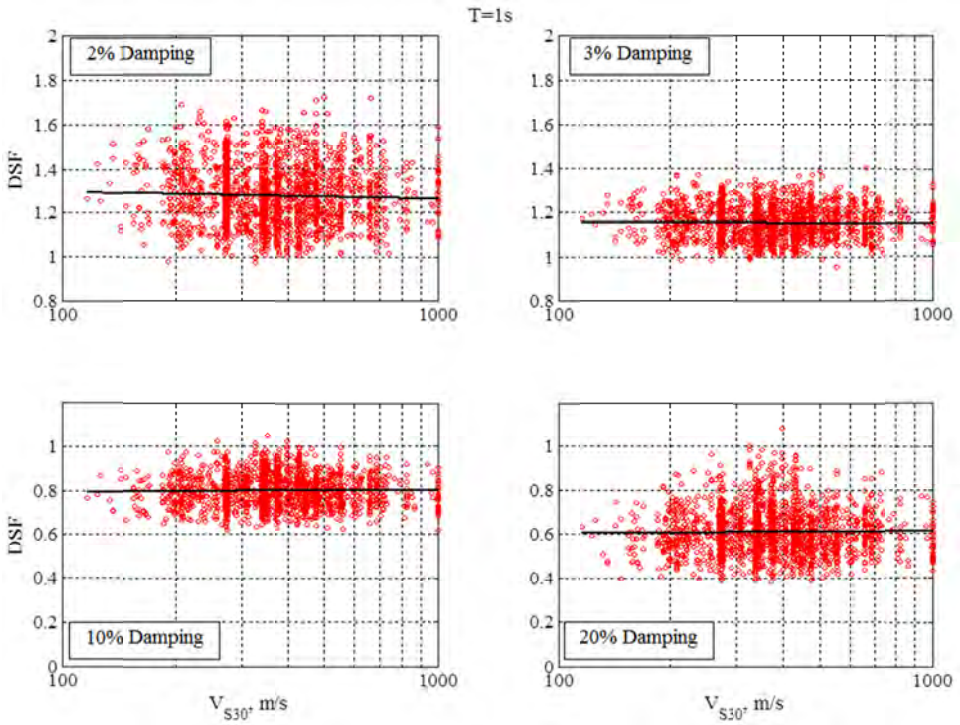

(b)

Figure 3.7 **Influence of V_{S30} on *DSF* at T = 1 sec and β = 2, 3, 10, 20%: (a) all data used; and (b) only records with R_{rup} < 50 km are used.**

4 Model Development

To develop a model of the form given in Equation (1.2), first, through statistical analyses of the recorded data, the probability distribution of the underlying population for the random variable DSF is investigated. Then, using the information in the previous chapter, the predictor variables are chosen and a functional form for the median value is selected. In this process, the functional forms used by previous researchers are examined and the trends observed between the DSF and other variables in the database are taken into consideration. Regression analysis is then performed to estimate the model coefficients and the variance component. Finally, the variance is modeled as a function of β. As in Chapter 3, the focus here is on the horizontal component of ground motion; the vertical component will be described in Chapter 6. Unless otherwise noted, the database of recorded ground motions with $R_{rup} < 50$ km is used.

4.1 DISTRIBUTION OF *DSF*

Traditionally, a lognormal distribution is assumed for the ground motion intensity (i.e., PSA) at specified earthquake and site characteristics (e.g., earthquake magnitude, source-to-site distance, etc.). If PSA is lognormally distributed, then $\ln(PSA)$ follows the normal distribution. Following Equation (2.1), one can write,

$$\ln(DSF) = \ln\left(PSA_{\beta\%}\right) - \ln(PSA_{5\%}) \tag{4.1}$$

where each term on the right hand side is assumed to be normally distributed. It is well-known that the linear combination of independent normally distributed random variables is normal. Therefore, if the PSAs at two different damping ratios were independent variables, then it is logical to assume a lognormal distribution for the *DSF*. But since PSA values at two different damping ratios can be dependent, we investigated the possibility that *DSF* follows a lognormal distribution independently by scrutinizing the available data. The results are outlined below.

At a specified T and β, the data for DSF are found to be well represented by the lognormal distribution (i.e., $\ln(DSF)$ is normally distributed). Figure 4.1 shows the normalized frequency diagrams of $\ln(DSF)$ at $\beta = 2\%$ and $T = 0.2, 1,$ and 7.5 sec. Figure 4.2 shows similar plots for $\beta = 20\%$. The parameters of the normal distribution are estimated by the method of moments, and the resulting probability density function (PDF) is superimposed on the figure. Furthermore, the corresponding empirical CDF is plotted against the CDF of the fitted distribution. By visual inspection of histograms, examining the fit to the empirical CDF, and scrutinizing the normal probability plots (not shown here), we graphically assessed the distribution of data and concluded that the fit of $\ln(DSF)$ to the normal distribution is very good

at shorter periods and acceptable at longer periods. At a specified T and β, the DSF can be reasonably assumed a lognormal random variable for the purposes of this study. It was decided that there was no need for any further hypothesis testing to prove that the sample is drawn from a lognormal distribution. These results are typical for all periods and damping ratios with the exception of two scenarios: (1) at very short T and very low β; and (2) at very short T and very high β. Examples of these two cases are shown in Figure 4.3 at $T = 0.05$ sec, and $\beta = 1\%$ and 20%.

Inconsistent use of DSF and $\ln(DSF)$ on the left hand side of Equation (1.2) in the literature is a source of confusion. DSF following a lognormal distribution supports the use of $\ln(DSF)$ in Equation (1.2). This is because the error term is assumed to be normally distributed; therefore, at specified values of the earthquake and site characteristics, the response variable (i.e., left hand side of equation) is also normally distributed. As a result, the choice of $\ln(DSF)$, which follows a normal distribution, is suitable. Choosing a suitable distribution for the response variable in the regression analysis could be an important factor when studying the symmetry of the residual diagnostic plots. This effect is discussed in more details at the end of Section 4.2.2 for the two scenarios where $\ln(DSF)$ is observed to deviate from a normal distribution. Additionally, the choice of $\ln(DSF)$ as the response variable in the regression analysis implies that the proposed model for $\mu(.)$ is for the median DSF under the assumption that DSF follows a lognormal distribution.

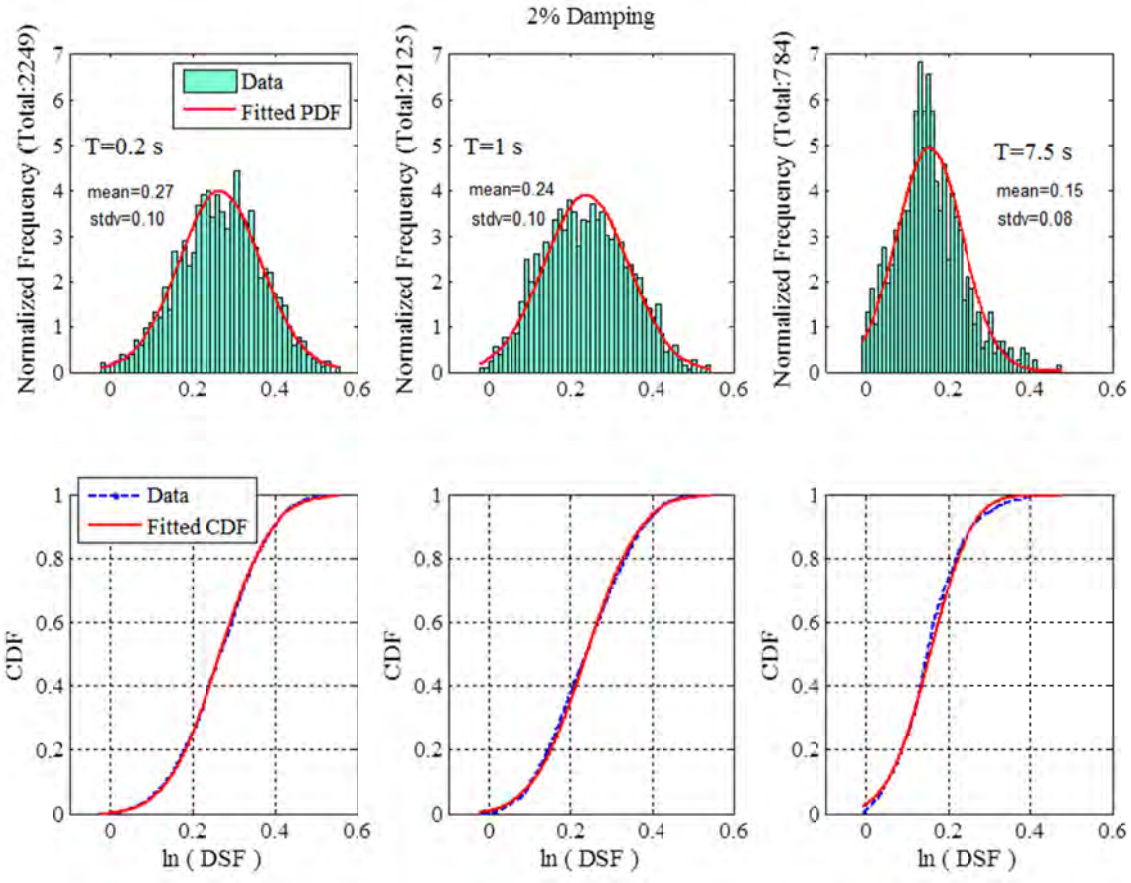

Figure 4.1 Distribution of ln(*DSF*) at specified periods and β = 2%.

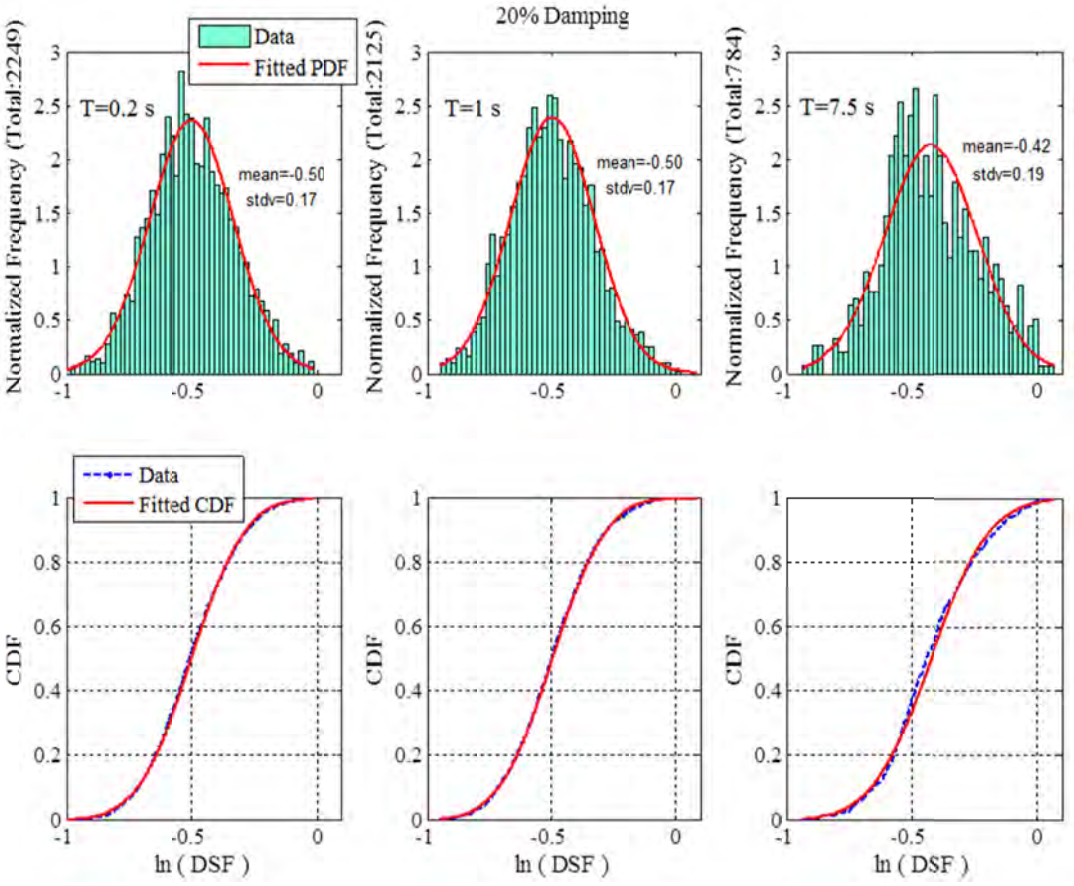

Figure 4.2 Distribution of ln(*DSF*) at specified periods and β = 20%.

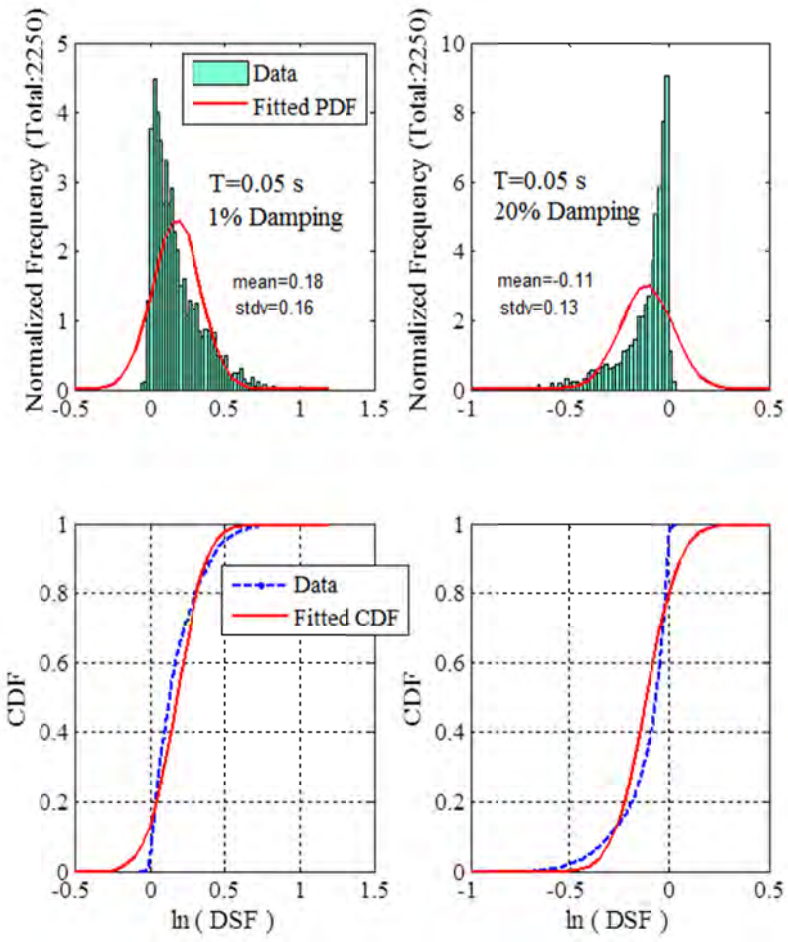

Figure 4.3 Extreme cases where ln(*DSF*) does not follow a normal distribution.

4.2 FUNCTIONAL FORM FOR MEDIAN *DSF*

4.2.1 Relevant Functional Forms Used in Literature

Commonly, two functional forms are used in the literature and building codes to describe DSF or $\ln(DSF)$ in terms of the damping ratio and sometimes the spectral period:

$$b_1 + b_2 \ln(\beta) \tag{4.2}$$

$$\left(\frac{b_1}{b_2 + \beta}\right)^{b_3} \tag{4.3}$$

where b_1, b_2, and b_3 are the period-dependent regression coefficients. The form in Equation (4.2) is used by Newmark and Hall [1982], U.S.-based building codes (see Appendix A for details), and Idriss [1993]. The form in Equation (4.3) is used by Tolis and Faccioli [1999], Priestley [2003], Eurocode 8 [2004], and the Caltrans [2001] guidelines for bridges. Note that assuming a

white-noise process and using random vibration theory as described in Chapter 1 (i.e., $DSF = \sqrt{5/\beta}$), *DSF* can be represented in the form of Equation (4.3), while $\ln(DSF)$ can be written in the form of Equation (4.2).

Some researchers use nonlinear regression analysis and search many mathematical equations to arrive at a functional form. For example, Lin and Chang [2003; 2004] and Hatzigeorgiou [2010] selected the following functions, respectively:

$$DSF = 1 - \frac{b_1 T^{b_2}}{(T+1)^{b_3}} \tag{4.4}$$

where b_1 depends on the damping ratio, and b_2 and b_3 depend on the site class; and

$$DSF = 1 + (\beta - 5)[1 + b_1 \ln(\beta) + b_2(\ln(\beta))^2][b_3 + b_4 \ln(T) + b_5(\ln(T))^2] \tag{4.5}$$

where b_1,…,b_5 are the regression coefficients.

Two functional forms that include magnitude or duration as predictor variables were developed by Abrahamson and Silva [1996] and Stafford et al. [2008]. Abrahamson and Silva included a quadratic magnitude term in their model

$$\ln(DSF) = \begin{cases} b_1 & if \quad T \leq 0.7s \\ b_1 + b_2(\mathbf{M} - 6) + b_3(8.5 - \mathbf{M})^2 & if \quad T > 0.7s \end{cases} \tag{4.6}$$

where the regression coefficients are tabulated for specified β and T. Stafford et al. selected the following function, where the regression coefficients are period-independent and D denotes a measure of duration as previously described in Section 3.2,

$$DSF = 1 - \frac{b_1 + b_2 \ln(\beta) + b_3 \ln(\beta)^2}{1 + \exp\left(-\frac{[\ln(D) + b_4]}{b_5}\right)} \tag{4.7}$$

4.2.2 The Proposed Model

Here, the *DSF* is calculated according to Equation (2.1) for the records in the database. These data are then regressed at each combination of the 21 specified periods and the 11 damping ratios (see Chapter 2) on the predictor variables **M** and R_{rup}. Different functions of each predictor variable are added to the model one at a time and the residual plots versus **M**, R_{rup}, and D_{5-75} are examined (see Appendix B for details). A linear magnitude term is found to be necessary and sufficient to capture the dependence of data on **M** and most of the dependence on D_{5-75}. The inclusion of a quadratic magnitude term does not provide significant improvements in the residual plots. The addition of a logarithmic function of R_{rup} reduces (not as much as the magnitude term) the remaining dependence on D_{5-75}. Trends in the residual plots against D_{5-95} are examined and similar behavior is found as observed for D_{5-75}. Note that, as described in

Chapter 2, only data with $R_{rup} < 50$ km are used in the regression; the behavior for larger distances is verified later, as explained in Section 4.4.

The relations between the constant term, the coefficient of the magnitude term, and the coefficient of the distance term with β are examined next. In the model building process, various potential functional forms are considered, examined, and kept or discarded. The details of the step-by-step model building are elaborated in Appendix B.

A multistep least squares regression process is carried out to arrive at the final model. At each step, the "primary" regression coefficients are estimated (i.e., regressing DSF on $\mathbf{M}$ and R_{rup} at a specified period and damping ratio); and then the coefficient with most dependence on the damping ratio is expressed in terms of β at a specified period. At the next step, the "secondary" regression coefficients (i.e., those describing a primary coefficient in terms of β) are fixed, and the process is repeated to capture the dependence of the remaining primary coefficients on β. Following this process (i.e., fixing the coefficients at each step), eventually leads to an accurate estimation of the standard deviation using the sample standard deviation of residuals, without a need to approximate the cross-correlations between the constant term, the magnitude term and the distance term. Furthermore, because the regression is performed separately on 11 subsets of the data (corresponding to the 11 damping ratios) at each specified period, no assumptions are made on the correlations between the data corresponding to different damping ratios during the regression process (as mentioned previously, there could be some correlation between PSA at two different damping ratios). More detail on the step-by-step regression process is provided in Appendix B.

The final model has the following functional form for a given value of T

$$\begin{aligned}\ln(DSF) = \\ & b_0 + b_1 \ln(\beta) + b_2(\ln(\beta))^2 \\ & +[b_3 + b_4 \ln(\beta) + b_5(\ln(\beta))^2]\mathbf{M} \\ & +[b_6 + b_7 \ln(\beta) + b_8(\ln(\beta))^2] \ln(R_{rup} + 1) \\ & + \epsilon\end{aligned} \tag{4.8}$$

where β is the damping ratio in percentage (e.g., $\beta = 2$ for 2% damping); and b_i, $i = 0, \ldots, 8$, are the regression coefficients, and are listed in Table 4.1 at each specified T for the horizontal component RotD50. The regression coefficients for GMRotI50 components are given in Appendix C, Table C.1. To obtain a simpler version of the model, the distance term may be eliminated at the cost of some loss in the accuracy and some additional pattern between residuals and the duration. (The regression coefficients for the simpler model are also provided in Appendix C, Table C.2.) Note that the dependence on the damping ratio is captured best by a quadratic function of $\ln(\beta)$ as is also seen in the models by Hatzigeorgiou [2010] and Stafford et al. [2008]. A linear function of $\ln(\beta)$, which has been used by many other researchers, works well only at certain periods. In Equation (4.8), ϵ is a zero-mean normally distributed random variable with standard deviation σ. A model for σ is presented in the next section.

Figure 4.4 shows the regression coefficients for the proposed model in Equation (4.8) plotted against period for both RotD50 and GMRotI50 components. Observe the insignificant difference between the results based on these two intensity measures. Smoothing of the coefficients (i.e., the constant term, the coefficient of the magnitude term, and the coefficient of

the distance term) is only done with respect to the damping ratio, because they show an obvious quadratic pattern with $\ln(\beta)$ [see Equation (4.8)], which allows direct inclusion of the damping ratio in the model. Smoothing with respect to the period is not done, as seen in Figure 4.4. Smoothing of the coefficients with respect to T is not considered necessary because the resulting DSF (see Figure 4.5 as example), and therefore the scaled GMPE (see Figure 4.6 as example), are smooth with respect to T. Figure 4.5 shows the predicted DSF values according to Equation (4.8) for the RotD50 component for $\mathbf{M} = 5, 6, 7, 8$ and $R_{rup} = 10$ km. This damping scaling factor is applied to the geometric mean of the five NGA-West1 GMPEs and is plotted versus period in Figure 4.6 for two different soil conditions. (For the case with $V_{S30} = 255$ m/sec, Idriss's 2008 NGA model is removed as this model cannot be used for $V_{S30} < 450$ m/sec.) Figure 4.6 shows the smoothness of the scaled GMPEs versus period. The worst case scenario (in terms of smoothness of the model) occurs at very small distances (about 1 km) and very low damping ratios (about 0.5%), as can be seen in Figures 4.7 and 4.8 for magnitude of 7.5.

As a validation measure for the proposed model, the diagnostic scatter plots of the residuals versus the predictor variables β, $\mathbf{M}$, and R_{rup}, and versus other parameters such as D_{5-75}, V_{S30}, and sediment depth (i.e., $Z_{1.0}$ and $Z_{2.5}$, respectively representing the depth to the 1.0 and 2.5 km/sec shear-wave velocity horizons) are examined. Sample residual plots are given in Appendix D. These plots show that the residuals are symmetrically scattered above and below the zero level with no obvious systematic patterns. This implies lack of bias and a good fit of the proposed model to the data. At $T = 0.1$ sec, the residual plots show an unsymmetrical behavior around zero. This could be due to the non-normality of $\ln(DSF)$ at the two extreme cases described in Section 4.1. Generally, the pattern in the residual plots is more significant when β deviates further away from 5%. Also, the pattern is opposite in the direction for β less than and greater than 5%. When examining the residuals, one should look at the data for individual damping ratios, as shown in the figures of Appendix D. Residual plots for data belonging to all damping ratios are also given in Appendix D to illustrate the cancellation of pattern for β less than and greater than 5%. The residual plots versus duration show that, in general, the duration-dependency of the *DSF* has been captured through other parameters (i.e., magnitude and distance).

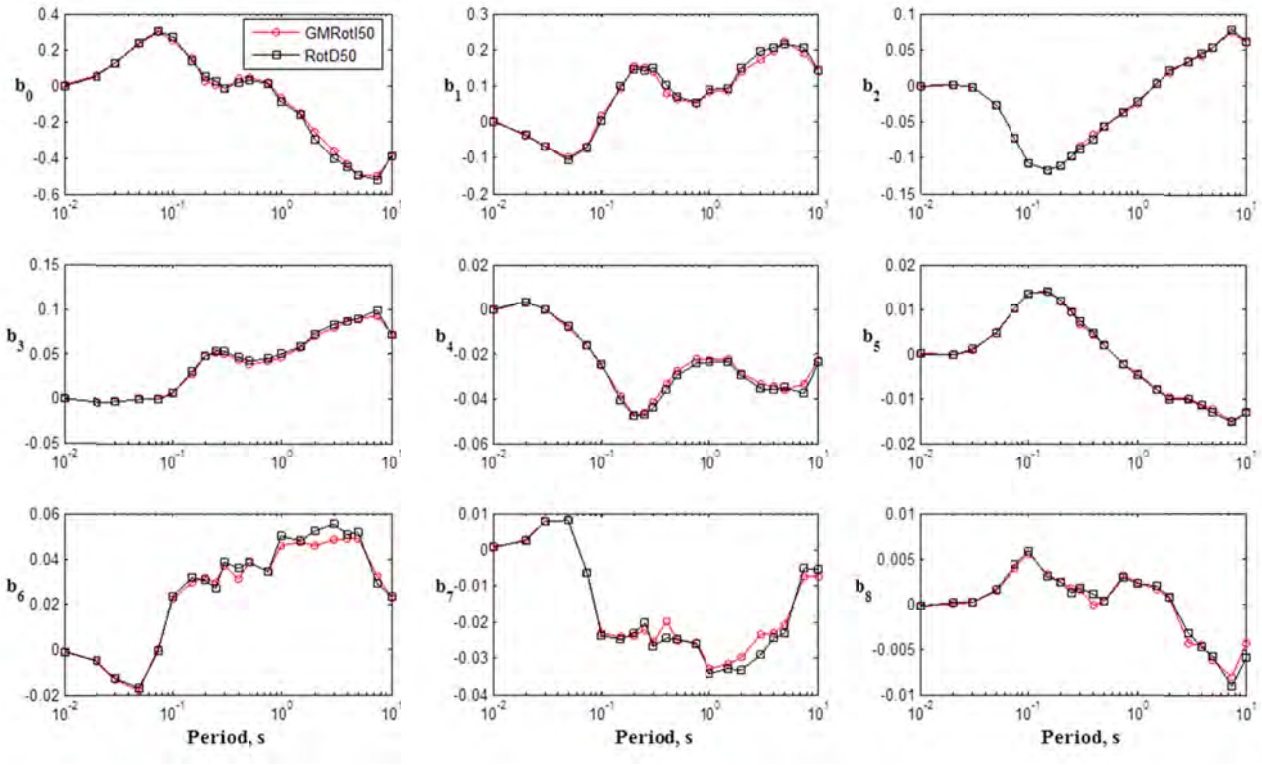

Figure 4.4 Regression coefficients plotted versus period for RotD50 and GMRotI50 components.

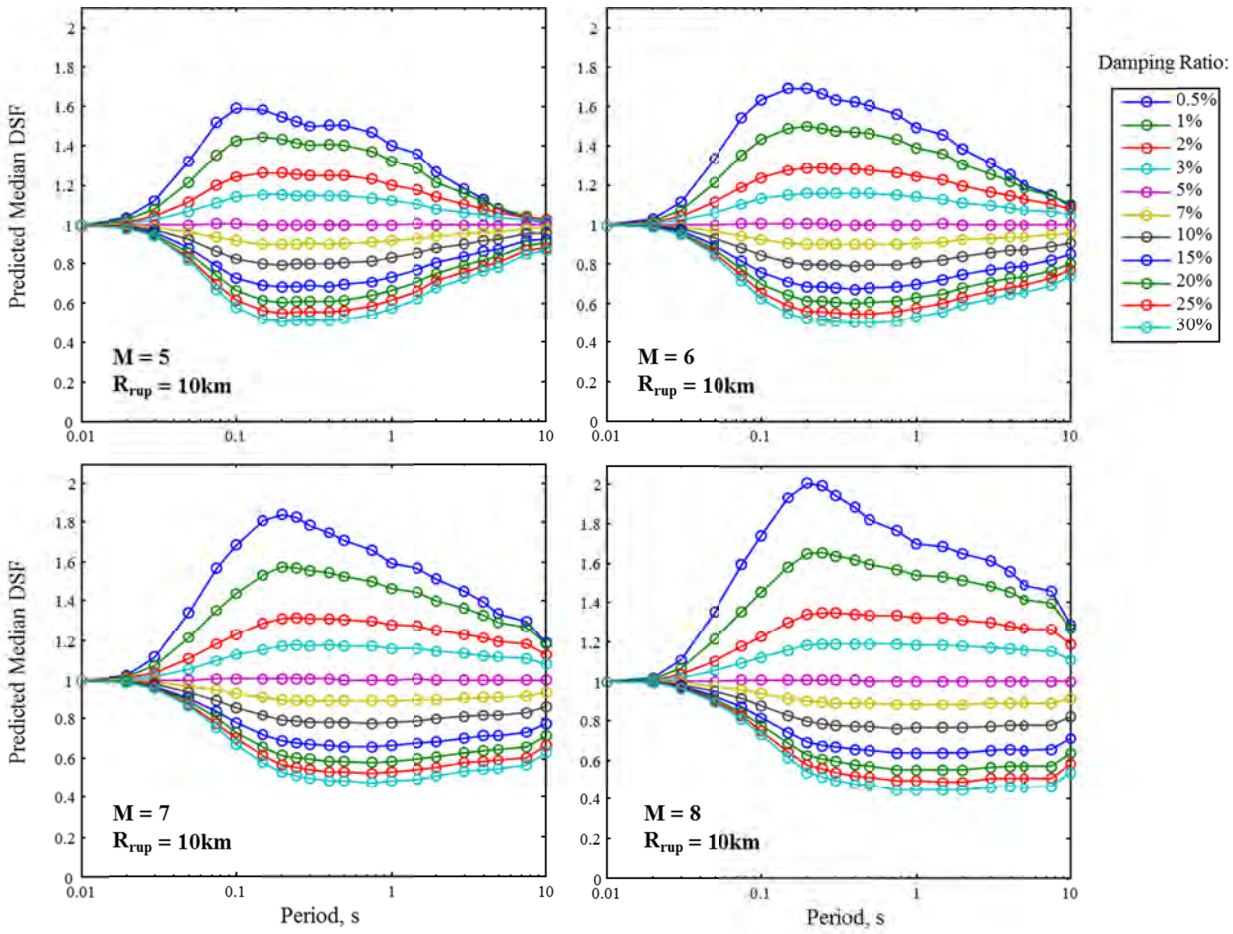

Figure 4.5 Predicted median *DSF* according to Equation (4.8) for RotD50.

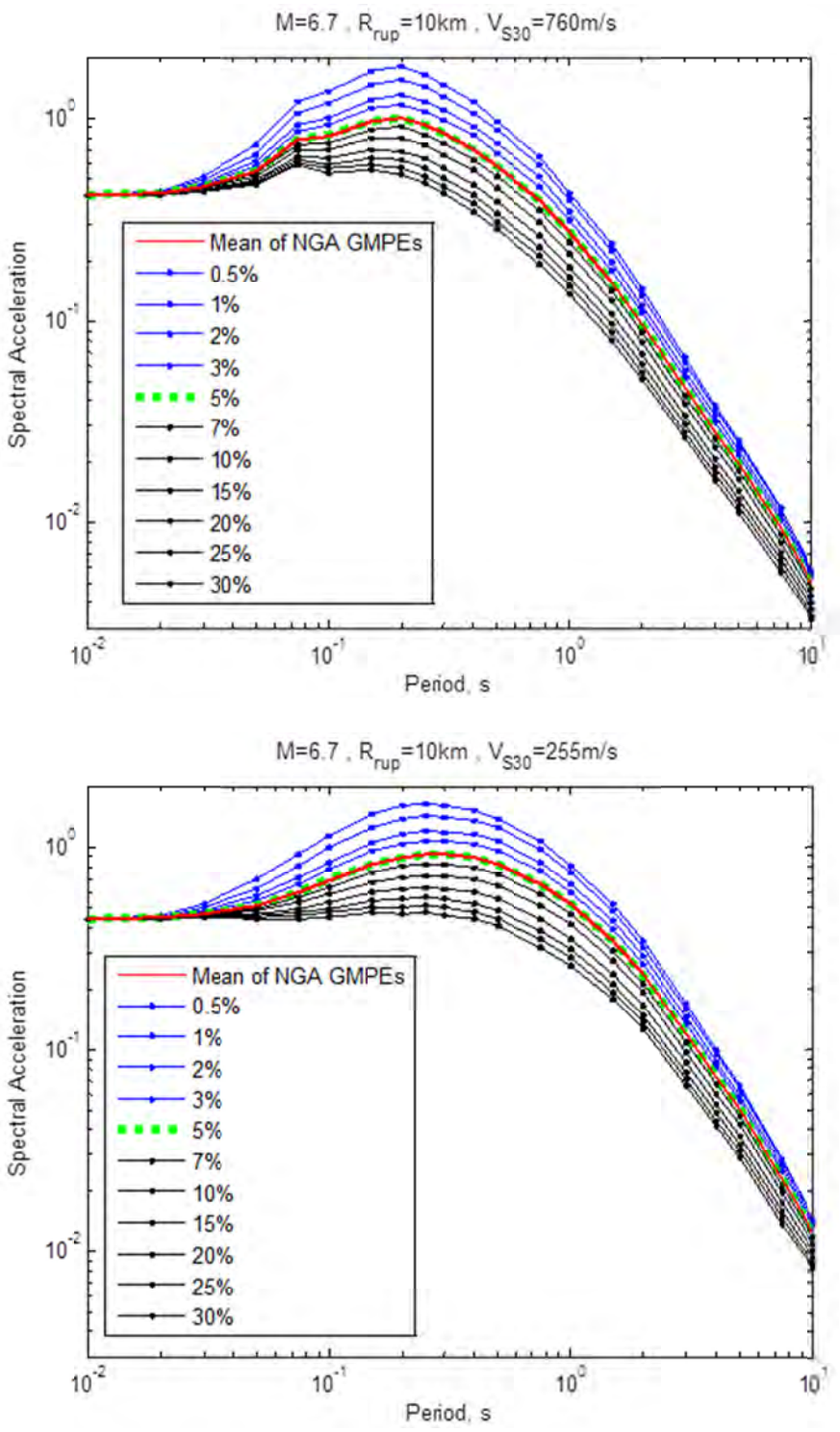

Figure 4.6 **The geometric mean of the five NGA-West1 GMPEs (red) is scaled to adjust for various damping ratios from 0.5% to 30%. The *DSF* model for RotD50 component is used. Assumptions to estimate the NGA-GMPEs: reverse fault, dip = 45°, hanging wall, fault rupture width = 15km, R_{jb} = 0 km, R_x = 7 km, V_{S30} = 760 m/sec (top), and V_{S30} = 255 m/sec (bottom).**

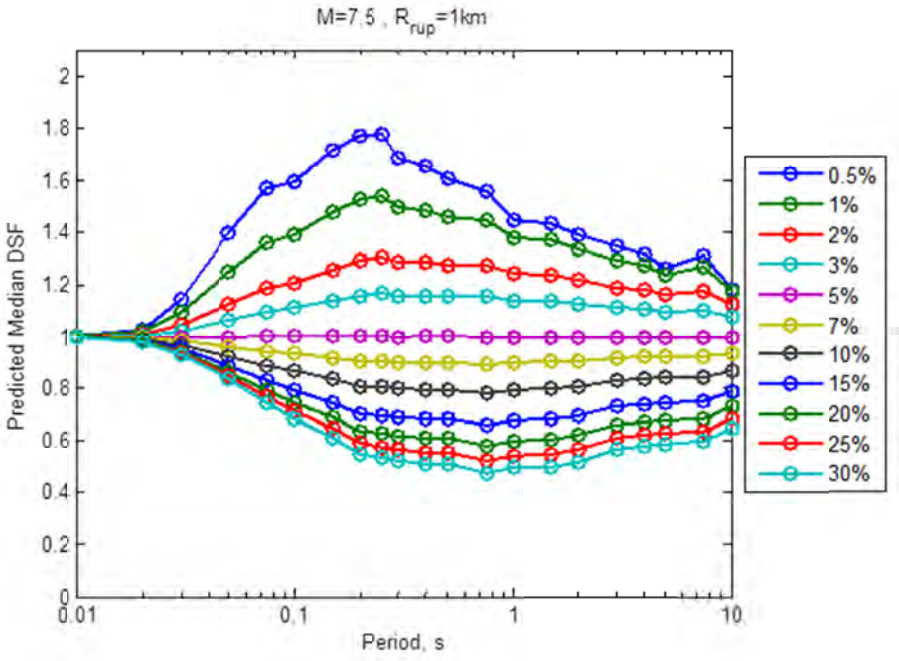

Figure 4.7 Predicted median *DSF* at R_{rup} = 1 km.

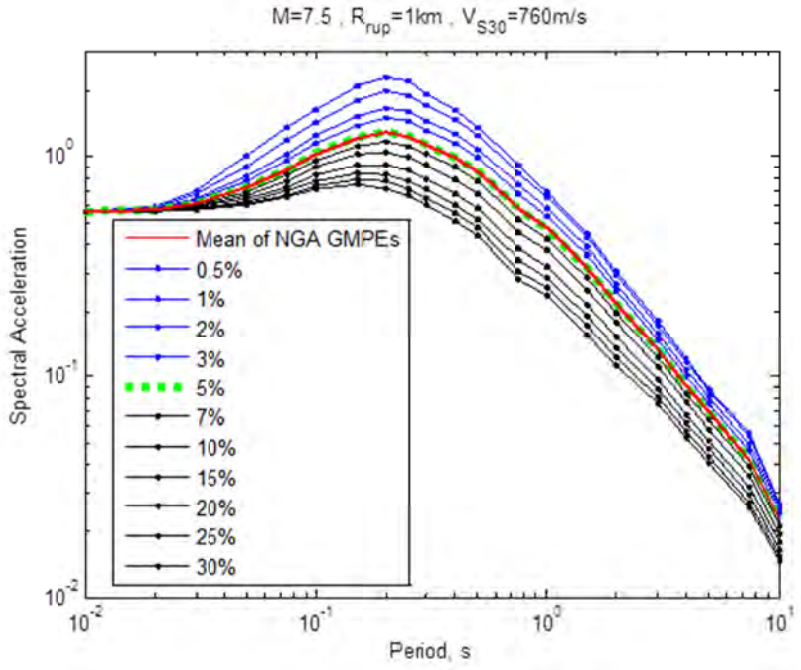

Figure 4.8 Scaled GMPE at R_{rup} = 1 km (GMPE assumptions are similar to Figure 4.6).

4.3 STANDARD DEVIATION

The standard deviation σ in Equation (4.8) is calculated for all combinations of T and β. In Section 3.2, the data suggested dependence of the variance on the damping ratio. Plotting the standard deviation at a given T versus β reveals a systematic pattern that can be seen in Figure 4.9 at four different periods. As expected, standard deviation is zero at 5% ($DSF = 1$ for $\beta = 5$) and it increases as the damping ratio deviates from 5% reaching a maximum of about 0.2.

The dependence of the standard deviation on the damping ratio can be captured by the following equation:

$$\sigma_{\ln(DSF)} = \begin{cases} a_0 \ln\left(\frac{\beta}{5}\right) + a_1 \left(\ln\left(\frac{\beta}{5}\right)\right)^2 & if \;\; \beta \leq 5\% \\ -a_0 \ln\left(\frac{\beta}{5}\right) - a_1 \left(\ln\left(\frac{\beta}{5}\right)\right)^2 & if \;\; \beta \geq 5\% \end{cases} \tag{4.9}$$

where β is the damping ratio in percentage (e.g., $\beta = 2$ for 2%); and a_0 and a_1 are obtained by fitting the model (using least squares regression) to the data for 11 damping values at a specified period. Their values are given in Table 4.1 for the RotD50 component (and in Appendix C for the GMRotI50 component) along with the standard error of the fit. Note that the reported standard errors are negligible. Also note that the behavior of the standard deviation for $\beta < 5\%$, and for $\beta > 5\%$ is exactly the same and just in the opposite direction. Division of β by 5% in Equation (4.9) is to ensure zero variance at 5% damping ratio.

Similar to the median model, smoothing is only done with respect to β as seen in Figure 4.9. We did not see it necessary to smooth a_0 and a_1 with respect to T. Their plots versus period are given in Figure 4.10 for the RotD50 component. The predicted standard deviation according to Equation (4.9) is plotted in Figure 4.11. These results are consistent with the few existing studies that have estimated the standard deviation. For example, Stafford et al. [2008], Cameron and Green [2007], Lin and Chang [2004], and Atkinson and Pierre [2004] reported estimates of standard deviation or coefficient of variation at certain periods and damping ratios. The reported values range anywhere between 0 to about 0.2 depending on the damping ratio; the variation with period and other parameters is of much less significance, as is also seen in this study. Values of the predicted $\sigma_{\ln(DSF)}$, according to the model in Equation (4.9), are calculated at specified T and β, and are given in Table 4.2.

The standard deviation of the scaled response spectrum can be calculated using the definition of DSF in Equation (2.1), written as follows:

$$\ln\left(PSA_{\beta\%}\right) = \ln(DSF) + \ln(PSA_{5\%}) \tag{4.10}$$

Taking the variance of both sides and taking the square root results in

$$\sigma_{\ln(PSA_{\beta\%})} = \sqrt{\sigma^2_{\ln(PSA_{5\%})} + \sigma^2_{\ln(DSF)} + 2\sigma_{\ln(PSA_{5\%})}\sigma_{\ln(DSF)}\rho} \tag{4.11}$$

where ρ represents the correlation coefficient between $\ln(DSF)$ and $\ln(PSA_{5\%})$. Assuming zero correlation, and estimating $\sigma_{\ln(DSF)}$ from Equation (4.9) and $\sigma_{\ln(PSA_{5\%})}$ from the corresponding

GMPE for $PSA_{5\%}$, the logarithmic standard deviation of $PSA_{\beta\%}$ can be calculated using Equation (4.11). We tested the validity of the assumption that $\rho = 0$ by calculating the sample correlation coefficients in our database for specified T and β. These values are given in Appendix E (Table E.1) using data with $R_{rup} < 50$ km.

Observe that ρ is insignificant at lower periods (the nonzero numbers could be simply due to the use of a sample data and do not necessarily reflect a dependence between the two parameters as error is inherent in statistical descriptors when they are estimated using sample realizations of random variables), and is negative for $\beta > 5\%$ (which reduces the total standard deviation). The highest value of ρ is around 0.5 at very long T and $\beta < 5\%$. We expect the first term in Equation (4.11) to dominate the overall standard deviation, and, consequently, we expect the effect of $\sigma_{\ln(DSF)}$ and ρ to be minimal. To examine this, Equation (4.11) is evaluated for $\sigma_{\ln(PSA_{5\%})}$ calculated from Campbell and Bozorgnia [2008] GMPE. The values of $\sigma_{\ln(PSA_{5\%})}$ are given in Table E.2. The resulting $\sigma_{\ln(PSA_{\beta\%})}$ are tabulated in Table E.3 assuming ρ is equal to the sample correlation coefficients of Table E.1, and in Table E.4 assuming $\rho = 0$. Observe that the deviations in the values of Tables E.3 and E.4 from those given in Table E.2 are small. It is being left to the user to decide what value of ρ to use. We are not making any recommendations on whether $\rho = 0$, but merely stating that the value of $\sigma_{\ln(PSA_{\beta\%})}$ is driven by $\sigma_{\ln(PSA_{5\%})}$.

4.4 BEYOND 50 KILOMETERS

As previously mentioned, the regression was done for $R_{rup} < 50$ km. We investigated the applicability of the proposed *DSF* model by studying the residual plots for records with $R_{rup} \geq 50$ km. Sample residual plots are provided in Appendix D for specified periods and damping ratios. We conclude that the model can be used for distances of up to 200 km without any modifications.

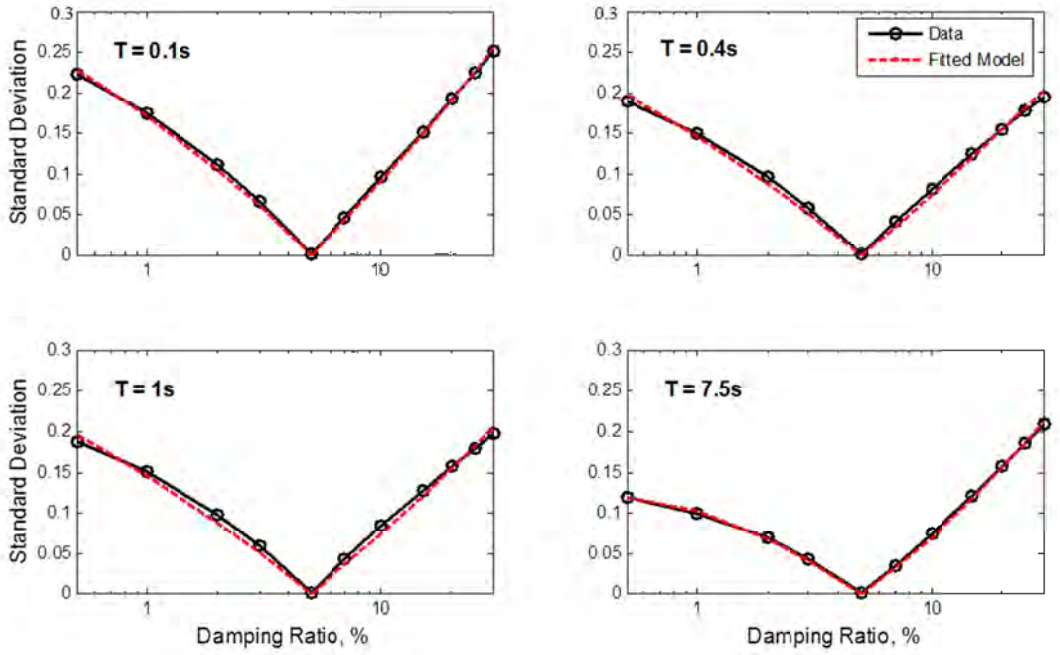

Figure 4.9 **Dependence of the standard deviation on β and the fitted function according to Equation (4.9).**

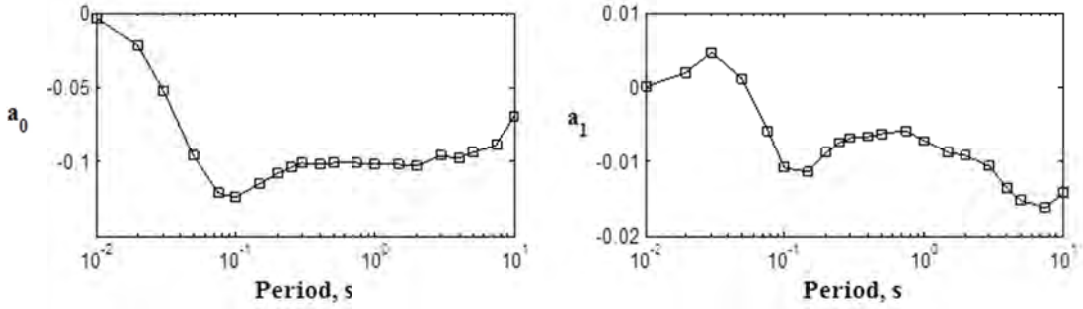

Figure 4.10 **Coefficients of the predicted standard deviation.**

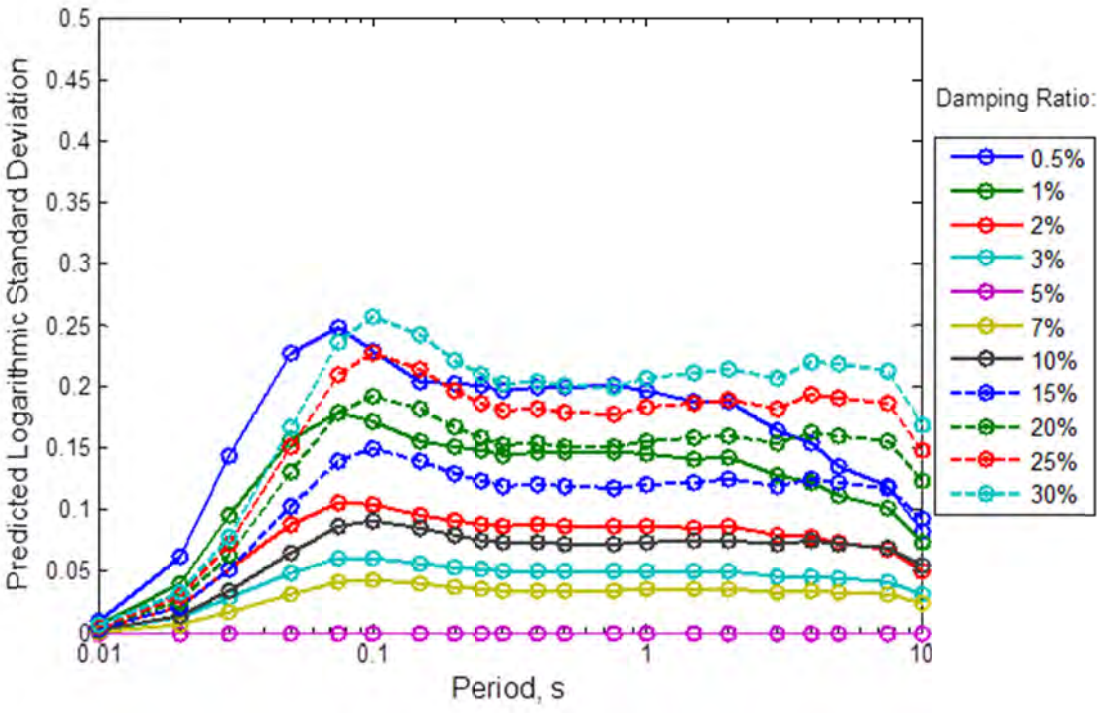

Figure 4.11 Predicted logarithmic standard deviation according to Equation (4.9).

Table 4.1 Regression coefficients for the horizontal component RotD50.

T, s	b0	b1	b2	b3	b4	b5	b6	b7	b8	a0	a1	$SE(\sigma)$*
0.01	1.73E-03	-2.07E-04	-6.29E-04	1.08E-06	-8.24E-05	7.36E-05	-1.07E-03	9.08E-04	-2.02E-04	-3.70E-03	2.30E-04	1.88E-04
0.02	5.53E-02	-3.77E-02	2.15E-03	-4.30E-03	3.21E-03	-3.32E-04	-4.75E-03	2.52E-03	2.29E-04	-2.19E-02	2.11E-03	4.99E-04
0.03	1.22E-01	-7.02E-02	-2.28E-03	-3.21E-03	6.91E-05	9.82E-04	-1.30E-02	7.82E-03	2.27E-04	-5.21E-02	4.60E-03	1.04E-03
0.05	2.39E-01	-1.06E-01	-2.63E-02	-8.57E-04	-7.43E-03	4.87E-03	-1.69E-02	8.08E-03	1.71E-03	-9.57E-02	1.31E-03	4.70E-03
0.075	3.05E-01	-7.32E-02	-7.29E-02	2.02E-04	-1.64E-02	1.03E-02	-9.26E-04	-6.40E-03	4.42E-03	-1.21E-01	-5.79E-03	4.60E-03
0.1	2.69E-01	4.18E-03	-1.07E-01	5.80E-03	-2.49E-02	1.34E-02	2.35E-02	-2.37E-02	5.84E-03	-1.24E-01	-1.08E-02	3.80E-03
0.15	1.41E-01	1.00E-01	-1.18E-01	3.01E-02	-4.09E-02	1.41E-02	3.16E-02	-2.47E-02	3.15E-03	-1.15E-01	-1.14E-02	3.97E-03
0.2	5.01E-02	1.45E-01	-1.11E-01	4.69E-02	-4.77E-02	1.18E-02	3.10E-02	-2.29E-02	2.41E-03	-1.08E-01	-8.85E-03	4.64E-03
0.25	2.28E-02	1.43E-01	-9.73E-02	5.20E-02	-4.70E-02	9.47E-03	2.71E-02	-2.02E-02	1.31E-03	-1.04E-01	-7.35E-03	4.66E-03
0.3	-1.58E-02	1.48E-01	-8.83E-02	5.21E-02	-4.36E-02	7.33E-03	3.87E-02	-2.66E-02	1.76E-03	-1.01E-01	-6.90E-03	5.31E-03
0.4	2.24E-02	1.03E-01	-7.41E-02	4.63E-02	-3.58E-02	4.65E-03	3.63E-02	-2.45E-02	1.18E-03	-1.02E-01	-6.71E-03	6.21E-03
0.5	3.19E-02	7.04E-02	-5.57E-02	4.25E-02	-2.94E-02	1.88E-03	3.87E-02	-2.47E-02	3.13E-04	-1.01E-01	-6.22E-03	7.13E-03
0.75	1.04E-02	5.33E-02	-3.72E-02	4.47E-02	-2.40E-02	-2.40E-03	3.47E-02	-2.59E-02	2.90E-03	-1.01E-01	-5.86E-03	6.85E-03
1	-8.84E-02	8.92E-02	-2.14E-02	4.98E-02	-2.36E-02	-4.70E-03	5.02E-02	-3.43E-02	2.32E-03	-1.02E-01	-7.31E-03	6.66E-03
1.5	-1.57E-01	9.33E-02	3.28E-03	5.85E-02	-2.36E-02	-8.02E-03	4.81E-02	-3.30E-02	2.10E-03	-1.02E-01	-8.75E-03	6.66E-03
2	-2.96E-01	1.50E-01	2.09E-02	7.30E-02	-2.96E-02	-9.95E-03	5.24E-02	-3.32E-02	6.86E-04	-1.03E-01	-9.22E-03	6.04E-03
3	-4.07E-01	1.97E-01	3.28E-02	8.35E-02	-3.54E-02	-1.01E-02	5.57E-02	-2.91E-02	-3.17E-03	-9.63E-02	-1.07E-02	6.03E-03
4	-4.49E-01	2.07E-01	4.42E-02	8.75E-02	-3.59E-02	-1.14E-02	5.07E-02	-2.43E-02	-4.67E-03	-9.83E-02	-1.37E-02	3.37E-03
5	-4.98E-01	2.17E-01	5.36E-02	9.03E-02	-3.48E-02	-1.29E-02	5.19E-02	-2.30E-02	-5.68E-03	-9.42E-02	-1.53E-02	2.99E-03
7.5	-5.25E-01	2.06E-01	7.79E-02	9.88E-02	-3.76E-02	-1.51E-02	2.91E-02	-4.93E-03	-9.02E-03	-8.95E-02	-1.63E-02	2.59E-03
10	-3.89E-01	1.43E-01	6.12E-02	7.14E-02	-2.36E-02	-1.30E-02	2.33E-02	-5.46E-03	-5.92E-03	-6.89E-02	-1.43E-02	1.94E-03

* Standard error in modeling σ according to Equation (4.9).

Table 4.2 Predicted standard deviation according to Equation (4.9).

	β, %										
***T*, s**	**0.5**	**1**	**2**	**3**	**5**	**7**	**10**	**15**	**20**	**25**	**30**
0.01	0.01	0.01	0.00	0.00	0.00	0.00	0.00	0.00	0.00	0.01	0.01
0.02	0.06	0.04	0.02	0.01	0.00	0.01	0.01	0.02	0.03	0.03	0.03
0.03	0.14	0.10	0.05	0.03	0.00	0.02	0.03	0.05	0.06	0.07	0.08
0.05	0.23	0.16	0.09	0.05	0.00	0.03	0.07	0.10	0.13	0.15	0.17
0.075	0.25	0.18	0.11	0.06	0.00	0.04	0.09	0.14	0.18	0.21	0.24
0.1	0.23	0.17	0.10	0.06	0.00	0.04	0.09	0.15	0.19	0.23	0.26
0.15	0.20	0.16	0.10	0.06	0.00	0.04	0.09	0.14	0.18	0.21	0.24
0.2	0.20	0.15	0.09	0.05	0.00	0.04	0.08	0.13	0.17	0.20	0.22
0.25	0.20	0.15	0.09	0.05	0.00	0.04	0.08	0.12	0.16	0.19	0.21
0.3	0.20	0.14	0.09	0.05	0.00	0.04	0.07	0.12	0.15	0.18	0.20
0.4	0.20	0.15	0.09	0.05	0.00	0.04	0.07	0.12	0.15	0.18	0.20
0.5	0.20	0.15	0.09	0.05	0.00	0.04	0.07	0.12	0.15	0.18	0.20
0.75	0.20	0.15	0.09	0.05	0.00	0.04	0.07	0.12	0.15	0.18	0.20
1	0.20	0.15	0.09	0.05	0.00	0.04	0.07	0.12	0.16	0.18	0.21
1.5	0.19	0.14	0.09	0.05	0.00	0.04	0.08	0.12	0.16	0.19	0.21
2	0.19	0.14	0.09	0.05	0.00	0.04	0.08	0.12	0.16	0.19	0.21
3	0.17	0.13	0.08	0.05	0.00	0.03	0.07	0.12	0.15	0.18	0.21
4	0.15	0.12	0.08	0.05	0.00	0.04	0.08	0.12	0.16	0.19	0.22
5	0.14	0.11	0.07	0.04	0.00	0.03	0.07	0.12	0.16	0.19	0.22
7.5	0.12	0.10	0.07	0.04	0.00	0.03	0.07	0.12	0.16	0.19	0.21
10	0.08	0.07	0.05	0.03	0.00	0.03	0.06	0.09	0.12	0.15	0.17

5 Comparison with Data and with Existing Models

This chapter compares the final model with the computed DSF values obtained from the database of recorded ground motions and with selected existing models. Since the proposed model is empirical and was designed to capture the observed trends in the database, close agreement between the model and the data is expected. To visually validate the model against data, plots similar to Figure 5.1 are generated, where the predicted median DSF is plotted for a moment magnitude of 6.5 and $R_{rup} = 10,\ 20$, and 30 km. Superimposed on all three plots is the median DSF calculated from the records in a magnitude-distance bin, where $6 \leq \mathbf{M} \leq 7$ and $0 \leq R_{rup} < 50$ km. The agreement between the model and data is excellent. The minor differences are due to the wide magnitude and distance bins, as is demonstrated by variation in the fit of the three plots with different distance measures. The most pronounced difference is seen around shorter periods, which reduces as the distance used in the proposed model approaches towards the mid-range values of the selected distance bin for the observed data (i.e., the fit is better at 30 km than 10 km when using a distance bin of 0 to 50 km). Depending on the exact values of $\mathbf{M}$ and R_{rup}, narrowing the magnitude and distance bins may give a better match to the corresponding prediction if enough data points are available, or due to the reduction in the sample size it may have the opposite effect.

In this chapter, a more direct and visual comparison is provided with selected existing models in the literature. Recall that different models use different databases and are applicable to different ranges of β, T, $\mathbf{M}$, and R_{rup} (see Appendix A for details on each model). Therefore, comparisons with models that use similar data and applicability range of the predictor variables are more appropriate.

In Figures 5.2 to 5.5, the median DSF for the proposed model is plotted versus period at the 11 damping ratios, $\beta = 0.5, 1, 2, 3, 5, 7, 10, 15, 20, 25, 30\%$, for $\mathbf{M} = 5.5, 6.5, 7.5$, and $R_{rup} = 5$ and 10 km. In Figure 5.2, the model developed by Idriss [1993] is superimposed on each plot. This model is only given and plotted for $\beta = 1, 2, 3, 5, 7, 10, 15\%$. It is applicable to T = 0.03–5 sec and is not a function of $\mathbf{M}$ or R_{rup}. It best agrees with the proposed model at higher magnitudes and periods greater than 0.1 sec.

In Figure 5.3, the model developed by Abrahamson and Silva [1996] is superimposed on each plot for $\beta = 0.5, 1, 2, 3, 5, 7, 10, 15, 20\%$. This model is applicable to T = 0.02–5 sec. It is calculated and plotted at select periods and is linearly interpolated in-between. It is a function of $\mathbf{M}$, but not R_{rup}. Except for very low damping, where the peak is at a longer period than the peak DSF in our model, there is a good agreement between this model and the proposed model. The

lack of R_{rup} as a predictor variable in this model can be observed in the figure: the fit is better at 10 km compared to 5 km, particularly at smaller magnitudes. (This is expected because there are probably more records with longer distances in their database, moving the average closer to 10 km than to 5 km.)

In Figure 5.4, the model is compared to the Newmark and Hall model [1982], which is the basis for most U.S. building codes. The model of Newmark and Hall is only applicable for $\beta \leq 20\%$ and is plotted for $\beta = 0.5, 1, 2, 3, 5, 7, 10, 15, 20\%$. Furthermore, it is applicable for $T = 0.125 - 10$ sec and is not a function of $\mathbf{M}$ or R_{rup}. Considering the limited number of records they used, their model is in good agreement with the proposed model, particularly for periods around 0.125 to 1 sec.

In Figure 5.5, the model of Eurocode 8 [2004] is superimposed on the plots of the proposed model for the same 11 damping ratios. This model is applicable to periods ranging roughly from 0.2 to 6 sec with unity imposed at very low and very high periods and should not be applied to β values resulting in a DSF smaller than 0.55. It is not a function of $\mathbf{M}$ or R_{rup}. For $\beta < 3\%$ this model tends to be relatively low. This might be expected because this model was based on the work of Bommer et al. [2000] that focused on high damping ratios. The figure demonstrates that the model underestimates or overestimates our prediction of DSF at long-period ranges depending on the specific values of $\mathbf{M}$ and R_{rup}. It compares best for T = 0.01–1 sec and high damping ratios.

Finally, Figure 5.6 compares the proposed model to that of Stafford et al. [2008]. This is not a direct comparison because the proposed model is a function of $\mathbf{M}$ and R_{rup}, while the model by Stafford et al. is a function of duration. The proposed model is plotted for a magnitude of 6.5 at 10 km distance. The model by Stafford et al. is plotted at four durations, $D_{5-75} = 5, 10, 15, 20$ sec, for $\beta = 2, 3, 5, 7, 10, 15, 20, 25, 30\%$. This model is not a function of period, and since their data is averaged over a period range of 1.5 to 3 sec, we plotted their model for this range only. As previously mentioned, duration is positively correlated with magnitude and distance. For $\mathbf{M} = 6.5$ and $R_{rup} = 10$ km used in Figure 5.6, the fit between the two models seems best at $D_{5-75} = 10$ sec. There are models in the literature to predict the duration of motion given magnitude, distance, and other variables (e.g., Kempton and Stewart [2006], Abrahamson and Silva [1996]). This figure does not rely on these previously derived empirical models, thereby avoiding their limitations and underlying assumptions in modeling.

Based on the comprehensiveness of the database used, detailed analyses of the model and residuals, and the wide range of applicability of the model, use of the model developed under the current study is recommended.

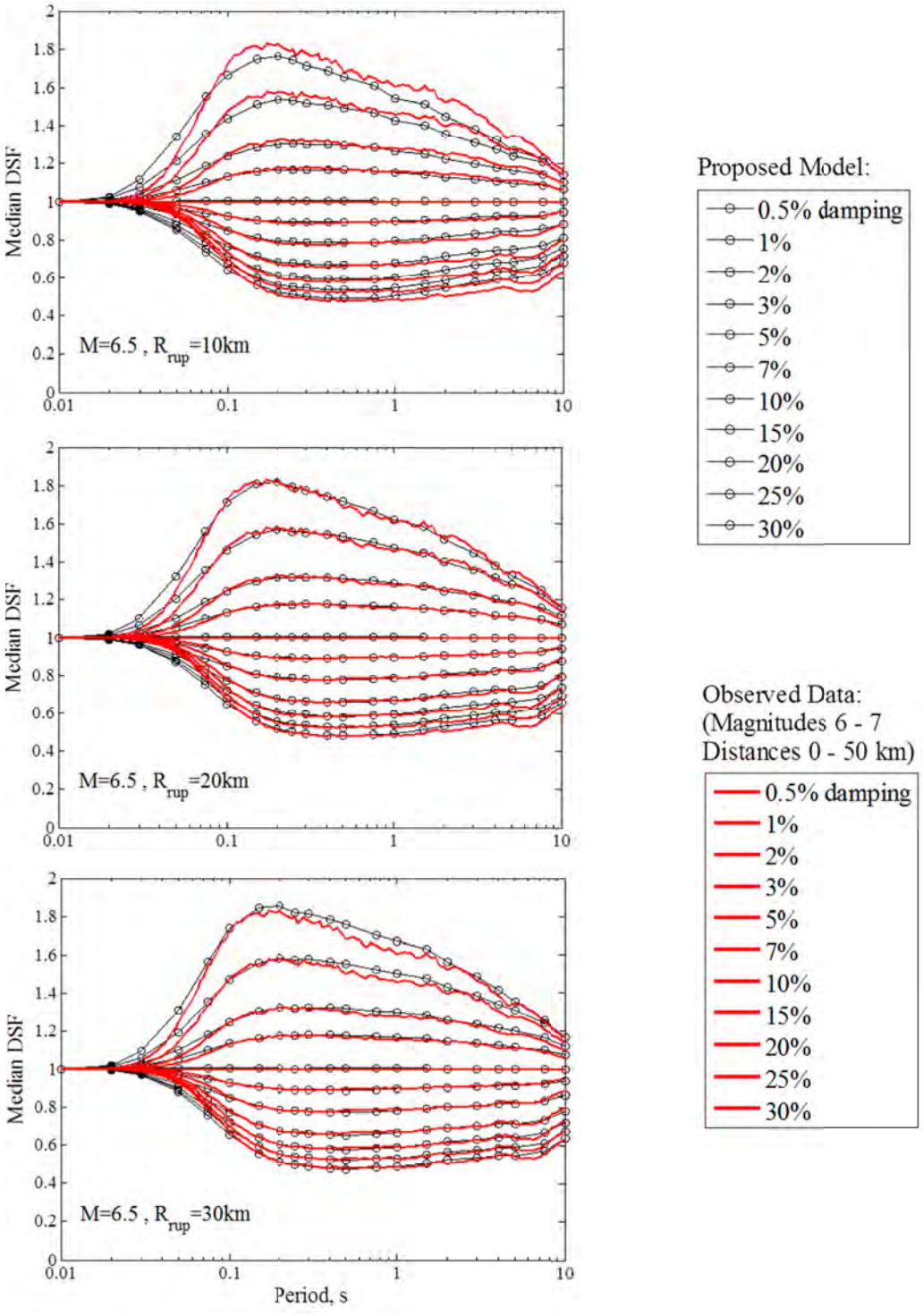

Figure 5.1 **Data binned for M and R_{rup} ($6 \leq M \leq 7$ and $0 \leq R_{rup} < 50$ km) is superimposed on the plots of the proposed model for M = 6.5 at three distances, R_{rup} = 10, 20, 30 km.**

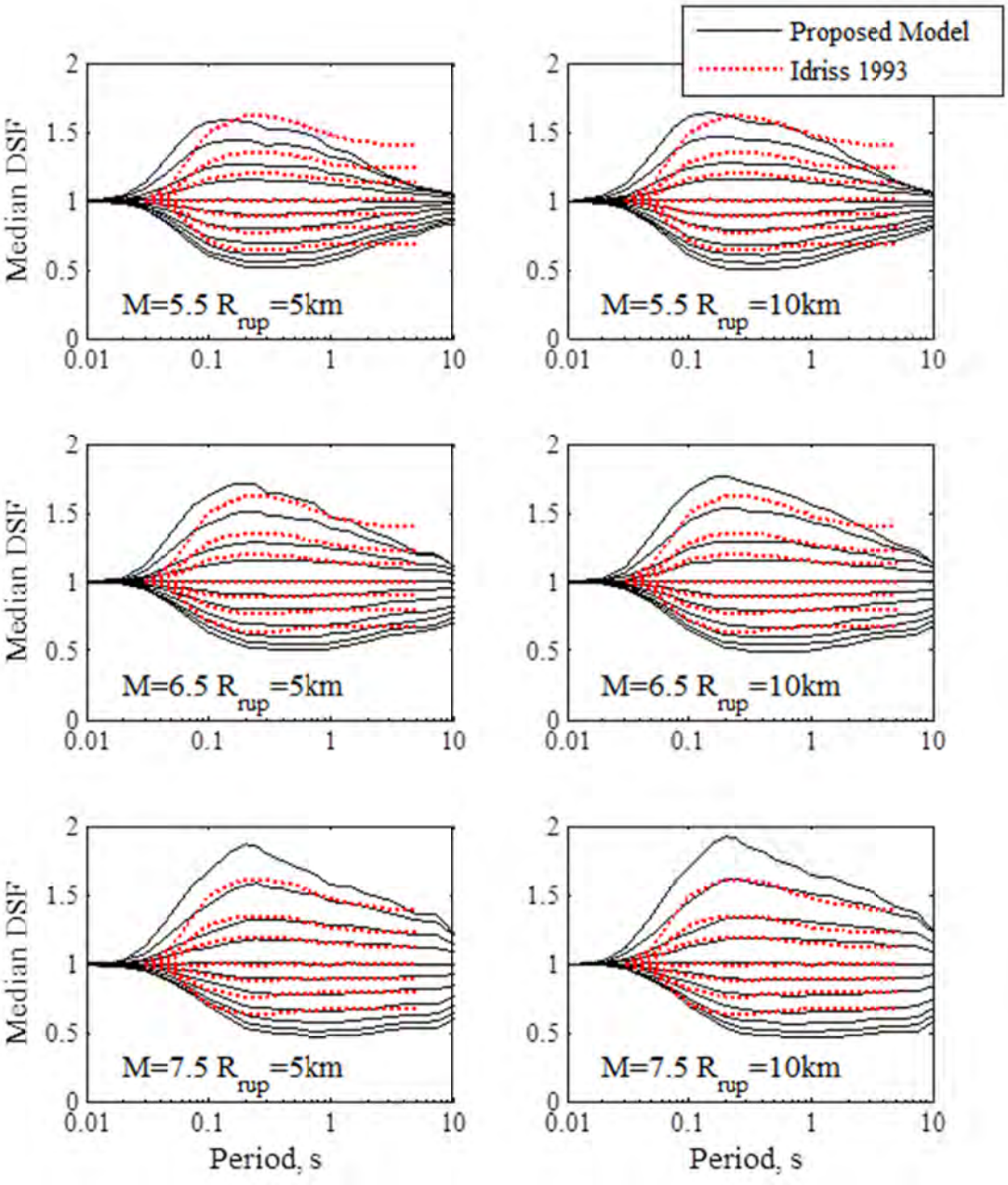

Figure 5.2 **The proposed model is plotted for all 11 damping ratios from 0.5% to 30%. Idriss [1993] is plotted for β = 1, 2, 3, 5, 7, 10, 15%. It is applicable to T = 0.03–5 sec, and is not a function of M or R_{rup}.**

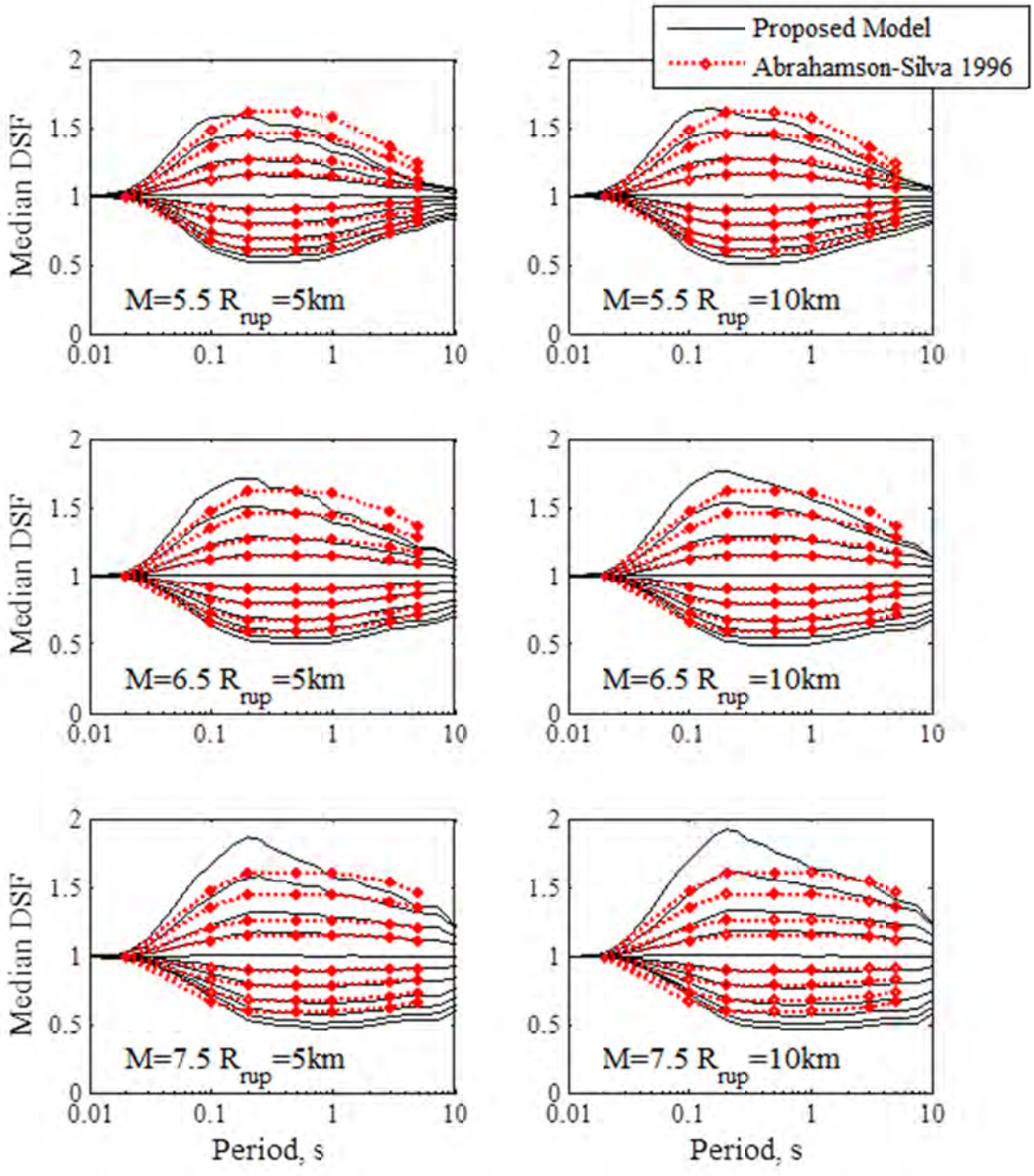

Figure 5.3 **The proposed model is plotted for all 11 damping ratios from 0.5% to 30%. Abrahamson and Silva [1996] is plotted for β = 0.5, 1, 2, 3, 7, 10, 15, 20% at select periods and interpolated in-between. It is applicable to T = 0.02–5 sec, and is a function of M but not R_{rup}.**

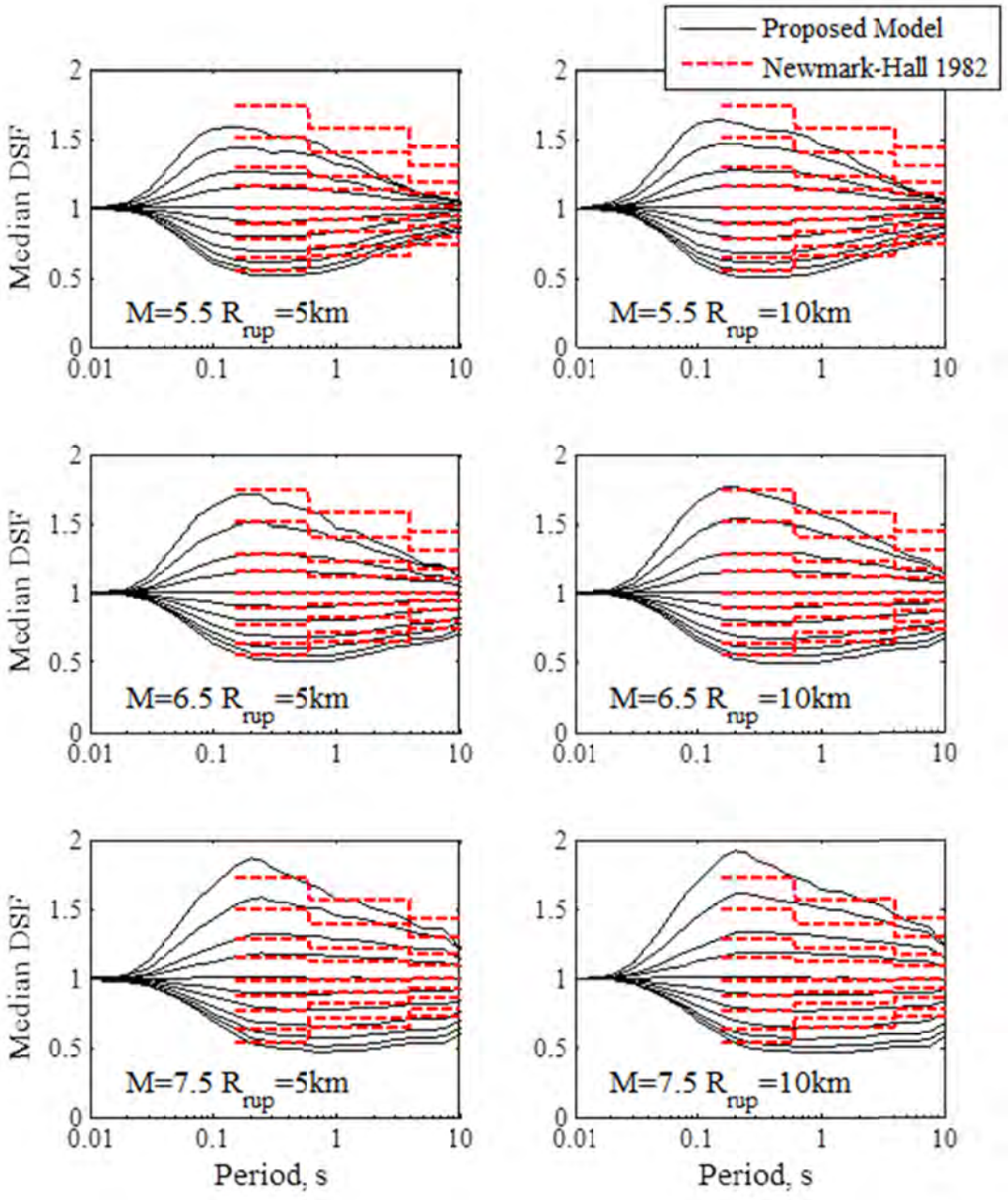

Figure 5.4 **The proposed model is plotted for all 11 damping ratios from 0.5% to 30%. Newmark and Hall [1982] is applicable for $\beta \leq 20\%$ and T = 0.125–10 sec. It is plotted for β = 0.5, 1, 2, 3, 5, 7, 10, 15, and 20%, and is a not a function of M or R_{rup}.**

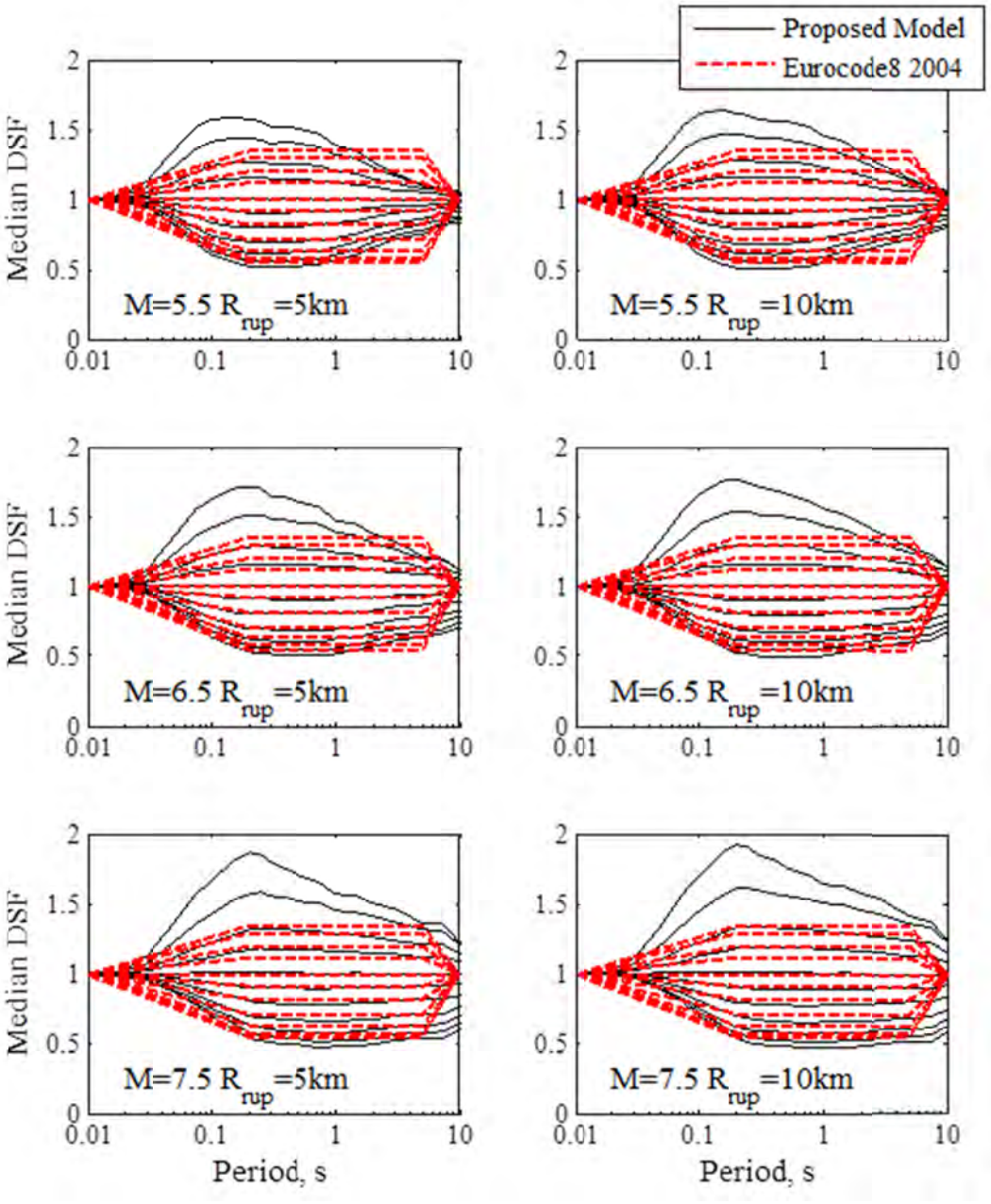

Figure 5.5 **The proposed model and the model by Eurocode 8 [2004] are plotted for all 11 damping ratios from 0.5% to 30%. The model by Eurocode 8 [2004] is not a function of M or R_{rup}. This figure assumes very low and very high periods, where the model by Eurocode 8 is equal to unity, are 0.01 and 10 sec (10 sec is the value used by Bommer and Mendis [2005]).**

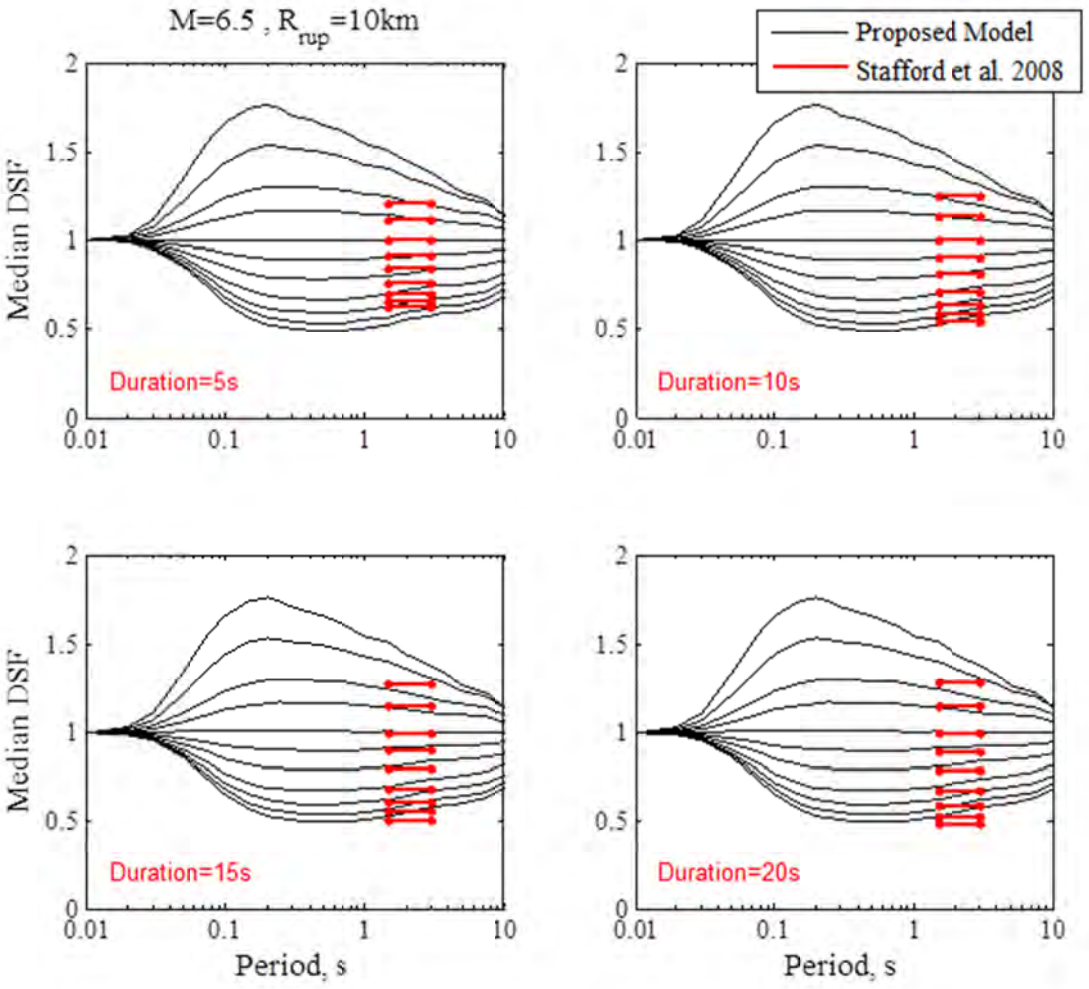

Figure 5.6 **The proposed model is plotted for M = 6.5 and R_{rup} = 10 km for all 11 damping ratios from 0.5% to 30%. The Stafford et al. [2008] model is plotted for β = 2, 3, 5, 7, 10, 15, 20, 25, 30% and D_{5-75} = 5, 10, 15, 20 sec. It is applicable to T = 1.5–3 sec.**

6 Vertical Component Model

In the previous chapters, we developed a model for the damping scaling factor, DSF, for the "average" of the two horizontal components of ground motion. This chapter focuses on the DSF for the vertical ground motion and highlights the differences between the models of the horizontal and vertical components.

The database of recorded ground motions used to develop the model was described in Chapter 2. Recall that for vertical component a subset of 2229 records with $R_{rup} < 50$ km is used in the regression analysis to ensure a proper damping scaling for near-source data. Distributions of $\mathbf{M}$, R_{rup}, D_{5-75}, and V_{S30} of the selected records were given in Figure 2.4. For each recorded vertical ground motion in the database, the DSF is calculated using the elastic pseudo-spectral acceleration at 21 selected periods and 11 damping ratios: 0.5, 1, 2, 3, 5, 7, 10, 15, 20, 25, and 30%.

After scrutinizing the data for potential predictor variables, the general trends seen between the vertical DSF and the predictor variables—discussed in Chapter 3—are similar to what was observed for the horizontal ground motion: Namely, systematic patterns with damping ratio and vibration period, significant dependence on duration and magnitude, a less significant dependence on distance, and a negligible dependence on soil conditions are observed. As examples, Figures 6.1 through 6.3 show the dependence of the vertical DSF on D_{5-75}, $\mathbf{M}$, and R_{rup} at a vibration period of $T = 1$ sec and four damping ratios.

Following the same approach of statistical analyses, step-by-step regression, and study of residual diagnostic plots that was described in Chapter 4, a functional form similar to that of the horizontal ground motion is selected. For the vertical ground motion, the median DSF and its logarithmic standard deviation are modeled by Equations (4.8) and (4.9) with the regression coefficients given in Table 6.1. Plots of the regression coefficients versus period are shown in Figures 6.4 and 6.5. Figure 6.6 shows the predicted median DSF for the vertical component for $\mathbf{M} = 5, 6, 7, 8$ and $R_{rup} = 10$ km (compare this with Figure 4.5 for RotD50).

For a more direct comparison with the horizontal component, Figures 6.7 and 6.8 show plots of horizontal DSF and vertical DSF at selected values of $\mathbf{M}$ and R_{rup}. Figure 6.7 shows the variation of DSF with distance; while Figure 6.8 shows the variation of DSF with magnitude. In general, the peak is shifted towards shorter periods and is more extreme for the vertical DSF. The most significant differences are seen at periods less than 0.2 sec.

The standard deviation versus period is plotted in Figure 6.9 at different damping ratios. Observe that the standard deviation varies between 0 and 0.3. This is a little higher than seen for the horizontal component (Figure 6.10); it is suspected that this effect is due to the "averaging"

of the two horizontal components, which is expected to reduce the standard deviation compared to the one component used for vertical ground motion.

Table 6.1 Regression coefficients for the vertical component.

T, s	b0	b1	b2	b3	b4	b5	b6	b7	b8	a0	a1	$SE(\sigma)$*
0.01	5.82E-03	-3.31E-03	-3.64E-04	-3.81E-04	2.15E-04	2.92E-05	-1.82E-03	1.54E-03	-2.48E-04	-6.15E-03	5.21E-04	4.17E-04
0.02	1.36E-01	-8.77E-02	1.65E-03	-1.02E-02	6.91E-03	-2.83E-04	-1.23E-02	6.98E-03	3.60E-04	-4.50E-02	3.16E-03	5.64E-04
0.03	3.49E-01	-1.94E-01	-1.19E-02	-1.61E-02	6.48E-03	1.95E-03	-2.59E-02	1.22E-02	2.19E-03	-1.06E-01	3.16E-03	4.25E-03
0.05	4.34E-01	-1.68E-01	-6.08E-02	-1.15E-03	-1.01E-02	6.59E-03	-1.37E-02	-3.18E-03	6.97E-03	-1.47E-01	-8.28E-03	8.02E-03
0.075	3.48E-01	-6.40E-02	-9.47E-02	1.69E-02	-2.37E-02	8.31E-03	6.22E-03	-1.97E-02	9.83E-03	-1.39E-01	-9.96E-03	6.85E-03
0.1	3.06E-01	-3.80E-02	-9.44E-02	2.63E-02	-2.96E-02	8.20E-03	1.14E-02	-1.80E-02	6.93E-03	-1.34E-01	-1.02E-02	8.38E-03
0.15	1.87E-01	6.67E-02	-1.16E-01	4.32E-02	-4.50E-02	1.15E-02	1.66E-02	-1.73E-02	4.82E-03	-1.23E-01	-6.66E-03	8.44E-03
0.2	1.86E-01	4.16E-02	-9.66E-02	3.55E-02	-3.56E-02	8.37E-03	2.73E-02	-2.37E-02	4.13E-03	-1.22E-01	-6.52E-03	9.09E-03
0.25	1.21E-01	7.76E-02	-9.75E-02	4.13E-02	-3.96E-02	8.98E-03	3.10E-02	-2.22E-02	1.97E-03	-1.20E-01	-5.99E-03	8.70E-03
0.3	1.41E-01	5.39E-02	-8.91E-02	3.79E-02	-3.61E-02	7.91E-03	2.76E-02	-1.85E-02	1.02E-03	-1.22E-01	-5.78E-03	9.76E-03
0.4	1.72E-01	1.29E-02	-7.08E-02	2.97E-02	-2.58E-02	4.42E-03	2.93E-02	-2.13E-02	1.05E-03	-1.20E-01	-5.74E-03	8.83E-03
0.5	2.21E-01	-3.86E-02	-6.00E-02	2.18E-02	-1.90E-02	3.21E-03	2.72E-02	-1.64E-02	-2.29E-04	-1.23E-01	-6.08E-03	1.03E-02
0.75	1.68E-01	-2.35E-02	-5.40E-02	2.49E-02	-1.57E-02	6.34E-04	3.10E-02	-2.21E-02	2.01E-03	-1.22E-01	-6.75E-03	9.14E-03
1	8.65E-02	2.28E-02	-5.28E-02	3.47E-02	-2.11E-02	4.55E-04	3.53E-02	-2.43E-02	1.75E-03	-1.24E-01	-8.33E-03	9.33E-03
1.5	-3.62E-02	7.02E-02	-3.20E-02	4.82E-02	-2.57E-02	-2.44E-03	3.63E-02	-2.24E-02	2.93E-04	-1.25E-01	-1.04E-02	8.14E-03
2	-8.29E-02	9.13E-02	-2.57E-02	5.37E-02	-2.64E-02	-4.34E-03	3.16E-02	-2.30E-02	2.38E-03	-1.22E-01	-1.11E-02	8.20E-03
3	-2.26E-01	1.21E-01	1.05E-02	6.50E-02	-2.59E-02	-8.86E-03	3.45E-02	-2.00E-02	-9.44E-04	-1.16E-01	-1.29E-02	6.07E-03
4	-4.08E-01	2.02E-01	3.12E-02	8.61E-02	-3.44E-02	-1.19E-02	4.15E-02	-2.23E-02	-2.25E-03	-1.11E-01	-1.63E-02	4.96E-03
5	-2.54E-01	1.11E-01	2.96E-02	6.37E-02	-2.13E-02	-1.15E-02	2.86E-02	-1.34E-02	-2.90E-03	-1.07E-01	-1.68E-02	3.89E-03
7.5	-4.41E-01	1.73E-01	6.26E-02	7.73E-02	-2.58E-02	-1.39E-02	3.84E-02	-1.44E-02	-5.92E-03	-9.36E-02	-1.63E-02	2.20E-03
10	-3.95E-01	1.23E-01	7.79E-02	7.10E-02	-2.12E-02	-1.43E-02	2.13E-02	-4.42E-03	-6.15E-03	-8.17E-02	-1.53E-02	2.16E-03

* Standard error in modeling σ according to Equation (4.9).

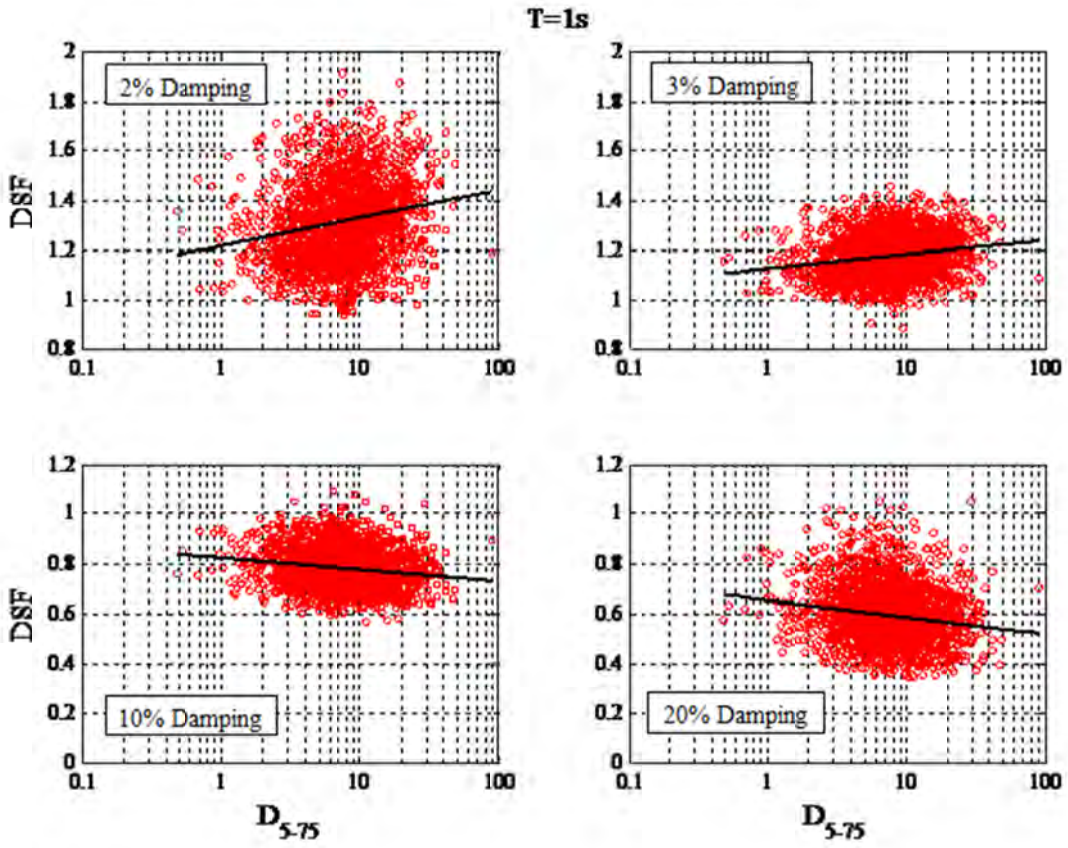

Figure 6.1 **Influence of duration on vertical *DSF* at T = 1 sec and β = 2, 3, 10, 20% (compare with Figure 3.3b for RotD50). Only data with R_{rup} < 50 km is used.**

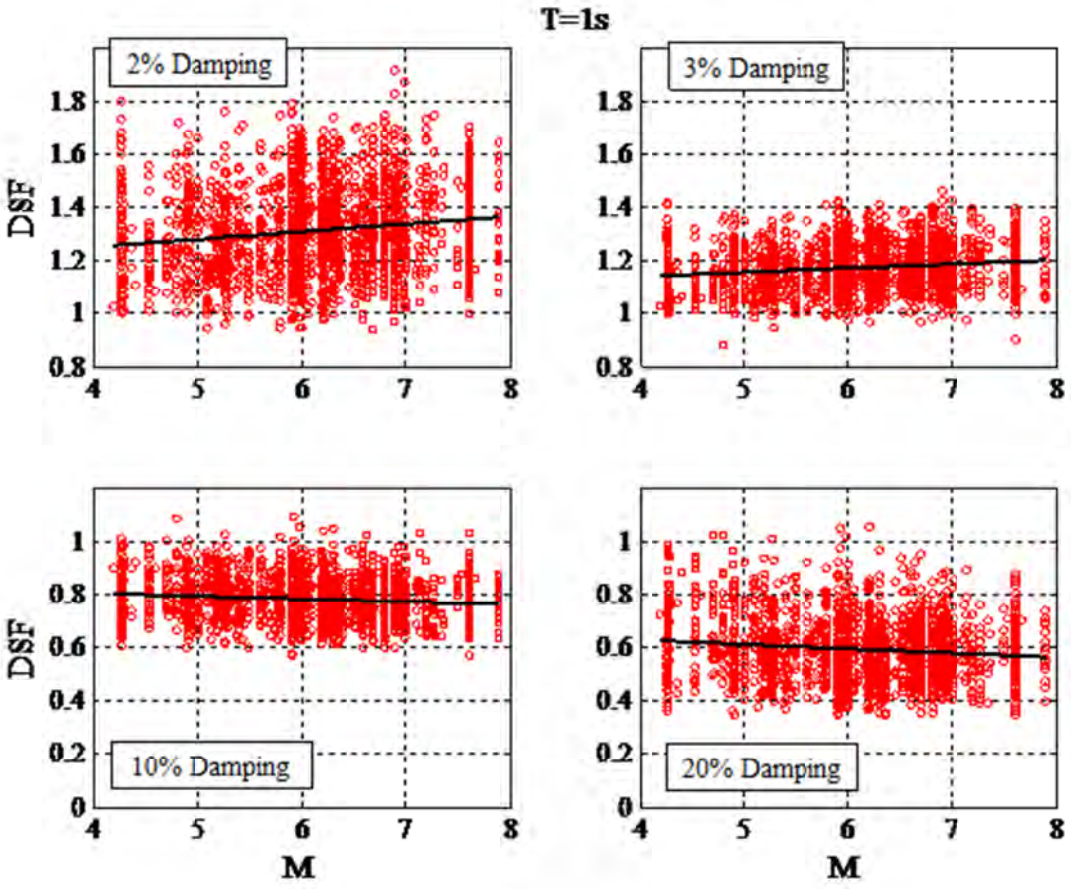

Figure 6.2 **Influence of magnitude on vertical *DSF* at T = 1 sec and β = 2, 3, 10, 20% (compare with Figure 3.4b for RotD50). Only data with R_{rup} < 50 km is used.**

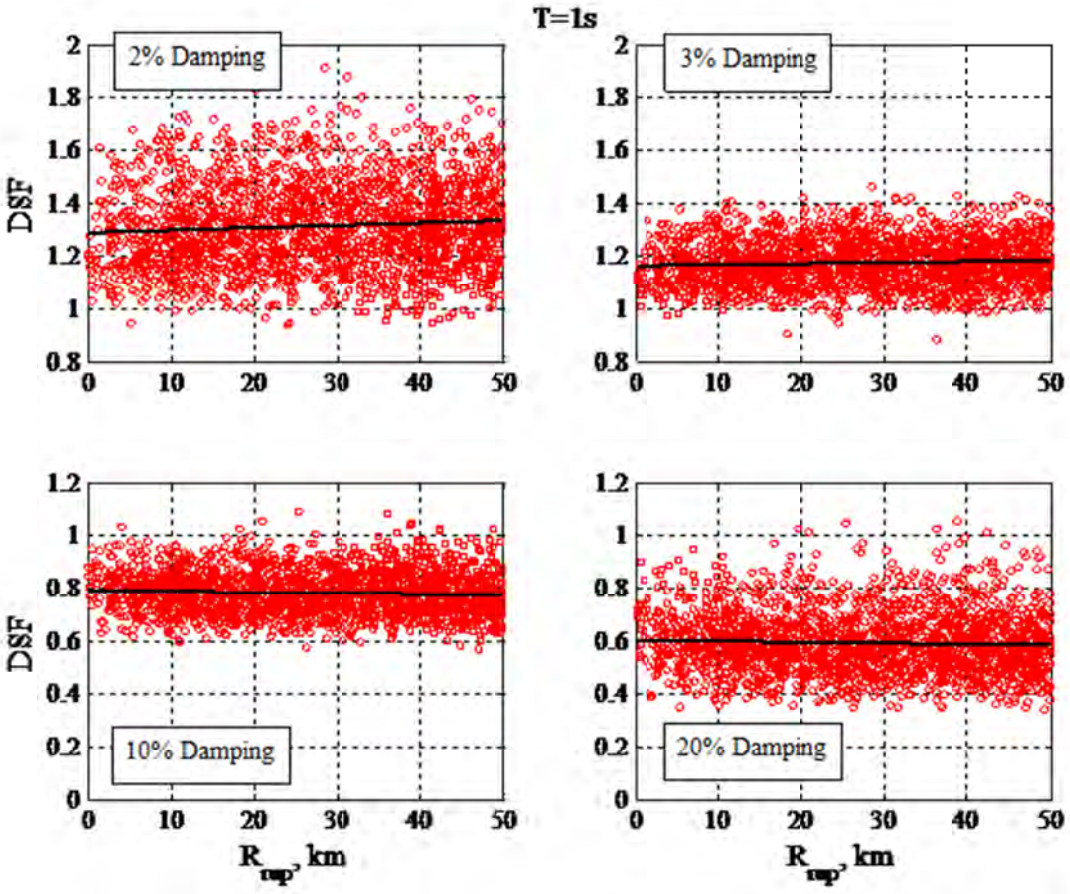

Figure 6.3 **Influence of distance on vertical *DSF* at T = 1 sec and β = 2, 3, 10, 20% (compare with Figure 3.5b for RotD50). Only data with R_{rup} < 50 km is used.**

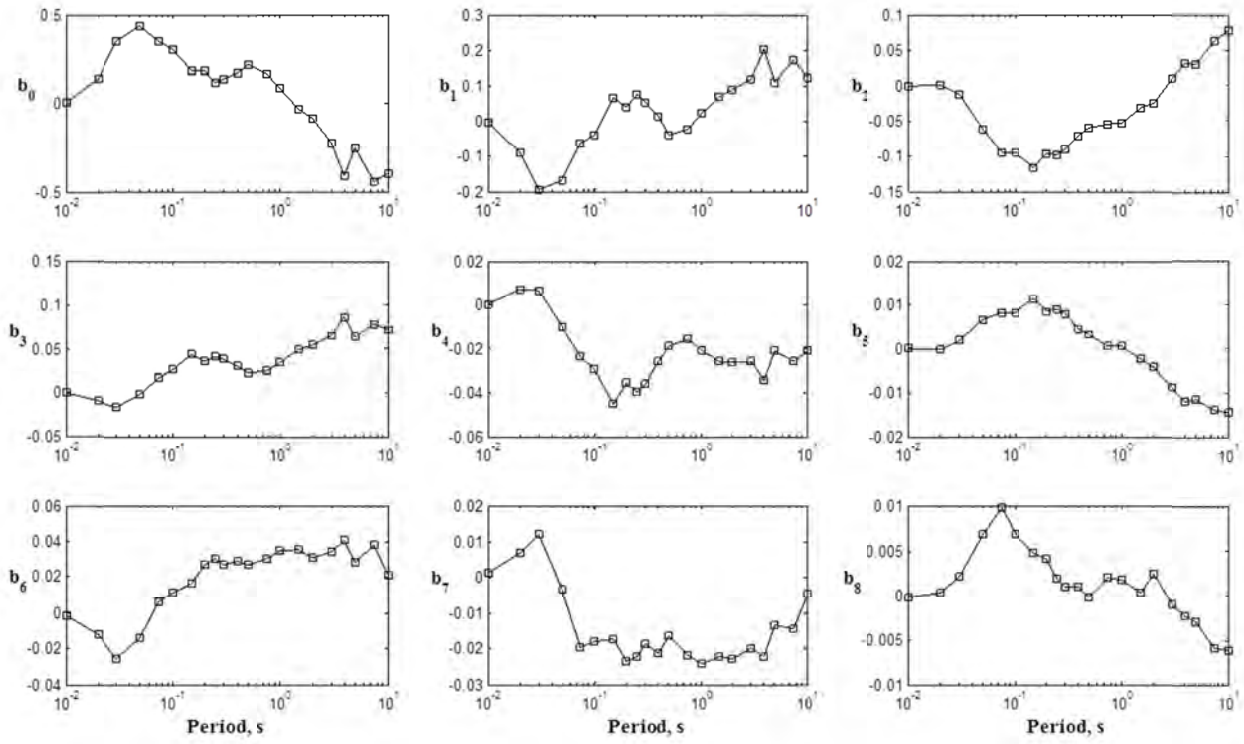

Figure 6.4 Regression coefficients for the vertical component.

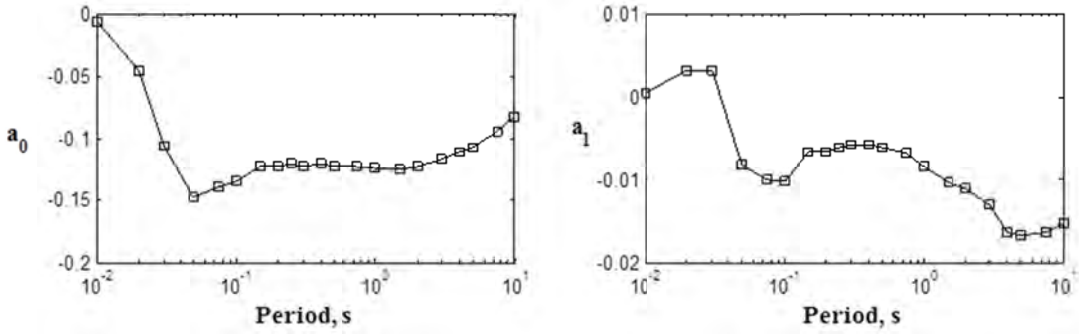

Figure 6.5 Coefficients of the predicted standard deviation for the vertical component.

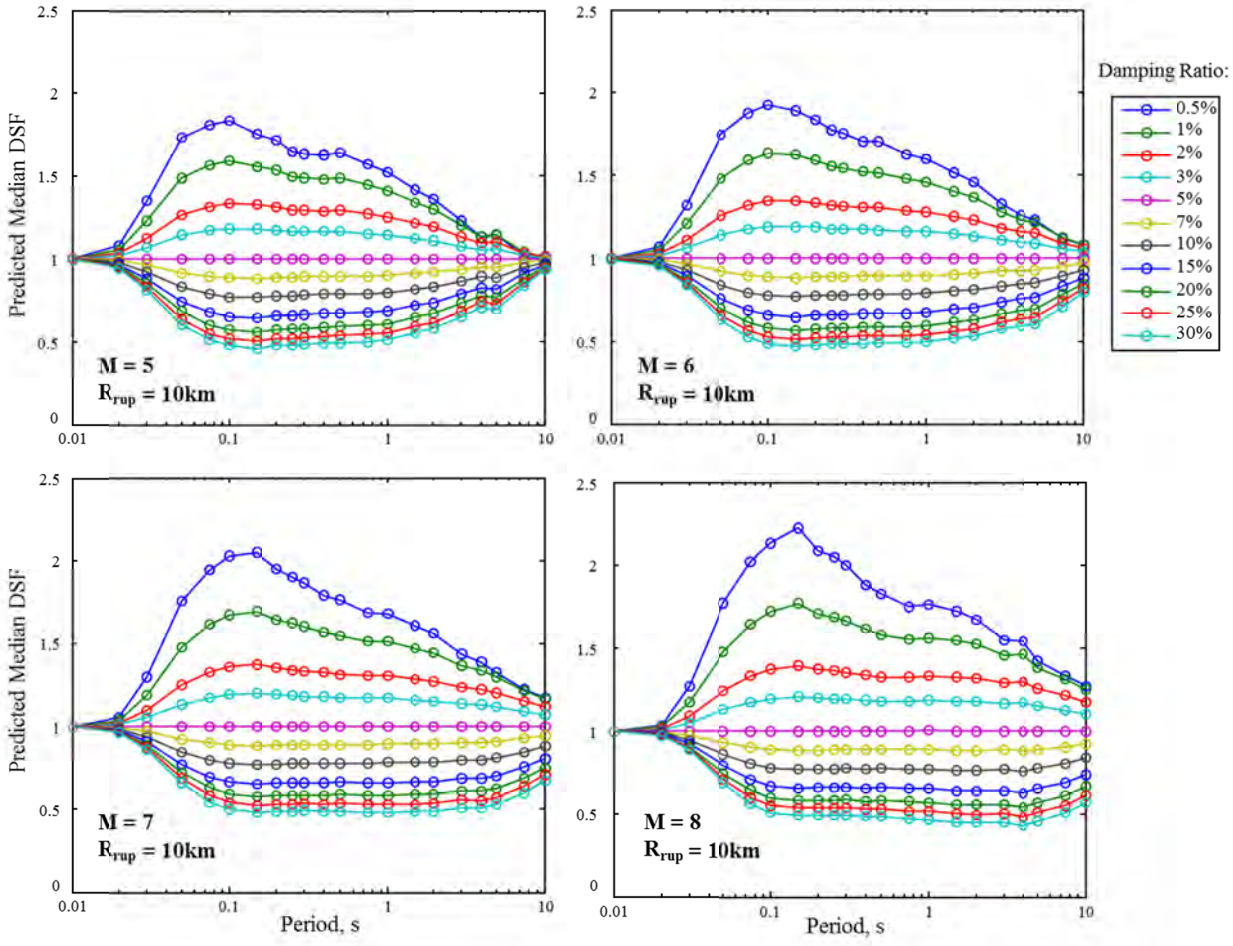

Figure 6.6 Predicted median *DSF* for the vertical component.

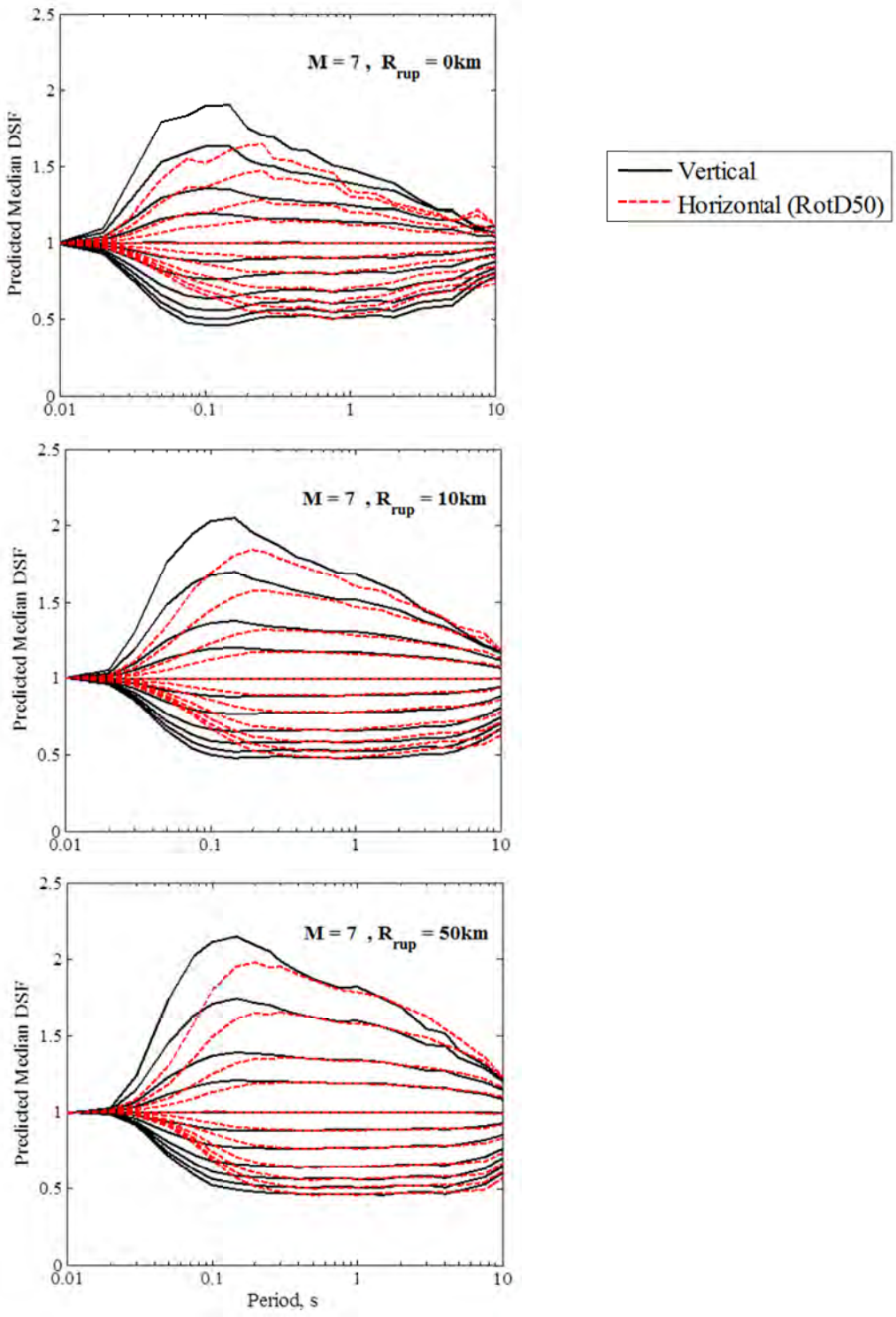

Figure 6.7 **Comparison between predicted *DSF* for the vertical and the horizontal components at M = 7 and R_{rup} = 0, 10, 50 km.**

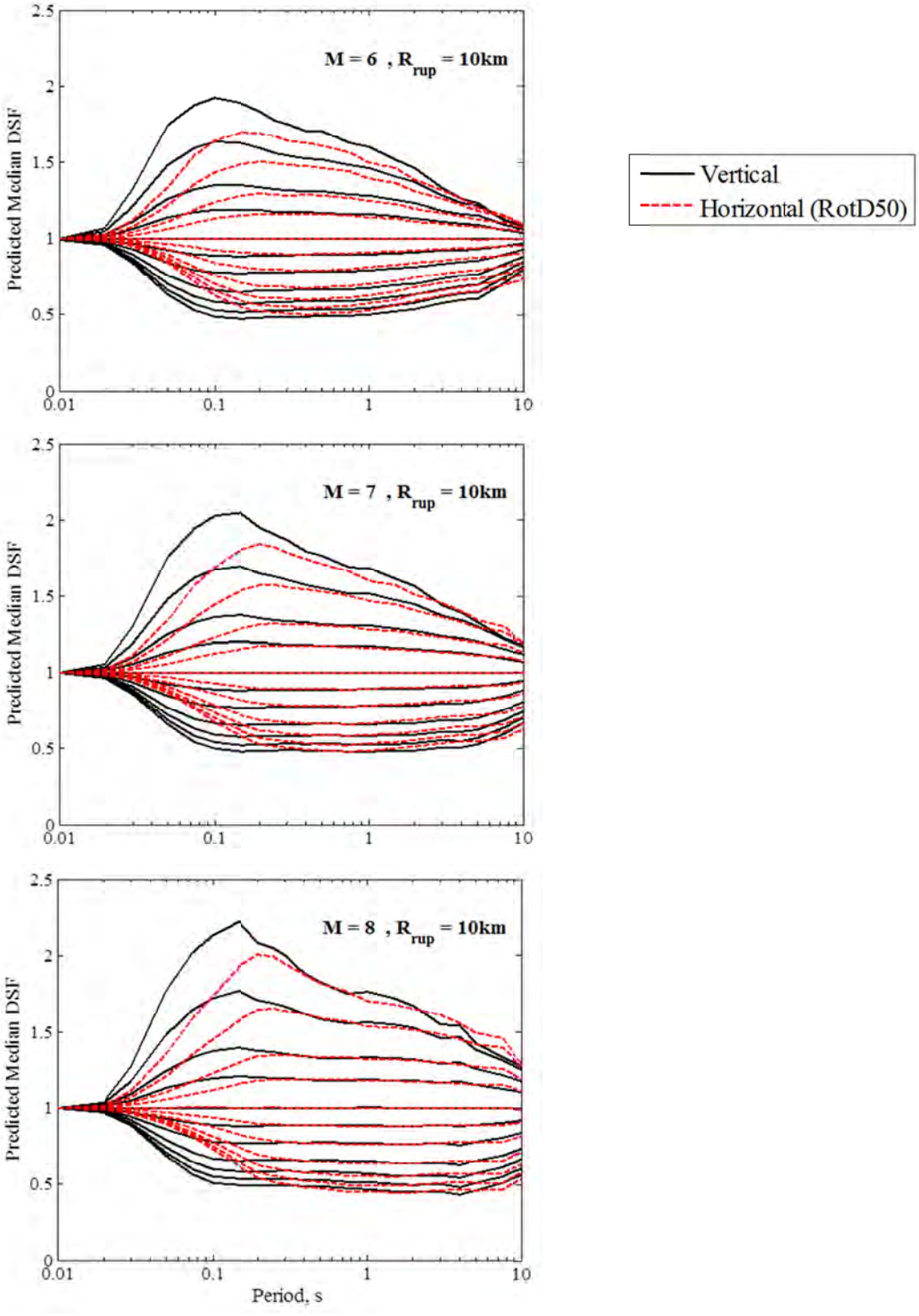

Figure 6.8 **Comparison between predicted *DSF* for the vertical and the horizontal components at M = 6, 7, 8 and R_{rup} = 10 km.**

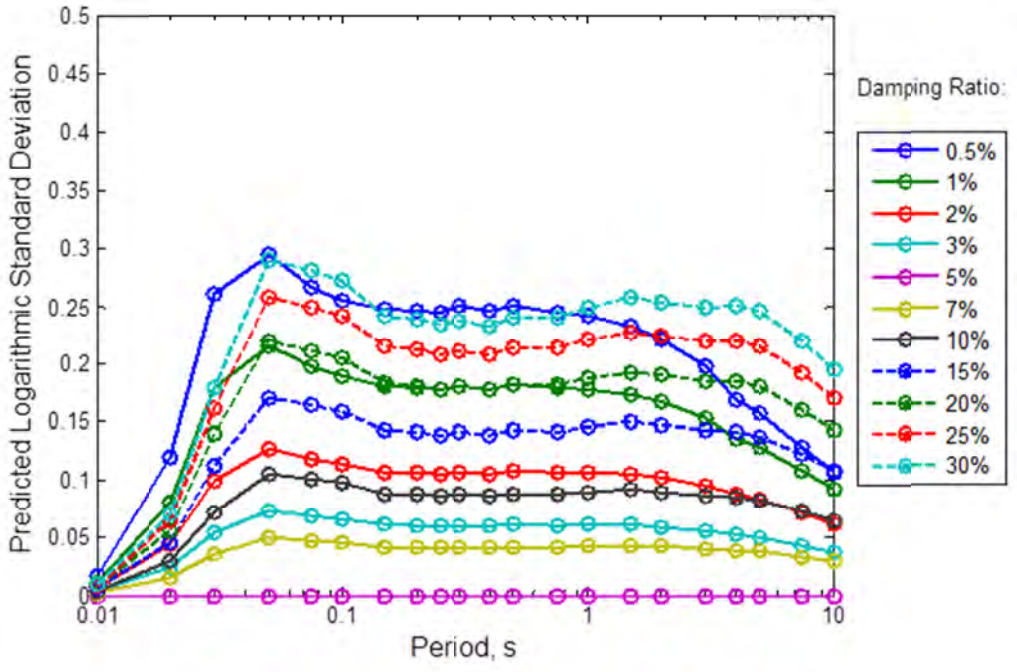

Figure 6.9 Predicted logarithmic standard deviation for the vertical component.

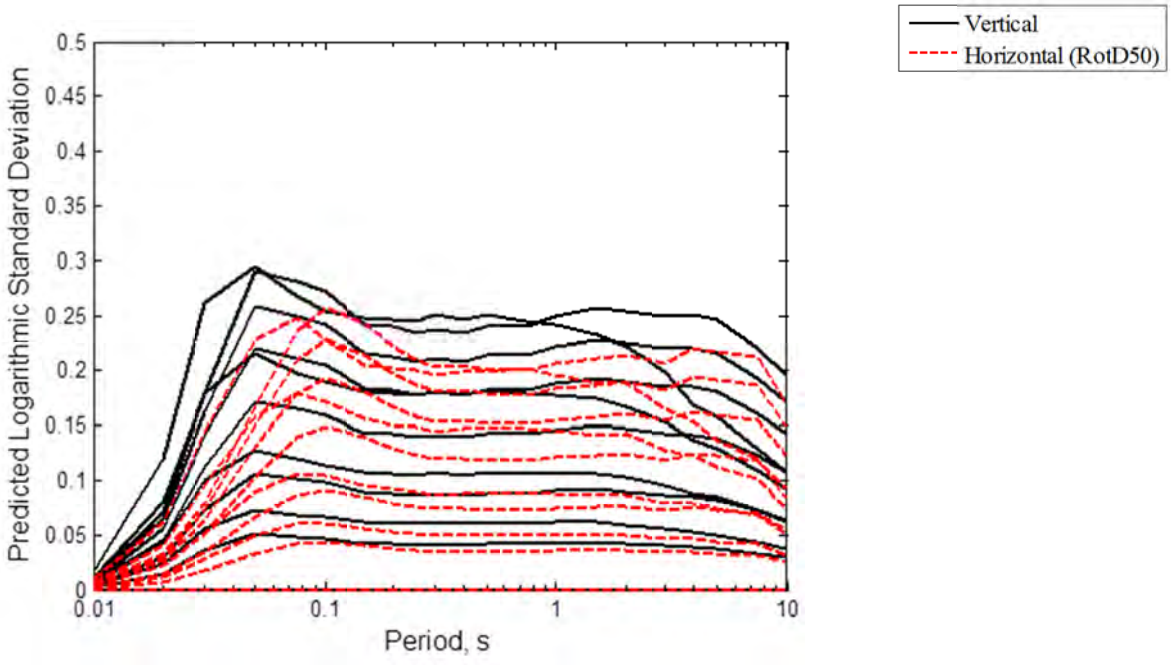

Figure 6.10 Comparison between the predicted standard deviation of the vertical and the horizontal components.

7 Conclusions

The new NGA-West2 database of recorded ground motions was used to develop a model for damping scaling factor (*DSF*), which can be used to scale *PSA* values predicted by GMPEs at a 5% damping ratio to *PSA* values at damping ratios other than 5%. A summary of the existing damping models was provided, and the general trends of the *DSF* with potential predictor variables (i.e., damping ratio, spectral period, duration, earthquake magnitude, source-to-site distance, and site conditions) were examined. In addition to the damping ratio and the spectral period, the predictor variables in the proposed *DSF* model are magnitude and distance. Duration is a variable that strongly influences *DSF*, however, since duration is correlated with magnitude and distance, most of the trend with duration was captured by the inclusion of magnitude and distance in the model. We found that the regression coefficients and the standard deviation have systematic patterns with the damping ratio. This allowed direct inclusion of the damping ratio in the model. The final form of the model is presented in Equations (4.8) and (4.9). Damping scaling models were derived for both horizontal (RotD50) and vertical components of ground motion with the estimated model parameters given at the 21 NGA periods in Tables 4.1 and 6.1. Appendix C provides the model coefficients for the GMRotI50 component. The damping scaling models in this study were developed based on the observed spectral ordinates; therefore, they are independent of any specific GMPE for *PSA*. The damping scaling models for horizontal and vertical components developed in this study are applicable to shallow crustal earthquakes in active tectonic regions for periods ranging from 0.01 to 10 sec, damping ratios from 0.5 to 30%, a magnitude range of 4.5 to 8.0, and distances of less than 200 km.

REFERENCES

Abrahamson NA, Silva WJ (1996). *Empirical Ground Motion Models*, Section 4: *Spectral Scaling for Other Damping Values*, Report to Brookhaven National Laboratory.

Abrahamson NA, Silva WJ (1996). *Empirical ground motion models*, *Section 5: Empirical model for duration of strong ground motion*, Report to Brookhaven National Laboratory.

Akkar S, Bommer J (2007). Prediction of elastic displacement response spectra in Europe and the Middle East, *Earthq. Engrg. Struct. Dyn.*, 36:1275–1301.

Ancheta T, Darragh R, Silva W, Abrahamson N, Atkinson G, Boore D, Bozorgnia Y, Campbell K, Chiou B, Graves R, Idriss IM, Stewart J, Shantz T, Youngs R (2012). PEER NGA-West2 Database: A database of ground motions recorded in shallow crustal earthquakes in active tectonic regimes. Abstract submitted to the *15th World Conference on Earthquake Engineering*, Lisbon, Portugal.

Applied Technology Council (2010). Modeling and acceptance criteria for seismic design and analysis of tall buildings*, ATC72-1*, Redwood City, CA.

Ashour SA (1987). *Elastic Seismic Response of Buildings with Supplemental Damping*, Ph.D. Dissertation, Department of Civil Engineering, University of Michigan, Ann Arbor, MI.

Atkinson GM, Pierre JR (2004). Ground-motion response spectra in eastern North America for different critical damping values*, Seismo. Res. Lett.*, 75:541-545.

Berge-Thierry C, Cotton F, Scotti O, Griot-Pommera DA, Fukushima Y (2003). New empirical response spectral attenuation laws for moderate European earthquakes, *J. Earthq. Engrg.*, **7**:193–222.

Bommer J, Mendis R (2005). Scaling of spectral displacement ordinates with damping ratios, *Earthq. Engrg. Struct. Dyn.*, 34:145–165.

Bommer J, Elnashai AS, Chlimintzas GO, Lee D (1998). Review and development of response spectra for displacement-based design, *ESEE Research Report No. 98-3*, Imperial College London.

Bommer J, Elnashai AS, Weir AG (2000). Compatible acceleration and displacement spectra for seismic design codes, *Proc., 12th World Conf. on Earthquake Engineering*, Auckland, New Zealand, New Zealand Society for Earthquake Engineering, Inc., Wellington, New Zealand, Paper No. 207.

Boore DM (2010). Orientation-independent, non geometric-mean measures of seismic intensity from two horizontal components of motion, *Bull. Seismo. Soc. Am.*, 100:1830–1835.

Boore DM, Joyner WB, Fumal TE (1993). Estimation of response spectra and peak accelerations from western North American earthquakes: an interim report, *US Geological Survey Open-File Report 93-509*, Menlo Park, CA.

Boore DM, Watson-Lamprey J, Abrahamson NA (2006). Orientation-independent measures of ground motion, *Bull. Seismo. Soc. Am.*, 96:1502–1511.

Bozorgnia Y, Bertero VV (eds.) (2004). *Earthquake Engineering: From Engineering Seismology to Performance-Based Engineering*, CRC Press, Boca Raton, FL.

Bozorgnia Y, Campbell KW (2004). Engineering characterization of ground motion, In: *Earthquake Engineering: From Engineering Seismology to Performance-Based Engineering*, Y. Bozorgnia and V.V. Bertero (eds.), CRC Press, Boca Raton, FL.

Bozorgnia, Y, Abrahamson, NA, Campbell, KW, Rowshandel, B., Shantz, T (2012). NGA-West2: A comprehensive research program to update ground motion prediction equations for shallow crustal earthquakes in active tectonic regions*, Proc., 15th World Conf. on Earthquake Engineering*, Lisbon, Portugal.

Cameron WI, Green I (2007). Damping correction factors for horizontal ground-motion response spectra, *Bull. Seismo. Soc. Am.*, 97:934–960.

California Department of Transportation (Caltrans) (2001). *Seismic Design Criteria Version 1.2*., Sacramento, CA.

Campbell KW, Bozorgnia Y (2008). NGA ground motion model for the geometric mean horizontal component of PGA, PGV, PGD and 5% damped linear elastic response spectra for periods ranging from 0.01 to 10 s, *Earthq. Spectra,* 24:139–171.

Chopra AK (2012). *Dynamics of Structures: Theory and Applications to Earthquake Engineering,* 4th ed., Prentice Hall: Upper Saddle River, NJ.

Eurocode 8 (2004). *Design of Structures for Earthquake Resistance—Part 1: General Rules, Seismic Actions and Rules for Buildings*, EN 1998-1: 2004. Comite Europeen de Normalisation, Brussels.

Faccioli E, Paolucci R, Rey J (2004). Displacement spectra for long periods, *Earthq. Spectra*, 20:347–376.

Federal Emergency Management Agency (1997). *Guidelines for Seismic Rehabilitation of Buildings, FEMA-273,* Washington, DC.

Federal Emergency Management Agency (1998). *1997 NEHRP Provisions for Seismic Regulations for New Buildings and Other Structures, FEMA-302,* Washington, DC.

Federal Emergency Management Agency (2003): *Recommended Provisions for Seismic Regulations for New Buildings and Other Structures*, *FEMA 450*, Building Seismic Safety Council, Washington, D.C.

Hatzigeorgiou GD (2010). Damping modification factors for SDOF systems subjected to near-fault, far-fault and artificial earthquakes, *Earthq. Engrg. Struct. Dyn.*, 39:1239-1258.

International Conference of Building Officials (1991). *Uniform Building Code*, Whittier, CA.

International Conference of Building Officials (1997). *Uniform Building Code*, Whittier, CA.

International Building Code (1999): International Code Conference, Final draft, ICC, Birmingham, AL.

Idriss IM (1993). Procedures for selecting earthquake ground motions at rock sites, *Report NIST GCR 93–625*, National Institute of Standards and Technology, Washington, D.E.

Iwan, WD, Gates, NC (1979). Estimating earthquake response of simple hysteretic structures, ASCE, *J. Engrg. Mech. Div.*, **94**, EM3, 391–405.

Kawashima K, Aizawa K (1986). Modification of earthquake response spectra with respect to damping ratio, *Proceedings of the 3rd US National Conference on Earthquake Engineering*, Charleston, South Caroline, Vol. 2, pp. 1107–1116.

Kempton JJ, Stewart JP (2006). Prediction equations for significant duration of earthquake ground motions considering site and near-source effects, *Earthq. Spectra*, 22:985–1013.

Lin YY, Chang KC (2003). Study on damping reduction factor for buildings under earthquake ground motions, ASCE, *J. Struct. Engrg.*, 129:206–214.

Lin YY, Chang KC (2004). Effects of site classes on damping reduction factors, ASCE, *J. Struct. Engrg.*,:1667–1675.

Lin YY, Miranda E, Chang KC (2005). Evaluation of damping reduction factors for estimating elastic response of structures with high damping, *Earthq. Engrg. Struct. Dyn.*, 34:1427–1443.

Malhotra PK (2006). Smooth spectra of horizontal and vertical ground motions, *Bulletin of the Seismological Society of America*, 96: 506-518.

McGuire RK, Silva WJ, Costantino CJ (2001). Technical basis for revision of regulatory guidance on design ground motions: Hazard- and risk-consistent ground motion spectra guidelines (Section 4.9: Estimation of spectra for other dampings), *Report, NUREG/CR-6728*. Prepared for Division of Engineering Technology, Office of Nuclear Regulatory Research, U.S. Nuclear Regulatory Commission, Washington, DC.

Naeim F, Kircher CA (2001). On the damping adjustment factors for earthquake response spectra, *The Structural Design of Tall Buildings,* 10:361-369.

Newmark NM, Hall WJ (1982). *Earthquake Spectra and Design*, Earthquake Engineering Research Institute, Berkeley, CA.

Power M, Chiou B, Abrahamson NA, Roblee C, Bozorgnia Y, Shantz, T (2008). An introduction to NGA, *Earthq. Spectra*, 24:3–21.

Priestley MJN (2003). *Myths and Fallacies in Earthquake Engineering, Revisited*, The Mallet Milne Lecture, IUSS Press, Istituto Universitario di Studi Superiori di Pavia, Pavia, Italy.

Ramirez OM, Constantinou MC, Kircher CA, Whittaker AS, Johnson MW, Gomez JD, Chrysostomou CZ (2000). Development and evaluation of simplified procedures for analysis and design of buildings with passive energy dissipation systems, *Report No: MCEER-00-0010*, Multidisciplinary Center for Earthquake Engineering Research, University of New York, Buffalo, NY.

Ramirez OM, Constantinou MC, Whittaker AS, Kircher CA, Chrysostomou CZ (2002). Elastic and inelastic seismic response of buildings with damping systems, *Earthq. Spectra*, 18:531–547.

Regulatory Guide 1.61 Revision 1 (2007). Damping values for seismic design of nuclear power plants, U.S. Nuclear Regulatory Commission, Washington, DC.

Rosenblueth E (1980). Characteristics of earthquakes, In: *Design of Earthquake Resistant Structures*, E. Rosenblueth (ed.), John Wiley, New York, NY.

Ruiz-Garcia J, Miranda E (2003). Inelastic displacement ratios for evaluation of existing structures, *Earthq. Engrg. Struct. Dyn.*, 32:1237–1258.

Structural Engineers Association of California (1990). *Recommended Lateral Force Requirements and Commentary*, 'Blue Book', 5th ed., SEAOC, Sacramento, CA.

Stafford PJ, Mendis R, Bommer, JJ (2008). Dependence of damping correction factors for response spectra on duration and numbers of cycles, ASCE, *J Struct. Engrg.*, **134**:1364–1373.

Pacific Earthquake Engineering Research Center (2010). Guidelines for performance-based seismic design of tall buildings*, PEER Report 2010/05*, prepared by the Tall Building Initiative Guidelines Working Group, Pacific Earthquake Engineering Research Center, University of California, Berkeley, CA.

Tolis SV, Faccioli E (1999). Displacement design spectra, *J. Earthq. Engrg.*, 3:107–125.

Trifunac MD, Lee VW (1989). Empirical models for scaling pseudo relative velocity spectra of strong earthquake accelerations in terms of magnitude, distance, site intensity and recording site conditions, *Soil Dyn. Earthq. Engrg.*, 8:126 –144.

Vanmarcke EH (1976). Structural response to earthquakes, in *Seismic Risk and Engineering Decisions*, C. Lomnitz and E. Rosenblueth (eds.), Elsevier Publishing Co., Amsterdam, London, New York.

Wu J, Hanson RD (1989). Study of inelastic spectra with high damping, ASCE, *J Struct. Engrg.*, 115:1412–1431.

Appendix A: Summary of Damping Scaling Models in Literature[1]

[1] All references to Tables and Figures in this appendix correspond to those in the respective papers.

	Relation		Model	Notes
GMPEs for $\beta \neq 5\%$	Akkar and Bommer [2007]		Geometric mean elastic spectral displacement (*SD*): $\log[SD(T,\beta)] =$ $b_1 + b_2\mathbf{M} + b_3\mathbf{M}^2 + (b_4 + b_5\mathbf{M})log\sqrt{R_{jb}^2 + b_6^2} + b_7S_S + b_8S_A + b_9F_N + b_{10}F_R$ Regression coefficients b_i, $i = 1, \ldots, 10$, and standard deviations are given in tables at specified periods for damping ratios of 2, 5, 10, 20, and 30%	• **Applicability:** Periods up to 4 sec Magnitudes between 5 and 7.6 Distances up to 100 km • **Database:** 532 accelerograms from Europe and the Middle East • Acknowledge dependence of DSF on magnitude, distance, and therefore duration.
	(See Bommer and Mendis, 2005 for a review and comparison of these relations)	Berge-Thierry et al. [2003]	GMPE for pseudo acceleration response spectrum (*PSA*) is provided for damping ratios of 5, 7, 10, and 20%	• **Applicability:** Periods up to 10 sec Magnitudes between 4 and 7.9 Distances up to 330 km • **Database:** 965 horizontal and 485 vertical components from Europe (83%) and California (17%)
		Bommer et al. [1998]	GMPE for relative displacement response spectrum (*SD*) is provided for damping ratios of 5, 10, 15, 20, 25, and 30%	• **Applicability:** Magnitudes between 5.5 and 7.9 Distances up to 260 km • **Database:** 183 records from Europe
		Boore et al. [1993]	GMPE for pseudo velocity response spectrum (*PSV*) is provided for damping ratios of 5, 10, and 20%	• **Applicability:** Periods up to 2 sec Magnitudes between 5.3 and 7.7 Distances up to 100 km • **Database:** 271 records from western North America
		Trifunac and Lee [1989]	GMPEs for pseudo velocity response spectrum (*PSV*) are provided with regression coefficients tabulated at specified periods for damping ratios of 0, 2, 5, 10, and 20%	• **Applicability:** Periods between 0.04 and 14 sec • **Database:** 438 records from 104 earthquakes, mostly from California up to the year 1981

GMPEs for $\beta \neq 5\%$	Faccioli et al. [2004]	Propose a model for the displacement spectra. Consider damping ratios of 0 and 5% only.	• **Applicability:** Periods between 0.01 and 10 sec Magnitudes between 5.4 and 7.6 Distances up to 50 km • **Database:** 253 records (3 components each) from Taiwan, Japan, Italy, and Greece • Conclude that the influence of damping ratio is limited at long periods

	Relation	Model	Predictor Variables	Notes
Random Vibration Methods	White-Noise Assumption	$DSF \cong \sqrt{\frac{5}{\beta}}$	1. Damping ratio, β	• A white-noise process is wide-band and stationary, which is not necessarily true for a real earthquake ground motion
	Recommended method by McGuire et al. [2001] (NUREG/CR-6728)	**<u>If $1 \leq f < 5$ Hz :</u>** Using Rosenblueth [1980] $SA(f,\beta)$ $= SA(f,0.05)\left[\frac{1+4.9\beta fD}{1+4.9\times 0.05fD}\right]^{-0.41}$ **<u>If $f \geq 5$ Hz :</u>** Using Vanmarcke [1976] $SA(f,\beta)$ $= \left\{PGA^2 + [SA(f,0.05)^2 - PGA^2\,]\left[\frac{1+4.9\beta fD}{1+4.9\times 0.05fD}\right]^{-0.82}\right\}^{0.5}$	1. Damping ratio, β 2. Frequency, f 3. Duration, D (distance dependent; use Abrahamson and Silva 1997 model for Western U.S.; and Atkinson and Boore 1997 model for Central Eastern U.S.)	• **Applicability:** Horizontal and vertical components $\beta = 0.5 - 20\%$ • The most theoretically consistent method

	Relation	Model	Predictor Variables	Notes
Empirical *DSF* Models	Hatzigeorgiou [2010]	$DSF = 1 + (\beta - 5)[1 + b_1 \ln(\beta) + b_2 (\ln(\beta))^2][b_3 + b_4 \ln(T) + b_5(\ln(T))^2]$ Regression coefficients b_i, $i = 1, \ldots, 5$, are tabulated for different soil conditions for acceleration, velocity and displacement response spectra.	1. Damping ratio, β 2. Period, T 3. Soil conditions	• **Applicability:** $T = 0.1 - 5$ sec $\beta = 0.5 - 50\%$ Magnitudes between 5–8 Distances up to 60 km • **Database:** 100 far-fault records, 110 near-fault records, 100 artificial accelerograms • States that fault distance has no impact on DSF • Performs nonlinear regression analysis test on about 8000 mathematical equations (i.e., DSF models)
	Stafford et al. [2008]	$DSF = 1 - \frac{b_1 + b_2 \ln(\beta) + b_3 \ln(\beta)^2}{1 + \exp\{-[\ln(x) + b_4]/b_5\}}$ x is a measure of duration and can be any of the following parameters: D_{5-75} : significant duration D_{5-95} : significant duration $N_{rr}(2.0)$: number of equivalent load cycles Regression coefficients b_i, $i = 1, \ldots, 5$, and standard deviations are given in Table 2 for relative displacement spectra	1. Damping ratio, β 2. Duration, x Data are averaged over periods of 1.5 to 3 sec.	• **Applicability:** $T = 1.5 - 3$ sec $\beta = 2 - 55\%$ Magnitudes between 4.2–7.9 Distances up to 300 km • **Database:** 1699 records from NGA database excluding Chi-Chi and records with missing metadata • Confirm and quantify the strong dependence on Duration, which is strongly related to Magnitude. Mild dependence on Period is reported. • A modified logistic model is used in modeling.
	Malhotra [2006]	$DSF = b_0 + b_1 ln\beta + b_2 (ln\beta)^2$	1. Damping ratio, β 2. Period, T (model coefficients are given for the acceleration	

			constant, velocity-constant, and displacement-constant regions of the horizontal and vertical spectra	
Empirical *DSF* Models	Cameron and Green [2007] (Built on the work of Bommer and Mendis [2005])	Median and logarithmic standard deviation of *DSF* (for *PSA* or *SD*) are **tabulated** for different magnitude and distance bins: - $\beta \geq 2\%$, WUS, Rock (Table 7) - $\beta \geq 2\%$, WUS, Soil (Table 8) - $\beta \geq 2\%$, CEUS, Rock (Table 9) - $\beta \geq 2\%$, CEUS, Soil (Table 10) - $\beta = 1\%$, WUS (Table 11) - $\beta = 1\%$, CEUS (Table 12)	1. Damping ratio, β 2. Period, T 3. Magnitude, **M** 4. Tectonic setting (WUS / CEUS) 5. Rock / Soil 6. Distance, if $\beta = 1\%$	• **Applicability:** WUS and CEUS horizontal motions $T = 0.05 - 10$ sec $\beta = 1 - 50\%$ Magnitude bins: 5–6, 6–7, 7+ Distance bins: 0–50, 50–200 km • **Database:** 676 recorded and 592 simulated motions taken from McGuire et al. [2001]. • **Analysis Approach:** Use analytical response to a sinusoidal excitation to show dependence on **frequency content** and **duration** of motion**.** Use point-source models to show that frequency and duration depend on **Magnitude, Distance** and **Tectonic Setting**. *DSF* is then calculated empirically and tabulated.
	Bommer and Mendis [2005]	This is a review paper. Considering only $\beta > 5\%$. Results are **plotted.** • **Existing models reviewed in this paper:** - Building codes (see Figure 4) - GMPEs (see Table 1) - Simulation based approach - Newmark and Hall (1982), Lin and Chang (2003), Priestley (2003), Wu and Hanson (1989), etc.	• **General trends:** - DSF is weakly dependent on T. - DSF decreases as magnitude increases. - DSF decreases as distance increases. - DSF increases for softer sites (to a lesser extent). → DSF decreases as duration increases. • Conclude that duration is an important factor. • State that there is significant disagreement amongst proposed models.	

<table>
<tr><td rowspan="2">Empirical DSF Models</td><td>Lin et al. [2005]</td><td colspan="3">This is a review paper that compares/evaluates existing models against a database of recorded motions.

• Introduce an error term:
Mean: $\bar{E}(T,\beta) = \frac{1}{n}\sum_{i=1}^{n}\left(DSF \times \frac{SD_{5\%}}{SD_{\beta}}\right)$
Dispersion: $\sigma(T,\beta)$
DSF: predicted from an existing model
$SD_{5\%}$, SD_{β}: calculated from the database
It is desired for $\bar{E}(T,\beta)$ and $\sigma(T,\beta)$ to approach 1 and 0, respectively.

• Review and evaluate 5 models (see Figure 2):
- Newmark and Hall [1982]
- Ashour [1987]
- Wu and Hanson [1989]
- Ramirez et al. [2000; 2002]
- Lin and Chang [2003]</td><td>• Database:
216 records from 12 earthquakes in California (same as Ruiz-Garcia and Miranda [2003])
$5.7 \le M_S \le 7.7$
$PGA > 45$ gal
$V_{S30} > 180$ m/sec (Site classes B, C, D)

$\beta = 2 - 50\%$
$T = 0.1 - 6$ sec

• Conclusions:
$\bar{E}(T,\beta)$ increases as β increases.
Maximum $\bar{E}(T,\beta)$ occurs at short T.
Newmark and Hall is the smallest at short T.
Ramirez et al. model is greater than others.
Variation with β is similar among 5 models.
Variation with T can be very different.</td></tr>
<tr><td>Lin and Chang [2004]
(Site effects)</td><td>Mean DSF for SD (or PSA):
$B_d = 1 - \frac{aT^b}{(T+1)^c}$
a, b and c: functions of site class and β

Mean DSF for SA:
$B_a = \begin{cases} 1 & if\ T = 0^* \\ linear\ interpolation & \\ d + e^T & if\ T \ge 0.15^{**} or\ 0.2^{***} \end{cases}$
* Site classes AB, C or D
** Site class AB
*** Site classes C or D
d and e: functions of site class and β

Dispersion of DSF:
C.O.V is tabulated and plotted</td><td>1. Damping ratio, β
2. Period, T
3. Site class (can be neglected if 5% error is acceptable in structural design and $\beta < 20\%$, or if 10% error is acceptable in structural design and $\beta < 50\%$)</td><td>• Applicability:
$T = 0.05 - 6$ sec
$\beta = 2 - 50\%$
Magnitudes greater than 5.4
• Database:
1037 records from 102 earthquakes (from U.S. PEER database)
$V_{S30} > 180$ m/sec
A and B: $V_{S30} > 760$ m/sec
C: 360-760 m/sec
D: 180-360 m/sec
$PGA > 25$ gal
• Conclude that B_a is more sensitive to site class than B_d.</td></tr>
</table>

Empirical *DSF* Models	Lin and Chang [2003]	*DSF* is calculated and **tabulated** for the mean spectrum (Table 2, Figure 3) and for the mean+1σ spectrum (Table 3, Figure 4). This is done separately for displacement, velocity and acceleration. $$DSF = 1 - \frac{aT^{0.30}}{(T+1)^{0.65}}$$ $$a = 1.303 + 0.436\ln(\beta)$$ The above equation is given in Lin and Chang, 2004 (without site effects).	1. Damping ratio, β 2. Period, T	• **Applicability:** Active seismic regions $\beta = 2 - 50\%$ $T = 0.01 - 10$ sec Magnitudes between 5.5 and 7.5 Distances up to 180 km Effects of soft soil and near-fault are not considered • **Database:** McGuire et al. (2001) database, 1053 records from 102 earthquakes 25gal$< PGA <$1.6g • **Absolute vs. Pseudo spectral acceleration:** State that in building codes *DSF* is derived for spectral displacement (*SD*), but is used to reduce design forces. This is inconsistent and un-conservative especially for $\beta > 10\%$ and $T > 0.15$ sec. In forced-based design, *DSF* must be derived from absolute spectral acceleration (*SA*). In displacement-based design, DSF must be derived from pseudo spectral acceleration (*PSA*). Use of *DSF* derived from (*PSA*) is acceptable if substitute structure method is used.

Empirical *DSF* Models	Atkinson and Pierre [2004]	Average and standard deviation of *DSF* are calculated and **tabulated** (see Table 1 and Figure 5). • Acknowledge the importance of Duration. Observe weak dependence on magnitude and distance in general, but strong dependence on distance at low β. • Observe weak dependence on T for β>5%, strong dependence on T for β<3%.	1. Damping ratio, β 2. Frequency, f (results are averaged over magnitude and distance)	• **Applicability:** Eastern-North America (including Central Eastern U.S.) $\beta = 1 - 15\%$ $T = 0.05 - 2$ sec Magnitudes between 4 and 7.25 Distances between 10-500 km $360 < V_{S30} < 760$ m/sec • **Database:** Use stochastic source-based simulations (Atkinson and Boore, 1995)
	Priestley [2003] (Near-fault) (as given in Cameron and Green [2007])	$DSF = \left(\frac{10}{5+\beta}\right)^{0.25}$	1. Damping ratio, β	• **Applicability:** Near-fault $\beta > 5\%$ $T = 0.2 - 6$ sec • Model is similar to that of Eurocode 8. The power is reduced from 0.5 to 0.25 based on the fact that near-fault velocity pulses may reduce effectiveness of the system damping.
	Ramirez et al. [2000; 2002] (as given in Lin et al. [2005)]	Bilinear function of T for $\beta \leq 50\%$ Trilinear function of T for $\beta > 50\%$ (see Figure 3 of Lin et al., 2005) (Implemented in NEHRP 2000 for design of buildings with damping systems)	1. Damping ratio, β 2. Period, T	• **Applicability:** Elastic and inelastic response spectra $\beta = 2 - 100\%$ $T < 4$ sec Magnitudes greater than 6.5 Distances between 10–20 km • **Database:** 20 horizontal components from 10 earthquakes
	McGuire et al. [2001] (NUREG/CR-6728)	Section 4.9 of this report (estimation of spectra for other dampings) reviews three empirical methods: Abrahamson and Silva, 1996; Idriss, 1993; Newmark and Hall, 1978.		

Empirical *DSF* Models	Naeim and Kircher [2001]	Mean and standard deviation of $1/DSF$ are **tabulated**. Review and evaluate existing models with an emphasis on U.S.-based building codes.	1. Damping ratio, β 2. Period, T (weak influence)	• **Applicability:** $\beta = 2, 10, 20\%$ $T = 0.1 - 4$ sec Magnitudes between 5 and 7.5 Distances between 10–20 km • **Database:** 1047 horizontal components of ground motions (1933 to 1994) from North American, Alaskan, and Hawaiian Island events with $PGA \geq 0.05$g. • Observe no significant dependence on T (due to large scatter of data), contrary to existing studies. • Conclude that building code values are accurate for lower β and slightly conservative for $\beta \geq 20\%$.
	Tolis and Faccioli, 1999	$DSF = \sqrt{\frac{15}{10+\beta}}$	1. Damping ratio, β	• **Applicability:** $\beta = 5 - 50\%$ • **Database:** 1995 Kobe earthquake
	Abrahamson and Silva [1996] (reviewed in McGuire et al. [2001], NUREG/CR-6728)	$\ln\left(\frac{SA_\beta}{SA_{5\%}}\right) = \begin{cases} c_1 & \text{if} \quad f > 1.43\ Hz \\ c_1 + g_2(\mathbf{M}-6) + g_3(8.5-\mathbf{M})^2 & \text{if} \quad f < 1.43 Hz \end{cases}$ Regression coefficients c_1, g_2, g_3 are given in tables for specified f and β values.	1. Damping ratio, β 2. Frequency, f 3. Magnitude, **M**	• **Applicability:** Vertical and horizontal ground motions $\beta = 0.5 - 20\%$ $T = 0.02 - 5$ sec

Empirical *DSF* Models	Idriss [1993] (as given in McGuire et al. [2001], NUREG/CR-6728)	$\left(\frac{SA_\beta}{SA_{5\%}}\right) = \begin{cases} a_1 - b_1 \ln(\beta) & \beta \le 5\% \\ a_2 - b_2 \ln(\beta) & \beta > 5\% \end{cases}$ Regression coefficients a_1, a_2, b_1, b_2 are functions of T and are given in Table 4-9 of McGuire et al. [2001].	1. Damping ratio, β 2. Period, T	• **Applicability:** Horizontal ground motion $\beta = 1 - 15\%$ $T = 0.03 - 5$ sec • **Database:** 1971 San Fernando 1979 Imperial Valley
	Wu and Hanson [1989] (reviewed in Lin et al. [2005] and in Bommer and Mendis [2005])	$DSF = \frac{\psi(\beta, T)}{\psi(5\%, T)}$ $\psi = \begin{cases} -0.349 \ln(0.0959\beta) & if\ T = 0.1\text{s} \\ -0.547 \ln(0.417\beta) & if\ T = 0.5\text{s} \\ -0.471 \ln(0.524\beta) & if\ 0.5 < T < 3\text{s} \\ -0.478 \ln(0.475\beta) & if\ T = 3\text{s} \\ -0.291 \ln(0.0473\beta) & if\ T = 10\text{s} \end{cases}$ (for $\mu = 1.0$)	1. Damping ratio, β 2. Period, T	• **Applicability:** Inelastic response spectra with high damping ratios. Ductility ratio: $1 < \mu < 6$ $\beta = 10 - 50\%$ $T = 0.1 - 10$ sec • **Database:** 10 records
	Ashour [1987] (as given in Lin et al. [2005])	$DSF = \sqrt{\frac{0.05(1 - e^{-\alpha\beta})}{\beta(1 - e^{-0.05\alpha})}}$ $\alpha = 18$ or 65 (upper/lower bounds) ($\alpha = 18$ in NEHRP 1994)	1. Damping ratio, β	• **Applicability:** $\beta = 0 - 150\%$ $T = 0.5 - 3$ sec • **Database:** 3 real (1940 El Centro NS, 1952 Taft N69W, and 1975 Alameda Park) and 12 artificial records
	Newmark and Hall [1982] (reviewed in Cameron and Green [2007], Lin et al. [2005], McGuire et al. [2001], and Naeim and Kircher [2001])	$DSF_{median} = \begin{cases} 1.51 - 0.32 \ln(\beta) \\ 1.40 - 0.25 \ln(\beta) \\ 1.31 - 0.19 \ln(\beta) \end{cases}$ Corresponding to the constant acceleration, velocity, and displacement period ranges, roughly approximated as $0.125 < T < 0.6$ sec $0.6 < T < 4$ sec $4 < T < 10$ sec	1. Damping ratio, β 2. Periods, T 3. The exact period ranges vary depending on the peak ground acceleration (PGA), velocity (PGV), displacement (PGD), β, etc.	• **Applicability:** Active seismic regions $\beta = 0 - 20\%$ Magnitudes between 5.3 and 7.5 • **Database:** 28 records from 9 earthquakes prior to 1973 • In addition to the median, the relation is also given for the 84^{th} percentile.

	Relation	Model	Predictor Variables	Notes
Building Codes	Eurocode 8 [2004] (see Bommer and Mendis [2005, page 148]; see Akkar and Bommer [2007, page 1291])	$\left(\frac{10}{5+\beta}\right)^{0.5} \geq 0.55$ Original form (1994): $\sqrt{\frac{7}{2+\beta}}$	1. Damping ratio, β	$T = 0.2 - 6$ sec Unity at very low (i.e., 0 sec) and very high periods (i.e., 10 sec used in Bommer and Mendis [2005] is imposed. Should not apply to β resulting in $DSF < 0.55$. Records represent European strong ground motions with magnitudes between 4.0 and 7.5 and distances up to 200 km.
	NEHRP [2003] (FEMA 450) (see Table 13 of Cameron and Green [2007])	**Tabulated** for seismically isolated buildings and structures with damping devices.	For seismic isolation: (Table 13.3-1) 1. Damping ratio, β For damping devices: (Table 15.6-1) 1. Damping ratio, β 2. Period, T	
	Caltrans, 2001 (Reviewed in Bommer and Mendis [2005])	$\frac{1.5}{0.4\beta + 1} + 0.5$	1. Damping ratio, β	For $\beta = 5 - 10\%$ on bridges. Based on Kawashima and Aizawa, 1986 for absolute acceleration.
	U.S. codes that are based on Newmark and Hall [1982] and are reviewed in Naeim and Kircher [2001].	• SEAOC Blue Book [1990]: based on Newmark and Hall [1982] • 1991 UBC [ICBO 1991]: based on 1990 Blue Book **Tabulated** for base-isolated buildings (velocity domain) • ATC [1996], NEHRP/FEMA [1997]: Extension to both velocity and acceleration domains: **Tabulated** B_L and B_1 for long T, and B_S for short T. (B_L is for base-isolated buildings. B_S is for buildings with damper systems and for nonlinear pushover analysis using capacity-spectrum method). ATC-40 [1996] FEMA 273 [1997] • 1997 UBC (see ICBO [1997]), 2000 IBC (see ICC [1999]): Based on NEHRP1997 /FEMA 1998 (See Table 2 of Naeim and Kircher [2001], or Table II of Lin et al. [2005])		

Building Codes	UBC [1994] NEHRP, 1994	Based on Wu and Hanson [1989]. (See Table II of Lin et al. [2005]		
	1990 French code 1994 Spanish code	$\left(\frac{5}{\beta}\right)^{0.4}$	1. Damping ratio, β	
	1983 Portuguese 1984 Indian code	Graphically represent the acceleration spectrum at more than one damping ratios. (see Figure 4 of Bommer and Mendis [2005])		

Appendix B: Modeling Process for Damping Scaling Factor

The DSF model was built step-by-step by trying various functions of the key predictor variables influencing the damping scaling. We began with the simplest model for the *DSF*, and added terms as needed to eliminate any systematic pattern between the residuals and the predictor variables. This appendix describes the modeling process for the *DSF* from the simplest to the final model.

First, we calculated the DSF according to Equation (2.1) for the records with $R_{rup} < 50$ km. At each combination of the 21 specified periods and 11 damping ratios, the data were analyzed and the dependence of DSF on potential predictor variables (e.g., duration, magnitude, distance, and site conditions) was investigated (see Chapter 3). By visual inspection of the plotted data, we observed strong dependence of DSF on duration and magnitude (stronger at longer periods), weaker but noticeable dependence on distance, and negligible dependence on soil conditions (i.e., 30 m shear-wave velocity and sediment depths to the 1.0 and 2.5 km/sec shear-wave velocity horizons). A logarithmic dependence on duration and a possible linear or quadratic dependence on magnitude were observed. Intending to capture the dependence on duration with inclusion of magnitude and distance in the model, we regressed $\ln(DSF)$ on the predictor variables $\mathbf{M}$ and R_{rup} at specified T and β. Different functions of each predictor variable were added to the model one at a time and plots of the residuals versus each possible predictor variable (e.g., $\mathbf{M}$, R_{rup}, V_{S30}, and D_{5-75}) were examined as described below.

At each of the following steps, a summary of the observations and final conclusions from the analysis of residuals are provided. Only sample residual diagnostic plots for the RoTD50 component are shown in this appendix at selected periods and damping ratios and for selected predictor variables. (Sample residual plots for the final model are provided in Appendix D.) In the following, c_i, $i = 0,1, ...$, represent the "primary" regression coefficients (i.e., when regressing $\ln(DSF)$ on predictor variables at a specified T and β); b_i, $i = 0,1, ...$, represent the "secondary" regression coefficients (i.e., when regressing a primary coefficient on β at a specified T); ϵ represents the error term for $\ln(DSF)$; and ϵ_i represents the error term for c_i.

Step 0: $\ln(DSF) = c_0 + \epsilon$

We regressed $\ln(DSF)$ on a constant at specified values of T and β. Residual plots revealed an almost linear relationship with **M** and a possible break in the pattern (i.e., change of slope in the linear relationship) around magnitude of 7 (this is more pronounced at longer periods), a strong nonlinear relationship (possibly quadratic or logarithmic) with D_{5-75}, and a mild linear pattern with $\ln(R_{rup})$. Figures B.1-B.6 show example plots of residuals versus $\mathbf{M}, D_{5-75}$, and R_{rup} at selected periods and damping ratios. In these figures, a black line represents the average values of the residuals over equally spaced bins of data. In the subsequent steps, we tried to capture these observed patterns by inclusion of one or more of the predictor variables in the model (i.e., the residuals of the final model will not show any pattern with the potential predictor variables).

Step 1: $\ln(DSF) = c_0 + c_1\mathbf{M} + \epsilon$

In this model, we added a linear magnitude term. The residual plots showed almost no pattern with magnitude (see Figures B.7-B.8 for sample plots of residuals versus **M**). Additionally, the inclusion of the linear magnitude term reduced the dependence on duration significantly as was seen from the residual plots versus D_{5-75}. For example, compare Figures B.9 and B.10 with Figures B.3 and B.4 (the difference is more pronounced at $T = 7.5$ sec). Still, we saw a mild and almost logarithmic pattern with R_{rup} (see Figures B.11-B.12 for sample plots of residuals versus R_{rup}).

Step 2: $\ln(DSF) = c_0 + c_1\mathbf{M} + \mathrm{c}_2\mathbf{M}^2 + \epsilon$

We examined adding a quadratic magnitude term. However, the residual plots did not show significant improvements compared to the previous step. In the interest of keeping the model simple and avoiding unnecessary terms, we decided on a linear magnitude term in the final model. Inclusion of a shifted magnitude term, e.g., $(\mathbf{M} - 7)$, was also considered, but the residual plots did not show any obvious improvements.

Step 3: $\ln(DSF) = c_0 + c_1\mathbf{M} + \mathrm{c}_2\ln(R_{rup} + 1) + \epsilon$

We observed that the addition of a logarithmic function of R_{rup} reduced (not as much as the magnitude term) the remaining dependence on D_{5-75} (e.g., the pattern seen in Figures B.9-B.10). Also as expected, it eliminated the mild pattern seen with distance (e.g., the pattern seen in Figures B.11-B.12). Figures B.13-B.18 show sample plots of residuals versus $\mathbf{M}, D_{5-75}$, and R_{rup}. The $+1$ term is to ensure the model is stable and can be applied at very short distances. Other distance functions such as $\ln\left(\sqrt{R_{rup}^2 + c_3^2}\right)$ were also investigated; however, no significant improvement of residuals was observed.

Step 4: $\ln(DSF) = c_0 + c_1 \ln(D_{5-75}) + c_2 \ln(D_{5-75})^2 + \epsilon$

To obtain a better understanding of the data and the trends observed between DSF and other variables, we considered a function of duration as is given in this step. In general, the resulting residuals showed no pattern with duration, some pattern with magnitude at very long periods, and very weak pattern with distance. See Figures B.19-B.24 for sample plots of residuals versus $\mathbf{M}, D_{5-75}$, and R_{rup}. Because direct inclusion of duration in the model is not practical (e.g., a design engineer is not given the duration of motion) and since the model in Step 3 captures most of the dependence on duration, we discarded this model.

We selected the model in Step 3 and estimated the regression coefficients at specified values of T and β. The relations between the constant term, the coefficient of the magnitude term, and the coefficient of the distance term with β were examined next. c_0 was the coefficient with the strongest dependence on the damping ratio. Estimated values of c_0 and its 95% confidence intervals versus β are plotted in Figure B.25 at select periods.

Step 3-1: $c_0 = b_0 + b_1 \ln(\beta) + b_2(\ln(\beta))^2 + \epsilon_0$

At a specified T, the dependence of c_0 on the damping ratio can be captured by a quadratic function of $\ln(\beta)$. The coefficients b_0, b_1, and b_2 were estimated by performing regression on the 11 data points (corresponding to the 11 β values). Figure B.26 shows the fit of the resulting model at the same periods as in Figure B.25.

Step 3-2: $\ln(DSF) - b_1 \ln(\beta) - b_2(\ln(\beta))^2 = \mathrm{c}_0 + c_1\mathbf{M} + \mathrm{c}_2\ln(R_{rup} + 1) + \epsilon$

At specified values of T and β, the above regression was performed while b_1 and b_2 were assigned fixed values using the results of Step 3-1. As expected, the dependence of c_0 on β was eliminated. The next coefficient with the strongest dependence on damping was c_1 as can be seen in Figure B.27.

Step 3-3: $c_1 = b_3 + b_4 \ln(\beta) + b_5(\ln(\beta))^2 + \epsilon_1$

At a specified T, similar to c_0, the dependence of c_1 on the damping ratio can be captured by a quadratic function of $\ln(\beta)$. The coefficients b_3, b_4, and b_5 were estimated by performing regression on the 11 data points. Figure B.28 shows the fit of the resulting model.

Step 3-4: $\ln(DSF) - b_1 \ln(\beta) - b_2(\ln(\beta))^2 - b_4 \ln(\beta)\,\mathbf{M} - b_5(\ln(\beta))^2\mathbf{M}$

$$= \mathrm{c}_0 + c_1\mathbf{M} + \mathrm{c}_2\ln(R_{rup} + 1) + \epsilon$$

At specified values of T and β, the above regression was performed while b_1 and b_2 were assigned fixed values using the results of Step 3-1 and b_4 and b_5 were assigned fixed values using the results of Step 3-3. As expected, the dependence of c_0 and c_1 on β were eliminated.

The next coefficient with the strongest dependence on damping was c_2 as can be seen in Figure B.29.

Step 3-5: $c_2 = b_6 + b_7 \ln(\beta) + b_8(\ln(\beta))^2 + \epsilon_2$

The dependence of c_2 on β was captured using a function similar to those of c_0 and c_1. The coefficients b_6, b_7, and b_8 were estimated. The fit of the model is shown in Figure B.30.

Step 3-6: $\ln(DSF) - b_1 \ln(\beta) - b_2(\ln(\beta))^2 - b_4 \ln(\beta)\,\mathbf{M} - b_5(\ln(\beta))^2\mathbf{M}$

$$-b_7 \ln(\beta) \ln(R_{rup} + 1) - b_8(\ln(\beta))^2 \ln(R_{rup} + 1) = \mathrm{c}_0 + c_1\mathbf{M} + \mathrm{c}_2 \ln(R_{rup} + 1) + \epsilon$$

At specified values of T and β, the above regression was performed where b_1, b_2, b_4, and b_5 are the same as in Step 3-4 and b_7 and b_8 are taken from Step 3-5. As expected, c_0, c_1, and c_2 (plotted in Figures B.31, B.32, and B.33) are no longer dependent on β. We modeled these coefficients with constant numbers with respect to β (see the red lines in Figures B.31-B.33) at specified periods.

Step 3-7: $\ln(DSF) - b_1 \ln(\beta) - b_2(\ln(\beta))^2 - b_4 \ln(\beta)\,\mathbf{M} - b_5(\ln(\beta))^2\mathbf{M}$

$$-b_7 \ln(\beta) \ln\left(R_{rup} + 1\right) - b_8(\ln(\beta))^2 \ln\left(R_{rup} + 1\right) - b_0 - b_3\mathbf{M} - b_6 \ln\left(R_{rup} + 1\right)$$

$$= \mathrm{c}_0 + \epsilon$$

Finally, at specified values of T and β, the above regression was performed. b_1, b_2, b_4, b_5, b_7, and b_8 are the same as those in Step 3-6. b_0, b_3, and b_6 are, respectively, the constant estimates of c_0, c_1, and c_2 from Step 3-6. After performing the regression, we observed that c_0 can be taken equal to zero (see Figure B.34). We also observed that the standard deviation of ϵ, σ, has a systematic pattern with β (see Figure B.35). This dependence was captured by Equation (4.9) and the fit can be seen in Figure B.36.

Setting $c_0 = 0$ and rearranging the equation given in Step 3–7, we arrived at the final model for the DSF. Using this model, we calculated and examined the residuals and did not observe significant trends with potential predictor variables (sample residual plots are given in Appendix D).

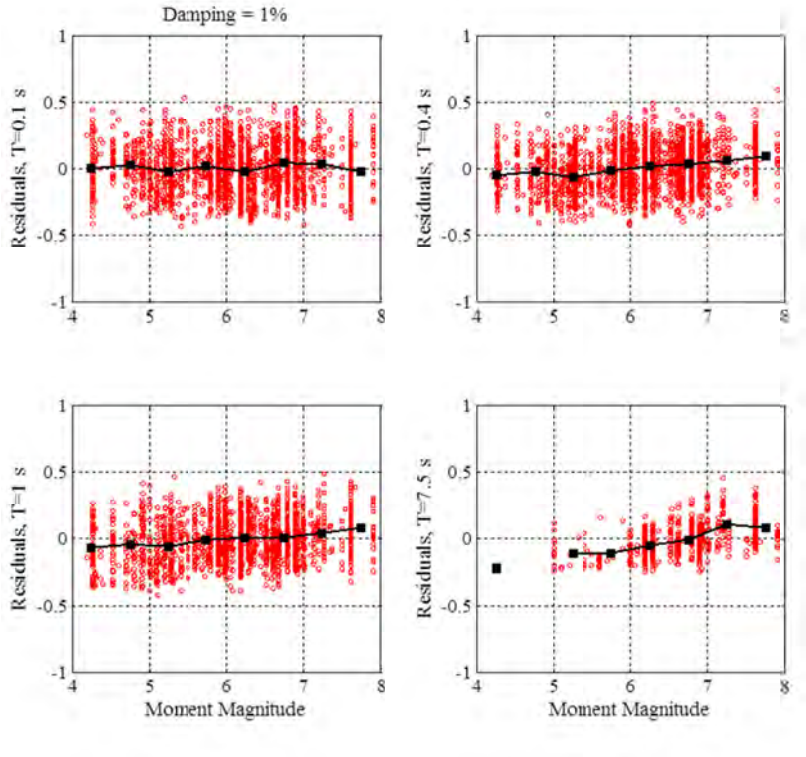

Figure B.1 Residuals versus earthquake magnitude at Step 0 for $\beta = 1\%$.

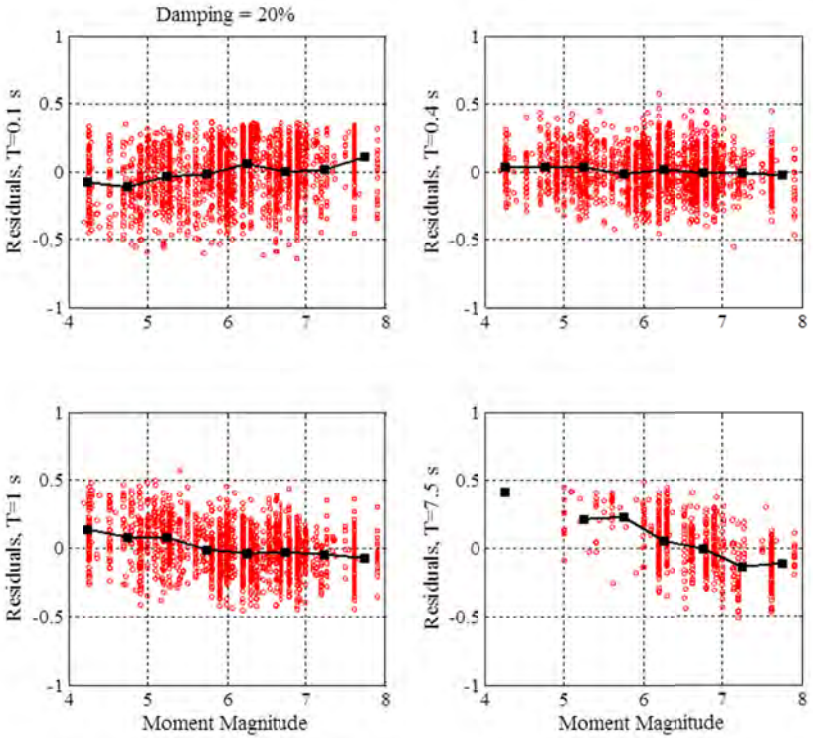

Figure B.2 Residuals versus earthquake magnitude at Step 0 for $\beta = 20\%$.

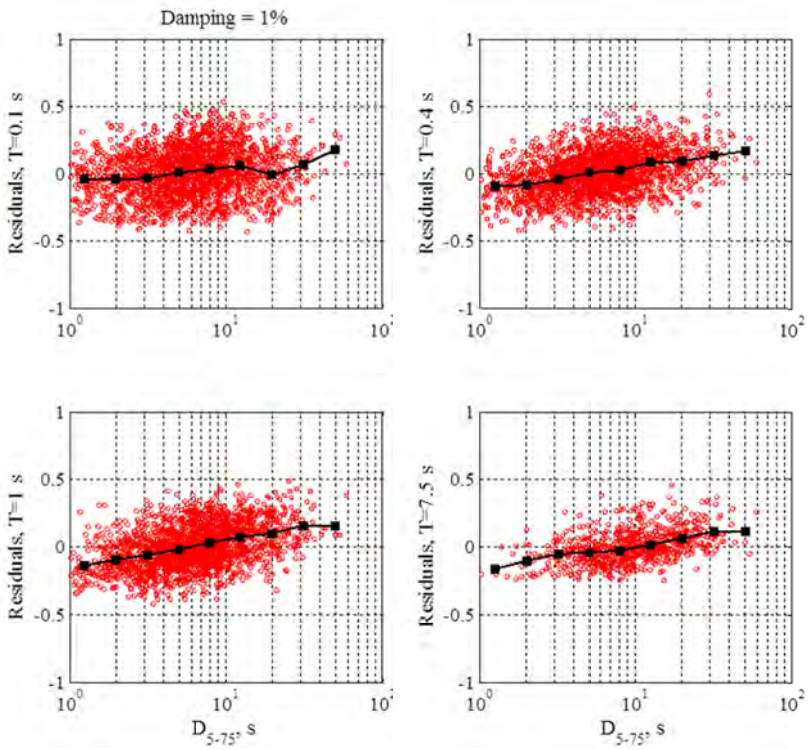

Figure B.3 Residuals versus duration at Step 0 for $\beta = 1\%$.

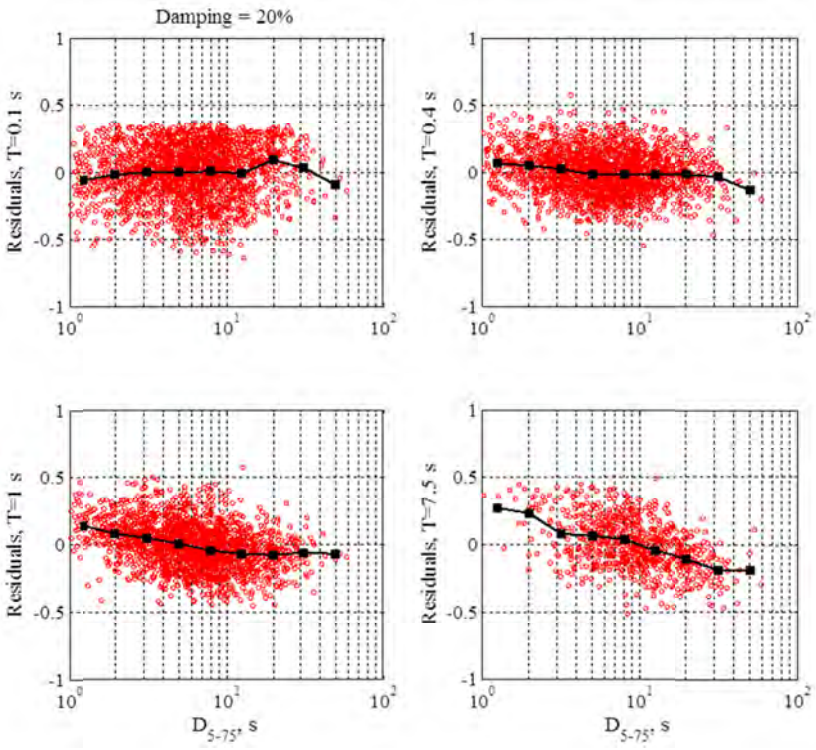

Figure B.4 Residuals versus duration at Step 0 for $\beta = 20\%$.

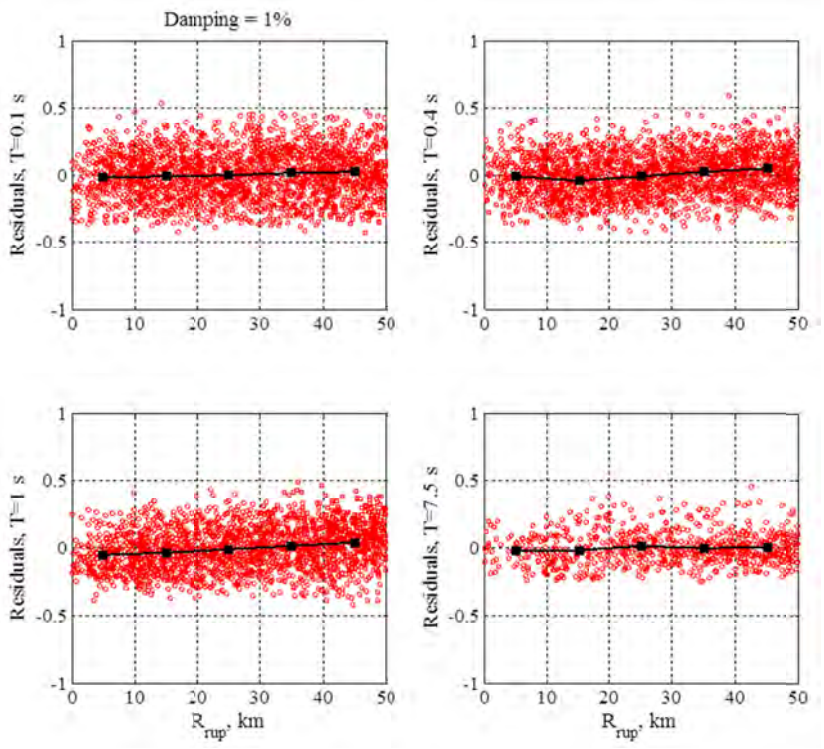

Figure B.5 Residuals versus distance at Step 0 for $\beta = 1\%$.

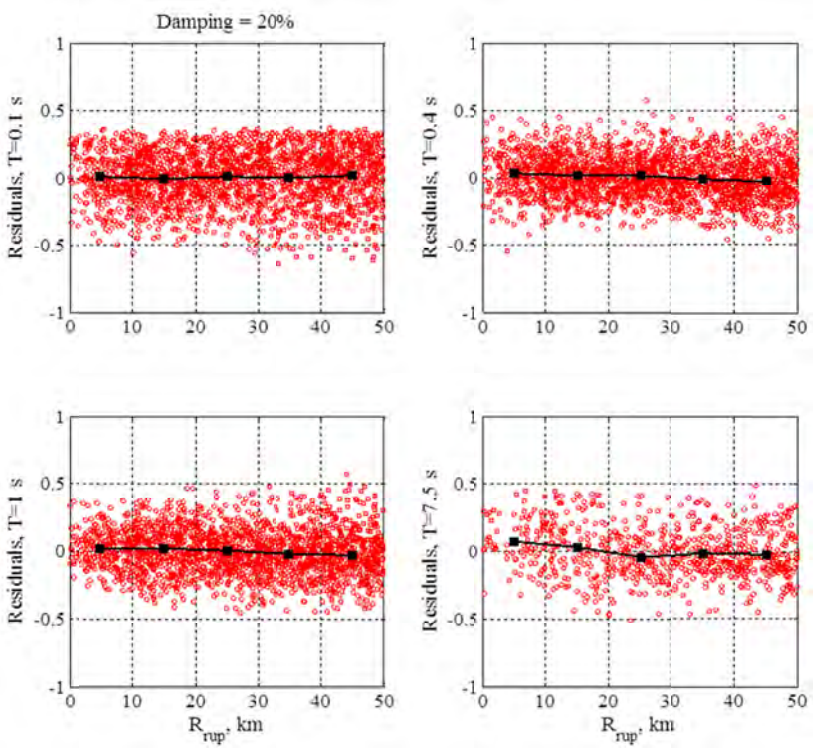

Figure B.6 Residuals versus distance at Step 0 for $\beta = 20\%$.

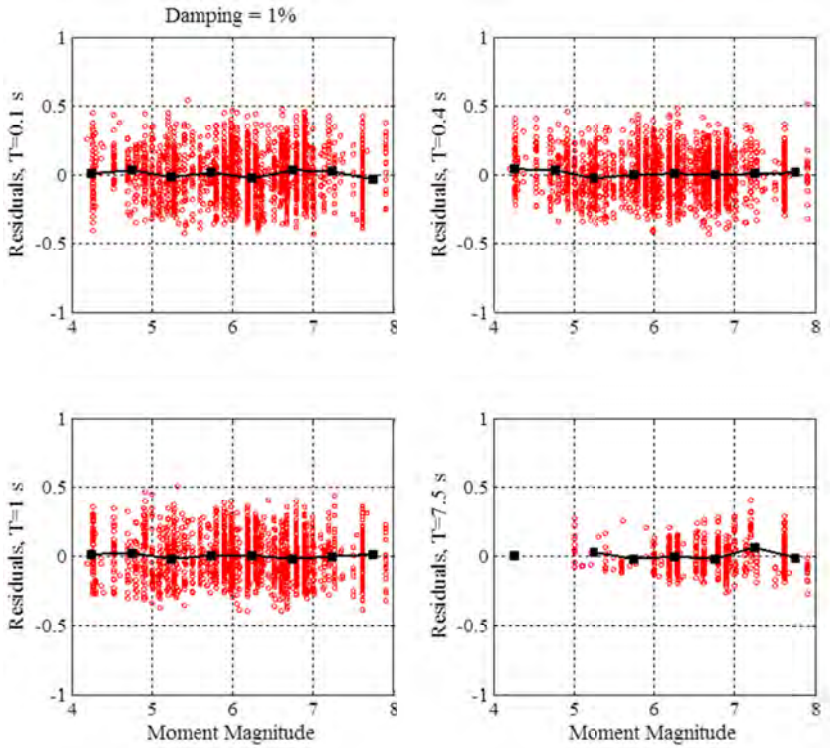

Figure B.7 Residuals versus earthquake magnitude at Step 1 for $\beta = 1\%$.

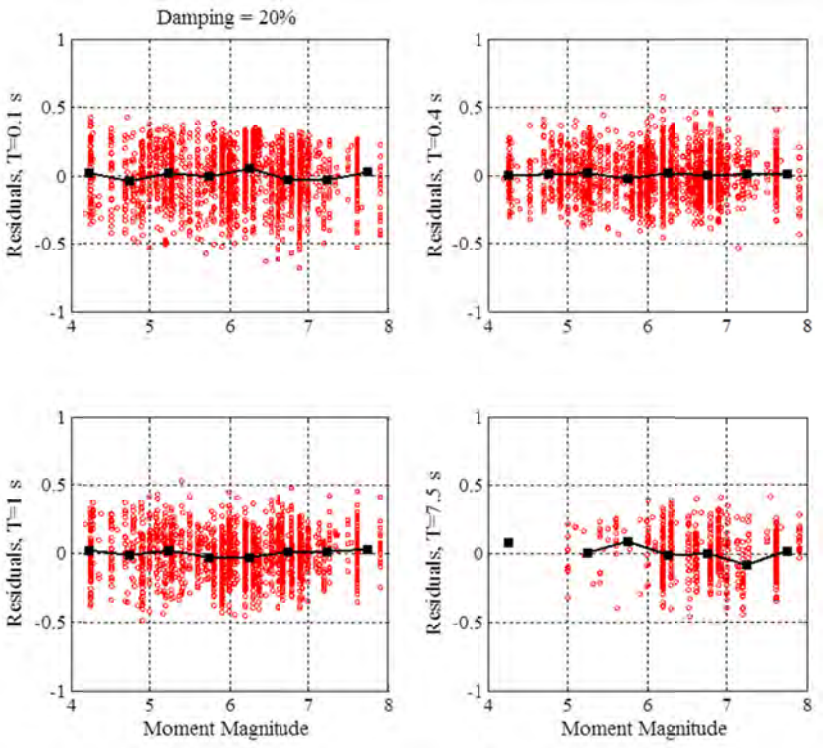

Figure B.8 Residuals versus earthquake magnitude at Step 1 for $\beta = 20\%$.

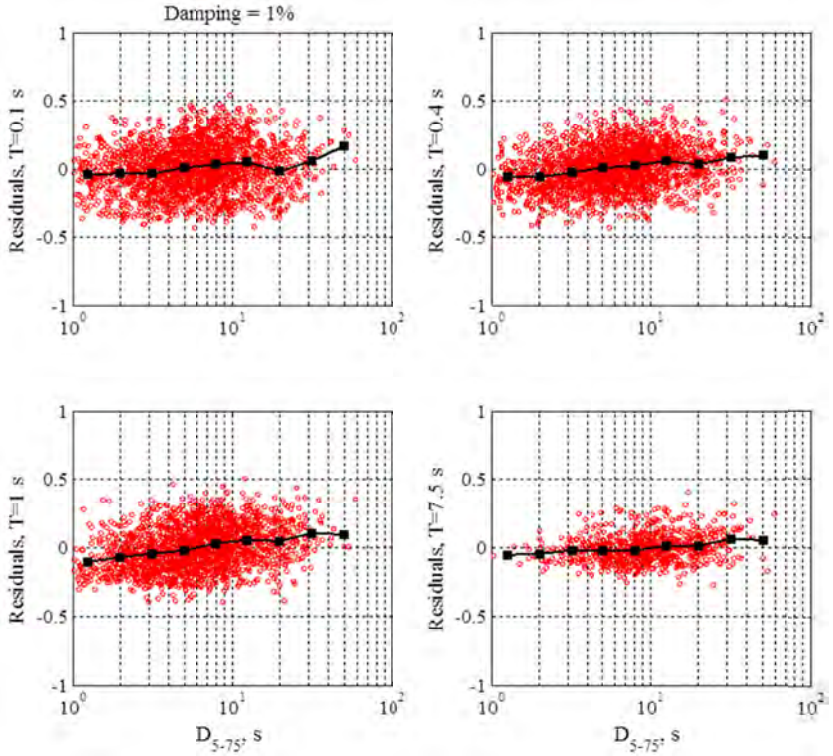

Figure B.9 Residuals versus duration at Step 1 for $\beta = 1\%$.

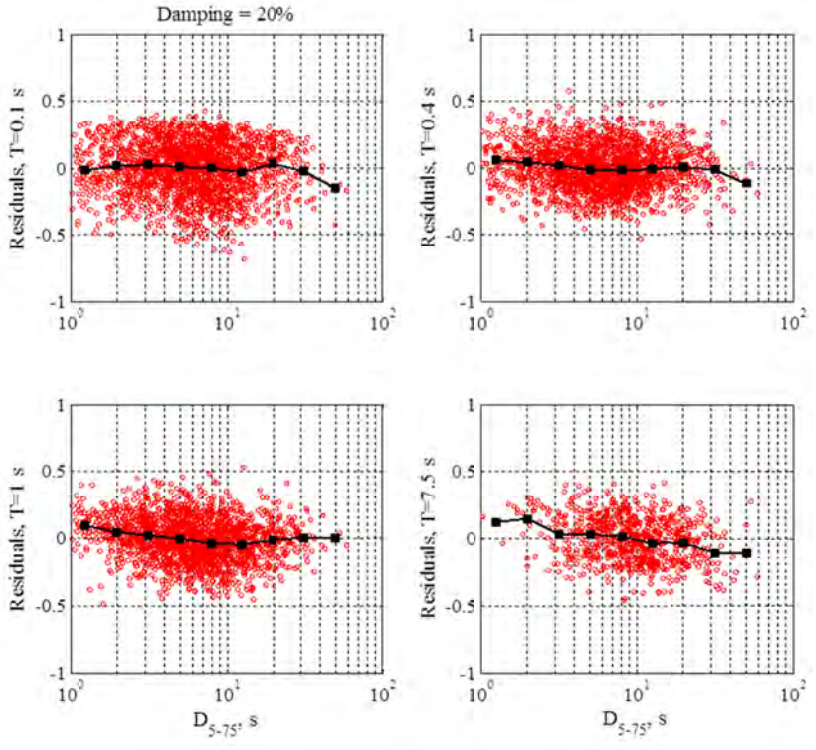

Figure B.10 Residuals versus duration at Step 1 for $\beta = 20\%$.

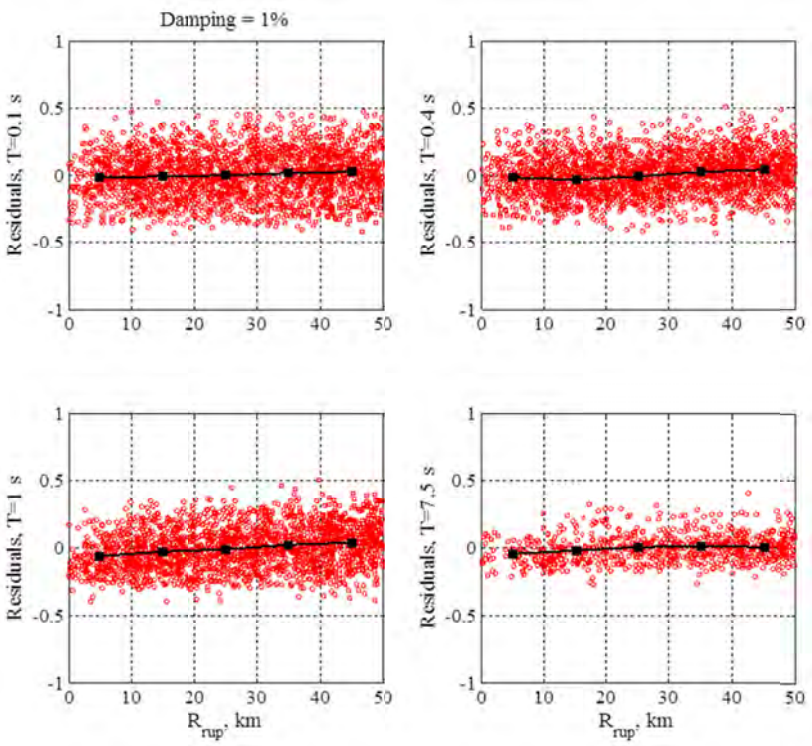

Figure B.11 Residuals versus distance at Step 1 for $\beta = 1\%$.

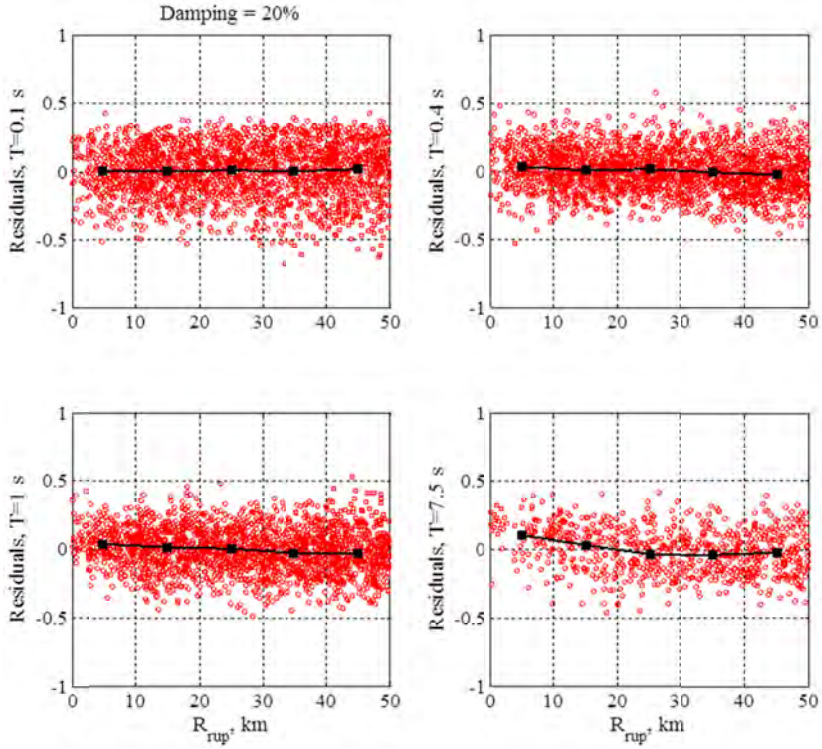

Figure B.12 Residuals versus distance at Step 1 for $\beta = 20\%$.

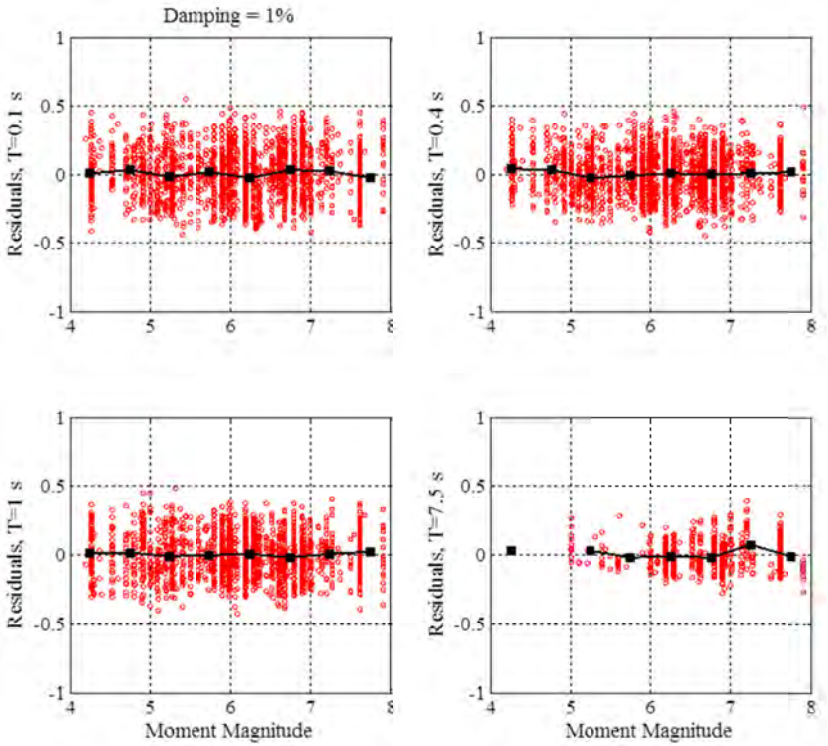

Figure B.13 Residuals versus earthquake magnitude at Step 3 for $\beta = 1\%$.

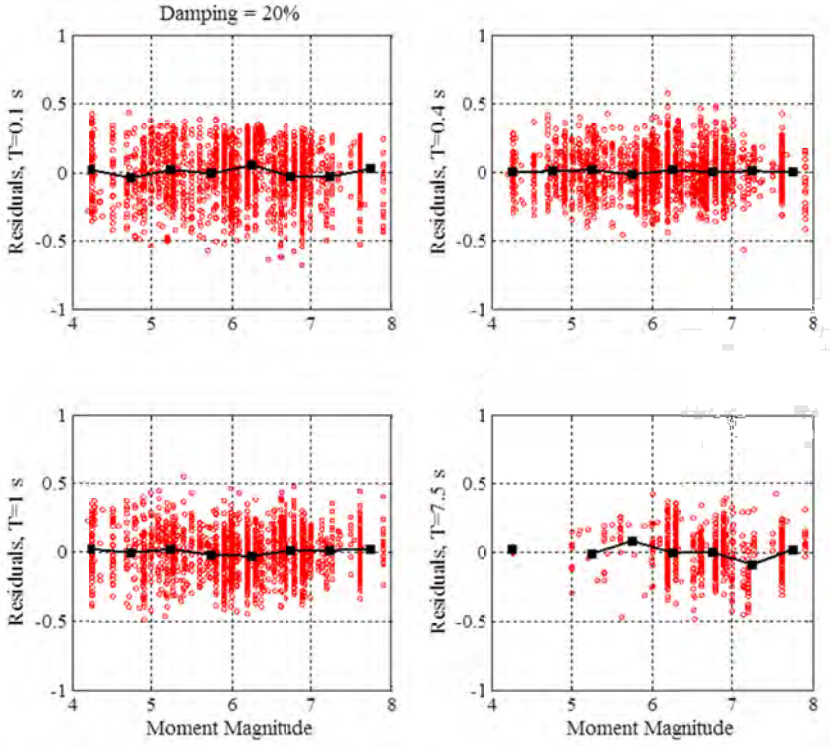

Figure B.14 Residuals versus earthquake magnitude at Step 3 for $\beta = 20\%$

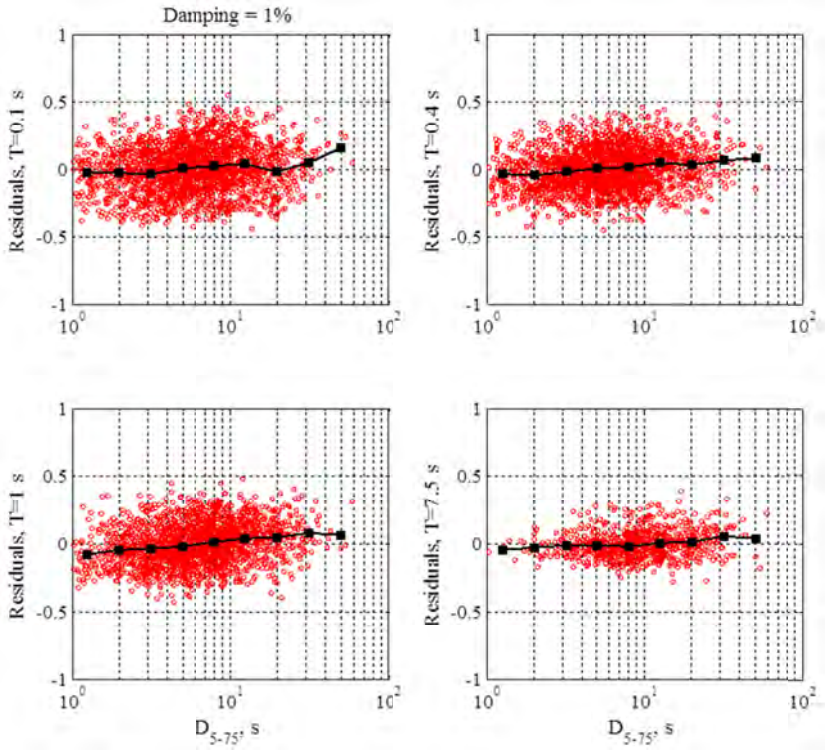

Figure B.15 Residuals versus duration at Step 3 for $\beta = 1\%$.

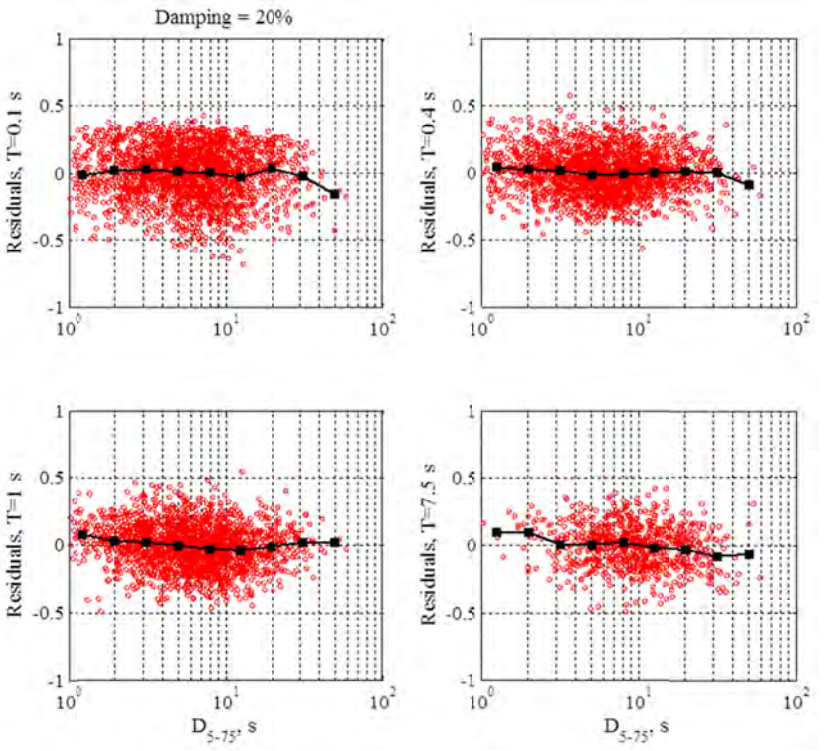

Figure B.16 Residuals versus duration at Step 3 for $\beta = 20\%$.

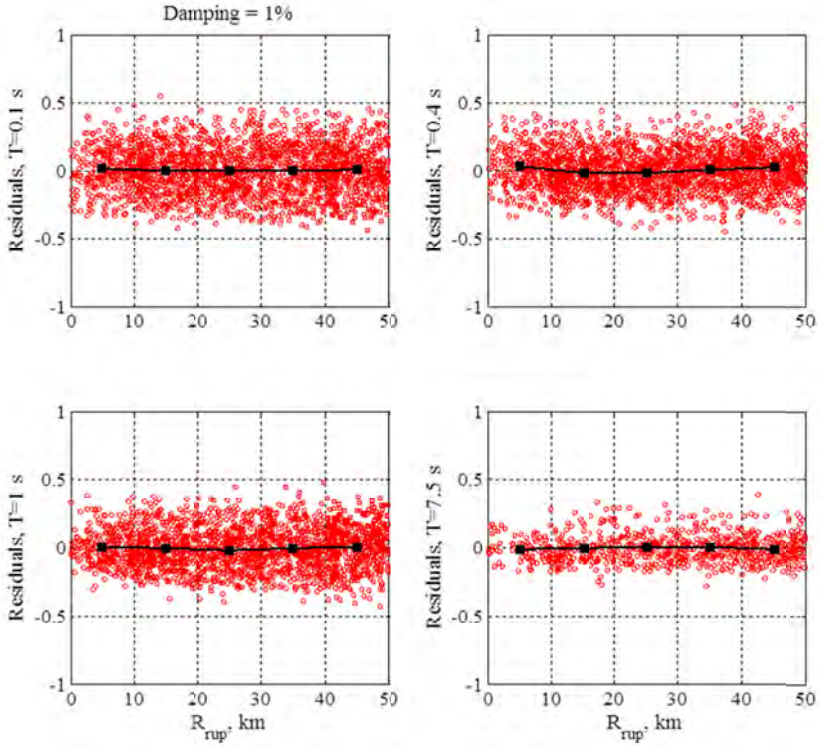

Figure B.17 Residuals versus distance at Step 3 for $\beta = 1\%$.

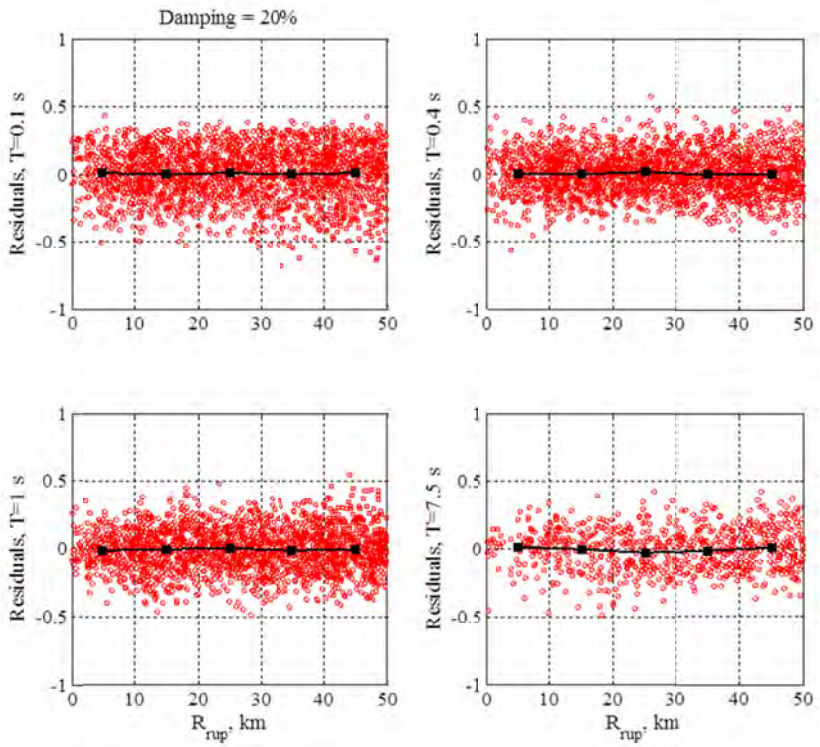

Figure B.18 Residuals versus distance at Step 3 for $\beta = 20\%$.

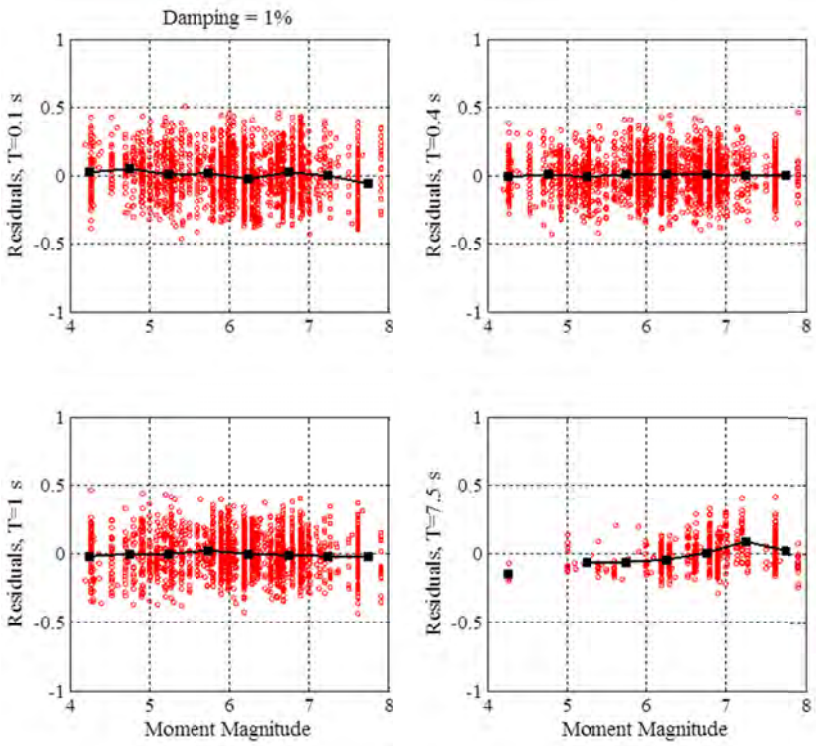

Figure B.19 Residuals versus earthquake magnitude at Step 4 for $\beta = 1\%$.

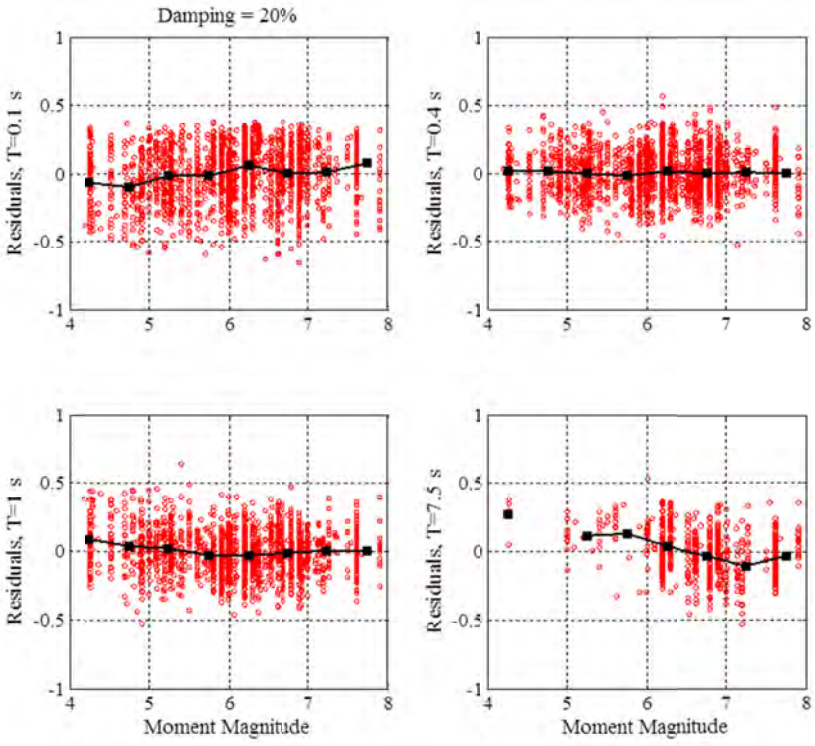

Figure B.20 Residuals versus earthquake magnitude at Step 4 for $\beta = 20\%$.

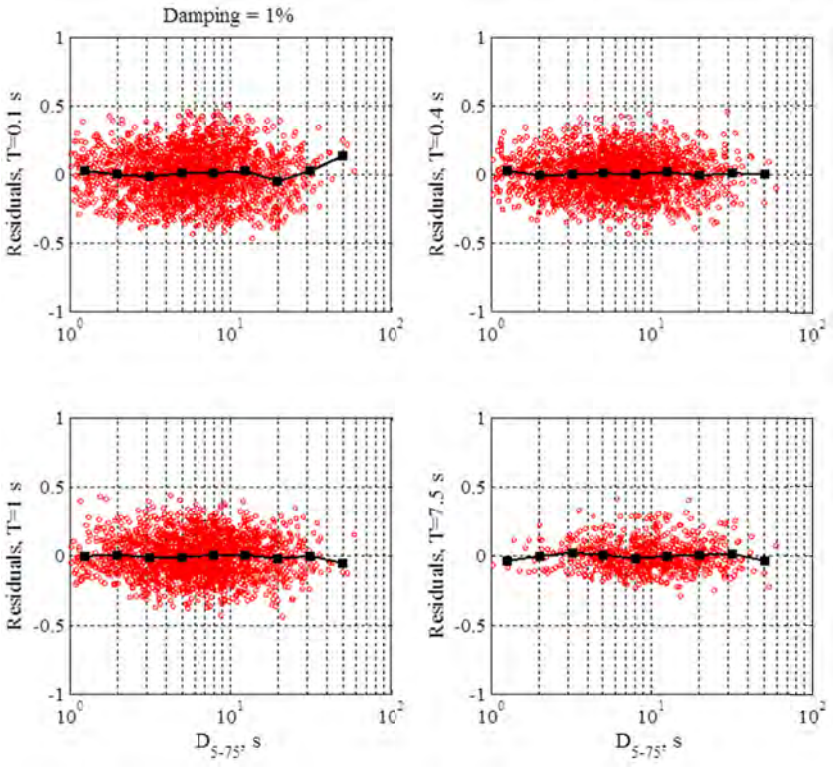

Figure B.21 Residuals versus duration at Step 4 for $\beta = 1\%$.

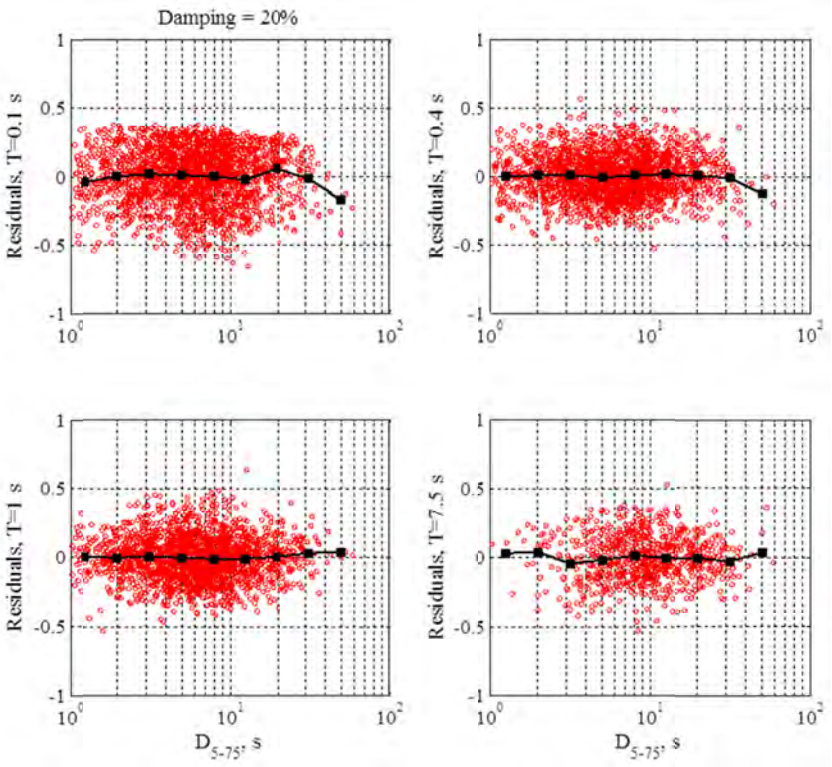

Figure B.22 Residuals versus duration at Step 4 for $\beta = 20\%$.

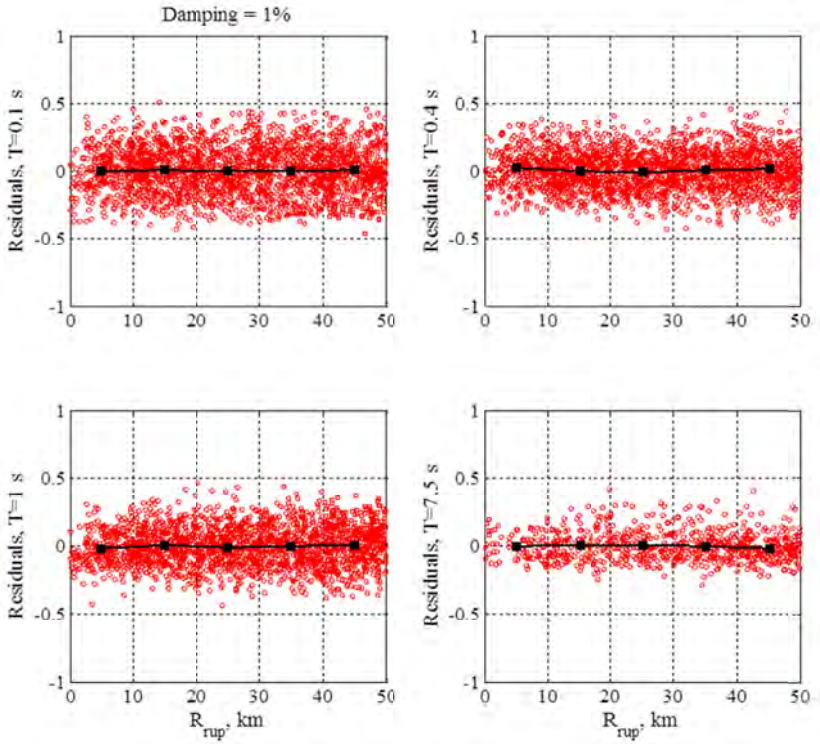

Figure B.23 Residuals versus distance at Step 4 for $\beta = 1\%$.

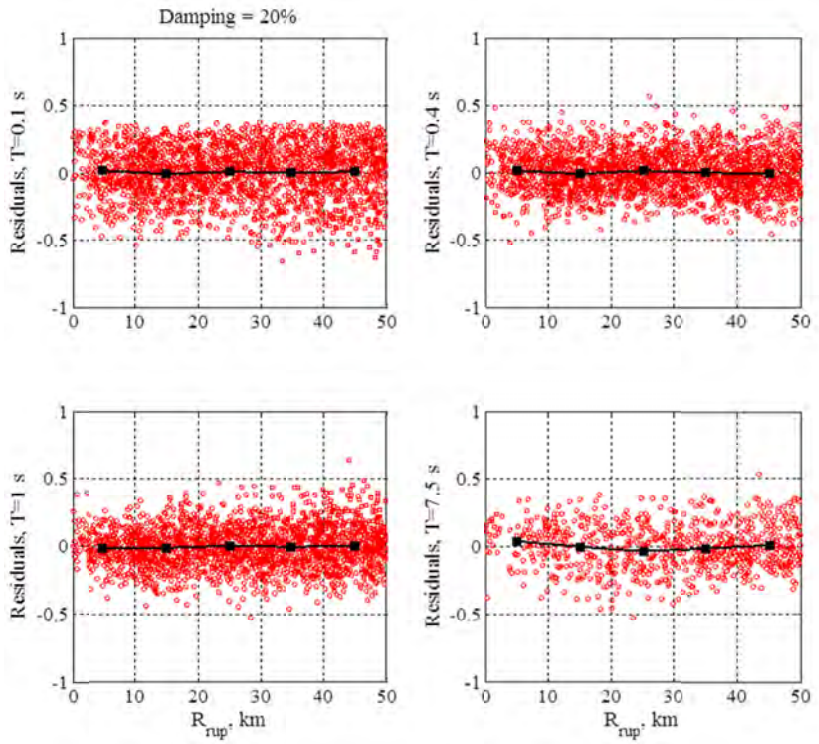

Figure B.24 Residuals versus distance at Step 4 for $\beta = 20\%$.

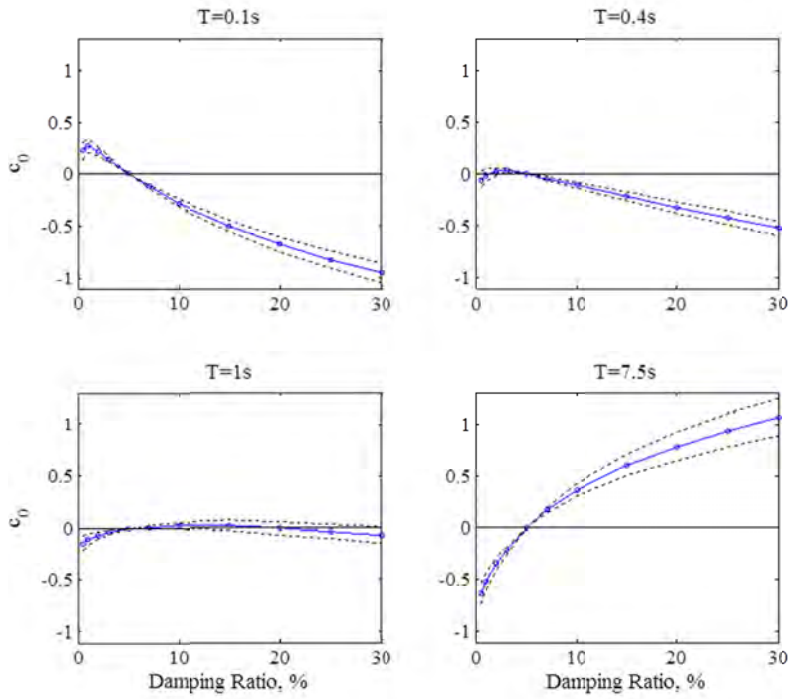

Figure B.25 Estimated values (solid line) and 95% confidence intervals (dotted lines) of c_0 at Step 3.

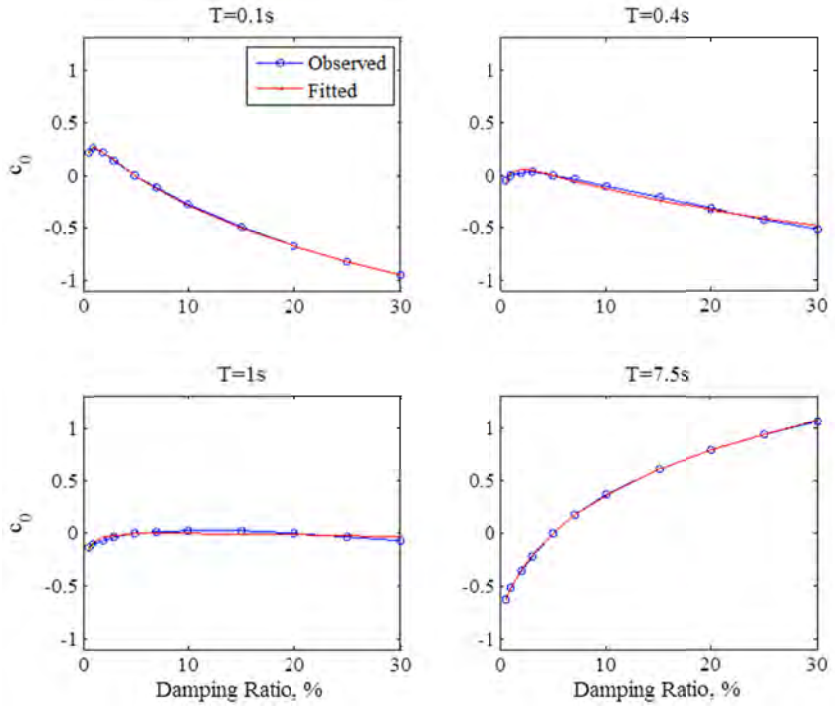

Figure B.26 Fitted model to c_0 at Step 3-1.

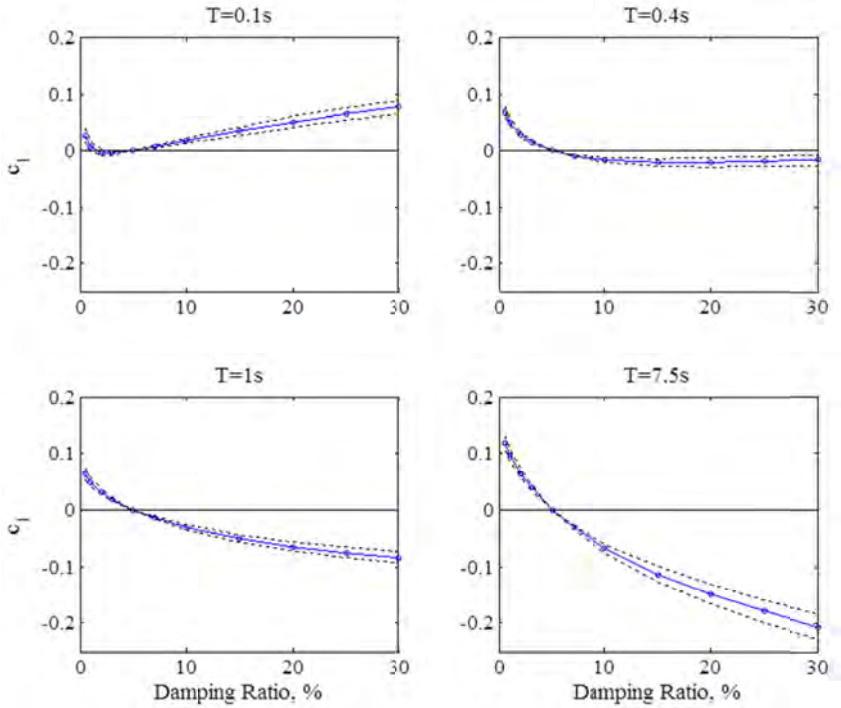

Figure B.27 Estimated values (solid line) and 95% confidence intervals (dotted lines) of c_1 at Step 3-2.

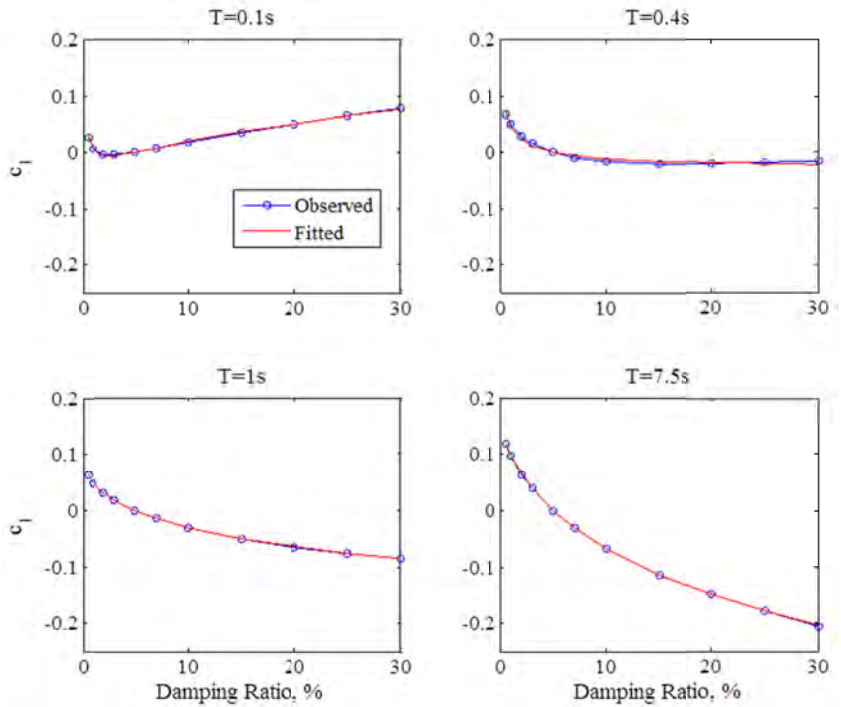

Figure B.28 Fitted model to c_1 at Step 3-3.

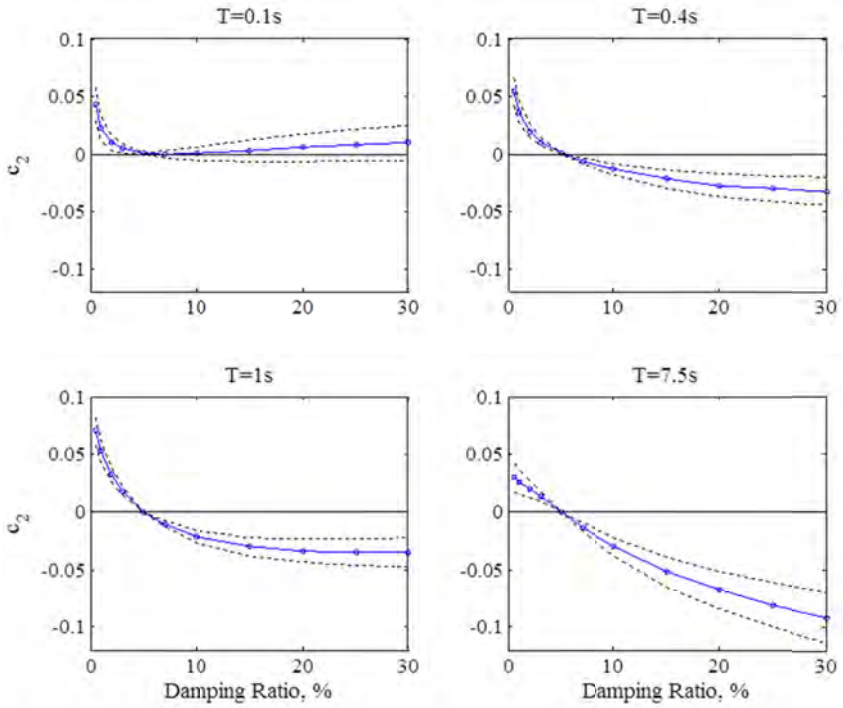

Figure B.29 Estimated values (solid line) and 95% confidence intervals (dotted lines) of c_2 at Step 3-4.

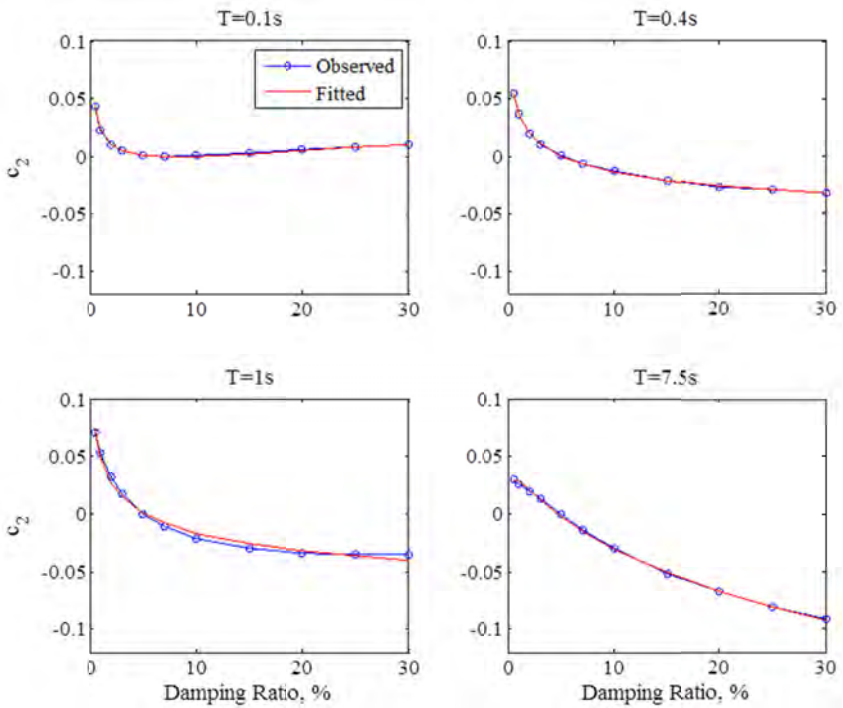

Figure B.30 Fitted model to c_2 at Step 3-5.

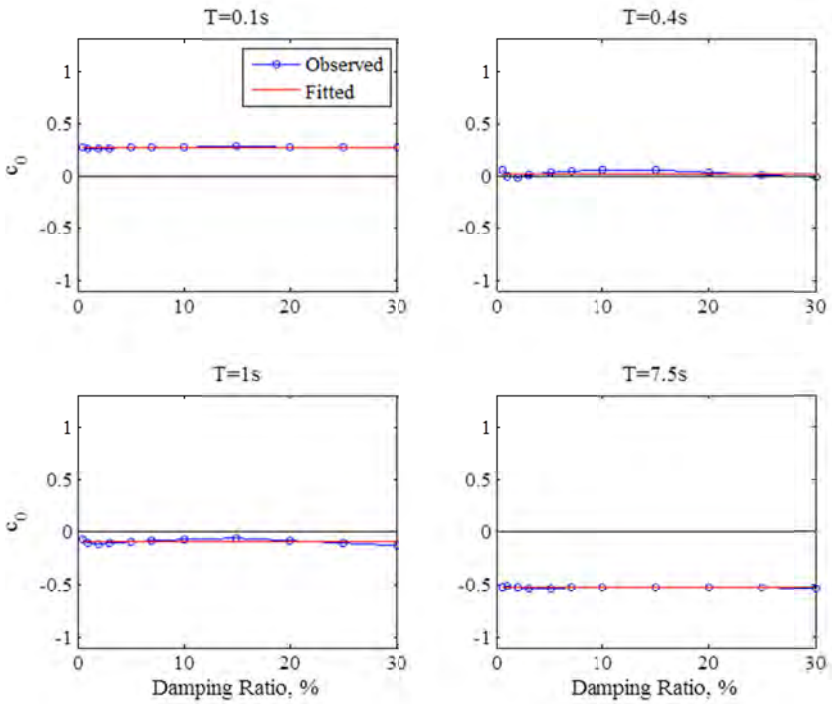

Figure B.31 Estimated (observed) values of c_0 and the fitted constant at Step 3-6.

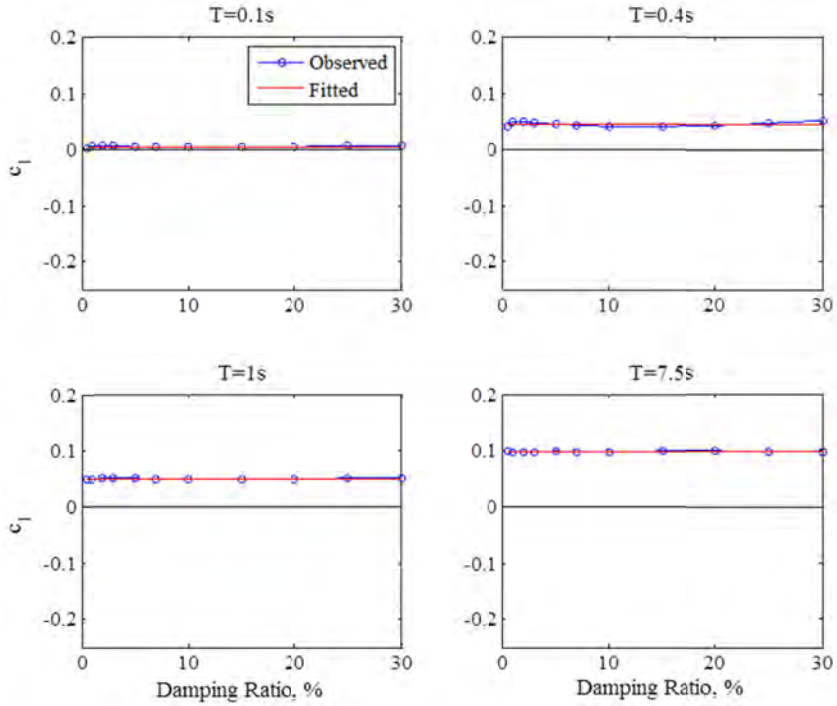

Figure B.32 Estimated (observed) values of c_1 and the fitted constant at Step 3-6.

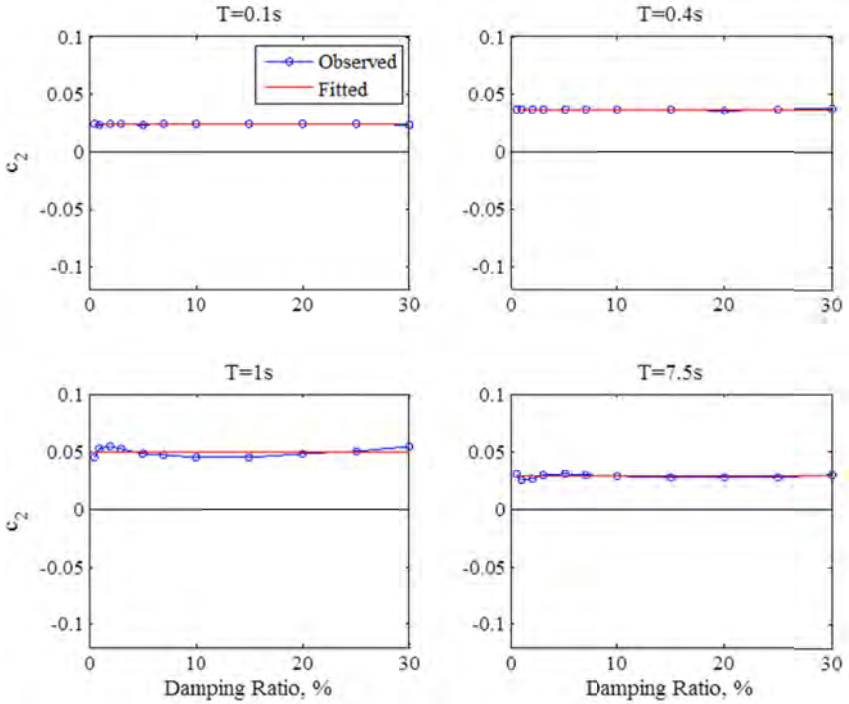

Figure B.33 Estimated (observed) values of c_2 and the fitted constant at Step 3-6.

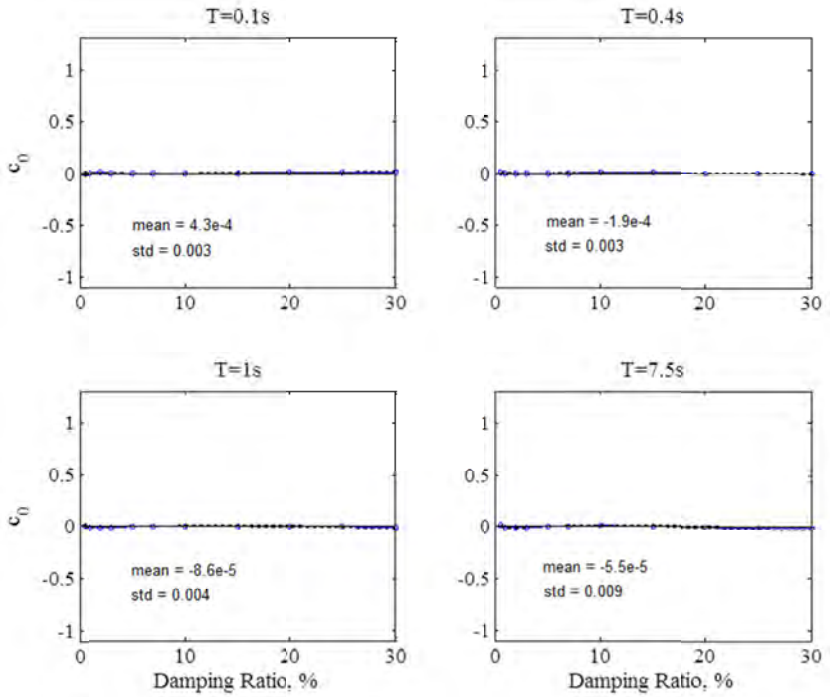

Figure B.34 Estimated values (solid line) and 95% confidence intervals (dotted lines) of c_0 at Step 3-7 (scale of the vertical axis is the same as in Figure B.25 to see the relative loss of dependence on the damping ratio and the closeness of c_0 to zero compared to the initial model).

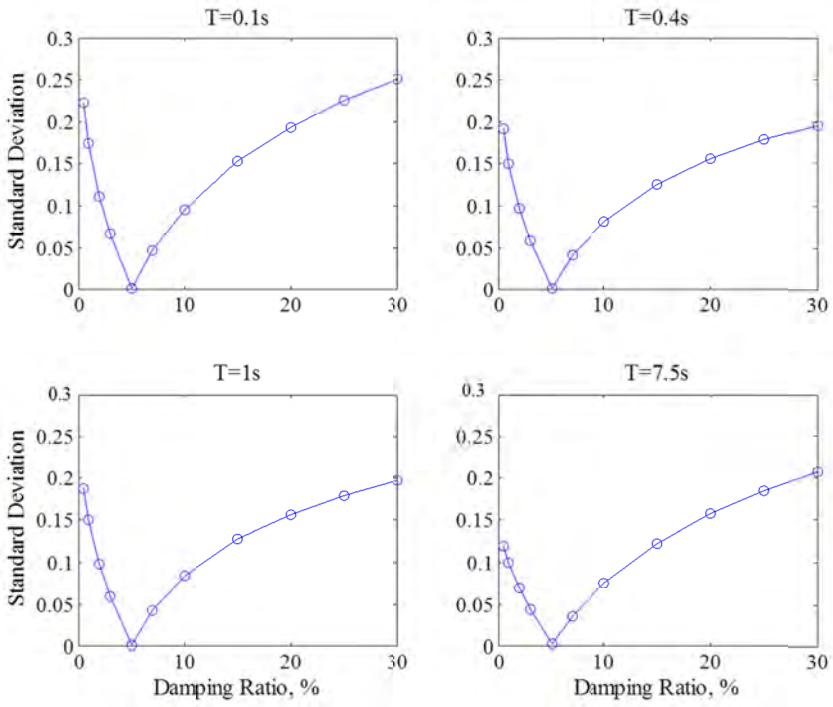

Figure B.35 Standard deviation of the error term at Step 3-7.

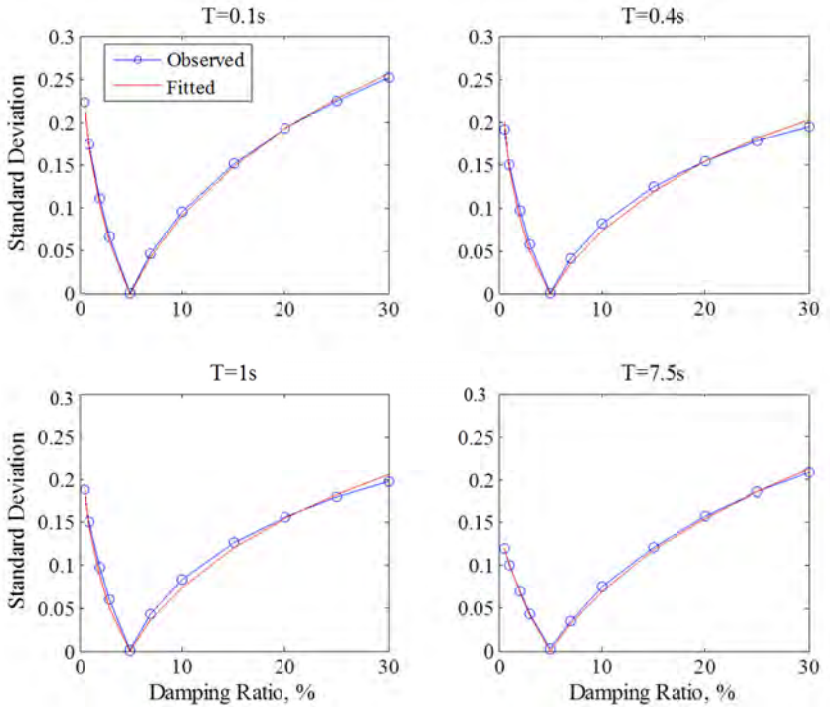

Figure B.36 Fitted model to the standard deviation.

Appendix C: Other Regression Coefficients

Table C.1 Regression coefficients for the horizontal component GMRotI50.

T, s	b0	b1	b2	b3	b4	b5	b6	b7	b8	a0	a1	$SE(\sigma)$*
0.01	3.01E-03	2.78E-03	-1.52E-03	-3.17E-04	-2.43E-04	1.55E-04	-9.93E-04	5.77E-04	-1.98E-04	-2.43E-02	-1.37E-03	8.54E-03
0.02	6.10E-02	-3.83E-02	1.85E-03	-4.92E-03	3.20E-03	-2.58E-04	-5.43E-03	2.98E-03	5.81E-05	-3.21E-02	1.64E-04	6.75E-03
0.03	1.22E-01	-6.98E-02	-2.11E-03	-3.36E-03	3.48E-04	8.94E-04	-1.33E-02	7.75E-03	1.56E-04	-5.48E-02	3.34E-03	5.16E-03
0.05	2.34E-01	-9.75E-02	-2.74E-02	-4.11E-04	-8.08E-03	5.03E-03	-1.79E-02	8.12E-03	1.48E-03	-9.45E-02	9.22E-04	6.36E-03
0.075	3.00E-01	-6.77E-02	-7.37E-02	-5.64E-04	-1.61E-02	1.03E-02	3.11E-05	-6.23E-03	4.00E-03	-1.20E-01	-6.18E-03	6.99E-03
0.1	2.54E-01	1.55E-02	-1.08E-01	7.09E-03	-2.54E-02	1.34E-02	2.24E-02	-2.32E-02	5.59E-03	-1.22E-01	-1.04E-02	7.22E-03
0.15	1.49E-01	9.41E-02	-1.17E-01	2.77E-02	-3.88E-02	1.37E-02	2.97E-02	-2.39E-02	3.29E-03	-1.14E-01	-1.08E-02	6.98E-03
0.2	2.57E-02	1.54E-01	-1.11E-01	4.76E-02	-4.73E-02	1.18E-02	3.20E-02	-2.38E-02	2.49E-03	-1.07E-01	-8.14E-03	8.67E-03
0.25	7.91E-03	1.50E-01	-9.77E-02	5.14E-02	-4.60E-02	9.24E-03	2.98E-02	-2.22E-02	1.79E-03	-1.03E-01	-6.91E-03	8.40E-03
0.3	-1.32E-02	1.39E-01	-8.50E-02	5.05E-02	-4.13E-02	6.75E-03	3.69E-02	-2.55E-02	1.59E-03	-1.01E-01	-6.37E-03	8.88E-03
0.4	4.02E-02	8.04E-02	-6.86E-02	4.39E-02	-3.31E-02	4.32E-03	3.14E-02	-1.99E-02	-1.26E-04	-1.01E-01	-6.38E-03	9.82E-03
0.5	4.76E-02	6.49E-02	-5.60E-02	3.83E-02	-2.72E-02	1.87E-03	3.89E-02	-2.50E-02	3.41E-04	-1.01E-01	-6.61E-03	1.08E-02
0.75	1.93E-02	4.86E-02	-3.90E-02	4.16E-02	-2.20E-02	-2.40E-03	3.46E-02	-2.58E-02	3.26E-03	-1.02E-01	-6.23E-03	1.09E-02
1	-6.40E-02	8.34E-02	-2.47E-02	4.64E-02	-2.24E-02	-4.30E-03	4.63E-02	-3.28E-02	2.49E-03	-1.03E-01	-6.82E-03	1.08E-02
1.5	-1.52E-01	8.58E-02	5.17E-03	5.63E-02	-2.21E-02	-8.06E-03	4.76E-02	-3.17E-02	1.65E-03	-1.02E-01	-8.91E-03	1.04E-02
2	-2.61E-01	1.38E-01	1.85E-02	6.94E-02	-2.85E-02	-9.59E-03	4.61E-02	-2.97E-02	6.49E-04	-1.04E-01	-8.98E-03	1.10E-02
3	-3.65E-01	1.71E-01	3.48E-02	7.88E-02	-3.34E-02	-9.86E-03	4.86E-02	-2.33E-02	-4.26E-03	-9.84E-02	-1.05E-02	1.07E-02
4	-4.38E-01	1.97E-01	4.19E-02	8.53E-02	-3.43E-02	-1.11E-02	4.91E-02	-2.31E-02	-4.36E-03	-9.85E-02	-1.22E-02	9.29E-03
5	-4.97E-01	2.21E-01	5.20E-02	8.98E-02	-3.59E-02	-1.23E-02	4.93E-02	-2.07E-02	-6.11E-03	-9.60E-02	-1.45E-02	6.68E-03
7.5	-5.05E-01	1.89E-01	7.36E-02	9.27E-02	-3.33E-02	-1.48E-02	3.22E-02	-7.26E-03	-7.98E-03	-9.21E-02	-1.53E-02	7.59E-03
10	-3.98E-01	1.41E-01	5.92E-02	7.22E-02	-2.26E-02	-1.31E-02	2.29E-02	-7.35E-03	-4.33E-03	-7.23E-02	-1.19E-02	8.93E-03

* Standard error in modeling σ according to Equation (4.9).

Table C.2 Regression coefficients for the horizontal component RotD50 if the distance term is eliminated.

T, s	b0	b1	b2	b3	b4	b5	a0	a1	$SE(\sigma)$*
0.01	-1.93E-03	2.93E-03	-1.33E-03	5.12E-05	-1.25E-04	8.31E-05	-3.72E-03	2.38E-04	-1.93E-03
0.02	3.91E-02	-2.91E-02	2.94E-03	-4.07E-03	3.09E-03	-3.43E-04	-2.20E-02	2.09E-03	3.91E-02
0.03	7.71E-02	-4.34E-02	-1.43E-03	-2.59E-03	-3.04E-04	9.72E-04	-5.25E-02	4.56E-03	7.71E-02
0.05	1.81E-01	-7.82E-02	-2.03E-02	-1.11E-04	-7.81E-03	4.80E-03	-9.62E-02	1.20E-03	1.81E-01
0.075	3.02E-01	-9.51E-02	-5.78E-02	3.83E-04	-1.62E-02	1.01E-02	-1.22E-01	-5.87E-03	3.02E-01
0.1	3.48E-01	-7.73E-02	-8.65E-02	4.83E-03	-2.38E-02	1.31E-02	-1.24E-01	-1.06E-02	3.48E-01
0.15	2.49E-01	1.52E-02	-1.07E-01	2.84E-02	-3.98E-02	1.40E-02	-1.16E-01	-1.11E-02	2.49E-01
0.2	1.58E-01	6.62E-02	-1.03E-01	4.53E-02	-4.66E-02	1.17E-02	-1.09E-01	-8.66E-03	1.58E-01
0.25	1.17E-01	7.29E-02	-9.28E-02	5.08E-02	-4.61E-02	9.41E-03	-1.05E-01	-7.24E-03	1.17E-01
0.3	1.18E-01	5.59E-02	-8.22E-02	5.02E-02	-4.23E-02	7.25E-03	-1.02E-01	-6.65E-03	1.18E-01
0.4	1.48E-01	1.82E-02	-7.00E-02	4.44E-02	-3.46E-02	4.60E-03	-1.03E-01	-6.53E-03	1.48E-01
0.5	1.66E-01	-1.54E-02	-5.45E-02	4.04E-02	-2.81E-02	1.87E-03	-1.02E-01	-6.15E-03	1.66E-01
0.75	1.32E-01	-3.77E-02	-2.69E-02	4.27E-02	-2.25E-02	-2.57E-03	-1.02E-01	-5.59E-03	1.32E-01
1	9.14E-02	-3.34E-02	-1.32E-02	4.65E-02	-2.13E-02	-4.86E-03	-1.04E-01	-6.89E-03	9.14E-02
1.5	1.96E-02	-2.81E-02	1.11E-02	5.45E-02	-2.09E-02	-8.17E-03	-1.04E-01	-8.33E-03	1.96E-02
2	-9.99E-02	2.60E-02	2.34E-02	6.85E-02	-2.65E-02	-1.01E-02	-1.05E-01	-8.88E-03	-9.99E-02
3	-1.99E-01	8.88E-02	2.09E-02	7.85E-02	-3.30E-02	-9.74E-03	-1.00E-01	-1.08E-02	-1.99E-01
4	-2.57E-01	1.15E-01	2.64E-02	8.20E-02	-3.33E-02	-1.09E-02	-1.02E-01	-1.42E-02	-2.57E-01
5	-3.01E-01	1.30E-01	3.19E-02	8.48E-02	-3.24E-02	-1.23E-02	-9.88E-02	-1.58E-02	-3.01E-01
7.5	-3.99E-01	1.84E-01	3.93E-02	9.41E-02	-3.67E-02	-1.37E-02	-9.24E-02	-1.74E-02	-3.99E-01
10	-2.80E-01	1.18E-01	3.35E-02	6.66E-02	-2.24E-02	-1.18E-02	-7.09E-02	-1.49E-02	-2.80E-01

* Standard error in modeling σ according to Equation (4.9).

Appendix D: Residual Diagnostic Plots (RotD50 Component)

The model residual is defined as the difference between the observed and predicted values of $\ln(DSF)$. One can write

$$residual = \ln(DSF_{observed}) - \ln\widehat{(DSF)}$$

where $\ln\widehat{(DSF)}$ is the predicted value according to Equation (4.8) given the observed earthquake magnitude, source-to-site distance, and damping ratio. Figures D.1-D.19 show the residual plots for data with $R_{rup} < 50$ km. These are the data used in the regression analysis. The residual diagnostic plots are presented at four different spectral periods: $T = 0.1$, 0.4, 1, and 7.5 sec. In all figures, a black line represents the average values of residuals over equally spaced bins of data. The dependence on the damping ratio is shown in Figure D.1. The dependence on moment magnitude is shown in Figures D.2-D.4. Figure D.2 combines the data for all 11 damping ratios considered in this report, whereas Figures D.3 and D.4 show the residuals for individual damping ratios, i.e., 1% and 20%. Similarly, Figures D.5-D.7 show the dependence on the closest distance to the ruptured area, R_{rup}. Figures D.8-D.10 show the dependence on the duration of motion, D_{5-75}. Figures D.11-D.13 show the dependence on 30-m shear-wave velocity, V_{S30}. Figures D.14-D.16 and D.17-D.19 respectively show the dependence on sediment depths $Z_{1.0}$ (depth to the 1.0 km/sec shear-wave velocity horizon) and $Z_{2.5}$ (depth to the 2.5 km/sec shear-wave velocity horizon).

Figures D.20-D.29 show the residual plots for data with $50 \leq R_{rup} < 200$ km. Even though these data are not used in modeling, the residual diagnostic plots reveal minimal pattern with the predictor variables, i.e., damping ratio, magnitude, distance, and the duration of motion. Beyond 200 km (up to a distance of 2000 km), significant patterns are observed with R_{rup} at individual damping ratios and therefore the use of model is not advisable.

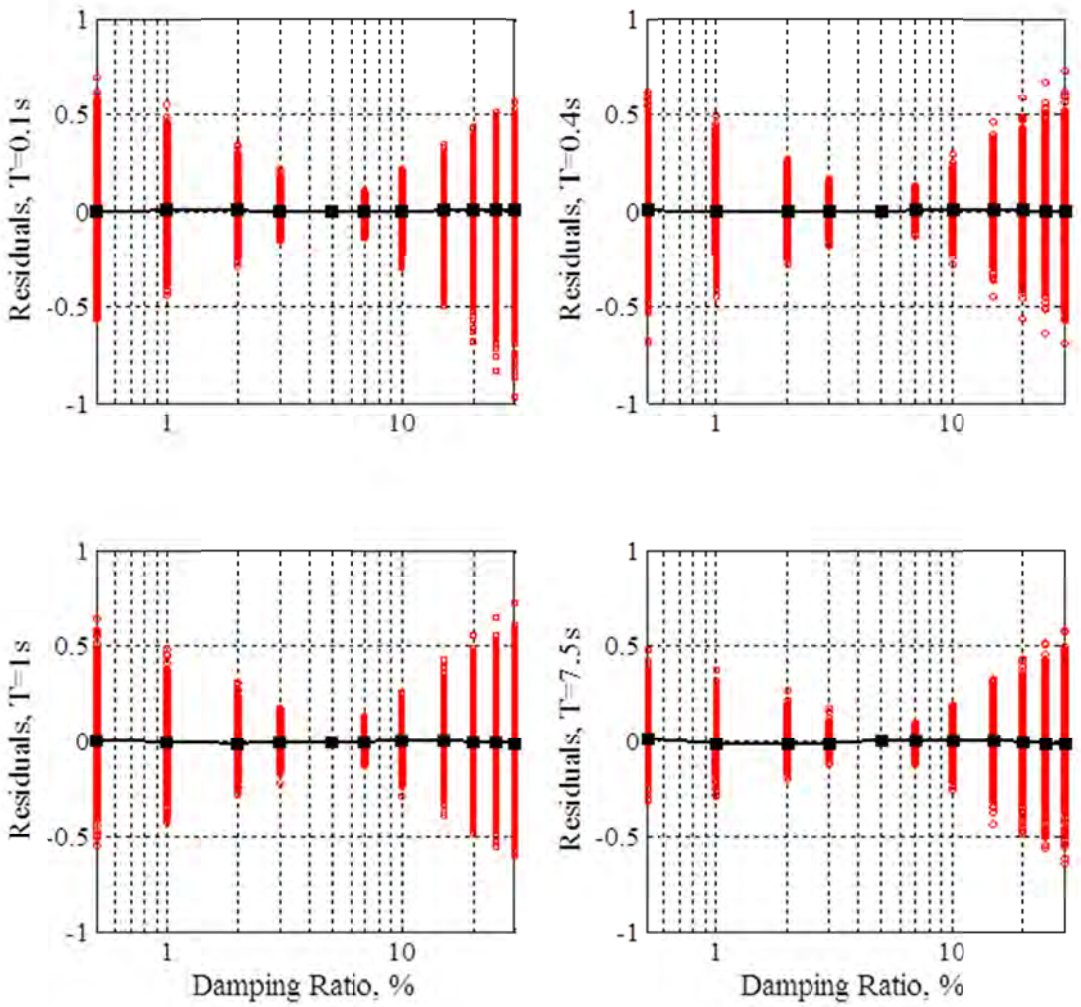

Figure D.1 **Dependence of residuals on damping ratio, β. Data with $R_{rup} < 50$ km are used.**

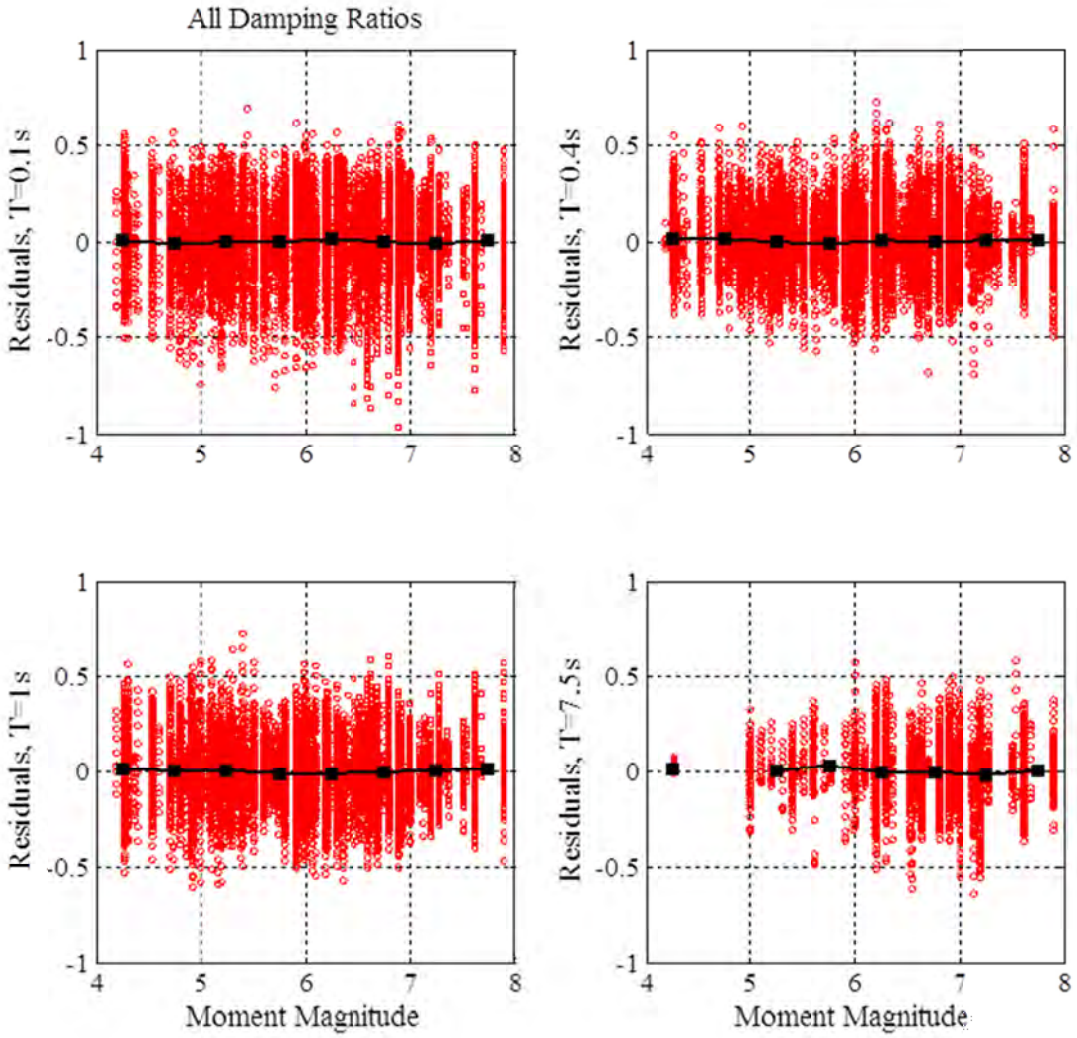

Figure D.2 **Dependence of residuals on earthquake magnitude, M. Data with $R_{rup} < 50$ km (i.e., data used in regression) for all 11 damping ratios are plotted.**

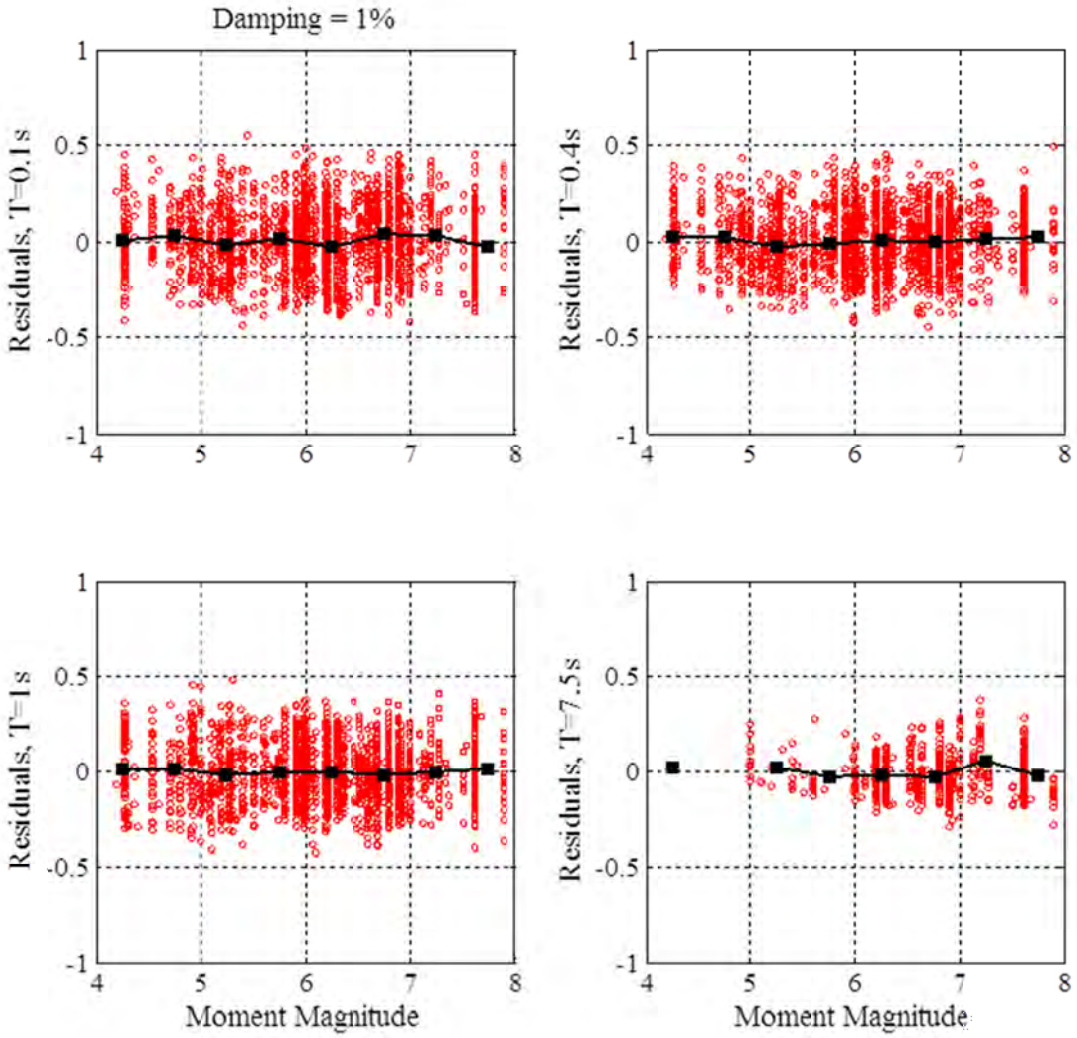

Figure D.3 Dependence of residuals on earthquake magnitude, M. Data with $R_{rup} < 50$ km (i.e., data used in regression) and $\beta = 1\%$ are plotted.

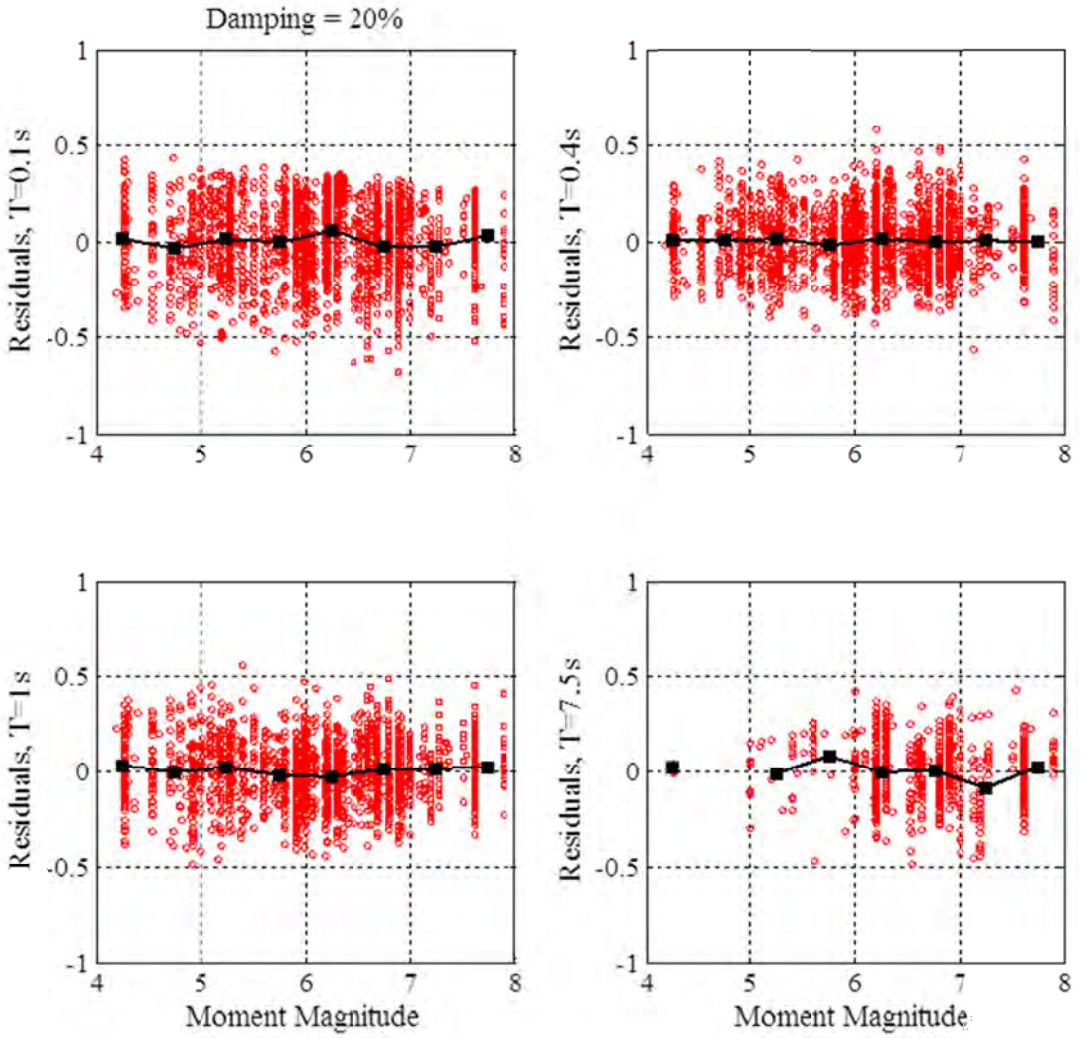

Figure D.4 **Dependence of residuals on earthquake magnitude, M. Data with $R_{rup} < 50$ km (i.e., data used in regression) and $\beta = 20\%$ are plotted.**

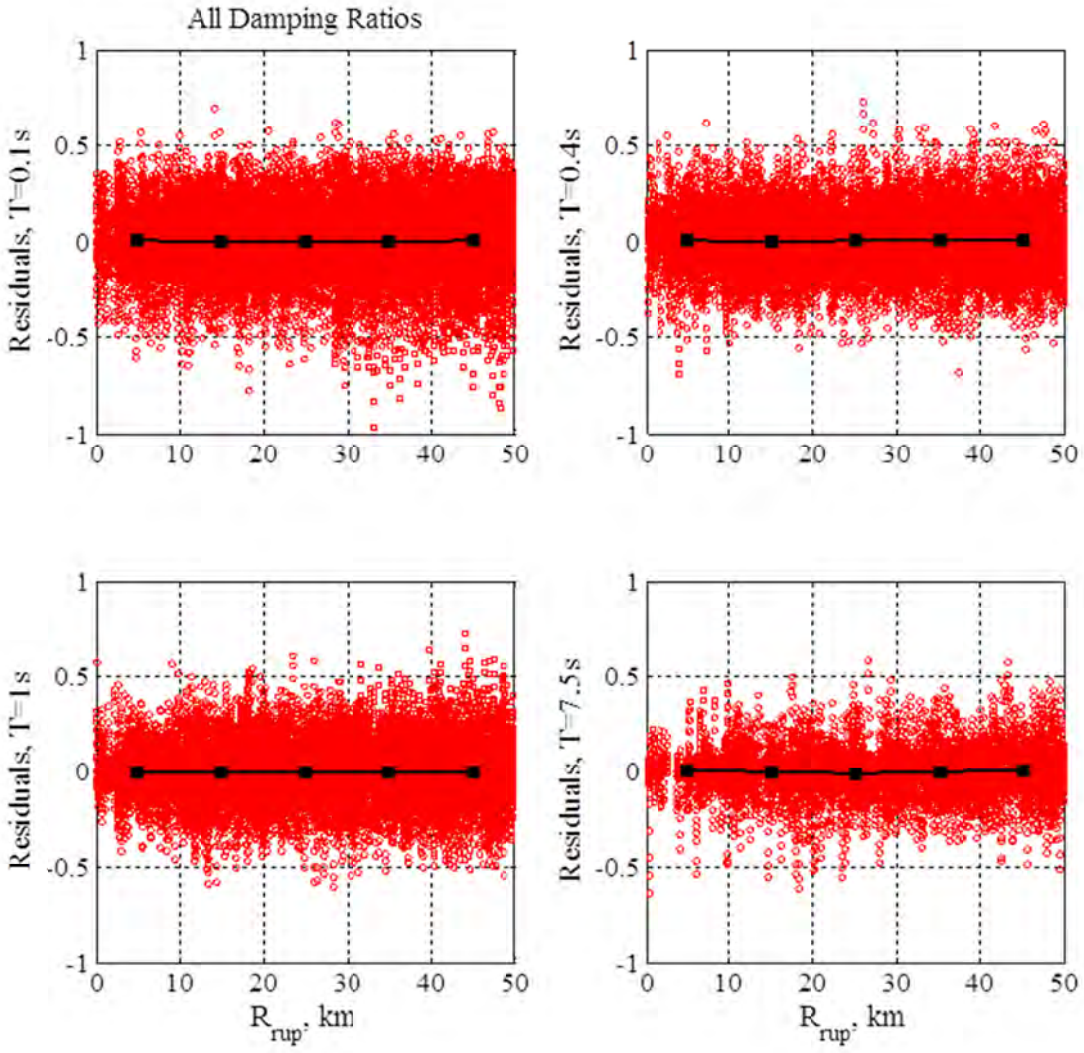

Figure D.5 **Dependence of residuals on rupture distance, R_{rup}. Data with $R_{rup} < 50$ km (i.e., data used in regression) for all 11 damping ratios are plotted.**

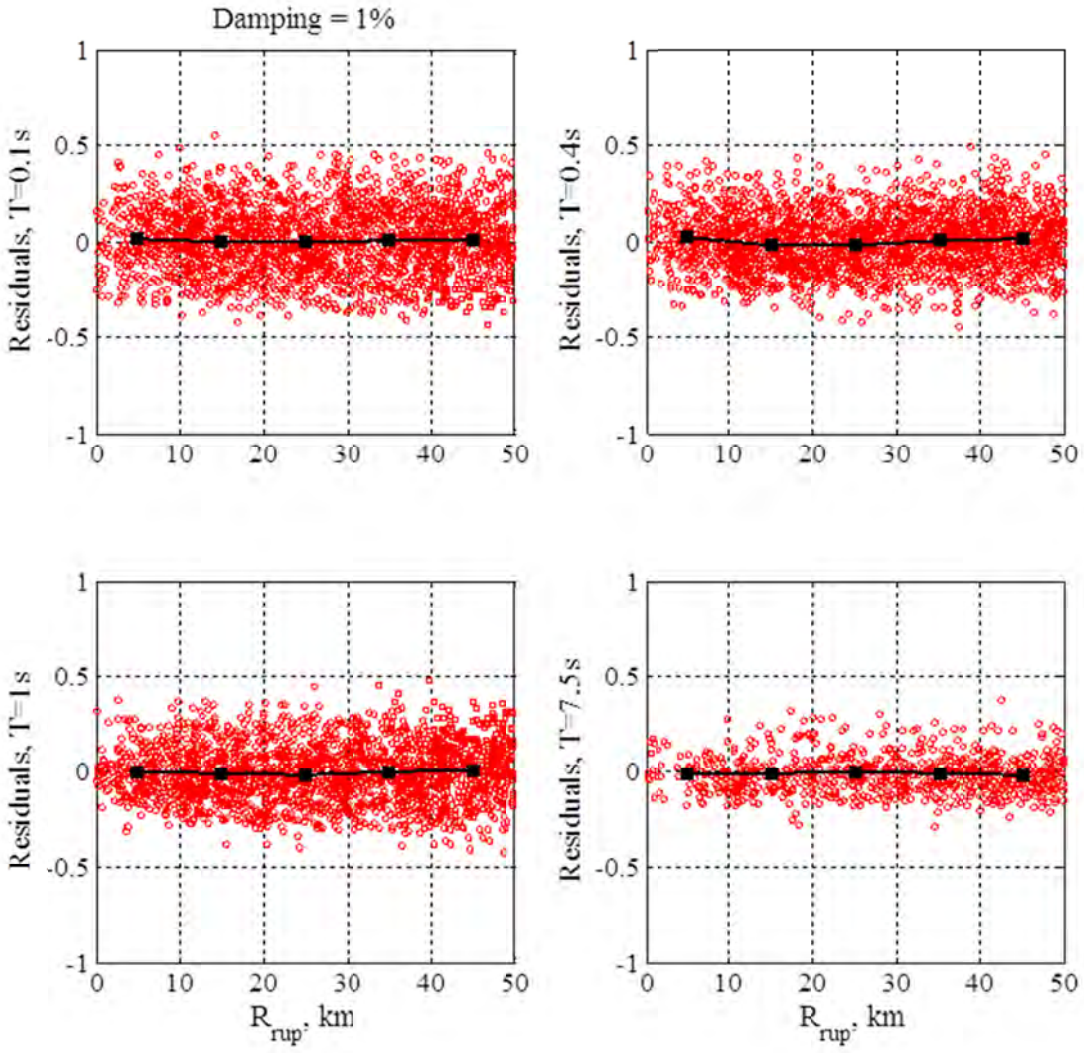

Figure D.6 **Dependence of residuals on rupture distance, R_{rup}. Data with $R_{rup} < 50$ km (i.e., data used in regression) and $\beta = 1\%$ are plotted.**

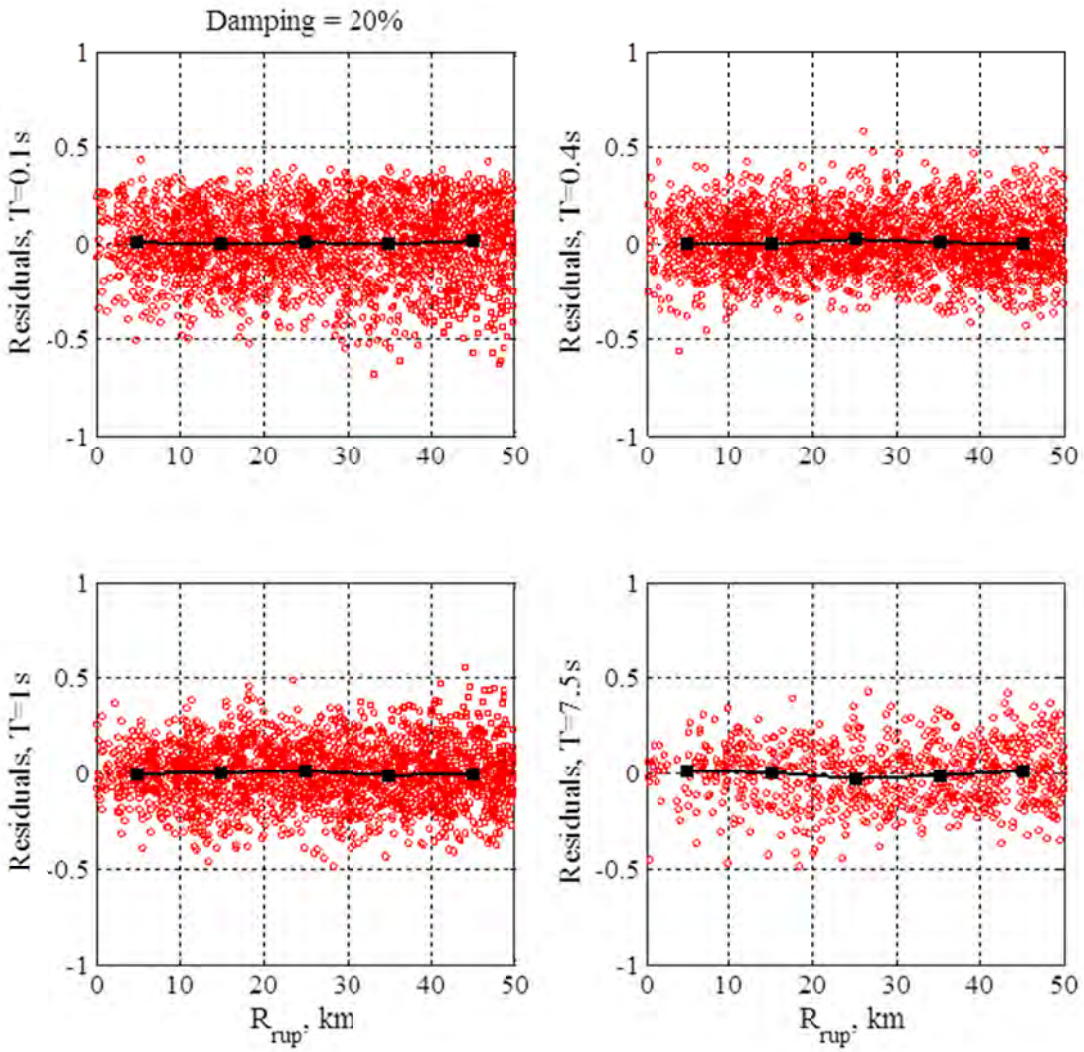

Figure D.7 **Dependence of residuals on rupture distance, R_{rup}. Data with $R_{rup} < 50$ km (i.e., data used in regression) and $\beta = 20\%$ are plotted.**

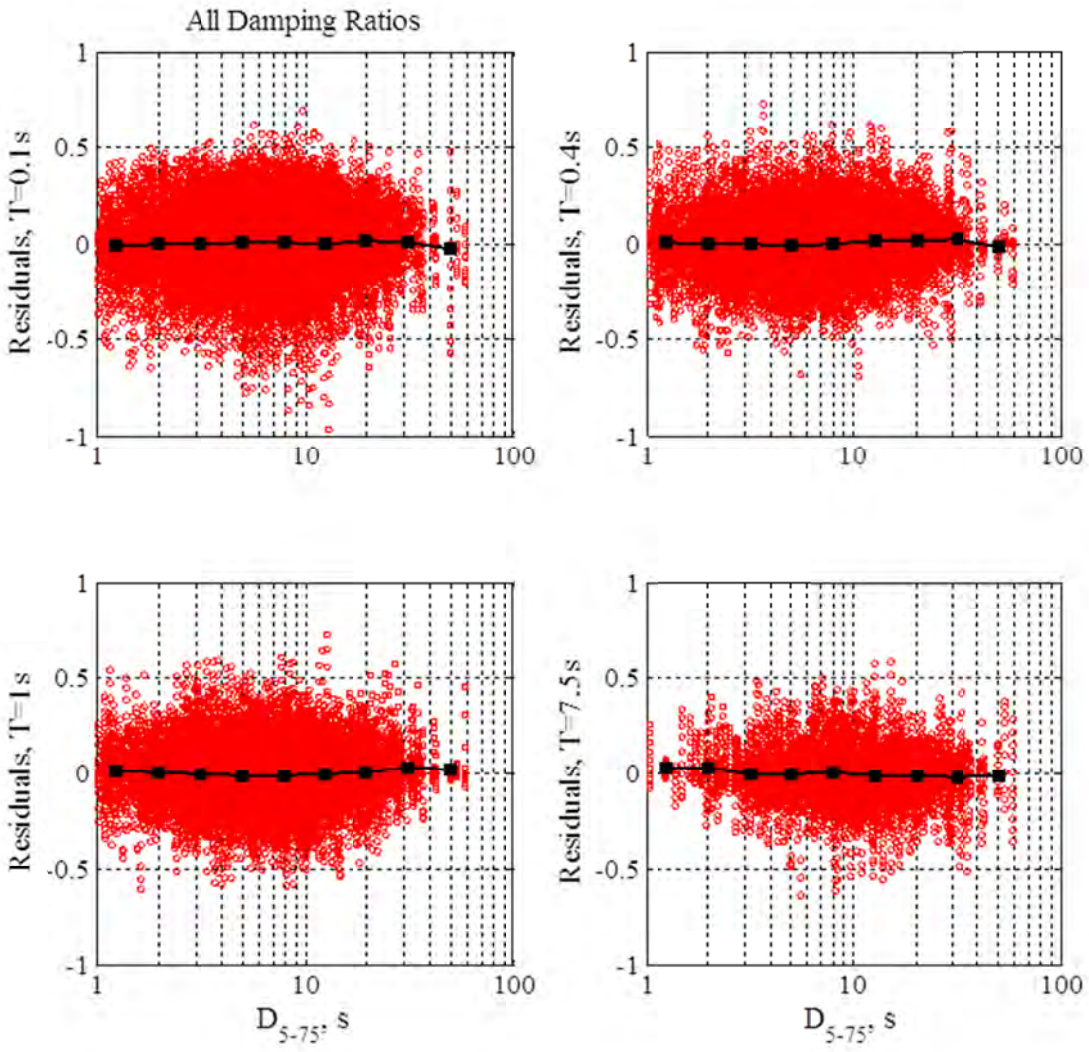

Figure D.8 **Dependence of residuals on duration of motion, D_{5-75}. Data with $R_{rup} < 50$ km (i.e., data used in regression) for all 11 damping ratios are plotted.**

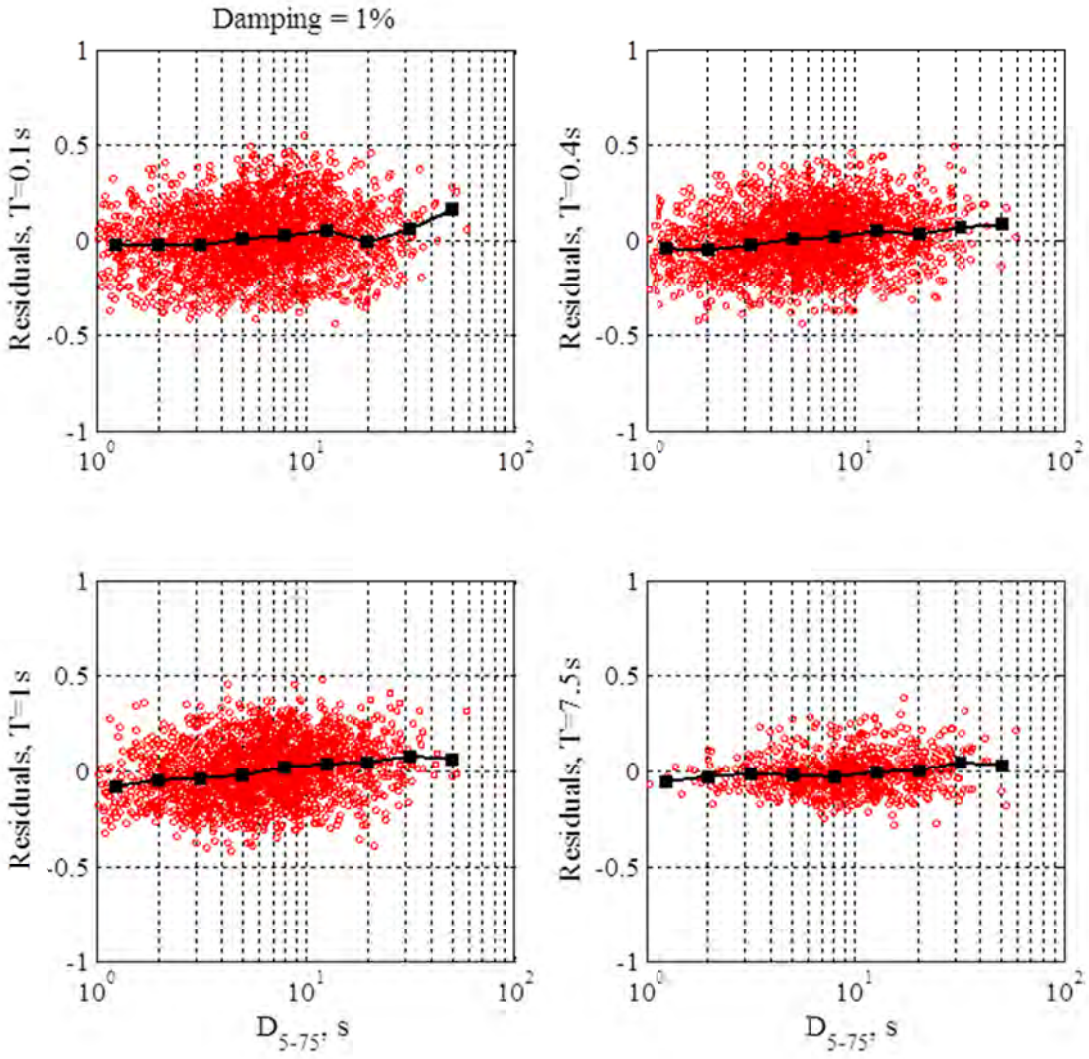

Figure D.9 **Dependence of residuals on duration of motion, D_{5-75}. Data with $R_{rup} < 50$ km (i.e., data used in regression) and $\beta = 1\%$ are plotted.**

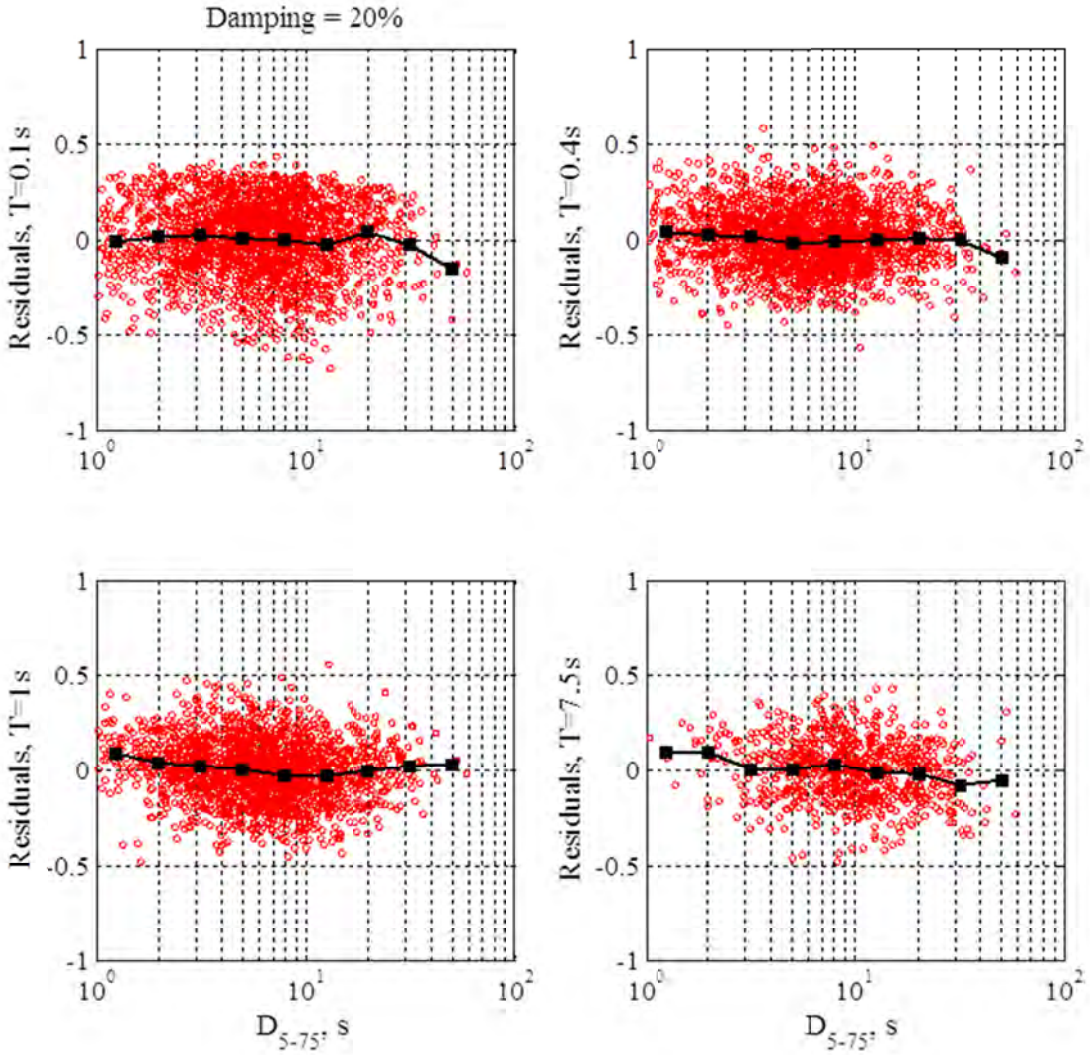

Figure D.10 Dependence of residuals on duration of motion, D_{5-75}. Data with $R_{rup} < 50$ km (i.e., data used in regression) and $\beta = 20\%$ are plotted.

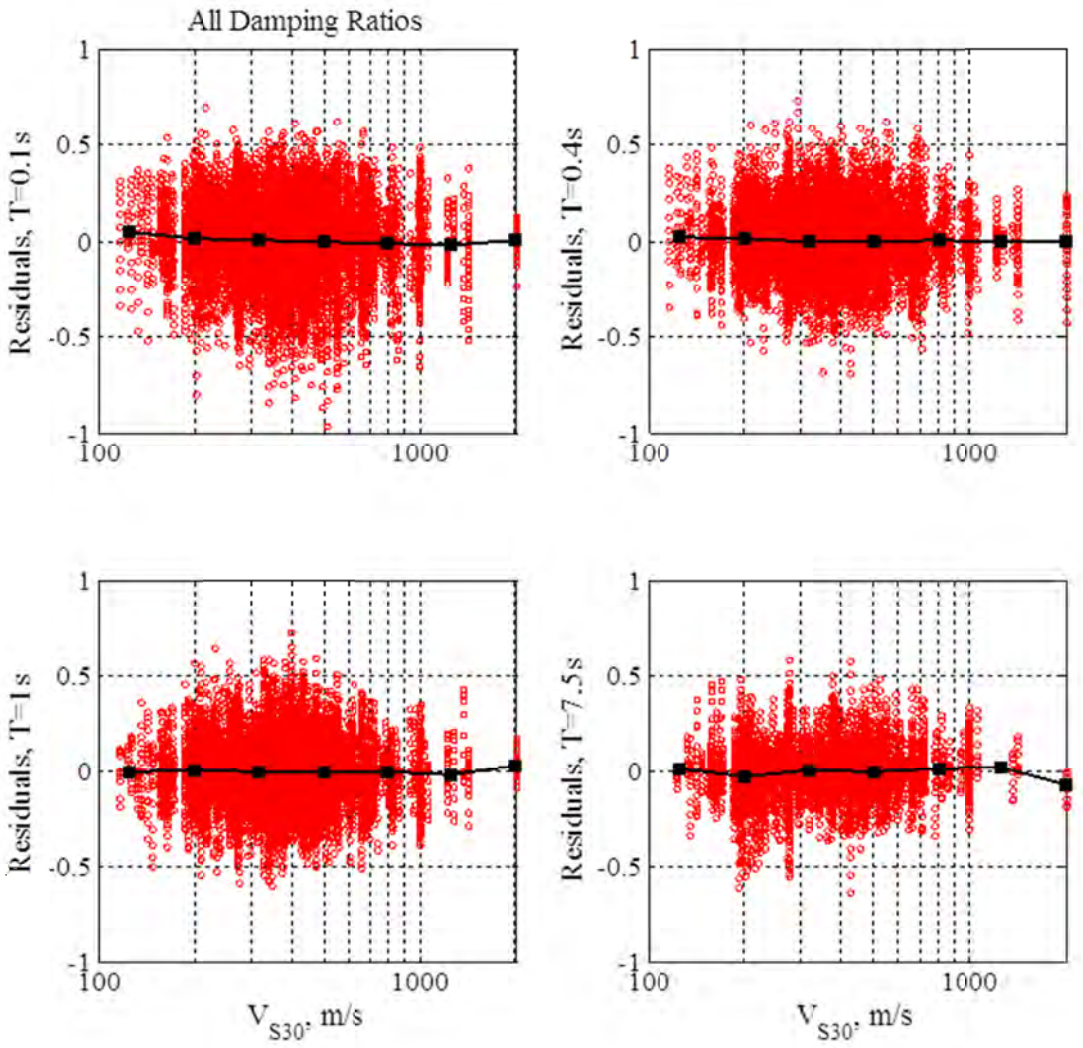

Figure D.11 **Dependence of residuals on 30-m shear-wave velocity, V_{S30}. Data with $R_{rup} < 50$ km (i.e., data used in regression) for all 11 damping ratios are plotted.**

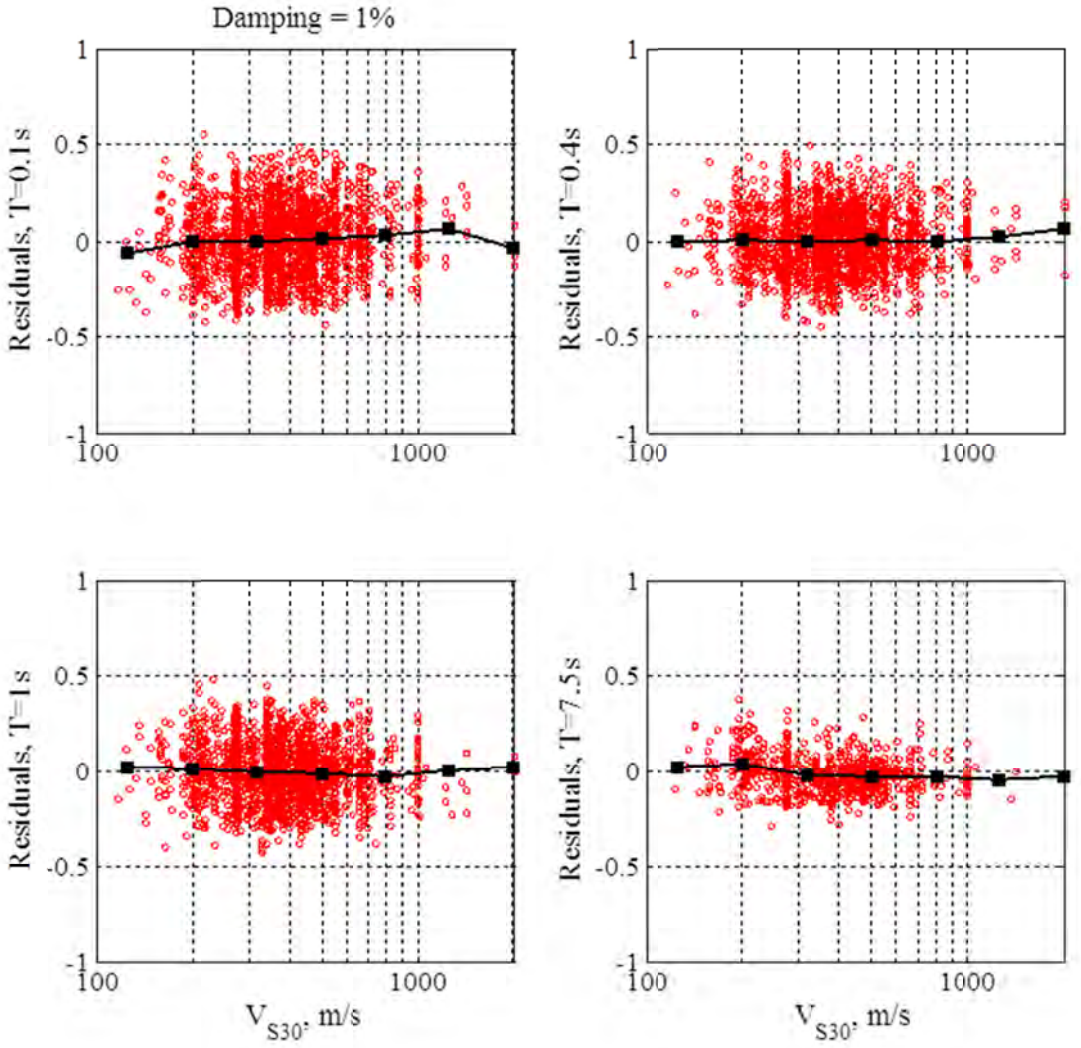

Figure D.12 Dependence of residuals on 30-m shear-wave velocity, V_{S30}. Data with $R_{rup} < 50$ km (i.e., data used in regression) and $\beta = 1\%$ are plotted.

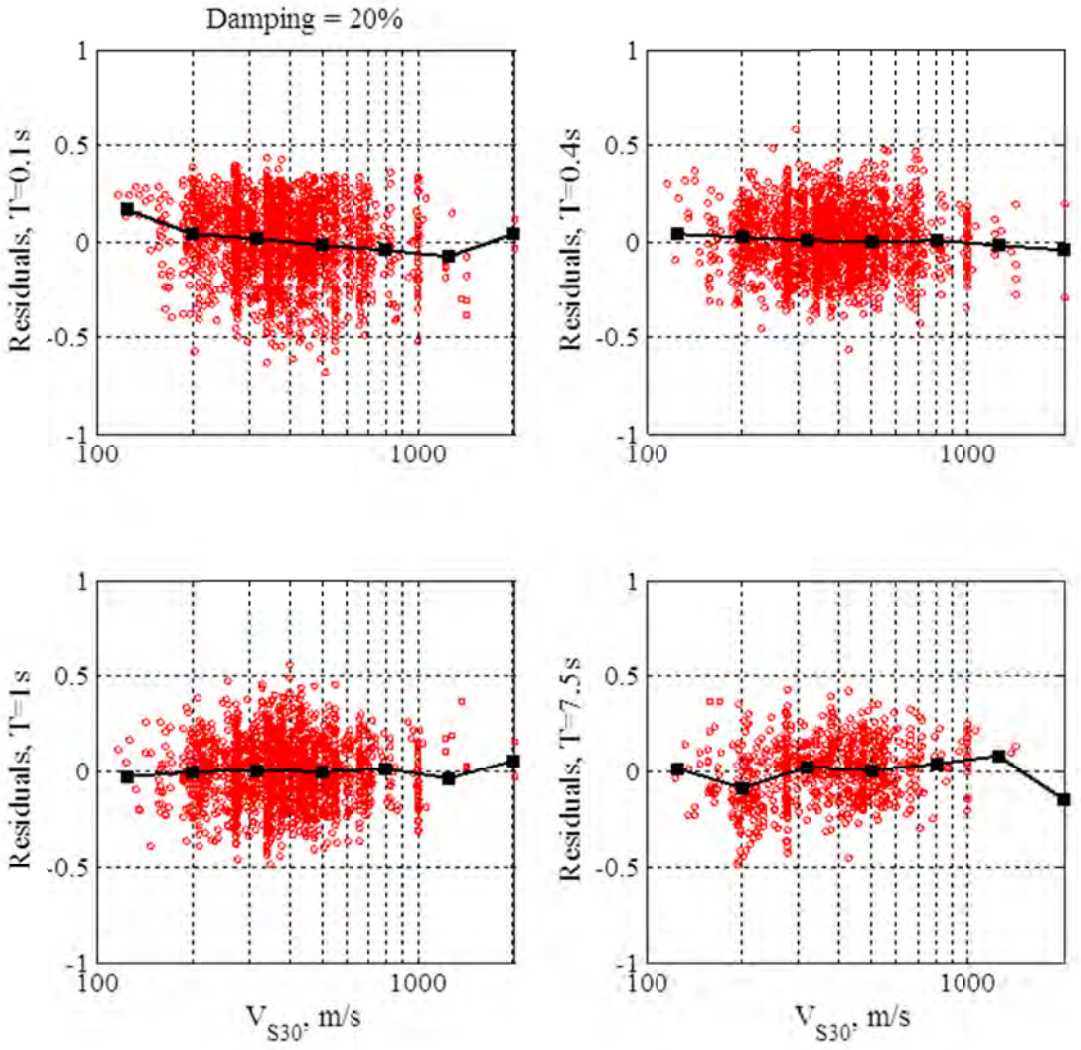

Figure D.13 Dependence of residuals on 30-m shear-wave velocity, V_{S30}. Data with $R_{rup} < 50$ km (i.e., data used in regression) and $\beta = 20\%$ are plotted.

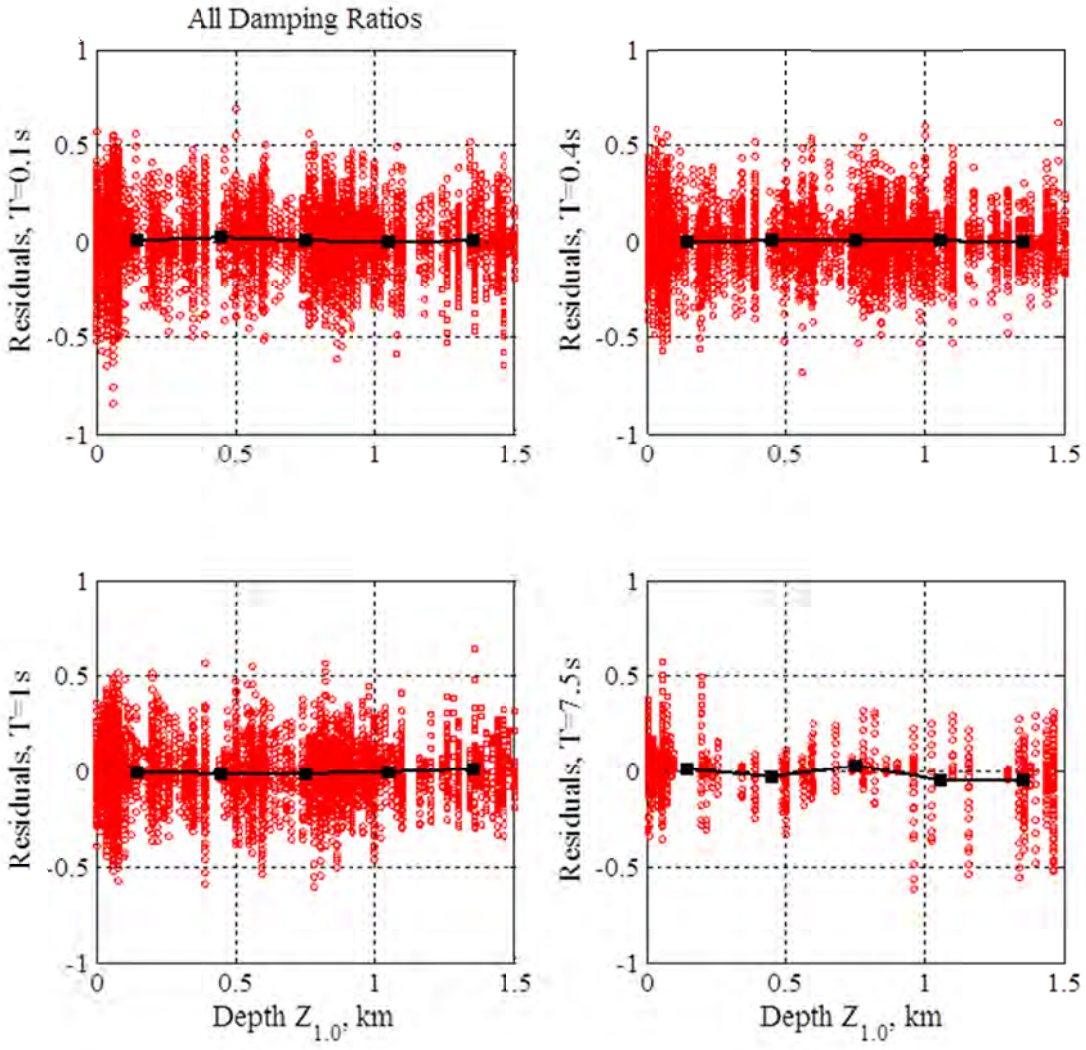

Figure D.14 Dependence of residuals on sediment depth, $Z_{1.0}$ (depth to the 1.0 km/sec velocity horizon). Data with $R_{rup} < 50$ km (i.e., data used in regression) for all 11 damping ratios are plotted.

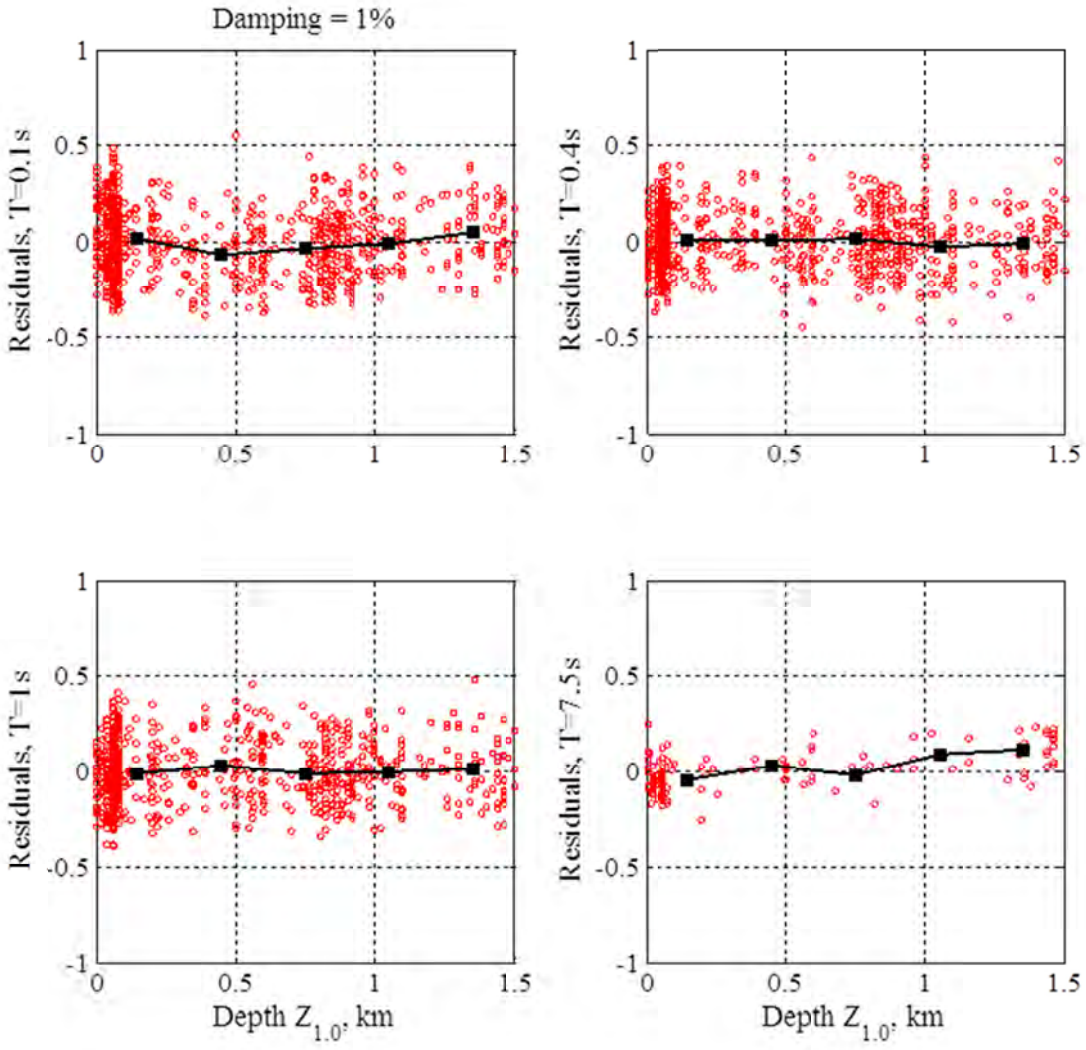

Figure D.15 Dependence of residuals on sediment depth, $Z_{1.0}$ (depth to the 1.0 km/sec velocity horizon). Data with $R_{rup} < 50$ km (i.e., data used in regression) and $\beta = 1\%$ are plotted.

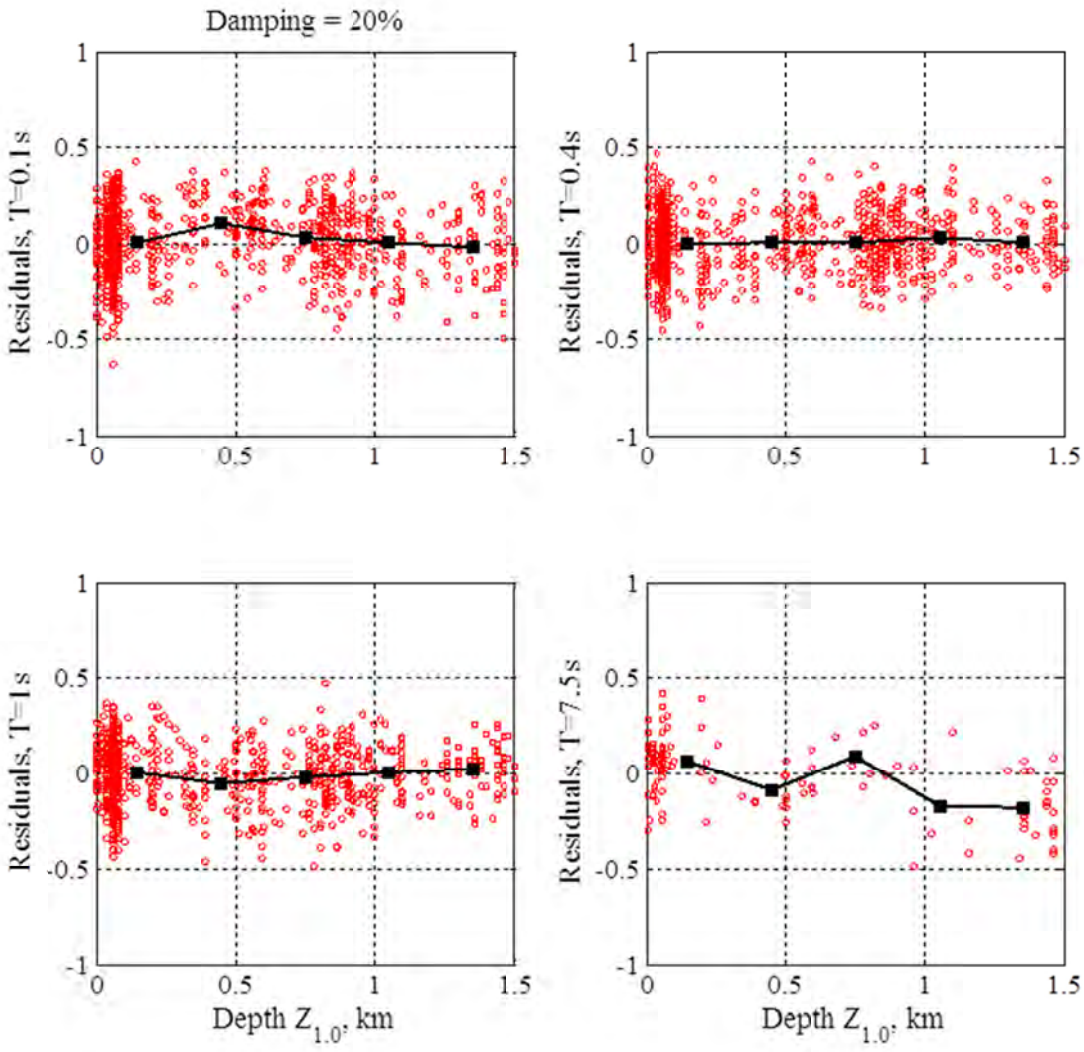

Figure D.16 **Dependence of residuals on sediment depth, $Z_{1.0}$ (depth to the 1.0 km/sec velocity horizon). Data with $R_{rup} < 50$ km (i.e., data used in regression) and $\beta = 20\%$ are plotted.**

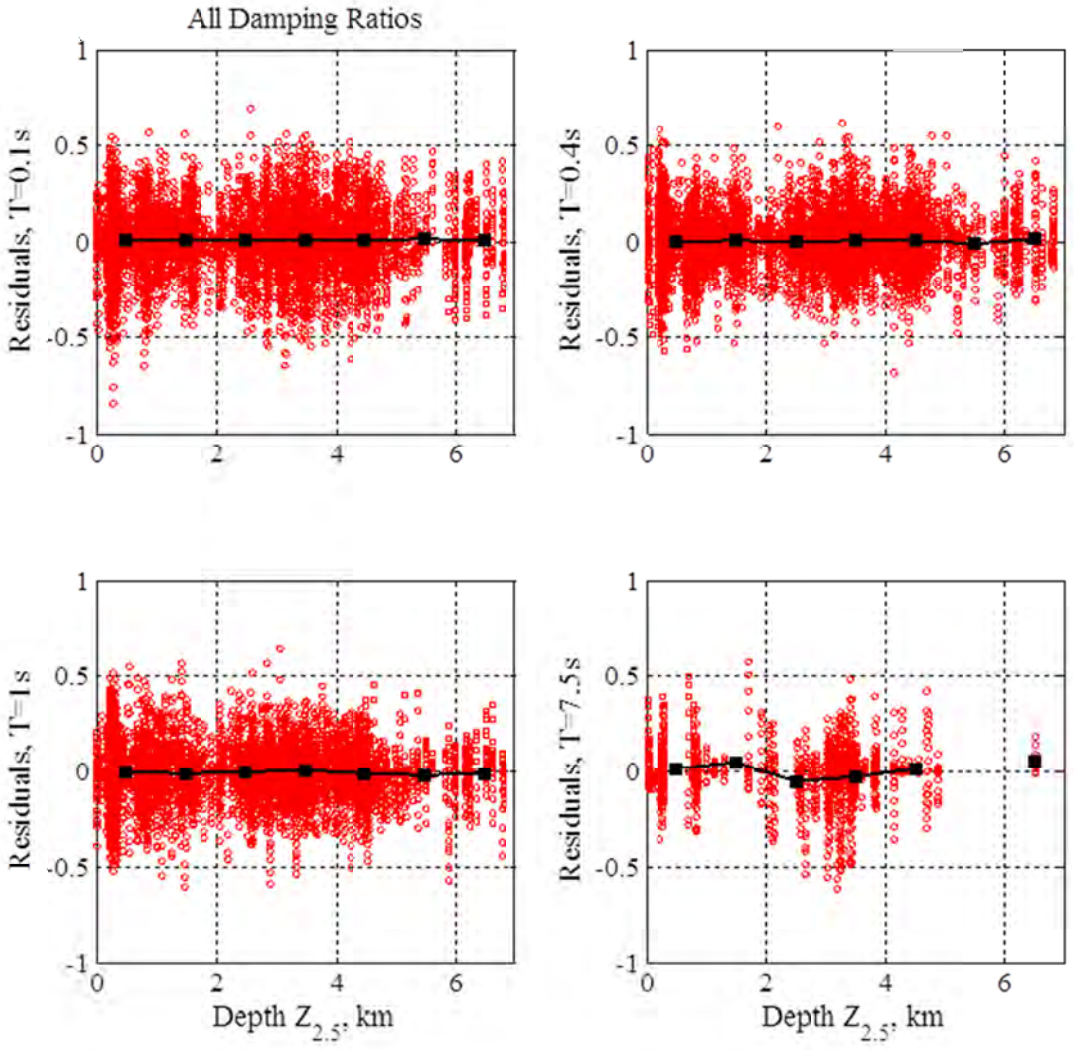

Figure D.17 **Dependence of residuals on sediment depth, $Z_{2.5}$ (depth to the 2.5 km/sec velocity horizon). Data with $R_{rup} < 50$ km (i.e., data used in regression) for all 11 damping ratios are plotted.**

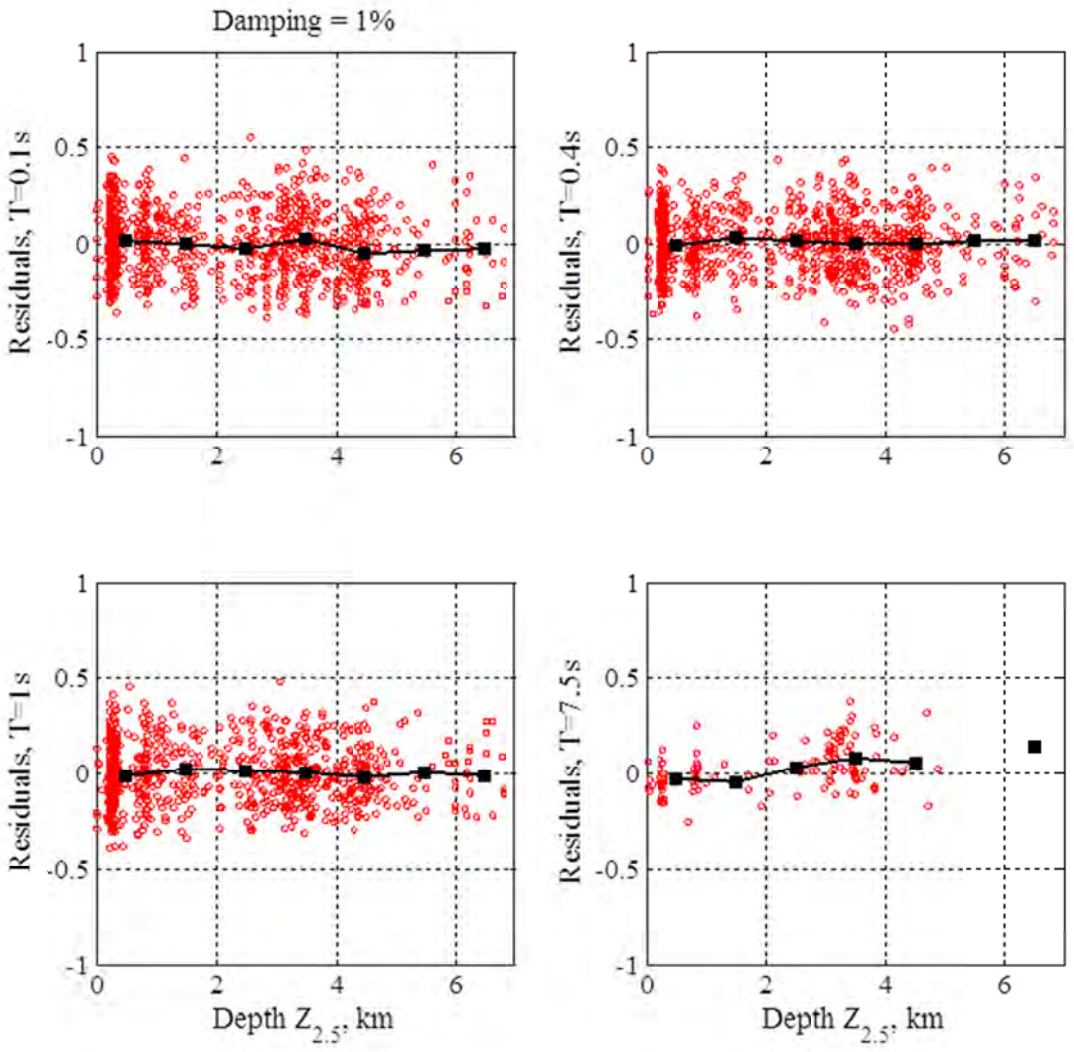

Figure D.18 **Dependence of residuals on sediment depth, $Z_{2.5}$ (depth to the 2.5 km/sec velocity horizon). Data with $R_{rup} < 50$ km (i.e., data used in regression) and $\beta = 1\%$ are plotted.**

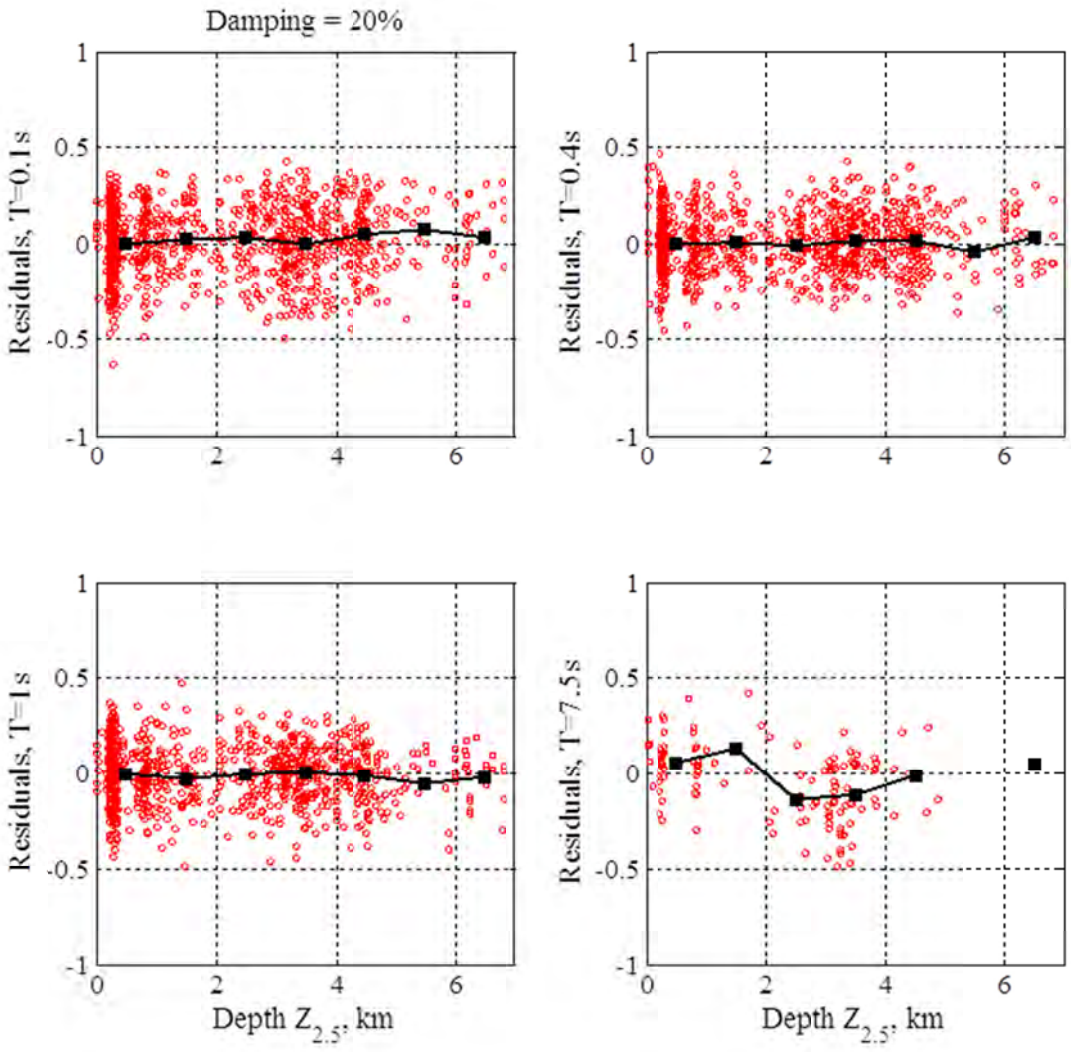

Figure D.19 **Dependence of residuals on sediment depth, $Z_{2.5}$ (depth to the 2.5 km/sec velocity horizon). Data with $R_{rup} < 50$ km (i.e., data used in regression) and $\beta = 20\%$ are plotted.**

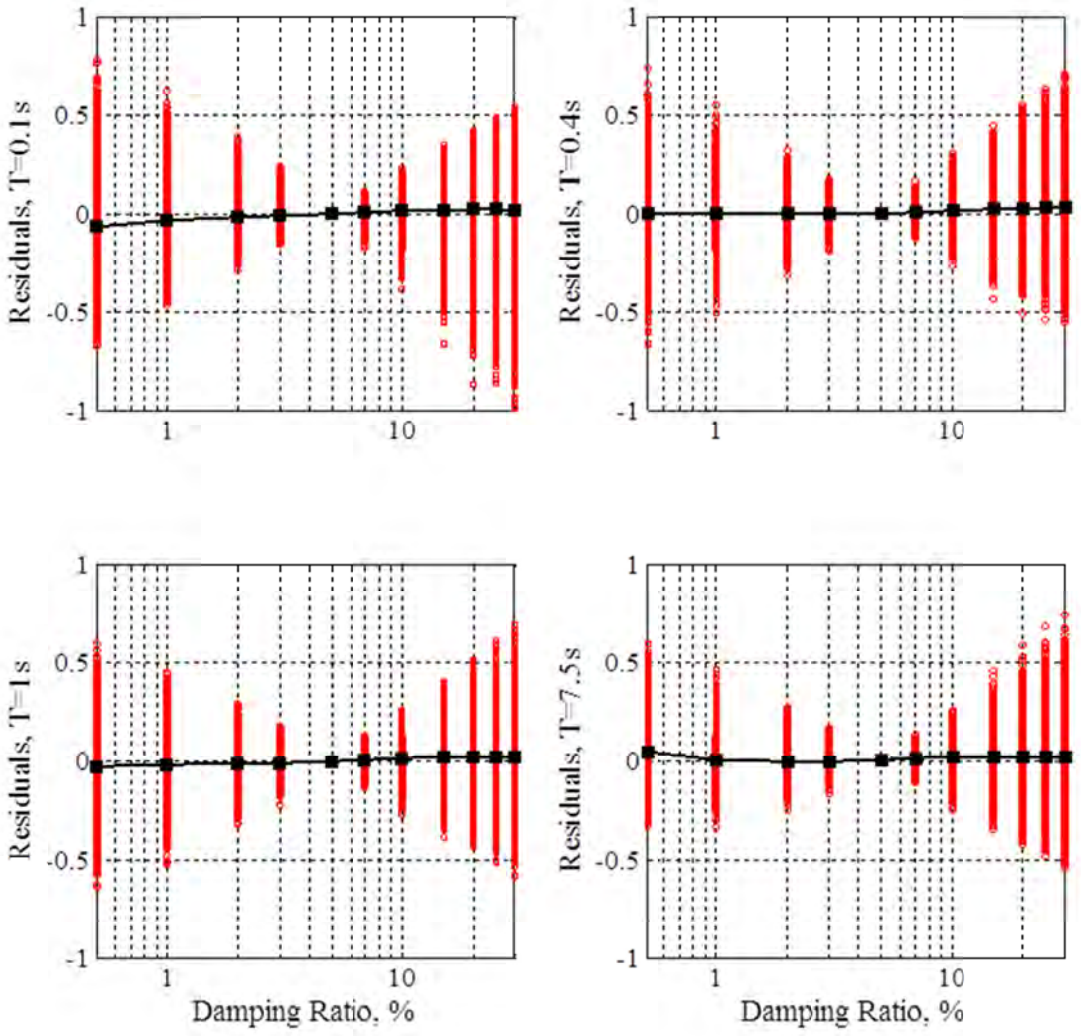

Figure D.20 Dependence of residuals on damping ratio, β. Data with $50 \leq R_{rup} < 200$ km are used.

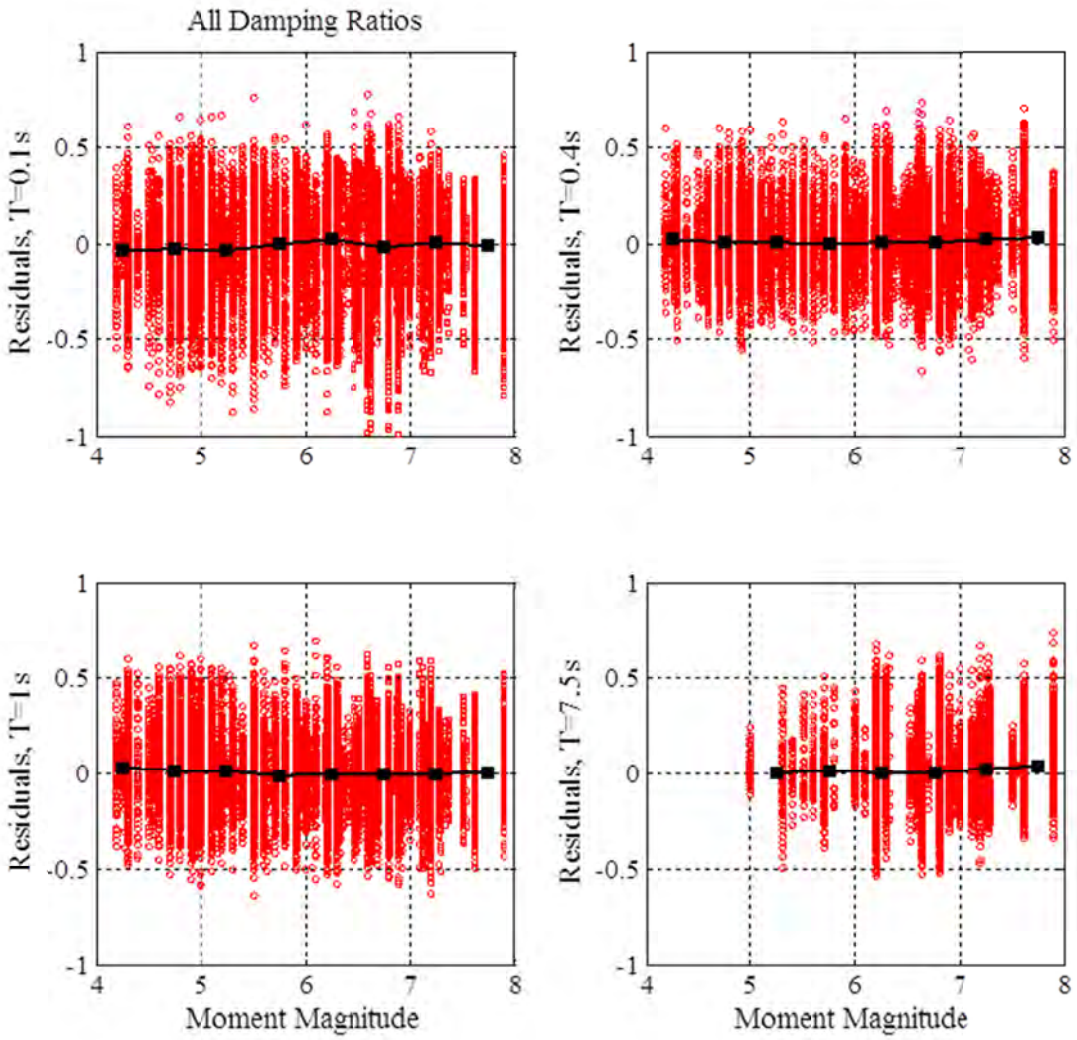

Figure D.21 Dependence of residuals on earthquake magnitude, M. Data with $50 \leq R_{rup} < 200$ km (i.e., data used in regression) for all 11 damping ratios are plotted.

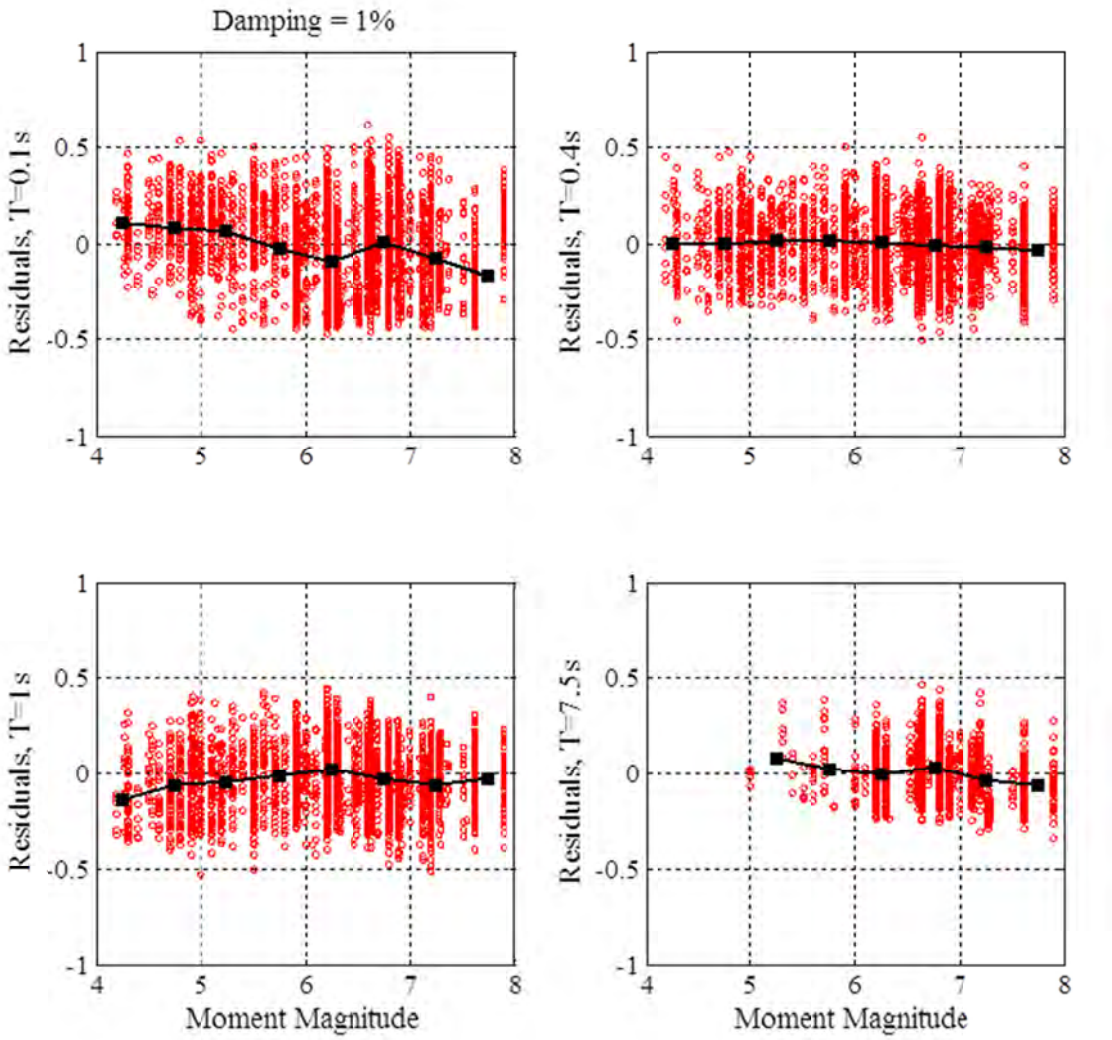

Figure D.22 Dependence of residuals on earthquake magnitude, M. Data with $50 \leq R_{rup} < 200$ km (i.e., data used in regression) and $\beta = 1\%$ are plotted.

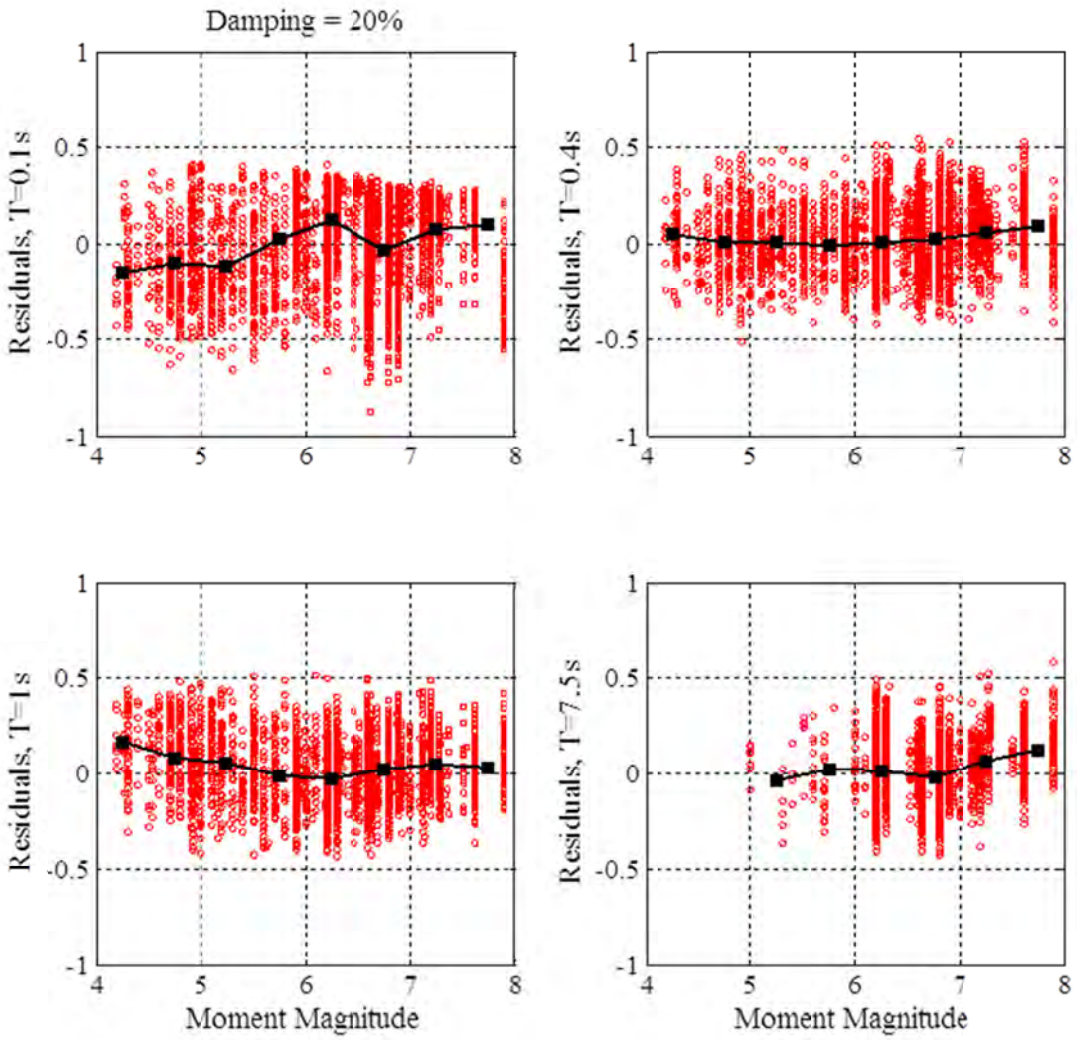

Figure D.23 Dependence of residuals on earthquake magnitude, M. Data with $50 \leq R_{rup} < 200$ km (i.e., data used in regression) and $\beta = 20\%$ are plotted.

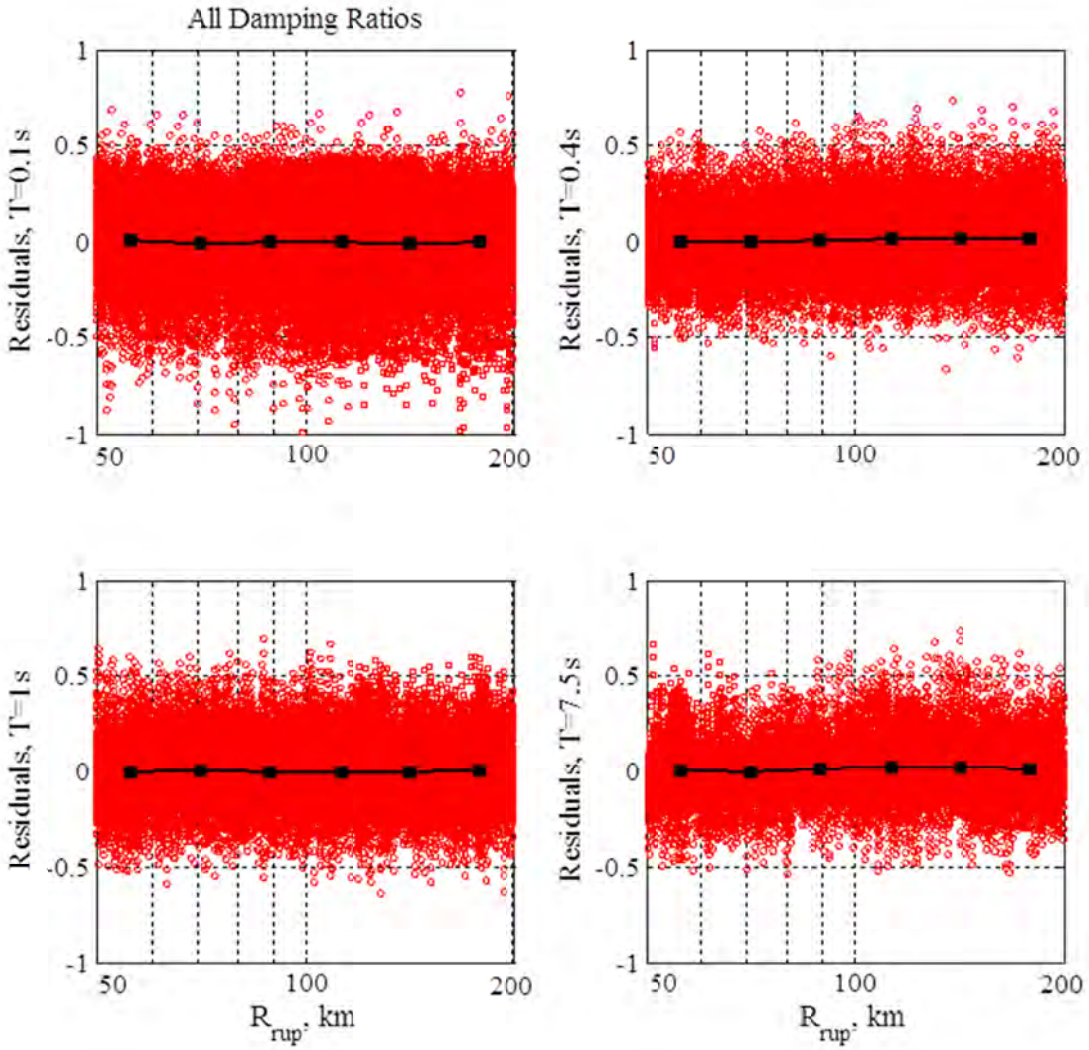

Figure D.24 Dependence of residuals on rupture distance, R_{rup}. Data with $50 \leq R_{rup} < 200$ km (i.e., data used in regression) for all 11 damping ratios are plotted.

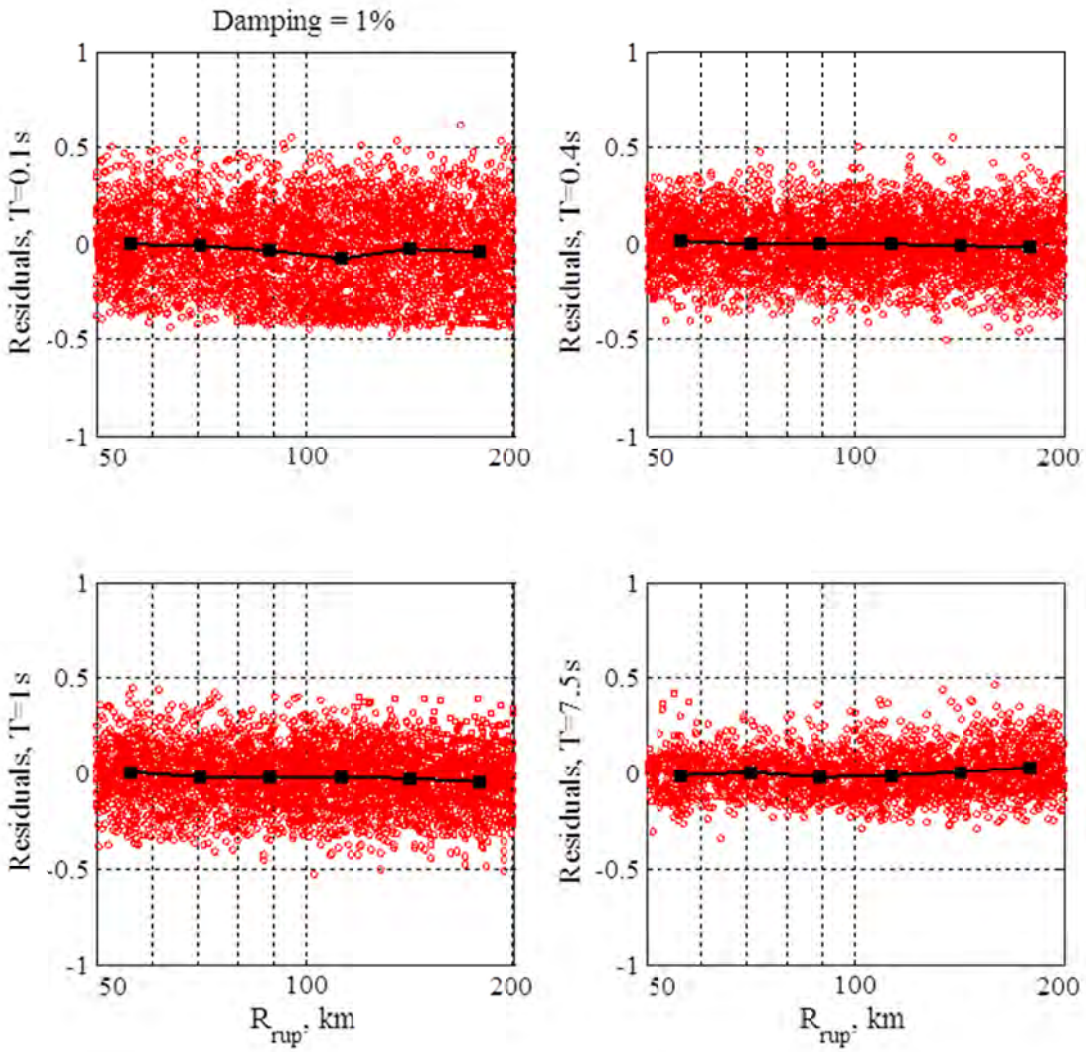

Figure D.25 Dependence of residuals on rupture distance, R_{rup}. Data with $50 \leq R_{rup} < 200$ km (i.e., data used in regression) and $\beta = 1\%$ are plotted.

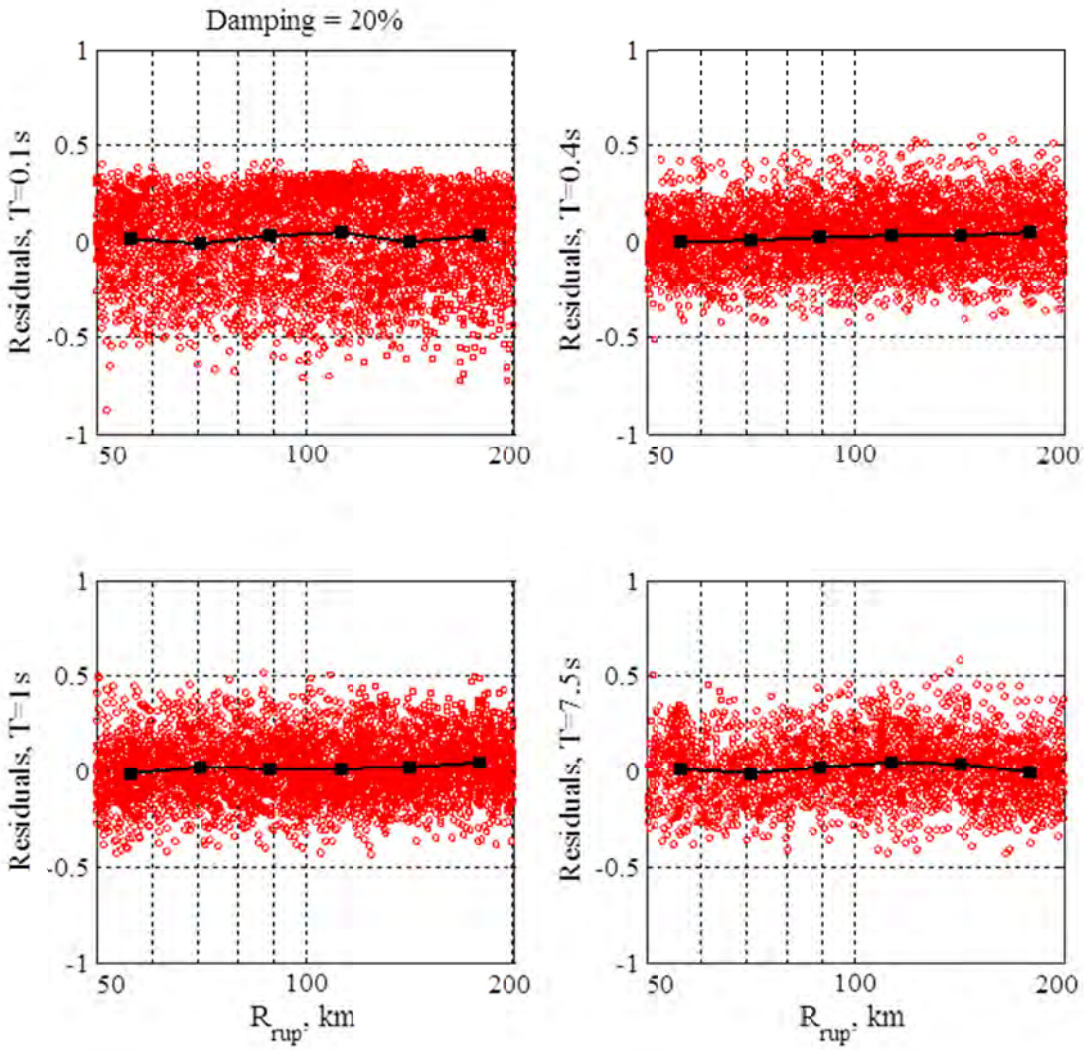

Figure D.26 Dependence of residuals on rupture distance, R_{rup}. Data with $50 \leq R_{rup} < 200$ km (i.e., data used in regression) and $\beta = 20\%$ are plotted.

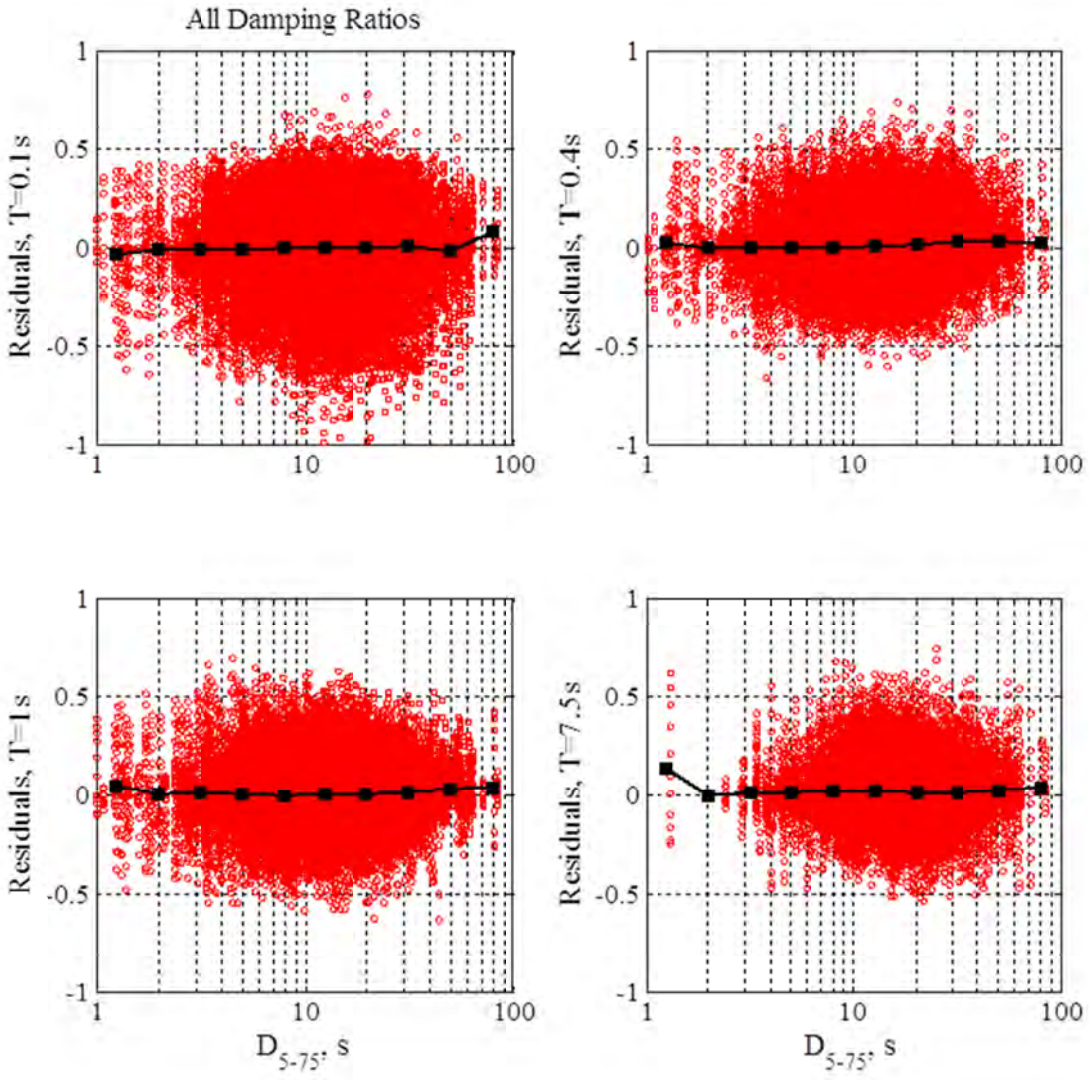

Figure D.27 Dependence of residuals on duration of motion, D_{5-75}. Data with $50 \leq R_{rup} < 200$ km (i.e., data used in regression) for all 11 damping ratios are plotted.

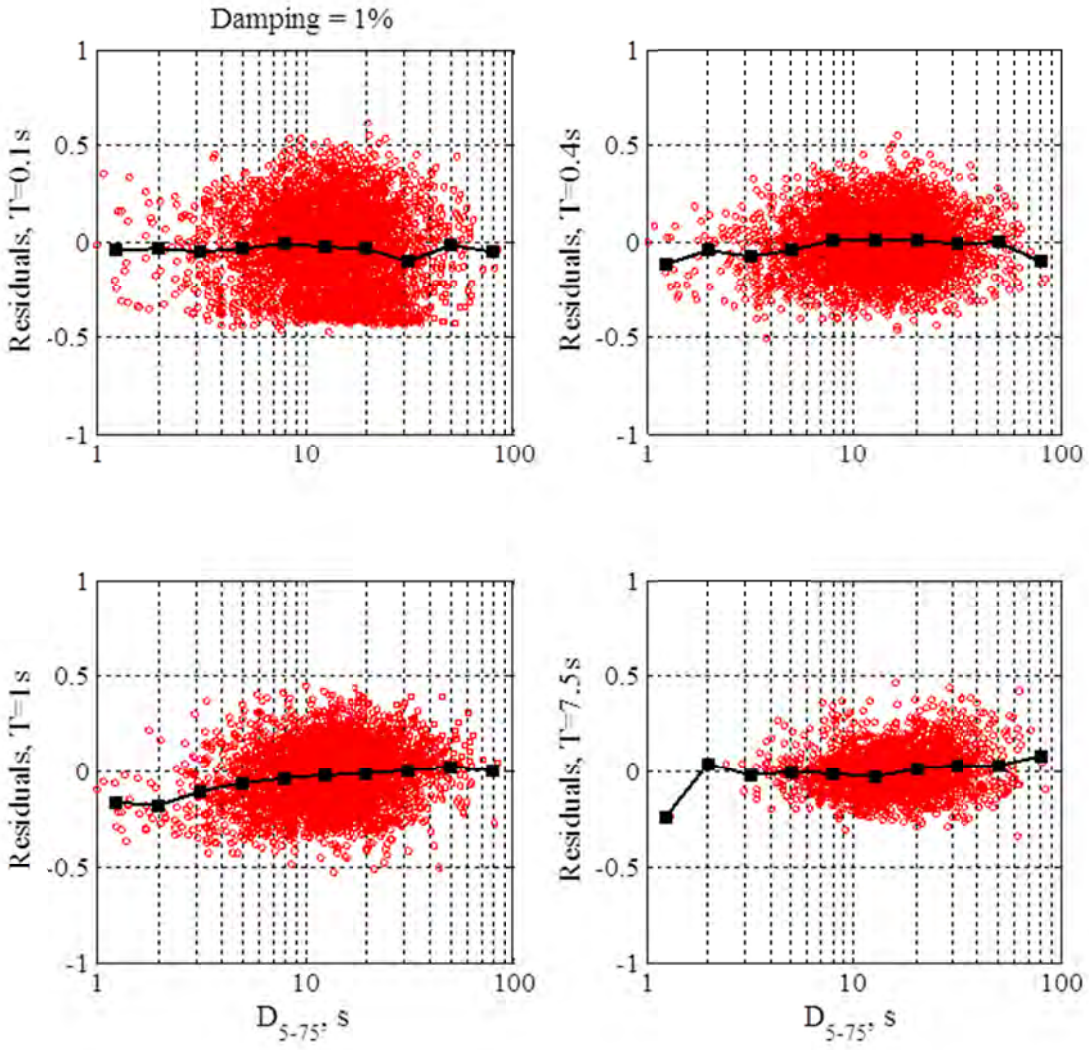

Figure D.28 Dependence of residuals on duration of motion, D_{5-75}. Data with $50 \leq R_{rup} < 200$ km (i.e., data used in regression) and $\beta = 1\%$ are plotted.

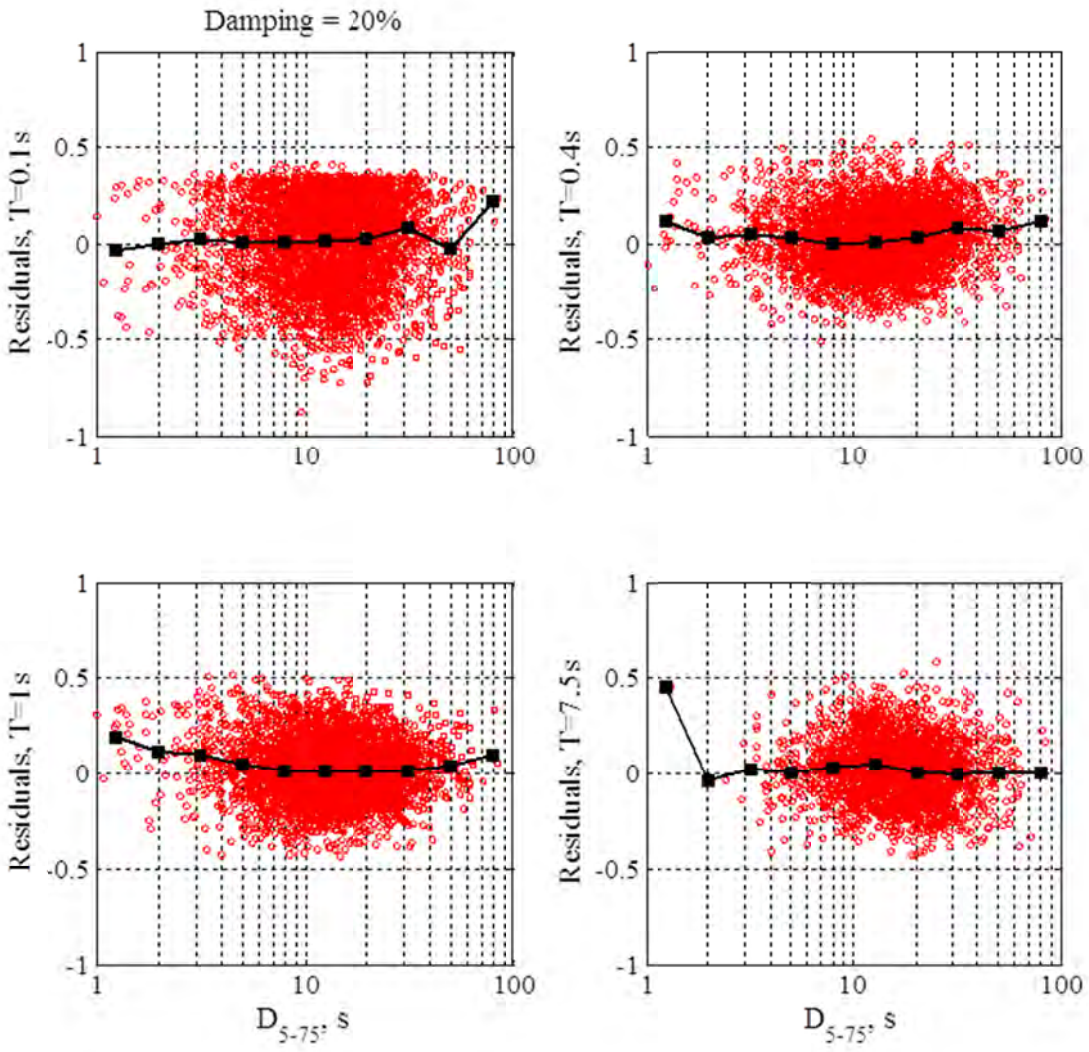

Figure D.29 Dependence of residuals on duration of motion, D_{5-75}. Data with $50 \leq R_{rup} < 200$ km (i.e., data used in regression) and $\beta = 20\%$ are plotted.

Appendix E: Sample Correlation Coefficients between ln(*DSF*) and ln($PSA_{5\%}$)

Table E.1 Sample correlation coefficients between $ln(DSF)$ and $ln(PSA_{5\%})$ using data with $R_{rup} < 50$ km.

	β, %										
***T*, s**	**0.5**	**1**	**2**	**3**	**5**	**7**	**10**	**15**	**20**	**25**	**30**
0.01	0.01	0.00	0.00	0.00	-	0.02	0.02	0.01	-0.01	-0.02	-0.03
0.02	0.01	0.03	0.04	0.06	-	-0.06	-0.06	-0.07	-0.08	-0.09	-0.09
0.03	0.12	0.12	0.12	0.13	-	-0.14	-0.15	-0.17	-0.17	-0.17	-0.17
0.05	0.15	0.17	0.17	0.18	-	-0.21	-0.21	-0.22	-0.22	-0.22	-0.22
0.075	0.10	0.12	0.15	0.15	-	-0.16	-0.18	-0.19	-0.20	-0.20	-0.20
0.1	0.06	0.09	0.10	0.11	-	-0.14	-0.16	-0.18	-0.18	-0.18	-0.18
0.15	0.00	0.01	0.03	0.04	-	-0.10	-0.12	-0.14	-0.14	-0.15	-0.15
0.2	0.03	0.05	0.07	0.06	-	-0.10	-0.12	-0.14	-0.14	-0.14	-0.14
0.25	0.04	0.06	0.08	0.08	-	-0.09	-0.10	-0.11	-0.12	-0.12	-0.12
0.3	0.02	0.03	0.05	0.06	-	-0.09	-0.11	-0.13	-0.13	-0.13	-0.13
0.4	0.00	0.02	0.04	0.05	-	-0.10	-0.11	-0.12	-0.13	-0.13	-0.13
0.5	-0.01	0.01	0.03	0.05	-	-0.11	-0.13	-0.15	-0.16	-0.17	-0.17
0.75	0.08	0.09	0.11	0.13	-	-0.19	-0.23	-0.28	-0.30	-0.32	-0.34
1	0.07	0.08	0.10	0.11	-	-0.19	-0.24	-0.29	-0.32	-0.35	-0.37
1.5	0.17	0.19	0.22	0.22	-	-0.27	-0.32	-0.37	-0.40	-0.43	-0.44
2	0.25	0.25	0.25	0.26	-	-0.33	-0.37	-0.42	-0.46	-0.49	-0.51
3	0.32	0.32	0.31	0.32	-	-0.35	-0.39	-0.43	-0.46	-0.48	-0.50
4	0.33	0.33	0.34	0.34	-	-0.36	-0.38	-0.41	-0.43	-0.44	-0.46
5	0.38	0.38	0.39	0.38	-	-0.40	-0.42	-0.45	-0.47	-0.49	-0.51
7.5	0.49	0.49	0.49	0.49	-	-0.51	-0.53	-0.55	-0.57	-0.58	-0.59
10	0.38	0.39	0.41	0.41	-	-0.42	-0.44	-0.47	-0.49	-0.51	-0.52

Table E.2 **Logarithmic standard deviation of $PSA_{5\%}$ according to Campbell and Bozorgnia [2008] GMPE, assuming $V_{S30} \geq k_1$, where k_1 is a period-dependent variable given in Campbell and Bozorgnia [2008]. All values are rounded to two decimal places**

T, s	$\sigma_{ln(PSA_{5\%})}$
0.01	0.53
0.02	0.53
0.03	0.54
0.05	0.57
0.075	0.60
0.1	0.60
0.15	0.60
0.2	0.59
0.25	0.59
0.3	0.58
0.4	0.58
0.5	0.59
0.75	0.61
1	0.62
1.5	0.64
2	0.64
3	0.65
4	0.65
5	0.70
7.5	0.76
10	0.82

Table E.3 $\sigma_{ln(PSA_{\beta\%})}$ **evaluated according to Equation (4.11), assuming** $\sigma_{ln(PSA_{5\%})}$ **equals the values in Table E.2 and** ρ **equals the values in Table E.1.**

	β, %										
***T*, s**	**0.5**	**1**	**2**	**3**	**5**	**7**	**10**	**15**	**20**	**25**	**30**
0.01	0.53	0.53	0.53	0.53	-	0.53	0.53	0.53	0.53	0.53	0.53
0.02	0.53	0.53	0.53	0.53	-	0.53	0.53	0.53	0.53	0.53	0.53
0.03	0.58	0.56	0.55	0.54	-	0.54	0.54	0.53	0.53	0.53	0.53
0.05	0.64	0.62	0.59	0.58	-	0.56	0.56	0.56	0.56	0.56	0.56
0.075	0.67	0.65	0.62	0.61	-	0.59	0.59	0.59	0.59	0.59	0.60
0.1	0.65	0.64	0.62	0.61	-	0.60	0.59	0.59	0.60	0.60	0.61
0.15	0.63	0.62	0.61	0.60	-	0.60	0.60	0.60	0.60	0.61	0.61
0.2	0.63	0.62	0.60	0.60	-	0.59	0.59	0.59	0.59	0.60	0.60
0.25	0.63	0.62	0.60	0.60	-	0.59	0.59	0.59	0.59	0.60	0.60
0.3	0.62	0.60	0.59	0.59	-	0.58	0.58	0.58	0.58	0.58	0.59
0.4	0.61	0.60	0.59	0.58	-	0.58	0.58	0.58	0.58	0.58	0.59
0.5	0.62	0.61	0.60	0.59	-	0.59	0.59	0.58	0.59	0.59	0.59
0.75	0.66	0.64	0.63	0.62	-	0.60	0.60	0.59	0.58	0.58	0.57
1	0.66	0.65	0.63	0.63	-	0.61	0.61	0.60	0.59	0.58	0.58
1.5	0.70	0.68	0.66	0.65	-	0.63	0.62	0.61	0.59	0.58	0.58
2	0.71	0.69	0.67	0.65	-	0.63	0.62	0.60	0.58	0.57	0.56
3	0.72	0.70	0.68	0.67	-	0.64	0.63	0.61	0.60	0.58	0.58
4	0.72	0.70	0.68	0.67	-	0.64	0.63	0.61	0.60	0.59	0.58
5	0.76	0.75	0.73	0.72	-	0.69	0.67	0.65	0.64	0.63	0.62
7.5	0.83	0.81	0.80	0.78	-	0.74	0.73	0.70	0.68	0.67	0.66
10	0.85	0.85	0.84	0.83	-	0.81	0.80	0.78	0.77	0.76	0.75

Table E.4 $\sigma_{ln(PSA_{\beta\%})}$ **evaluated according to Equation (4.11), assuming** $\sigma_{ln(PSA_{5\%})}$ **equals the values in Table E.2 and** $\rho = 0$.

	β, %										
***T*, s**	**0.5**	**1**	**2**	**3**	**5**	**7**	**10**	**15**	**20**	**25**	**30**
0.01	0.53	0.53	0.53	0.53	0.53	0.53	0.53	0.53	0.53	0.53	0.53
0.02	0.53	0.53	0.53	0.53	0.53	0.53	0.53	0.53	0.53	0.53	0.53
0.03	0.56	0.55	0.54	0.54	0.54	0.54	0.54	0.54	0.54	0.54	0.55
0.05	0.61	0.59	0.58	0.57	0.57	0.57	0.57	0.58	0.58	0.59	0.59
0.075	0.65	0.63	0.61	0.60	0.60	0.60	0.61	0.62	0.63	0.64	0.64
0.1	0.64	0.62	0.61	0.60	0.60	0.60	0.61	0.62	0.63	0.64	0.65
0.15	0.63	0.62	0.61	0.60	0.60	0.60	0.61	0.62	0.63	0.64	0.65
0.2	0.62	0.61	0.60	0.59	0.59	0.59	0.60	0.60	0.61	0.62	0.63
0.25	0.62	0.61	0.60	0.59	0.59	0.59	0.59	0.60	0.61	0.62	0.63
0.3	0.61	0.60	0.59	0.58	0.58	0.58	0.58	0.59	0.60	0.61	0.61
0.4	0.61	0.60	0.59	0.58	0.58	0.58	0.58	0.59	0.60	0.61	0.61
0.5	0.62	0.61	0.60	0.59	0.59	0.59	0.59	0.60	0.61	0.62	0.62
0.75	0.64	0.63	0.62	0.61	0.61	0.61	0.61	0.62	0.63	0.64	0.64
1	0.65	0.64	0.63	0.62	0.62	0.62	0.62	0.63	0.64	0.65	0.65
1.5	0.67	0.66	0.65	0.64	0.64	0.64	0.64	0.65	0.66	0.67	0.67
2	0.67	0.66	0.65	0.64	0.64	0.64	0.64	0.65	0.66	0.67	0.67
3	0.67	0.66	0.65	0.65	0.65	0.65	0.65	0.66	0.67	0.68	0.68
4	0.67	0.66	0.65	0.65	0.65	0.65	0.65	0.66	0.67	0.68	0.69
5	0.71	0.71	0.70	0.70	0.70	0.70	0.70	0.71	0.72	0.73	0.73
7.5	0.77	0.77	0.76	0.76	0.76	0.76	0.76	0.77	0.78	0.78	0.79
10	0.82	0.82	0.82	0.82	0.82	0.82	0.82	0.83	0.83	0.83	0.84

PEER REPORTS

PEER reports are available individually or by yearly subscription. PEER reports can be ordered at http://peer.berkeley.edu/publications/peer_reports.html or by contacting the Pacific Earthquake Engineering Research Center, 325 Davis Hall mail code 1792, Berkeley, CA 94720. Tel.: (510) 642-3437; Fax: (510) 665-1655; Email: peer_editor@berkeley.edu

PEER 2012/01 *Spectral Damping Scaling Factors for Shallow Crustal Earthquakes in Active Tectonic Regions.* Sanaz Rezaeian, Yousef Bozorgnia, I. M. Idriss, Kenneth Campbell, Norman Abrahamson, and Walter Silva. July 2012.

PEER 2011/10 *Earthquake Engineering for Resilient Communities: 2011 PEER Internship Program Research Report Collection.* Eds. Heidi Faison and Stephen A. Mahin. December 2011.

PEER 2011/09 *Calibration of Semi-Stochastic Procedure for Simulating High-Frequency Ground Motions.* Jonathan P. Stewart, Emel Seyhan, and Robert W. Graves. December 2011.

PEER 2011/08 *Water Supply in regard to Fire Following Earthquake.* Charles Scawthorn. November 2011.

PEER 2011/07 *Seismic Risk Management in Urban Areas. Proceedings of a U.S.-Iran-Turkey Seismic Workshop.* September 2011.

PEER 2011/06 *The Use of Base Isolation Systems to Achieve Complex Seismic Performance Objectives.* Troy A. Morgan and Stephen A. Mahin. July 2011.

PEER 2011/05 *Case Studies of the Seismic Performance of Tall Buildings Designed by Alternative Means.* Task 12 Report for the Tall Buildings Initiative. Jack Moehle, Yousef Bozorgnia, Nirmal Jayaram, Pierson Jones, Mohsen Rahnama, Nilesh Shome, Zeynep Tuna, John Wallace, Tony Yang, and Farzin Zareian. July 2011.

PEER 2011/04 *Recommended Design Practice for Pile Foundations in Laterally Spreading Ground.* Scott A. Ashford, Ross W. Boulanger, and Scott J. Brandenberg. June 2011.

PEER 2011/03 *New Ground Motion Selection Procedures and Selected Motions for the PEER Transportation Research Program.* Jack W. Baker, Ting Lin, Shrey K. Shahi, and Nirmal Jayaram. March 2011.

PEER 2011/02 *A Bayesian Network Methodology for Infrastructure Seismic Risk Assessment and Decision Support.* Michelle T. Bensi, Armen Der Kiureghian, and Daniel Straub. March 2011.

PEER 2011/01 *Demand Fragility Surfaces for Bridges in Liquefied and Laterally Spreading Ground.* Scott J. Brandenberg, Jian Zhang, Pirooz Kashighandi, Yili Huo, and Minxing Zhao. March 2011.

PEER 2010/05 *Guidelines for Performance-Based Seismic Design of Tall Buildings.* Developed by the Tall Buildings Initiative. November 2010.

PEER 2010/04 *Application Guide for the Design of Flexible and Rigid Bus Connections between Substation Equipment Subjected to Earthquakes.* Jean-Bernard Dastous and Armen Der Kiureghian. September 2010.

PEER 2010/03 *Shear Wave Velocity as a Statistical Function of Standard Penetration Test Resistance and Vertical Effective Stress at Caltrans Bridge Sites.* Scott J. Brandenberg, Naresh Bellana, and Thomas Shantz. June 2010.

PEER 2010/02 *Stochastic Modeling and Simulation of Ground Motions for Performance-Based Earthquake Engineering.* Sanaz Rezaeian and Armen Der Kiureghian. June 2010.

PEER 2010/01 *Structural Response and Cost Characterization of Bridge Construction Using Seismic Performance Enhancement Strategies.* Ady Aviram, Božidar Stojadinović, Gustavo J. Parra-Montesinos, and Kevin R. Mackie. March 2010.

PEER 2009/03 *The Integration of Experimental and Simulation Data in the Study of Reinforced Concrete Bridge Systems Including Soil-Foundation-Structure Interaction.* Matthew Dryden and Gregory L. Fenves. November 2009.

PEER 2009/02 *Improving Earthquake Mitigation through Innovations and Applications in Seismic Science, Engineering, Communication, and Response. Proceedings of a U.S.-Iran Seismic Workshop.* October 2009.

PEER 2009/01 *Evaluation of Ground Motion Selection and Modification Methods: Predicting Median Interstory Drift Response of Buildings.* Curt B. Haselton, Ed. June 2009.

PEER 2008/10 *Technical Manual for Strata.* Albert R. Kottke and Ellen M. Rathje. February 2009.

PEER 2008/09 *NGA Model for Average Horizontal Component of Peak Ground Motion and Response Spectra.* Brian S.-J. Chiou and Robert R. Youngs. November 2008.

PEER 2008/08 *Toward Earthquake-Resistant Design of Concentrically Braced Steel Structures.* Patxi Uriz and Stephen A. Mahin. November 2008.

PEER 2008/07 *Using OpenSees for Performance-Based Evaluation of Bridges on Liquefiable Soils.* Stephen L. Kramer, Pedro Arduino, and HyungSuk Shin. November 2008.

PEER 2008/06 *Shaking Table Tests and Numerical Investigation of Self-Centering Reinforced Concrete Bridge Columns.* Hyung IL Jeong, Junichi Sakai, and Stephen A. Mahin. September 2008.

PEER 2008/05 *Performance-Based Earthquake Engineering Design Evaluation Procedure for Bridge Foundations Undergoing Liquefaction-Induced Lateral Ground Displacement.* Christian A. Ledezma and Jonathan D. Bray. August 2008.

PEER 2008/04 *Benchmarking of Nonlinear Geotechnical Ground Response Analysis Procedures.* Jonathan P. Stewart, Annie On-Lei Kwok, Yousseff M. A. Hashash, Neven Matasovic, Robert Pyke, Zhiliang Wang, and Zhaohui Yang. August 2008.

PEER 2008/03 *Guidelines for Nonlinear Analysis of Bridge Structures in California.* Ady Aviram, Kevin R. Mackie, and Božidar Stojadinović. August 2008.

PEER 2008/02 *Treatment of Uncertainties in Seismic-Risk Analysis of Transportation Systems.* Evangelos Stergiou and Anne S. Kiremidjian. July 2008.

PEER 2008/01 *Seismic Performance Objectives for Tall Buildings.* William T. Holmes, Charles Kircher, William Petak, and Nabih Youssef. August 2008.

PEER 2007/12 *An Assessment to Benchmark the Seismic Performance of a Code-Conforming Reinforced Concrete Moment-Frame Building.* Curt Haselton, Christine A. Goulet, Judith Mitrani-Reiser, James L. Beck, Gregory G. Deierlein, Keith A. Porter, Jonathan P. Stewart, and Ertugrul Taciroglu. August 2008.

PEER 2007/11 *Bar Buckling in Reinforced Concrete Bridge Columns.* Wayne A. Brown, Dawn E. Lehman, and John F. Stanton. February 2008.

PEER 2007/10 *Computational Modeling of Progressive Collapse in Reinforced Concrete Frame Structures.* Mohamed M. Talaat and Khalid M. Mosalam. May 2008.

PEER 2007/09 *Integrated Probabilistic Performance-Based Evaluation of Benchmark Reinforced Concrete Bridges.* Kevin R. Mackie, John-Michael Wong, and Božidar Stojadinović. January 2008.

PEER 2007/08 *Assessing Seismic Collapse Safety of Modern Reinforced Concrete Moment-Frame Buildings.* Curt B. Haselton and Gregory G. Deierlein. February 2008.

PEER 2007/07 *Performance Modeling Strategies for Modern Reinforced Concrete Bridge Columns.* Michael P. Berry and Marc O. Eberhard. April 2008.

PEER 2007/06 *Development of Improved Procedures for Seismic Design of Buried and Partially Buried Structures.* Linda Al Atik and Nicholas Sitar. June 2007.

PEER 2007/05 *Uncertainty and Correlation in Seismic Risk Assessment of Transportation Systems.* Renee G. Lee and Anne S. Kiremidjian. July 2007.

PEER 2007/04 *Numerical Models for Analysis and Performance-Based Design of Shallow Foundations Subjected to Seismic Loading.* Sivapalan Gajan, Tara C. Hutchinson, Bruce L. Kutter, Prishati Raychowdhury, José A. Ugalde, and Jonathan P. Stewart. May 2008.

PEER 2007/03 *Beam-Column Element Model Calibrated for Predicting Flexural Response Leading to Global Collapse of RC Frame Buildings.* Curt B. Haselton, Abbie B. Liel, Sarah Taylor Lange, and Gregory G. Deierlein. May 2008.

PEER 2007/02 *Campbell-Bozorgnia NGA Ground Motion Relations for the Geometric Mean Horizontal Component of Peak and Spectral Ground Motion Parameters.* Kenneth W. Campbell and Yousef Bozorgnia. May 2007.

PEER 2007/01 *Boore-Atkinson NGA Ground Motion Relations for the Geometric Mean Horizontal Component of Peak and Spectral Ground Motion Parameters.* David M. Boore and Gail M. Atkinson. May. May 2007.

PEER 2006/12 *Societal Implications of Performance-Based Earthquake Engineering.* Peter J. May. May 2007.

PEER 2006/11 *Probabilistic Seismic Demand Analysis Using Advanced Ground Motion Intensity Measures, Attenuation Relationships, and Near-Fault Effects.* Polsak Tothong and C. Allin Cornell. March 2007.

PEER 2006/10 *Application of the PEER PBEE Methodology to the I-880 Viaduct.* Sashi Kunnath. February 2007.

PEER 2006/09 *Quantifying Economic Losses from Travel Forgone Following a Large Metropolitan Earthquake.* James Moore, Sungbin Cho, Yue Yue Fan, and Stuart Werner. November 2006.

PEER 2006/08 *Vector-Valued Ground Motion Intensity Measures for Probabilistic Seismic Demand Analysis.* Jack W. Baker and C. Allin Cornell. October 2006.

PEER 2006/07 *Analytical Modeling of Reinforced Concrete Walls for Predicting Flexural and Coupled–Shear-Flexural Responses.* Kutay Orakcal, Leonardo M. Massone, and John W. Wallace. October 2006.

PEER 2006/06 *Nonlinear Analysis of a Soil-Drilled Pier System under Static and Dynamic Axial Loading.* Gang Wang and Nicholas Sitar. November 2006.

PEER 2006/05 *Advanced Seismic Assessment Guidelines.* Paolo Bazzurro, C. Allin Cornell, Charles Menun, Maziar Motahari, and Nicolas Luco. September 2006.

PEER 2006/04 *Probabilistic Seismic Evaluation of Reinforced Concrete Structural Components and Systems.* Tae Hyung Lee and Khalid M. Mosalam. August 2006.

PEER 2006/03 *Performance of Lifelines Subjected to Lateral Spreading.* Scott A. Ashford and Teerawut Juirnarongrit. July 2006.

PEER 2006/02 *Pacific Earthquake Engineering Research Center Highway Demonstration Project.* Anne Kiremidjian, James Moore, Yue Yue Fan, Nesrin Basoz, Ozgur Yazali, and Meredith Williams. April 2006.

PEER 2006/01 *Bracing Berkeley. A Guide to Seismic Safety on the UC Berkeley Campus.* Mary C. Comerio, Stephen Tobriner, and Ariane Fehrenkamp. January 2006.

PEER 2005/16 *Seismic Response and Reliability of Electrical Substation Equipment and Systems.* Junho Song, Armen Der Kiureghian, and Jerome L. Sackman. April 2006.

PEER 2005/15 *CPT-Based Probabilistic Assessment of Seismic Soil Liquefaction Initiation.* R. E. S. Moss, R. B. Seed, R. E. Kayen, J. P. Stewart, and A. Der Kiureghian. April 2006.

PEER 2005/14 *Workshop on Modeling of Nonlinear Cyclic Load-Deformation Behavior of Shallow Foundations.* Bruce L. Kutter, Geoffrey Martin, Tara Hutchinson, Chad Harden, Sivapalan Gajan, and Justin Phalen. March 2006.

PEER 2005/13 *Stochastic Characterization and Decision Bases under Time-Dependent Aftershock Risk in Performance-Based Earthquake Engineering.* Gee Liek Yeo and C. Allin Cornell. July 2005.

PEER 2005/12 *PEER Testbed Study on a Laboratory Building: Exercising Seismic Performance Assessment.* Mary C. Comerio, editor. November 2005.

PEER 2005/11 *Van Nuys Hotel Building Testbed Report: Exercising Seismic Performance Assessment.* Helmut Krawinkler, editor. October 2005.

PEER 2005/10 *First NEES/E-Defense Workshop on Collapse Simulation of Reinforced Concrete Building Structures.* September 2005.

PEER 2005/09 *Test Applications of Advanced Seismic Assessment Guidelines.* Joe Maffei, Karl Telleen, Danya Mohr, William Holmes, and Yuki Nakayama. August 2006.

PEER 2005/08 *Damage Accumulation in Lightly Confined Reinforced Concrete Bridge Columns.* R. Tyler Ranf, Jared M. Nelson, Zach Price, Marc O. Eberhard, and John F. Stanton. April 2006.

PEER 2005/07 *Experimental and Analytical Studies on the Seismic Response of Freestanding and Anchored Laboratory Equipment.* Dimitrios Konstantinidis and Nicos Makris. January 2005.

PEER 2005/06 *Global Collapse of Frame Structures under Seismic Excitations.* Luis F. Ibarra and Helmut Krawinkler. September 2005.

PEER 2005//05 *Performance Characterization of Bench- and Shelf-Mounted Equipment.* Samit Ray Chaudhuri and Tara C. Hutchinson. May 2006.

PEER 2005/04 *Numerical Modeling of the Nonlinear Cyclic Response of Shallow Foundations.* Chad Harden, Tara Hutchinson, Geoffrey R. Martin, and Bruce L. Kutter. August 2005.

PEER 2005/03 *A Taxonomy of Building Components for Performance-Based Earthquake Engineering.* Keith A. Porter. September 2005.

PEER 2005/02 *Fragility Basis for California Highway Overpass Bridge Seismic Decision Making.* Kevin R. Mackie and Božidar Stojadinović. June 2005.

PEER 2005/01 *Empirical Characterization of Site Conditions on Strong Ground Motion.* Jonathan P. Stewart, Yoojoong Choi, and Robert W. Graves. June 2005.

PEER 2004/09 *Electrical Substation Equipment Interaction: Experimental Rigid Conductor Studies.* Christopher Stearns and André Filiatrault. February 2005.

PEER 2004/08 *Seismic Qualification and Fragility Testing of Line Break 550-kV Disconnect Switches.* Shakhzod M. Takhirov, Gregory L. Fenves, and Eric Fujisaki. January 2005.

PEER 2004/07 *Ground Motions for Earthquake Simulator Qualification of Electrical Substation Equipment.* Shakhzod M. Takhirov, Gregory L. Fenves, Eric Fujisaki, and Don Clyde. January 2005.

PEER 2004/06 *Performance-Based Regulation and Regulatory Regimes.* Peter J. May and Chris Koski. September 2004.

PEER 2004/05 *Performance-Based Seismic Design Concepts and Implementation: Proceedings of an International Workshop.* Peter Fajfar and Helmut Krawinkler, editors. September 2004.

PEER 2004/04 *Seismic Performance of an Instrumented Tilt-up Wall Building.* James C. Anderson and Vitelmo V. Bertero. July 2004.

PEER 2004/03 *Evaluation and Application of Concrete Tilt-up Assessment Methodologies.* Timothy Graf and James O. Malley. October 2004.

PEER 2004/02 *Analytical Investigations of New Methods for Reducing Residual Displacements of Reinforced Concrete Bridge Columns.* Junichi Sakai and Stephen A. Mahin. August 2004.

PEER 2004/01 *Seismic Performance of Masonry Buildings and Design Implications.* Kerri Anne Taeko Tokoro, James C. Anderson, and Vitelmo V. Bertero. February 2004.

PEER 2003/18 *Performance Models for Flexural Damage in Reinforced Concrete Columns.* Michael Berry and Marc Eberhard. August 2003.

PEER 2003/17 *Predicting Earthquake Damage in Older Reinforced Concrete Beam-Column Joints.* Catherine Pagni and Laura Lowes. October 2004.

PEER 2003/16 *Seismic Demands for Performance-Based Design of Bridges.* Kevin Mackie and Božidar Stojadinović. August 2003.

PEER 2003/15 *Seismic Demands for Nondeteriorating Frame Structures and Their Dependence on Ground Motions.* Ricardo Antonio Medina and Helmut Krawinkler. May 2004.

PEER 2003/14 *Finite Element Reliability and Sensitivity Methods for Performance-Based Earthquake Engineering.* Terje Haukaas and Armen Der Kiureghian. April 2004.

PEER 2003/13 *Effects of Connection Hysteretic Degradation on the Seismic Behavior of Steel Moment-Resisting Frames.* Janise E. Rodgers and Stephen A. Mahin. March 2004.

PEER 2003/12 *Implementation Manual for the Seismic Protection of Laboratory Contents: Format and Case Studies.* William T. Holmes and Mary C. Comerio. October 2003.

PEER 2003/11 *Fifth U.S.-Japan Workshop on Performance-Based Earthquake Engineering Methodology for Reinforced Concrete Building Structures.* February 2004.

PEER 2003/10 *A Beam-Column Joint Model for Simulating the Earthquake Response of Reinforced Concrete Frames.* Laura N. Lowes, Nilanjan Mitra, and Arash Altoontash. February 2004.

PEER 2003/09 *Sequencing Repairs after an Earthquake: An Economic Approach.* Marco Casari and Simon J. Wilkie. April 2004.

PEER 2003/08 *A Technical Framework for Probability-Based Demand and Capacity Factor Design (DCFD) Seismic Formats*. Fatemeh Jalayer and C. Allin Cornell. November 2003.

PEER 2003/07 *Uncertainty Specification and Propagation for Loss Estimation Using FOSM Methods.* Jack W. Baker and C. Allin Cornell. September 2003.

PEER 2003/06 *Performance of Circular Reinforced Concrete Bridge Columns under Bidirectional Earthquake Loading*. Mahmoud M. Hachem, Stephen A. Mahin, and Jack P. Moehle. February 2003.

PEER 2003/05 *Response Assessment for Building-Specific Loss Estimation.* Eduardo Miranda and Shahram Taghavi. September 2003.

PEER 2003/04 *Experimental Assessment of Columns with Short Lap Splices Subjected to Cyclic Loads*. Murat Melek, John W. Wallace, and Joel Conte. April 2003.

PEER 2003/03 *Probabilistic Response Assessment for Building-Specific Loss Estimation.* Eduardo Miranda and Hesameddin Aslani. September 2003.

PEER 2003/02 *Software Framework for Collaborative Development of Nonlinear Dynamic Analysis Program.* Jun Peng and Kincho H. Law. September 2003.

PEER 2003/01 *Shake Table Tests and Analytical Studies on the Gravity Load Collapse of Reinforced Concrete Frames.* Kenneth John Elwood and Jack P. Moehle. November 2003.

PEER 2002/24 *Performance of Beam to Column Bridge Joints Subjected to a Large Velocity Pulse.* Natalie Gibson, André Filiatrault, and Scott A. Ashford. April 2002.

PEER 2002/23 *Effects of Large Velocity Pulses on Reinforced Concrete Bridge Columns.* Greg L. Orozco and Scott A. Ashford. April 2002.

PEER 2002/22 *Characterization of Large Velocity Pulses for Laboratory Testing.* Kenneth E. Cox and Scott A. Ashford. April 2002.

PEER 2002/21 *Fourth U.S.-Japan Workshop on Performance-Based Earthquake Engineering Methodology for Reinforced Concrete Building Structures*. December 2002.

PEER 2002/20 *Barriers to Adoption and Implementation of PBEE Innovations.* Peter J. May. August 2002.

PEER 2002/19 *Economic-Engineered Integrated Models for Earthquakes: Socioeconomic Impacts.* Peter Gordon, James E. Moore II, and Harry W. Richardson. July 2002.

PEER 2002/18 *Assessment of Reinforced Concrete Building Exterior Joints with Substandard Details.* Chris P. Pantelides, Jon Hansen, Justin Nadauld, and Lawrence D. Reaveley. May 2002.

PEER 2002/17 *Structural Characterization and Seismic Response Analysis of a Highway Overcrossing Equipped with Elastomeric Bearings and Fluid Dampers: A Case Study.* Nicos Makris and Jian Zhang. November 2002.

PEER 2002/16 *Estimation of Uncertainty in Geotechnical Properties for Performance-Based Earthquake Engineering.* Allen L. Jones, Steven L. Kramer, and Pedro Arduino. December 2002.

PEER 2002/15 *Seismic Behavior of Bridge Columns Subjected to Various Loading Patterns.* Asadollah Esmaeily-Gh. and Yan Xiao. December 2002.

PEER 2002/14 *Inelastic Seismic Response of Extended Pile Shaft Supported Bridge Structures.* T.C. Hutchinson, R.W. Boulanger, Y.H. Chai, and I.M. Idriss. December 2002.

PEER 2002/13 *Probabilistic Models and Fragility Estimates for Bridge Components and Systems.* Paolo Gardoni, Armen Der Kiureghian, and Khalid M. Mosalam. June 2002.

PEER 2002/12 *Effects of Fault Dip and Slip Rake on Near-Source Ground Motions: Why Chi-Chi Was a Relatively Mild M7.6 Earthquake.* Brad T. Aagaard, John F. Hall, and Thomas H. Heaton. December 2002.

PEER 2002/11 *Analytical and Experimental Study of Fiber-Reinforced Strip Isolators*. James M. Kelly and Shakhzod M. Takhirov. September 2002.

PEER 2002/10 *Centrifuge Modeling of Settlement and Lateral Spreading with Comparisons to Numerical Analyses***.** Sivapalan Gajan and Bruce L. Kutter. January 2003.

PEER 2002/09 *Documentation and Analysis of Field Case Histories of Seismic Compression during the 1994 Northridge, California, Earthquake.* Jonathan P. Stewart, Patrick M. Smith, Daniel H. Whang, and Jonathan D. Bray. October 2002.

PEER 2002/08 *Component Testing, Stability Analysis and Characterization of Buckling-Restrained Unbonded Braces™.* Cameron Black, Nicos Makris, and Ian Aiken. September 2002.

PEER 2002/07 *Seismic Performance of Pile-Wharf Connections.* Charles W. Roeder, Robert Graff, Jennifer Soderstrom, and Jun Han Yoo. December 2001.

PEER 2002/06 *The Use of Benefit-Cost Analysis for Evaluation of Performance-Based Earthquake Engineering Decisions*. Richard O. Zerbe and Anthony Falit-Baiamonte. September 2001.

PEER 2002/05 *Guidelines, Specifications, and Seismic Performance Characterization of Nonstructural Building Components and Equipment*. André Filiatrault, Constantin Christopoulos, and Christopher Stearns. September 2001.

PEER 2002/04 *Consortium of Organizations for Strong-Motion Observation Systems and the Pacific Earthquake Engineering Research Center Lifelines Program: Invited Workshop on Archiving and Web Dissemination of Geotechnical Data, 4–5 October 2001*. September 2002.

PEER 2002/03 *Investigation of Sensitivity of Building Loss Estimates to Major Uncertain Variables for the Van Nuys Testbed.* Keith A. Porter, James L. Beck, and Rustem V. Shaikhutdinov. August 2002.

PEER 2002/02 *The Third U.S.-Japan Workshop on Performance-Based Earthquake Engineering Methodology for Reinforced Concrete Building Structures*. July 2002.

PEER 2002/01 *Nonstructural Loss Estimation: The UC Berkeley Case Study.* Mary C. Comerio and John C. Stallmeyer. December 2001.

PEER 2001/16 *Statistics of SDF-System Estimate of Roof Displacement for Pushover Analysis of Buildings.* Anil K. Chopra, Rakesh K. Goel, and Chatpan Chintanapakdee. December 2001.

PEER 2001/15 *Damage to Bridges during the 2001 Nisqually Earthquake.* R. Tyler Ranf, Marc O. Eberhard, and Michael P. Berry. November 2001.

PEER 2001/14 *Rocking Response of Equipment Anchored to a Base Foundation.* Nicos Makris and Cameron J. Black. September 2001.

PEER 2001/13 *Modeling Soil Liquefaction Hazards for Performance-Based Earthquake Engineering.* Steven L. Kramer and Ahmed-W. Elgamal. February 2001.

PEER 2001/12 *Development of Geotechnical Capabilities in OpenSees.* Boris Jeremić. September 2001.

PEER 2001/11 *Analytical and Experimental Study of Fiber-Reinforced Elastomeric Isolators*. James M. Kelly and Shakhzod M. Takhirov. September 2001.

PEER 2001/10 *Amplification Factors for Spectral Acceleration in Active Regions.* Jonathan P. Stewart, Andrew H. Liu, Yoojoong Choi, and Mehmet B. Baturay. December 2001.

PEER 2001/09 *Ground Motion Evaluation Procedures for Performance-Based Design.* Jonathan P. Stewart, Shyh-Jeng Chiou, Jonathan D. Bray, Robert W. Graves, Paul G. Somerville, and Norman A. Abrahamson. September 2001.

PEER 2001/08 *Experimental and Computational Evaluation of Reinforced Concrete Bridge Beam-Column Connections for Seismic Performance*. Clay J. Naito, Jack P. Moehle, and Khalid M. Mosalam. November 2001.

PEER 2001/07 *The Rocking Spectrum and the Shortcomings of Design Guidelines.* Nicos Makris and Dimitrios Konstantinidis. August 2001.

PEER 2001/06 *Development of an Electrical Substation Equipment Performance Database for Evaluation of Equipment Fragilities*. Thalia Agnanos. April 1999.

PEER 2001/05 *Stiffness Analysis of Fiber-Reinforced Elastomeric Isolators.* Hsiang-Chuan Tsai and James M. Kelly. May 2001.

PEER 2001/04 *Organizational and Societal Considerations for Performance-Based Earthquake Engineering.* Peter J. May. April 2001.

PEER 2001/03 *A Modal Pushover Analysis Procedure to Estimate Seismic Demands for Buildings: Theory and Preliminary Evaluation.* Anil K. Chopra and Rakesh K. Goel. January 2001.

PEER 2001/02 *Seismic Response Analysis of Highway Overcrossings Including Soil-Structure Interaction.* Jian Zhang and Nicos Makris. March 2001.

PEER 2001/01 *Experimental Study of Large Seismic Steel Beam-to-Column Connections.* Egor P. Popov and Shakhzod M. Takhirov. November 2000.

PEER 2000/10 *The Second U.S.-Japan Workshop on Performance-Based Earthquake Engineering Methodology for Reinforced Concrete Building Structures.* March 2000.

PEER 2000/09 *Structural Engineering Reconnaissance of the August 17, 1999 Earthquake: Kocaeli (Izmit), Turkey.* Halil Sezen, Kenneth J. Elwood, Andrew S. Whittaker, Khalid Mosalam, John J. Wallace, and John F. Stanton. December 2000.

PEER 2000/08 *Behavior of Reinforced Concrete Bridge Columns Having Varying Aspect Ratios and Varying Lengths of Confinement.* Anthony J. Calderone, Dawn E. Lehman, and Jack P. Moehle. January 2001.

PEER 2000/07 *Cover-Plate and Flange-Plate Reinforced Steel Moment-Resisting Connections.* Taejin Kim, Andrew S. Whittaker, Amir S. Gilani, Vitelmo V. Bertero, and Shakhzod M. Takhirov. September 2000.

PEER 2000/06 *Seismic Evaluation and Analysis of 230-kV Disconnect Switches.* Amir S. J. Gilani, Andrew S. Whittaker, Gregory L. Fenves, Chun-Hao Chen, Henry Ho, and Eric Fujisaki. July 2000.

PEER 2000/05 *Performance-Based Evaluation of Exterior Reinforced Concrete Building Joints for Seismic Excitation.* Chandra Clyde, Chris P. Pantelides, and Lawrence D. Reaveley. July 2000.

PEER 2000/04 *An Evaluation of Seismic Energy Demand: An Attenuation Approach.* Chung-Che Chou and Chia-Ming Uang. July 1999.

PEER 2000/03 *Framing Earthquake Retrofitting Decisions: The Case of Hillside Homes in Los Angeles.* Detlof von Winterfeldt, Nels Roselund, and Alicia Kitsuse. March 2000.

PEER 2000/02 *U.S.-Japan Workshop on the Effects of Near-Field Earthquake Shaking.* Andrew Whittaker, ed. July 2000.

PEER 2000/01 *Further Studies on Seismic Interaction in Interconnected Electrical Substation Equipment.* Armen Der Kiureghian, Kee-Jeung Hong, and Jerome L. Sackman. November 1999.

PEER 1999/14 *Seismic Evaluation and Retrofit of 230-kV Porcelain Transformer Bushings*. Amir S. Gilani, Andrew S. Whittaker, Gregory L. Fenves, and Eric Fujisaki. December 1999.

PEER 1999/13 *Building Vulnerability Studies: Modeling and Evaluation of Tilt-up and Steel Reinforced Concrete Buildings.* John W. Wallace, Jonathan P. Stewart, and Andrew S. Whittaker, editors. December 1999.

PEER 1999/12 *Rehabilitation of Nonductile RC Frame Building Using Encasement Plates and Energy-Dissipating Devices.* Mehrdad Sasani, Vitelmo V. Bertero, James C. Anderson. December 1999.

PEER 1999/11 *Performance Evaluation Database for Concrete Bridge Components and Systems under Simulated Seismic Loads.* Yael D. Hose and Frieder Seible. November 1999.

PEER 1999/10 *U.S.-Japan Workshop on Performance-Based Earthquake Engineering Methodology for Reinforced Concrete Building Structures.* December 1999.

PEER 1999/09 *Performance Improvement of Long Period Building Structures Subjected to Severe Pulse-Type Ground Motions*. James C. Anderson, Vitelmo V. Bertero, and Raul Bertero. October 1999.

PEER 1999/08 *Envelopes for Seismic Response Vectors.* Charles Menun and Armen Der Kiureghian. July 1999.

PEER 1999/07 *Documentation of Strengths and Weaknesses of Current Computer Analysis Methods for Seismic Performance of Reinforced Concrete Members.* William F. Cofer. November 1999.

PEER 1999/06 *Rocking Response and Overturning of Anchored Equipment under Seismic Excitations.* Nicos Makris and Jian Zhang. November 1999.

PEER 1999/05 *Seismic Evaluation of 550 kV Porcelain Transformer Bushings.* Amir S. Gilani, Andrew S. Whittaker, Gregory L. Fenves, and Eric Fujisaki. October 1999.

PEER 1999/04 *Adoption and Enforcement of Earthquake Risk-Reduction Measures.* Peter J. May, Raymond J. Burby, T. Jens Feeley, and Robert Wood.

PEER 1999/03 *Task 3 Characterization of Site Response General Site Categories.* Adrian Rodriguez-Marek, Jonathan D. Bray, and Norman Abrahamson. February 1999.

PEER 1999/02 *Capacity-Demand-Diagram Methods for Estimating Seismic Deformation of Inelastic Structures: SDF Systems*. Anil K. Chopra and Rakesh Goel. April 1999.

PEER 1999/01 *Interaction in Interconnected Electrical Substation Equipment Subjected to Earthquake Ground Motions.* Armen Der Kiureghian, Jerome L. Sackman, and Kee-Jeung Hong. February 1999.

PEER 1998/08 *Behavior and Failure Analysis of a Multiple-Frame Highway Bridge in the 1994 Northridge Earthquake.* Gregory L. Fenves and Michael Ellery. December 1998.

PEER 1998/07 *Empirical Evaluation of Inertial Soil-Structure Interaction Effects.* Jonathan P. Stewart, Raymond B. Seed, and Gregory L. Fenves. November 1998.

PEER 1998/06 *Effect of Damping Mechanisms on the Response of Seismic Isolated Structures.* Nicos Makris and Shih-Po Chang. November 1998.

PEER 1998/05 *Rocking Response and Overturning of Equipment under Horizontal Pulse-Type Motions.* Nicos Makris and Yiannis Roussos. October 1998.

PEER 1998/04 *Pacific Earthquake Engineering Research Invitational Workshop Proceedings, May 14–15, 1998: Defining the Links between Planning, Policy Analysis, Economics and Earthquake Engineering.* Mary Comerio and Peter Gordon. September 1998.

PEER 1998/03 *Repair/Upgrade Procedures for Welded Beam to Column Connections.* James C. Anderson and Xiaojing Duan. May 1998.

PEER 1998/02 *Seismic Evaluation of 196 kV Porcelain Transformer Bushings.* Amir S. Gilani, Juan W. Chavez, Gregory L. Fenves, and Andrew S. Whittaker. May 1998.

PEER 1998/01 *Seismic Performance of Well-Confined Concrete Bridge Columns.* Dawn E. Lehman and Jack P. Moehle. December 2000.

ONLINE REPORTS

The following PEER reports are available by Internet only at http://peer.berkeley.edu/publications/peer_reports.html

PEER 2012/101 *Mechanics of Fiber Reinforced Bearings.* James M. Kelly and Andrea Calabrese. February 2012.

PEER 2011/107 *Nonlinear Site Response and Seismic Compression at Vertical Array Strongly Shaken by 2007 Niigata-ken Chuetsu-oki Earthquake.* Eric Yee, Jonathan P. Stewart, and Kohji Tokimatsu. December 2011.

PEER 2011/106 *Self Compacting Hybrid Fiber Reinforced Concrete Composites for Bridge Columns.* Pardeep Kumar, Gabriel Jen, William Trono, Marios Panagiotou, and Claudia Ostertag. September 2011.

PEER 2011/105 *Stochastic Dynamic Analysis of Bridges Subjected to Spacially Varying Ground Motions.* Katerina Konakli and Armen Der Kiureghian. August 2011.

PEER 2011/104 *Design and Instrumentation of the 2010 E-Defense Four-Story Reinforced Concrete and Post-Tensioned Concrete Buildings.* Takuya Nagae, Kenichi Tahara, Taizo Matsumori, Hitoshi Shiohara, Toshimi Kabeyasawa, Susumu Kono, Minehiro Nishiyama (Japanese Research Team) and John Wallace, Wassim Ghannoum, Jack Moehle, Richard Sause, Wesley Keller, Zeynep Tuna (U.S. Research Team). June 2011.

PEER 2011/103 *In-Situ Monitoring of the Force Output of Fluid Dampers: Experimental Investigation.* Dimitrios Konstantinidis, James M. Kelly, and Nicos Makris. April 2011.

PEER 2011/102 *Ground-motion prediction equations 1964 - 2010.* John Douglas. April 2011.

PEER 2011/101 *Report of the Eighth Planning Meeting of NEES/E-Defense Collaborative Research on Earthquake Engineering.* Convened by the Hyogo Earthquake Engineering Research Center (NIED), NEES Consortium, Inc. February 2011.

PEER 2010/111 *Modeling and Acceptance Criteria for Seismic Design and Analysis of Tall Buildings.* Task 7 Report for the Tall Buildings Initiative - Published jointly by the Applied Technology Council. October 2010.

PEER 2010/110 *Seismic Performance Assessment and Probabilistic Repair Cost Analysis of Precast Concrete Cladding Systems for Multistory Buildlings.* Jeffrey P. Hunt and Božidar Stojadinovic. November 2010.

PEER 2010/109 *Report of the Seventh Joint Planning Meeting of NEES/E-Defense Collaboration on Earthquake Engineering. Held at the E-Defense, Miki, and Shin-Kobe, Japan, September 18–19, 2009.* August 2010.

PEER 2010/108 *Probabilistic Tsunami Hazard in California.* Hong Kie Thio, Paul Somerville, and Jascha Polet, preparers. October 2010.

PEER 2010/107 *Performance and Reliability of Exposed Column Base Plate Connections for Steel Moment-Resisting Frames.* Ady Aviram, Božidar Stojadinovic, and Armen Der Kiureghian. August 2010.

PEER 2010/106 *Verification of Probabilistic Seismic Hazard Analysis Computer Programs.* Patricia Thomas, Ivan Wong, and Norman Abrahamson. May 2010.

PEER 2010/105 *Structural Engineering Reconnaissance of the April 6, 2009, Abruzzo, Italy, Earthquake, and Lessons Learned.* M. Selim Günay and Khalid M. Mosalam. April 2010.

PEER 2010/104 *Simulating the Inelastic Seismic Behavior of Steel Braced Frames, Including the Effects of Low-Cycle Fatigue.* Yuli Huang and Stephen A. Mahin. April 2010.

PEER 2010/103 *Post-Earthquake Traffic Capacity of Modern Bridges in California.* Vesna Terzic and Božidar Stojadinović. March 2010.

PEER 2010/102 *Analysis of Cumulative Absolute Velocity (CAV) and JMA Instrumental Seismic Intensity (I_{JMA}) Using the PEER–NGA Strong Motion Database.* Kenneth W. Campbell and Yousef Bozorgnia. February 2010.

PEER 2010/101 *Rocking Response of Bridges on Shallow Foundations.* Jose A. Ugalde, Bruce L. Kutter, and Boris Jeremic. April 2010.

PEER 2009/109 *Simulation and Performance-Based Earthquake Engineering Assessment of Self-Centering Post-Tensioned Concrete Bridge Systems.* Won K. Lee and Sarah L. Billington. December 2009.

PEER 2009/108 *PEER Lifelines Geotechnical Virtual Data Center.* J. Carl Stepp, Daniel J. Ponti, Loren L. Turner, Jennifer N. Swift, Sean Devlin, Yang Zhu, Jean Benoit, and John Bobbitt. September 2009.

PEER 2009/107 *Experimental and Computational Evaluation of Current and Innovative In-Span Hinge Details in Reinforced Concrete Box-Girder Bridges: Part 2: Post-Test Analysis and Design Recommendations.* Matias A. Hube and Khalid M. Mosalam. December 2009.

PEER 2009/106 *Shear Strength Models of Exterior Beam-Column Joints without Transverse Reinforcement.* Sangjoon Park and Khalid M. Mosalam. November 2009.

PEER 2009/105 *Reduced Uncertainty of Ground Motion Prediction Equations through Bayesian Variance Analysis.* Robb Eric S. Moss. November 2009.

PEER 2009/104 *Advanced Implementation of Hybrid Simulation.* Andreas H. Schellenberg, Stephen A. Mahin, Gregory L. Fenves. November 2009.

PEER 2009/103 *Performance Evaluation of Innovative Steel Braced Frames.* T. Y. Yang, Jack P. Moehle, and Božidar Stojadinovic. August 2009.

PEER 2009/102 *Reinvestigation of Liquefaction and Nonliquefaction Case Histories from the 1976 Tangshan Earthquake.* Robb Eric Moss, Robert E. Kayen, Liyuan Tong, Songyu Liu, Guojun Cai, and Jiaer Wu. August 2009.

PEER 2009/101 *Report of the First Joint Planning Meeting for the Second Phase of NEES/E-Defense Collaborative Research on Earthquake Engineering.* Stephen A. Mahin et al. July 2009.

PEER 2008/104 *Experimental and Analytical Study of the Seismic Performance of Retaining Structures.* Linda Al Atik and Nicholas Sitar. January 2009.

PEER 2008/103 *Experimental and Computational Evaluation of Current and Innovative In-Span Hinge Details in Reinforced Concrete Box-Girder Bridges. Part 1: Experimental Findings and Pre-Test Analysis.* Matias A. Hube and Khalid M. Mosalam. January 2009.

PEER 2008/102 *Modeling of Unreinforced Masonry Infill Walls Considering In-Plane and Out-of-Plane Interaction.* Stephen Kadysiewski and Khalid M. Mosalam. January 2009.

PEER 2008/101 *Seismic Performance Objectives for Tall Buildings.* William T. Holmes, Charles Kircher, William Petak, and Nabih Youssef. August 2008.

PEER 2007/101 *Generalized Hybrid Simulation Framework for Structural Systems Subjected to Seismic Loading.* Tarek Elkhoraibi and Khalid M. Mosalam. July 2007.

PEER 2007/100 *Seismic Evaluation of Reinforced Concrete Buildings Including Effects of Masonry Infill Walls.* Alidad Hashemi and Khalid M. Mosalam. July 2007.

The Pacific Earthquake Engineering Research Center (PEER) is a multi-institutional research and education center with headquarters at the University of California, Berkeley. Investigators from over 20 universities, several consulting companies, and researchers at various state and federal government agencies contribute to research programs focused on performance-based earthquake engineering.

These research programs aim to identify and reduce the risks from major earthquakes to life safety and to the economy by including research in a wide variety of disciplines including structural and geotechnical engineering, geology/seismology, lifelines, transportation, architecture, economics, risk management, and public policy.

PEER is supported by federal, state, local, and regional agencies, together with industry partners.

PEER Core Institutions:
University of California, Berkeley (Lead Institution)
California Institute of Technology
Oregon State University
Stanford University
University of California, Davis
University of California, Irvine
University of California, Los Angeles
University of California, San Diego
University of Southern California
University of Washington

PEER reports can be ordered at http://peer.berkeley.edu/publications/peer_reports.html or by contacting

Pacific Earthquake Engineering Research Center
University of California, Berkeley
325 Davis Hall, mail code 1792
Berkeley, CA 94720-1792
Tel: 510-642-3437
Fax: 510-642-1655
Email: peer_editor@berkeley.edu

ISSN 1547-0587X